R-08-96

Neutron data experiments for transmutation

Annual Report 2007/2008

J Blomgren, A al-Adili, P Andersson, R Bevilacqua,
L Nilsson, S Pomp, V Simutkin, A Öhrn, M Österlund
Department of Physics and Astronomy
Division of Applied Nuclear Physics
Uppsala University

August 2008

Svensk Kärnbränslehantering AB
Swedish Nuclear Fuel
and Waste Management Co
Box 250, SE-101 24 Stockholm
Tel +46 8 459 84 00

ISSN 1402-3091
SKB Rapport R-08-96

Neutron data experiments for transmutation

Annual Report 2007/2008

J Blomgren, A al-Adili, P Andersson, R Bevilacqua,
L Nilsson, S Pomp, V Simutkin, A Öhrn, M Österlund
Department of Physics and Astronomy
Division of Applied Nuclear Physics
Uppsala University

August 2008

Summary

The project NEXT, Neutron data Experiments for Transmutation, is performed within the nuclear reactions group of the Department of Physics and Astronomy, Division of Applied Nuclear Physics, Uppsala University. The activities of the group are directed towards experimental studies of nuclear reaction probabilities of importance for various applications, like transmutation of nuclear waste, biomedical effects and electronics reliability. The experimental work is primarily undertaken at the The Svedberg Laboratory (TSL) in Uppsala, where the group is operating two world-unique instruments, MEDLEY and SCANDAL.

Highlights from the past year:

- The SCANDAL facility has been upgraded.
- One PhD student has successfully defended her thesis.
- Two PhD students have been accepted.
- Vasily Simutkin has been selected as one of the top 12 PhD students within the European Nuclear Education Network. He has accordingly been invited to present his work at the ENEN PhD event held in connection with the PHYSOR conference in Interlaken, Switzerland, September 2008.
- A research collaboration with the dedicated EU laboratory for nuclear data research has been established.
- A well-attended workshop on nuclear data for ADS and Gen-IV has been organized as part of the EU project CANDIDE (Coordination Action on Nuclear Data for Industrial Development in Europe), coordinated by Jan Blomgren.
- Several experiments have been performed at TSL, with beamtime funded through the EU project EFNUDAT (European Facilities for Nuclear Data research), partly coordinated by Jan Blomgren.
- Nuclear power education has reached all-time high at Uppsala University. In particular, industry education has increased significantly.
- IAEA has visited Uppsala University to investigate the industry-related nuclear power education, as part of a safety culture review of the Forsmark nuclear power plant.

Sammanfattning

Projektet NEXT, NeutrondataEXperiment för Transmutation, bedrivs inom kärnreaktionsgruppen vid institutionen för fysik och astronomi, avdelningen för tillämpad kärnfysik, Uppsala universitet. Gruppens verksamhet är inriktad mot experimentella studier av kärnfysikaliska reaktionssannolikheter för olika tillämpningsområden, som transmutation av kärnavfall, biomedicinska effekter och tillförlitlighet hos elektronik. Den experimentella verksamheten bedrivs huvudsakligen vid The Svedberglaboratoriet (TSL) i Uppsala, där gruppen driver två världsunika instrument, MEDLEY och SCANDAL.

Höjdpunkter från det gångna verksamhetsåret:

- En omfattande uppgradering av experimentuppställningen SCANDAL har genomförts.
- En doktorand har disputerat.
- Två nya doktorander har antagits.
- Vasily Simutkin har utsetts till en av de 12 bästa doktoranderna inom ENEN (European Nuclear Education Network). Han har därför inbjudits att presentera sitt arbete vid ENEN:s doktorandmöte i samband med PHYSOR-konferensen i Interlaken, Schweiz, September 2008.
- Ett forskningssamarbete med EU:s kärndatalaboratorium har etablerats.
- En välbesökt workshop om kärndata har arrangerats inom ramen för EU-projektet CANDIDE (Coordination Action on Nuclear Data for Industrial Development in Europe), koordinerat av Jan Blomgren.
- Ett flertal experiment har genomförts vid TSL med finansiering av stråltiden genom EU-projektet EFNUDAT (European Facilities for Nuclear Data research), delvis koordinerat av Jan Blomgren.
- Kärnkraftutbildning har nått sin största volym någonsin vid Uppsala universitet. Detta gäller särskilt utbildning för industrin som har ökat snabbt.
- IAEA har besökt Uppsala Universitet och studerat uppdragsutbildningen för kärnkraftsindustrin i samband med en inspektion av säkerhetsarbetet vid Forsmark.

Contents

Appendices attached on CD

VI M Österlund, J Blomgren, M Hayashi, P Mermod, L Nilsson, S Pomp, A Öhrn, A V Prokofiev, U Tippawan, *Elastic neutron scattering studies at 96 MeV*, Tenth Symposium on Neutron Dosimetry, Uppsala, Sweden, June 12–16, 2006. Rad. Prot. Dosim. 126 (2007) 119.

VII S Pomp, J Blomgren, C Johansson, J Klug, A Öhrn, M Österlund, V Blideanu, F R Lecolley, J F Lecolley, T Lefort, M Louvel, N Marie, Ph. Eudes, A Guertin, F Haddad, Ch. Le Brun, A Prokofiev, U Tippawan, *Neutron-induced light-ion production from Fe, Pb and U at 96 MeV*, Tenth Symposium on Neutron Dosimetry, Uppsala, Sweden, June 12–16, 2006. Rad. Prot. Dosim. 126 (2007) 123.

VIII U Tippawan, S Dangtip, S Pomp, A Ataç, B Bergenwall, J Blomgren, C Johansson, J Klug, P Mermod, L Nilsson, N Olsson, A Öhrn, M Österlund, A Prokofiev, P Nadel-Turonski, V Corcalciuc, A J Koning, *Light charged-particle production in 96 MeV neutron-induced reactions on carbon and oxygen*, Tenth Symposium on Neutron Dosimetry, Uppsala, Sweden, June 12–16, 2006. Rad. Prot. Dosim. 126 (2007) 35.

IX A Öhrn, J Blomgren, H Park, S Khurana, R Nolte, D Schmidt, K Wilhelmsen, *A monitor for neutron flux measurements up to 20 MeV*, Tenth Symposium on Neutron Dosimetry, Uppsala, Sweden, June 12–16, 2006. Rad. Prot. Dosim. 126 (2007) 394.

X P Bilski, J Blomgren, A Esposito, F d'Errico, G Fehrenbacher, F Fernàndez, A Fuchs, N Golnik, V Lacoste, A Leuschner, S Sandri, M Silari, F Spurny, B Wiegel, P Wright, *Complex radiation fields at workplaces at European high-energy accelerators and fusion facilities*, Tenth Symposium on Neutron Dosimetry, Uppsala, Sweden, June 12–16, 2006. Rad. Prot. Dosim. 126 (2007) 491.

XI AV Prokofiev, O Byström, C Ekström, D Reistad, V Ziemann, J Blomgren, S Pomp, M Österlund, U Tippawan, *A New Neutron Beam Facility at TSL*, Tenth Symposium on Neutron Dosimetry, Uppsala, Sweden, June 12–16, 2006. Rad. Prot. Dosim. 126 (2007) 18.

XII H Jäderström, Yu Murin, Yu Babain, M Chubarov, V Pljuschev, M Zubkov, P Nomokonov, N Olsson, J Blomgren, U Tippawan, L Westerberg, P Golubev, B Jakobsson, L Gerén, P-E Tegnér, I Zartova, A Budzanowski, B Czech, I Skwirczynska, V Kondratiev, H H Tang, J Aichelin, Y Watanabe, K K Gudima, *200 and 300 MeV/nucleon nuclear reactions responsible for single-event effects in microelectronics*. Phys. Rev. C. 77 (2008) 044601.

XIII A Öhrn, J Blomgren, H Park, S Khurana, R Nolte, D Schmidt, K Wilhelmsen, *A monitor for neutron flux measurements up to 20 MeV*, Nucl. Instr. Meth. Phys. Res. A 592 (2008) 405.

XIV J Blomgren, E Bauge, D Cano Ott, S Czifrus, K Dahlbacka, E Gonzalez, H Henriksson, R Jacqmin, A Koning, D Lecarpentier, E Malambu, A Mengoni, R Mills, A Plompen, G Rimpault, V Stary, C Trakas, P Vaz, C Zimmerman, *CANDIDE - Coordination Action on Nuclear Data for Industrial Development in Europe*, International Conference on Nuclear Data for Science and Technology, Nice, France, April 22–27, 2007, p. 235.

XV A Öhrn, J Klug, J Blomgren, C Johansson, P Mermod, L Nilsson, S Pomp, M Österlund, A Prokofiev, G Tutin, U Tippawan, *Elastic neutron scattering at 96 MeV*, International Conference on Nuclear Data for Science and Technology, Nice, France, April 22–27, 2007, p. 269.

XVI P Mermod, J Blomgren, C Johansson, A Öhrn, M Österlund, S Pomp, B Bergenwall, J Klug, L Nilsson, N Olsson, U Tippawan, P Nadel-Turonski, O Jonsson, AV Prokofiev, P-U Renberg, Y Maeda, H Sakai, A Tamii, K Amos, R Crespo, A Moro, *95 MeV neutron scattering on hydrogen, deuterium, carbon and oxygen*, International Conference on Nuclear Data for Science and Technology, Nice, France, April 22–27, 2007, p. 273.

XVII J Blomgren, S Pomp, J-C Boursellier, M Österlund, AV Prokofiev, A Koning, *Mono-energy neutron testing of single-event effects*, International Conference on Nuclear Data for Science and Technology, Nice, France, April 22–27, 2007, p. 340.

XVIII V P Eismont, N P Filatov, A N Smirnov, J Blomgren, *Angular anisotropy of intermediate energy nucleon-induced fission of actinide and subactinide nuclei*, International Conference on Nuclear Data for Science and Technology, Nice, France, April 22–27, 2007, p. 283.

XIX A N Smirnov, O I Batenkov, V P Eismont, N P Filatov, J Blomgren, H Condé, A V Prokofiev, S G Mashnik, *Nucleon-induced fission cross-sections of tantalum and separated tungsten isotopes and "compound nucleus" effect in intermediate energy region*, International Conference on Nuclear Data for Science and Technology, Nice, France, April 22–27, p. 288.

XX U Tippawan, S Pomp, J Blomgren, M Hayashi, L Nilsson, A Öhrn, M Österlund, A Prokofiev, V Simutkin, P-A Söderström, Y Watanabe, *Studying neutron-induced light-ion production with the MEDLEY facility: status and future plans*, International Conference on Nuclear Data for Science and Technology, Nice, France, April 22–27, 2007, p. 356.

XXI M Hayashi, Y Watanabe, J Blomgren, L Nilsson, A Öhrn, M Österlund, S Pomp, A Prokofiev, V Simutkin, P-A Söderström, U Tippawan, *Measurement of light-ion production at the new Uppsala neutron beam facility*, International Conference on Nuclear Data for Science and Technology, Nice, France, April 22–27, 2007, p. 287.

XXII O Batenkov, G Boikov, V Eismont, M Majorov, S Soloviev, J Blomgren, W Loveland, *Comparison of prompt-fission neutron multiplicities and energy spectra for intermediate energy proton- and neutron-induced fission*, International Conference on Nuclear Data for Science and Technology, Nice, France, April 22–27, 2007, p. 285.

XXIII X Ledoux, M Aiche, G Ban, G Barreau, P Baumann, P Bém, V Blideanu, J Blomgren, S Czajkowski, P Dessagne, E Dupont, T Ethvignot, U Fischer, F Gunsing, B Jacquot, *A neutron beam facility at SPIRAL-2*, International Conference on Nuclear Data for Science and Technology, Nice, France, April 22–27, 2007, p. 122.

XXIV P Mermod, S Pomp, J Blomgren, C Johansson, J Klug, L Nilsson, N Olsson, A Öhrn, M Österlund, U Tippawan, O Jonsson, A V Prokofiev, P-U Renberg, B Bergenwall, P Nadel-Turonski, Y Maeda, H Sakai, A Tamii, *Evidence of three-body force effects in neutron-deuteron scattering at 95 MeV*, Proc. International Nuclear Physics Conference (INPC2007), (Tokyo 2007) Volume 2, pp. 449.

1 Background

1. 1 The NEXT project

The present project, Neutron data Experiments for Transmutation (NEXT), supported as a research task agreement by Statens Kärnkraftinspektion (SKI), Svensk Kärnbränslehantering AB (SKB) and Ringhalsverket AB, started 2006-07-01. The primary objective from the supporting organizations is to promote research and research education of relevance for development of the national competence within nuclear energy.

The aim of the project is in short to:

- promote development of the competence within nuclear physics and nuclear technology by supporting licenciate and PhD students,
- advance the international research front regarding fundamental nuclear data within the presently highlighted research area accelerator-driven transmutation,
- strengthen the Swedish influence within the mentioned research area by expanding the international contact network,
- provide a platform for Swedish participation in relevant EU projects,
- monitor the international development for the supporting organizations,
- constitute a basis for Swedish participation in the nuclear data activities at IAEA and OECD/NEA.

The project is operated by the Department of Physics and Astronomy, Division of Applied Nuclear Physics (TK, abbreviation of the Swedish division name Tillämpad Kärnfysik). TK is the successor of the late Department of Neutron Research (INF), that was merged with three other departments to form the new organization 2008-01-01. TK is utilizing the unique neutron beam facility at the The Svedberg Laboratory (TSL) at Uppsala University, which forms the backbone of the research of the NEXT project.

In this document, we give a status report after the second year (2007-07-01–2008-06-30) of the project.

2 Introduction

2.1 Why accelerator-driven transmutation?

During the operation of a commercial nuclear power reactor, energy is released due to fission of uranium and heavier elements, with U-235 being the most important nuclide. Fission results in the creation of a large number of elements roughly half the mass and atomic number of uranium. Essentially all these new elements are radioactive, most of them with short half-lives. Immediately after irradiation in a reactor, spent nuclear fuel would be lethally harmful to be close to, and therefore the handling of spent nuclear fuel is carried out with great precaution.

The radioactivity gets reduced over time. Of the elements created in large quantities, Sr-90 and Cs-137 have the longest half-lives, in both cases around 30 years. This means that the radioactivity is reduced by a factor 1,000 in about 300 years, after which the remaining radioactivity due to fission products is so small that it does no longer pose a significant risk.

In parallel with the fission processes in a reactor, heavier elements than uranium (i.e. trans-uranium elements) are being created via neutron capture reactions followed by beta decay. At outtake of spent nuclear fuel, most of the initial U-235 has been spent. Instead, the spent fuel contains a few percent of trans-uranium (TRU) elements, with plutonium being by far the most abundant.

Many of these TRUs are long-lived alpha emitters. This means that they pose essentially no risk as long as they are outside the body, but can be highly radiotoxic after intake. This means that two strategies have evolved concerning the handling of spent nuclear fuel:

- Wait for natural decay, and reduce the possibility for intake during the decay time.
- Convert the material via nuclear reactions to short-lived elements.

The first strategy leads to geological disposal. A number of countries are preparing for geological disposal, Sweden being one of the countries with the most advanced plans. The second strategy, often called transmutation, has some attractive features in principle, but suffers from a far less mature technology. This is manifested by the fact that no country is presently relying on transmutation as a main strategy.

It is, however, known already that in principle it is possible to incinerate these long-lived TRU elements via neutron-induced fission. A fraction of these elements can be treated with thermal neutrons, which makes transmutation in present-day reactors possible. It is, however, clear that fission induced by fast neutrons is a pre-requisite for a significant reduction of the long-term radio-toxicity. This points towards reactors of a type that presently exist only as research facilities. Thus, the challenge today is not to prove the underlying physics for transmutation, but to convert a research technology into industrial-scale operation.

Fast reactors can be of two types: critical and sub-critical. Critical reactors operate on self-sustaining nuclear chain reactions. In fission, 2–4 neutrons are released, which in turn can induce new fission reactions. Hence, a critical reactor needs no external input of neutrons. All TRUs are, however, not suitable as fuels in critical reactors. This is because of the role of delayed neutrons.

After fission, most of the neutrons are released immediately. In commercial reactors, the average time from one fission reaction until a released neutron induces a new fission reaction is of the order of less than 0.1 ms. This means that if only slightly more than one neutron per fission induces another fission reaction, the neutron flux will increase very rapidly, with the power increasing correspondingly rapidly. If this were the whole story, critical reactors could not operate. Nature, however, provides a solution to this dilemma: delayed neutrons.

A small fraction of the neutrons, typically around 0.5%, are not released directly after fission, but after beta decay of fission products. This means that they are emitted in up to about a minute after fission, with 15 seconds as average time in present commercial reactors. Although being a small fraction, they extend the average time between fissions significantly, making the time required for a change of the power in the reaction moving from the millisecond scale to seconds, given that the reactor is operated close to exact criticality.

It turns out, however, that for most of the TRU elements the fraction of delayed neutrons is smaller than for U-235, making incineration in critical reactors more difficult. In the case of americium, the fraction is very small, making a critical reactor loaded with a large fraction of americium practically impossible to control. Here sub-critical systems have a cutting edge. If the reactor is under-critical, delayed neutrons are not required for stability. The price to pay is that neutrons have to be externally produced and fed into the core to keep the system running.

The presently leading technology for driving an under-critical reactor is proton-induced spallation of heavy elements. If a 1 GeV proton beam hits a lead target, about 20 neutrons per incident proton are released. If this is placed at the centre of a reactor, the emitted neutrons can induce chain reactions in the surrounding core, and the power released is proportional to the proton beam power.

There is consensus that successful implementation of transmutation requires partitioning of the spent nuclear fuel before installation into a sub-critical reactor. The fission products produced in the critical reactor need to be separated, and only the actinides should be transmuted. Therefore, this entire research field is commonly referred to as partitioning and transmutation (P&T).

It should be stressed that even optimally successful operation of P&T does not alleviate the need for geological storage. Still the fission products need to be stored, and it is likely that some losses in the handling of actinides are unavoidable, leading to some storage needs also of actinides. P&T could possible change the requirements on the geological storage, but not remove the need completely.

2.2 Nuclear data for transmutation

Nuclear data research has been carried out for a long time resulting in nuclear data libraries utilized in development and optimization of thermal reactors. In an accelerator-driven system (ADS) there are some notable differences compared to critical reactors /Blomgren 2002, 2004/:

- Proton-induced neutron production.
- Neutrons at much higher energies than in critical reactors.

To meet the corresponding nuclear data demands, the EU-sponsored project HINDAS (High and Intermediate energy Nuclear Data for Accelerator-driven Systems) was carried out during 2000–03. HINDAS was a joint European effort, which gathered essentially all European competence on nuclear data for transmutation in the 20–2,000 MeV range /Koning et al. 2002/. The program was designed to obtain a maximal improvement in high-energy nuclear data knowledge for transmutation. It was conceived that this goal could only be achieved with a well-balanced combination of basic cross section measurements, nuclear model simulations and data evaluations. The work was focused on three elements, iron, lead and uranium, selected to give a representative coverage of typical materials for construction, target and core, respectively, especially relevant to ADS, as well as a wide coverage of the periodic table of elements.

In total, 16 universities or laboratories participated, whereof 6 had experimental facilities. This means that HINDAS involved essentially all relevant European laboratories in its energy range. This distribution and coordination of experiments at many laboratories made the work very efficient. What is noteworthy is that HINDAS involved many partners and even laboratories that had previously not been involved at all in activities on nuclear data for applications. Thus, HINDAS has contributed to a widening of the field of applied nuclear physics.

The work was divided into two main energy domains, 20–200 MeV and 200–2,000 MeV. This division into two energy ranges is natural, since there appears to be a transition region around 200 MeV for the theoretical models. Below this energy the theoretical calculations have to include direct interactions, as well as pre-equilibrium, fission and statistical models, whereas at higher energies the intra-nuclear cascade model, together with fission and evaporation models, has to be considered. As a coincidence, the experimental facilities and the measurement techniques are also different below and above about 200 MeV. Within each energy domain, the experimental work was structured according to type of particles produced. This means that for each energy range, there were work packages on production of light ions, neutrons and residues, respectively.

Notably, fission was not explicitly included in HINDAS, simply because a large majority of all fission studies were undertaken within ISTC (International Science and Technology center), i.e. in collaborative efforts between former weapons scientists of the former Soviet Union and civil European researchers.

The HINDAS project resulted in a wealth of new knowledge, and has been considered a raw model for international collaboration in the realm of nuclear data.

2.3 Previous Uppsala activities in the field

Uppsala took a very active part in HINDAS, was coordinating one work package and provided the most frequently used experimental facility, TSL. Connected to HINDAS, the Uppsala group ran two projects preceding NEXT, KAT (1998–2002) and NATT (2002–2006) with similar structure and scope as NEXT.

Quickly summarizing the achievements during the last ten years, it can be concluded that the Uppsala group has advanced the research frontier significantly on neutron-induced nuclear reactions of ADS relevance. Analysis and documentation has been finalized of previously performed measurements of elastic neutron scattering on five nuclei ranging from carbon to lead at 96 MeV /Klug et al. 2003, Mermod et al. 2006, Öhrn et al. 2008/. The precision in the results surpasses all previous data by at least an order of magnitude. These measurements represent the highest energy in neutron scattering where the ground state has been resolved. The results show that all previous theory work has underestimated the probability for neutron scattering at the present energy by 0–30%.

A new method for measurements of absolute probabilities for neutron-induced nuclear reactions with experimental techniques only has been developed /Klug et al. 2003/. Previously, only two such methods have been known.

Compelling evidence of the existence of three-body forces in nuclei has been obtained. The first publication on these matters from the group /Mermod et al. 2004/ turned out to qualify on the top-ten downloading list of Physics Letters B, one of the very most prestigious journals in subatomic physics.

Production of light ions from iron, lead and uranium has been studied in collaboration with a number of French research institutes /Blideanu et al. 2004/, and studies of the same reactions on carbon, oxygen and silicon have been undertaken by the local group /Tippawan et al. 2004, 2006/. These data have provided valuable benchmarking of present state-of-the-art theory models.

Fission has been studied in collaboration with a number of Russian research institutes. In these studies, the Uppsala contribution has primarily been limited to providing the beam and auxiliary equipment.

Another important result of the KAT and NATT projects is that five PhD theses with data from TSL have been successfully defended.

2.4 International outlook

During the last decade, the leading research on nuclear data for ADS has been undertaken in Europe including Russia. There is a striking imbalance around the World on nuclear data for ADS. Europe, including Russia, dominates heavily. The other large nuclear energy countries, i.e. USA and Japan, have only limited research in this field, in spite of previously having hosted important activities.

In the fifth EU framework program (FP5), a large fraction of the P&T research was devoted to nuclear data. Two large projects, HINDAS and NTOF were financed by the EC. As outlined above, HINDAS resulted in a wealth of new nuclear data and advanced the frontier significantly. NTOF was primarily focused on the low-energy range and dominated by activities at CERN, Geneva, Switzerland, where a spallation neutron source was developed. The agenda comprised mostly capture and fission cross-section measurements in the eV to keV neutron energy range. The development of the facility was significantly delayed compared with the original time table, and therefore the project was extended. At present, the facility is operational with parameters close to the specifications, and the first results have been presented.

In FP6, a notable shift in focus on European nuclear data research for ADS has taken place. With the successful completion of the HINDAS project, it was concluded that the nuclear data requirements had to a large degree been fulfilled, and therefore the EUROTRANS project was focused on other problem areas. Still, however, a work package on nuclear data was included, but at a lower ambition level than in FP5.

In parallel with the EU activities, ISTC has financed important activities on nuclear data for transmutation. It should be especially pointed out that our present knowledge of fission cross sections above 20 MeV is heavily dominated by ISTC-supported data. From a Swedish perspective, it is noteworthy that a significant fraction of these results has been produced by Russian groups working at TSL.

2.5 Scientific scope of NEXT

In the 20–200 MeV range, the most important remaining data requests from the ADS community are:

- Neutron-induced light-ion production at around 200 MeV. Up to now, high-quality data up to 100 MeV are available.
- Neutron-induced fission in the 20–200 MeV range. Data on total fission cross sections are available. What is requested now are other types of information, like distributions in angle, mass and energy of the fission products. Moreover, most data sets are relative measurements, implying that accurate calibration of the cross section scale for one or a few fission reactions would be very advantageous.
- Neutron elastic scattering at around 200 MeV. Up to now, high-quality data up to 100 MeV are available.
- Neutron inelastic scattering in the 100–200 MeV range. Up to now, high-quality data up to 30 MeV are available, and one single data set at 65 MeV has been published.

The NEXT project was originally designed to address the first two items above, with one PhD student working on each of the two topics. After NEXT was initiated, a large grant for instrument upgrade was provided by VR, allowing the third issue also to be addressed. As a consequence, a third PhD student has been recruited.

In the present FP6 project EUROTRANS (2004-08), UU participates with a joint Swedish-French experiment on neutron inelastic scattering, for which a world-unique experimental equipment has been developed. Thus, the fourth item is also dealt with, outside NEXT.

It should be mentioned that KAT and NATT were originally intended to be focused on elastic scattering, and a measurement techniques was adopted that was not considered suitable for inelastic scattering studies. It has been shown recently, however, that the existing data from the SCANDAL setup can in fact be analyzed to extract also inelastic scattering cross sections.

As outlined above, several ISTC projects have been carried out at TSL in close collaboration with the TK group. This has matured to involve joint experimental work also at other facilities. A joint fission experiment in Louvain-la-Neuve, Belgium was initiated in May 2007, and several experiment campaigns are foreseen, in which the NEXT PhD students participate. In particular, for the fission-oriented student, this offers a valuable opportunity for quality improvement.

2.6 Outlook

As described above, in the realm of ADS, two classes of nuclear data are clearly discernable, above and below 20 MeV. Above 20 MeV, no previous nuclear energy applications have been developed, and consequently the database is meagre. During the last decade, the situation on proton- and neutron-induced production of charged particles has improved considerably, and presently the situation is satisfactory for the demands as long as the aim is to build a demonstrator or prototype system. If a future full-scale ADS plant for large-scale incineration were to be built, the situation would, however, probably need to be revisited due to the higher demands of a production facility.

Concerning neutron-induced nuclear reactions at around 200 MeV, there is still room for considerable improvement. The present upgrades at TSL are dictated to fill these demands. It can be foreseen that a 5–10 year experimental campaign is required to reach a situation resembling the present situation at 100 MeV.

Up to now, all experimental activities have been focused on cross section measurements. The natural next step would be to carry out integral experiments, i.e. an experiment where the quality of the entire data library is assessed. This could for instance be measurements of neutron transmission through large blocks of various materials. Only one such experiment has been performed worldwide /Nakashima et al. 1996/. TSL is well suited for such experiments, and it is conceivable that such integral experiments could be important in FP7. A series of studies, conducted as part of NEXT and presented at an international symposium, indicates that such an experiment could be performed with existing equipment at TSL /Blomgren and Chtioui 2007/.

At lower energies, the nuclear data situation is fundamentally different. The development of critical reactors has motivated large efforts in data production and therefore the present work is dedicated to filling important gaps in the literature. In general, the nuclear data status is satisfactory for uranium and plutonium, whilst there is room for improvement on the minor actinides (neptunium, americium and curium). At present and in the near future, the activities on americium dominate. This is due to two factors. First, americium is the nucleus that has the largest deficiencies in the nuclear data bases and second, it is probably the element where incineration in ADS is best motivated.

Nuclear data activities at lower energies could be expected to grow in a near future, because of the interest in Gen-IV reactor systems. The nuclear data required for development of Gen-IV are more or less identical with those needed for ADS.

If realization of a full-scale ADS or Gen-IV system would be carried out, another nuclear data activity might be motivated. The nuclear data on the most important elements, i.e. uranium and plutonium, were often produced thirty years ago or more. It is not unlikely that some of the key nuclear data in the adopted databases suffer from systematic errors. This might motivate some of these data to be revisited, taking advantage of the development of novel experimental techniques in the recent years.

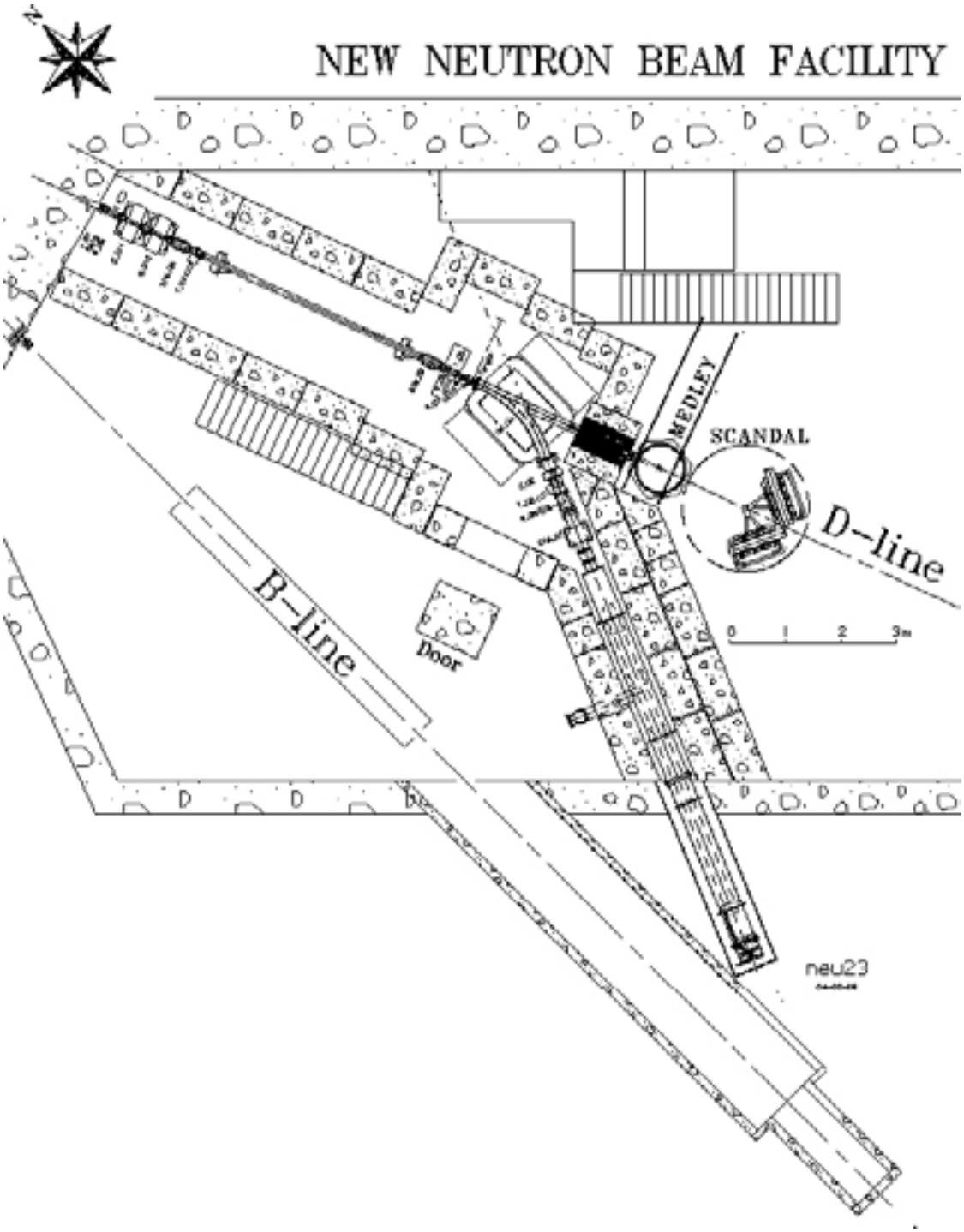

Figure 2-1. *The TSL neutron beam facility.*

3 Experimental setup and techniques

3.1 The TSL neutron beam facility

At TSL, quasi-monoenergetic neutrons are produced by the reaction ^{7}Li(p,n)^{7}Be in a ^{7}Li target bombarded by 50–180 MeV protons from the cyclotron, as is illustrated in Figure 2-1. After the target, the proton beam is bent by a dipole magnet into a concrete tunnel, where it is stopped in a well-shielded Faraday cup, used to measure the proton beam current. A narrow neutron beam is formed in the forward direction by a collimator with a total thickness of about one metre.

The energy spectrum of the neutron beam consists of a high-energy peak, having approximately the same energy as the incident proton beam, and a low-energy tail. About half of all neutrons appear in the high-energy peak, while the rest are roughly equally distributed in energy, from the maximum energy and down to zero. The low-energy tail of the neutron beam can be reduced using time-of-flight (TOF) techniques over the distance between the neutron source and the reaction target.

The relative neutron beam intensity is monitored by integrating the charge of the primary proton beam, as well as by using thin film breakdown counters, placed in the neutron beam, measuring the number of neutron-induced fissions in ^{238}U.

Two multi-purpose experimental setups are semi-permanently installed at the neutron beam line, namely MEDLEY and SCANDAL. These were described in detail in the annual report 1999/2000 of the previous KAT project, and only a brief presentation is given here.

3.2 The MEDLEY setup

The MEDLEY detector array /Dangtip et al. 2000/, shown in Figure 3-1, has been designed for measurements of neutron-induced light-ion production cross sections of relevance for applications within ADS and fast-neutron cancer therapy and related dosimetry. It consists of eight particle telescopes, installed at emission angles of 20–160 degrees with 20 degrees separation, in a 1 m diameter scattering chamber, positioned directly after the last neutron collimator. All the telescopes are fixed on a turnable plate at the bottom of the chamber, which can be rotated without breaking the vacuum.

Each telescope is a ΔE–ΔE–E detector combination, where the ΔE detectors are silicon surface barrier detectors and the E detector is an inorganic CsI(Tl) crystal. Detectors of various thicknesses are being used, with different combinations depending on the application. ΔE–ΔE or ΔE–E techniques are used to identify light charged particles (p, d, t, 3He, α). The chosen design gives a sufficient dynamic range to distinguish all charged particles from a few MeV up to 175 MeV, being the maximum energy of the facility.

3.3 The SCANDAL setup

The SCANDAL setup /Klug et al. 2002/ is primarily intended for studies of elastic neutron scattering, i.e. (n,n) reactions. Neutron detection is accomplished via conversion to protons by the H(n,p) reaction. In addition, (n,xp) reactions in nuclei can be studied by direct detection of protons. This feature is also used for calibration, and the setup has therefore been designed for a quick and simple change from one mode to the other.

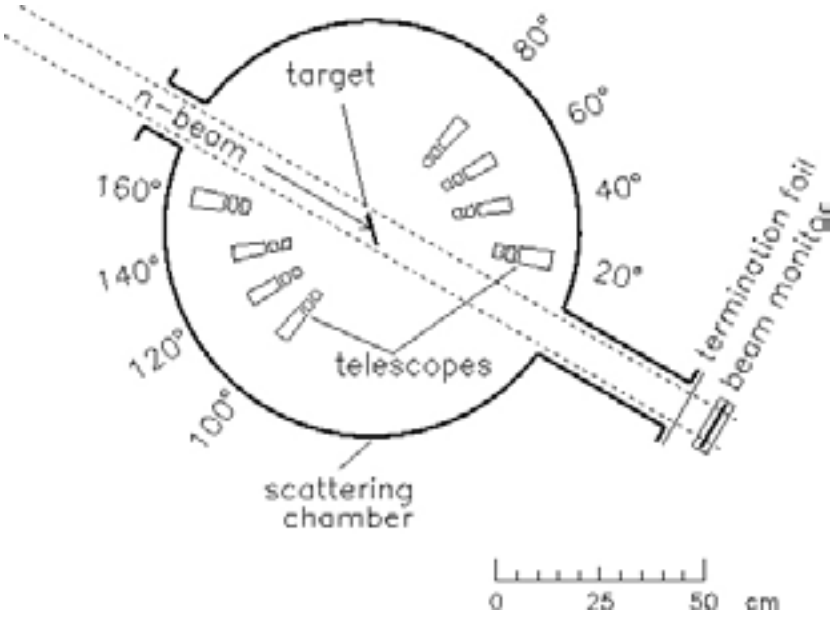

Figure 3-1. *The MEDLEY setup.*

The device is illustrated in Figure 3-2. It consists of two identical systems, in most cases located on each side of the neutron beam. The design allows the neutron beam to pass through the drift chambers of the right-side setup, making low-background measurements close to zero degrees feasible.

In neutron detection mode, each arm consists of a 2 mm thick veto scintillator for fast charged-particle rejection, a neutron-to-proton converter which is a 10 mm thick plastic scintillator, a 2 mm thick plastic scintillator for triggering, two drift chambers for proton tracking, a 2 mm thick ΔE plastic scintillator, which is also part of the trigger, and an array of 12 large CsI detectors for energy determination. The trigger is provided by a coincidence of the two trigger scintillators, vetoed by the front scintillator. The compact geometry allows a large solid angle for protons emitted from the converter. Recoil protons are selected using the ΔE and E information from the plastic scintillators and the CsI detectors, respectively. The energy resolution is about 3.7 MeV (FWHM), which is sufficient to resolve elastic and inelastic scattering in several nuclei. The angular resolution is calculated to be about 1.4 degrees (rms) when using a cylindrical scattering sample of 5 cm diameter.

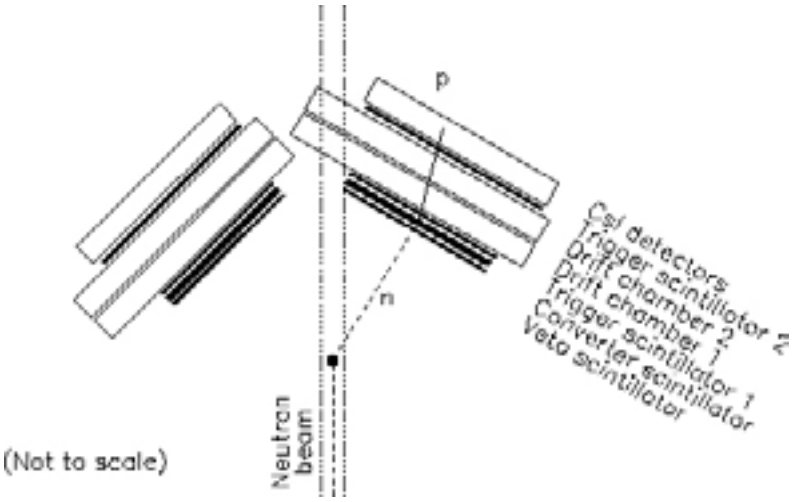

Figure 3-2. *The SCANDAL setup.*

When SCANDAL is used for (n,xp) studies, the veto and converter scintillators are removed. A multitarget arrangement can be used to increase the target content without impairing the energy resolution, which is typically 3.0 MeV (FWHM). This multitarget box allows up to seven targets to be mounted simultaneously, interspaced with multi-wire

proportional counters (MWPC). In this way it is possible to determine in which target layer the reaction took place, and corrections for energy loss in the subsequent targets can be applied. In addition, different target materials can be studied simultaneously, thus facilitating absolute cross section normalization by filling a few of the multitarget slots with CH2 targets. The first two slots are normally kept empty, and used to identify charged particles contaminating the neutron beam.

During the last project year, SCANDAL has undergone an upgrade. The CsI crystals have been replaced by thicker ones to allow studies at the TSL maximum energy (175 MeV). A test run has shown that the resolution specifications have been met, and production experiments are presently being prepared.

4 Recent results

4.1 Elastic scattering

New experimental data on elastic scattering of 96 MeV neutrons from iron and yttrium /Öhrn et al. 2007/ have recently been published (see Figure 4-1). The previously published data on lead have been extended, as a new method has been developed to obtain more information from data, namely to increase the number of angular bins at the most forward angles. The results are compared with modern optical model predictions, based on phenomenology and microscopic nuclear theory, and are in general in good agreement with the model predictions.

These nuclei are all of interest from ADS point of view, since they represent construction material (iron), fuel cladding (zirconium, replaced by yttrium) and target/coolant (lead). The choice of yttrium might need a clarification. For physics interpretation, it is advantageous to have a mono-isotopic target. Zirconium has five isotopes, none accounting for more than about 50% of the abundance, while yttrium is naturally mono-isotopic.

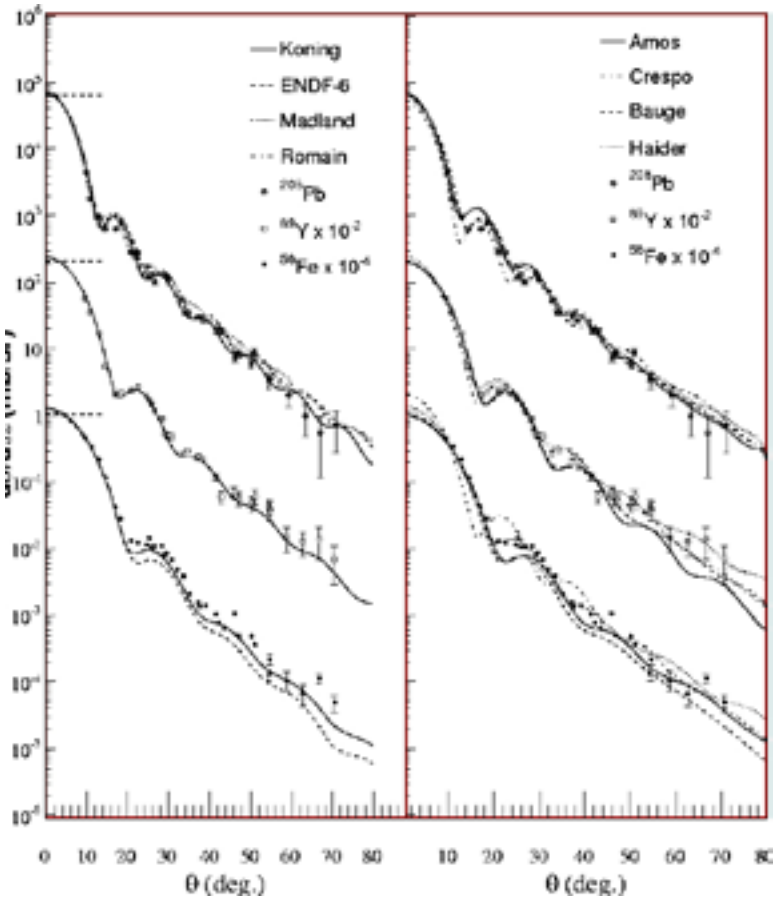

Figure 4-1. *Neutron elastic scattering cross sections on iron, yttrium and lead at 95 MeV. The lines refer to various theory predictions.*

4.2 (n,xlcp) reactions

In parallel with the other experiments mentioned above and below, data have been taken with the MEDLEY setup on light-ion production reactions. During the last years, results on oxygen, silicon, iron, lead and uranium have been published. Preliminary carbon data have been presented at an international conference. During late autumn 2007, a large measurement campaign was undertaken, in which data on carbon and iron were acquired at 175 MeV. Presently, Riccardo Bevilacqua is analyzing these data.

4.3 (n,xn') reactions

We have a collaboration project with a group from Caen, France, on (n,xn') reactions. For these studies, a modified SCANDAL converter (CLODIA) has been designed and built in Caen. A large experiment on lead and iron targets was conducted in August 2004. This experiment is our deliverable in the EU 6th FWP EUROTRANS. Preliminary data were presented at the International workshop on Fast Neutron Detectors and Applications, Cape Town, South Africa, April 3–6, 2006 /Sagrado Garcia et al. 2006/.

A method to extend the analysis of previously obtained data has been developed, resulting in the spectra shown in Figure 4-2. A publication is underway.

4.4 Fission

In 2006, our group performed an experiment on fission at the CYCLONE laboratory as in Louvain-la-Neuve, Belgium, in collaboration with a fission experiment group at Khlopin Radium Institute (KRI) in St. Petersburg, Russia. This collaboration has been deepened during the present project year. Vasily Simutkin, one of the NEXT PhD students, has spent a few months in St. Petersburg for data analysis. The results clearly show that the mechanism for fission changes significantly with incident neutron energy. Especially the final products created in fission change, implying that if ADS is implemented, the fission products to be geologically stored will be different from those of present power reactors.

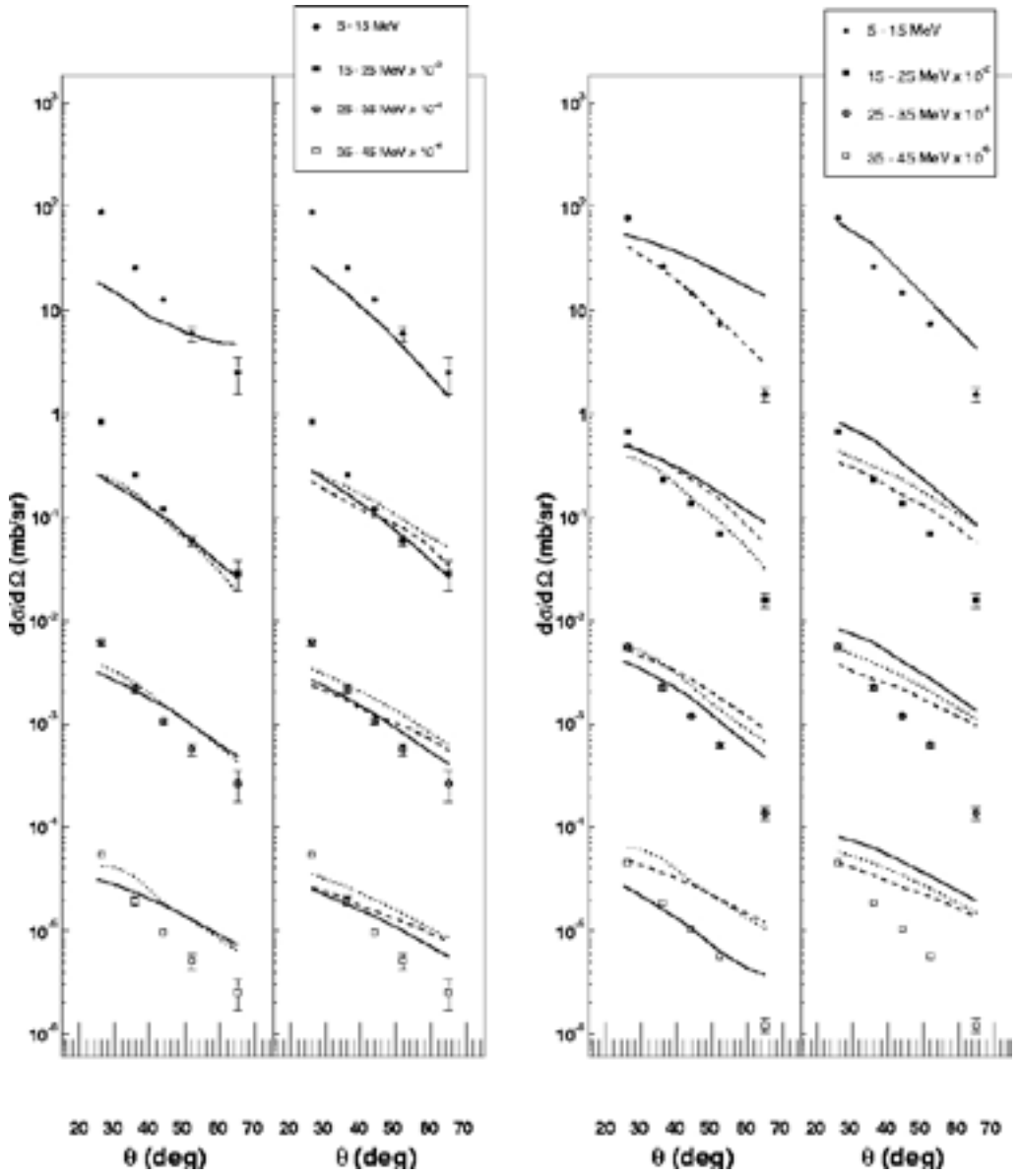

Figure 4-2. *Neutron inelastic scattering cross sections on iron at 95 MeV. The lines refer to various theory predictions.*

5 International activities

5.1 Collaborations

During 2005, the 6th EU framework program EUROTRANS started. Our group and our long-term collaborators from LPC Caen, France, have merged our activities in EUROTRANS, and we have a joint deliverable concerning (n,xn') reactions (see above).

Our group has been active in two EU projects during the present project year. The four-year project EFNUDAT (European Facilities for Nuclear Data Measurements) aims at establishing a joint European infrastructure for nuclear data measurements by networking existing facilities. Our role is to provide access to The Svedberg Laboratory to other European users, and to coordinate the networking activities, i.e. organize workshops and training courses, as well as exchange programmes of technical staff. The total EU support is 2.4 M Euro, whereof 311,000 Euro is coordinated by UU/TK. The project involves 10 partners with 9 facilities in 7 countries.

TK is coordinating the two-year EU project CANDIDE (Coordination Action on Nuclear Data for Industrial Development in Europe) /Blomgren et al. 2007/. The project aims at enhancing the European collaboration on nuclear data for nuclear waste management. This will be accomplished via networking activities (workshops, training of young professionals in the nuclear power industry) and via an assessment of the status and needs of present and future nuclear data. The project involves 15 partners from 11 countries, spanning from very large business corporations (e.g. Electricité de France and Areva) to research centres and universities. The role of TK is to coordinate the entire project, to lead the development of a school for young professionals in the field, and to contribute experience in high-energy neutron experiments in the assessment. The total EU support to the project is 779,000 Euro.

5.2 Meetings and conferences

The international workshop on Neutron Measurements, Evaluations and Applications (NEMEA) was organized October 16–18 in Prague, Czech Republic, as part of the CANDIDE project. This workshop was dedicated to nuclear data needs for Generation-IV and accelerator-driven systems.

Jan Blomgren is Swedish representative in the OECD/NEA Nuclear Science Committee (NSC) and its Executive Group. Minutes from the annual meeting is found in appendix XXV and XXVI.

6 Administrative matters

6.1 Staff and students

During the project year, Jan Blomgren has been project leader, active on a 20% basis within the project. His other major activities are teaching and duties as director of studies. Associate professor (universitetslektor) Stephan Pomp has worked essentially all his time within the project with research and student supervision. Associate professor Michael Österlund is involved in part-time research within the group. Leif Nilsson, retired professor, has been employed on about 10% time for student supervision. Assistant professor Udomrat Tippawan of Chiang Mai University, Thailand, is a frequent guest scientist within the group.

Two PhD students are directly connected to and financed by the present project, Vasily Simutkin and Riccardo Bevilacqua. Simutkin's thesis work is primarily on fission and Bevilacqua is working with light-ion production reactions. In addition, Pernilla Andersson has been working with upgrading the SCANDAL setup during the present year, and was accepted for PhD studies on elastic scattering early 2008. Her work has up to now been financed by VR, and from now on as part of the EFNUDAT project.

In June 2008, Ali al-Adili was accepted as PhD student on a project on fission studies to be conducted at the EU dedicated nuclear data laboratory, JRC-IRMM in Geel, Belgium. This is a joint undertaking, in which JRC finances three out of four years of PhD studies, and he spends these three years on site in Geel. He is enrolled as PhD student at Uppsala University and takes courses at UU. After the research work has been completed, he will return to UU for finalizing the thesis.

Angelica Öhrn (born Hildebrand), PhD student of the previous NATT project, defended her thesis on neutron scattering February 29, 2008, with dr. Bob Haight, Los Alamos National Laboratory, USA, as faculty opponent. She is presently employed by Westinghouse, Västerås, working on nuclear power safety issues.

6.2 Reference group

The reference group consists of Fred Karlsson (SKB), Benny Sundström (SKI), and Fredrik Winge (BKAB). The progress of the work has continuously been communicated to the reference group members by short, written, quarterly reports.

7 References

Blideanu V, Lecolley F R, Lecolley J F, Lefort T, Marie N, Atac A, Ban G, Bergenwall B, Blomgren J, Dangtip S, Elmgren K, Eudes Ph, Foucher Y, Guertin A, Haddad F, Hildebrand A, Johansson C, Jonsson O, Kerveno M, Kirchner T, Klug J, Le Brun Ch, Lebrun C, Louvel M, Nadel-Turonski P, Nilsson L, Olsson N, Pomp S, Prokofiev A V, Renberg P-U, Rivière G, Slypen I, Stuttgé L, Tippawan U, Österlund M, 2004. Nucleon-induced reactions at intermediate energies: New data at 96 MeV and theoretical status, Phys. Rev. C 70, 014607.

Blomgren J, 2002. Experimental activities at high energies, Proceedings from an international symposium on Accelerator Driven Systems for Energy production and Waste Incineration: Physics, Design and Related Nuclear Data, Trieste, 2002, p. 327. (Invited talk).

Blomgren J, 2004. Nuclear data for accelerator-driven systems – Experiments above 20 MeV, Proceedings from EU enlargement workshop on Neutron Measurements and Evaluations for Applications, Bucharest, Romania, October 20–23, 2004 (invited). EUR Report 22794 EN, Luxembourg: Office for Official Publications of the European Communities, ISBN 978-92-79-06158-5, European Communities, 2007, p. 7.

Blomgren J, Bauge E, Cano Ott D, Czifrus S, Dahlbacka K, Gonçalves I, Gonzalez E, Henriksson H, Jacqmin R, Koning A, Lecarpentier D, Malambu E, Mengoni A, Mills R, Plompen A, Rimpault G, Stary V, Trakas C, Vaz P, Zimmerman C, 2007. CANDIDE – Coordination Action on Nuclear Data for Industrial Development in Europe, Proceedings of 4th Workshop on Neutron Measurements, Evaluations and Applications – Nuclear data needs for Generation IV and accelerator driven systems, Prague, Czech Republic, October 16–18, 2007. NEMEA-4, Neutron Measurements, Evaluations and Applications, EUR Report 23235 EN, Luxembourg: Office for Official Publications of the European Communities, ISBN 978-92-79-08274-0, European Communities, 2008, p. 1.

Blomgren J, Chtioui K, 2007. A proposal for an integral neutron data experiment in the 100–200 MeV region, Proceedings of 4th Workshop on Neutron Measurements, Evaluations and Applications – Nuclear data needs for Generation IV and accelerator driven systems, Prague, Czech Republic, October 16–18, 2007. NEMEA-4, Neutron Measurements, Evaluations and Applications, EUR Report 23235 EN, Luxembourg: Office for Official Publications of the European Communities, ISBN 978-92-79-08274-0, European Communities, 2008, p. 59.

Dangtip S, Atac A, Bergenwall B, Blomgren J, Elmgren K, Johansson C, Klug J, Olsson N, Alm Carlsson G, Söderberg J, Jonsson O, Nilsson L, Renberg P-U, Nadel-Turonski P, Le Brun C, Lecolley F-R, Lecolley J-F, Varignon C, Eudes Ph, Haddad F, Kerveno M, Kirchner T, Lebrun C, 2000. A facility for measurements of nuclear cross sections for fast neutron cancer therapy, Nucl. Instr. Meth. A452, 484.

Klug J, Blomgren J, Atac A, Bergenwall B, Dangtip S, Elmgren K, Johansson C, Olsson N, Rahm J, Jonsson O, Nilsson L, Renberg P-U, Nadel-Turonski P, Ringbom A, Oberstedt A, Tovesson F, Le Brun C, Lecolley J-F, Lecolley F-R, Louvel M, Marie N, Schweitzer C, Varignon C, Eudes Ph, Haddad F, Kerveno M, Kirchner T, Lebrun C, Stuttgé L, Slypen I, Prokofiev A, Smirnov A, Michel R, Neumann S, Herpers U, 2002. SCANDAL – A facility for elastic neutron scattering studies in the 50–130 MeV range, Nucl. Instr. Meth. A489, 282.

Klug J, Blomgren J, Atac A, Bergenwall B, Hildebrand A, Johansson C, Mermod P, Nilsson L, Pomp S, Tippawan U, Elmgren K, Olsson N, Jonsson O, Prokofiev A V, Renberg P-U, Nadel-Turonski P, Dangtip S, Phansuke P, Österlund M, Le Brun C, Lecolley J-F, Lecolley F-R, Louvel M, Marie-Noury N, Schweitzer C, Eudes Ph, Haddad F, Lebrun C, Koning A J, Ledoux X, 2003. Elastic neutron scattering at 96 MeV from ^{12}C and ^{208}Pb, Phys. Rev. C. 68 064605.

Koning A, Beijers H, Benlliure J, Bersillon O, Blomgren J, Cugnon J, Duijvestijn M, Eudes Ph, Filges D, Haddad F, Hilaire S, Lebrun C, Lecolley F-R, Leray S, Meulders J-P, Michel R, Neef R-D, Nolte R, Olsson N, Ostendorf E, Ramström E, Schmidt K-H, Schuhmacher H, Slypen I, Synal H-A, Weinreich R, 2002. In Proceedings of Int. Conf. on Nuclear Data for Science and Technology, Tsukuba, Japan (2001); J. Nucl. Sci. Tech, Suppl. 2, 1161.

Mermod P, Blomgren J, Bergenwall B, Hildebrand A, Johansson C, Klug J, Nilsson L, Olsson N, Österlund M, Pomp S, Tippawan U, Jonsson O, Prokofiev A V, Renberg P-U, Nadel-Turonski P, Maeda Y, Sakai H, Tamii A, 2004. Search for three-body force effects in neutron-deuteron scattering at 95 MeV, Phys. Lett. B 597, 243.

Mermod P, Blomgren J, Johansson C, Öhrn A, Österlund M, Pomp S, Bergenwall B, Klug J, Nilsson L, Olsson N, Tippawan U, Nadel-Turonski P, Jonsson O, Prokofiev A V, Renberg P-U, Maeda Y, Sakai H, Tamii A, Amos K, Crespo R, Moro A, 2006. 95 MeV neutron scattering on hydrogen, deuterium, carbon and oxygen, Phys. Rev. C. 74, 054002.

Nakashima H, Nakao N, Tanaka S, Nakamura T, Shin K, Tanaka S, Takada H, Meigo S, Nakane Y, Sakamoto Y, Baba M, 1996. Transmission through shields of quasi-monoenergetic neutrons generated by 43- and 68-MeV protons – II: Iron shielding experiment and analysis for investigating calculational method and cross-section data, J. Nucl. Sci. Eng. 124, 243.

Sagrado Garcia I, Ban G, Blideanu V, Blomgren J, Eudes P, Fontbonne J M, Foucher Y, Guertin A, Haddad F, Hay L, Hildebrand A, Iltis G, Le Brun C, Lecolley F R, Lecolley J F, Lecouey J L, Lefort T, Marie N, Olsson N, Pomp S, Österlund M, Prokofiev A, Steckmeyer J-C, 2006. A Novel Fast Neutron Detector for Nuclear Data Measurements, International workshop on Fast Neutron Detectors and Applications, Cape Town, South Africa, April 3–6, 2006. Proceedings of Science, PoS(FNDA2006)009. http://pos.sissa.it/.

Tippawan U, Pomp S, Atac A, Bergenwall B, Blomgren J, Dangtip S, Hildebrand A, Johansson C, Klug J, Mermod P, Nilsson L, Österlund M, Olsson N, Elmgren K, Jonsson O, Prokofiev A V, Renberg P-U, Nadel-Turonski P, Corcalciuc V, Watanabe Y, Koning A, 2004. Light-Ion Production in the Interaction of 96 MeV Neutrons with Silicon, Phys. Rev. C 69, 064609.

Tippawan U, Pomp S, Atac A, Bergenwall B, Blomgren J, Dangtip S, Hildebrand A, Johansson C, Klug J, Mermod P, Nilsson L, Österlund M, Olsson N, Elmgren K, Jonsson O, Prokofiev A.V, Renberg P-U, Nadel-Turonski P, Corcalciuc V, Koning A, 2006. Light-Ion Production in the Interaction of 96 MeV Neutrons with Oxygen, Phys. Rev. C 73 (2006) 034611.

Öhrn A, Blomgren J, Andersson P, Atac A , Johansson C, Klug J, Mermod P, Pomp S, Wolniewicz P, Österlund M, Nilsson L, Bergenwall B, Elmgren K, Olsson N, Tippawan U, Dangtip S, Phansuke P, Nadel-Turonski P, Jonsson O, Prokofiev A V, Renberg P-U, Blideanu V, Le Brun C, Lecolley J F, Lecolley F.R, Louvel M, Marie-Noury N, Schweitzer C, Eudes Ph, Haddad F, Lebrun C, Bauge E, Delaroche J P, Girod M, Ledoux X, Amos K, Karataglidis S, Crespo R, Haider W. Elastic neutron scattering of 96 MeV neutrons from iron, yttrium and lead, Phys. Rev. C. 77 (2008) 024605.

PRAMANA
— journal of
physics

Vol. xx, No. x
xxxxx 2006
pp. 1–10

Neutron cross-sections above 20 MeV for design and modeling of ADS

J BLOMGREN
Department of Neutron Research, Uppsala University, Box 525, S-751 20 Uppsala, Sweden
E-mail:

Abstract. One of the outstanding new developments in the field of partitioning and transmutation (P&T) concerns accelerator-driven systems (ADS) which consist of a combination of a high-power, high-energy accelerator, a spallation target for neutron production and a sub-critical reactor core. The development of the commercial critical reactors of today motivated a large effort on nuclear data up to about 20 MeV, and presently several million data points can be found in various data libraries. At higher energies, data are scarce or even non-existent. With the development of nuclear techniques based on neutrons at higher energies, nowadays there is a need also for higher-energy nuclear data. To provide alternative to this lack of data, a wide program on neutron-induced data related to ADS for P&T is running at the 20–180 MeV neutron beam facility at the the 'the Svedberg laboratory' (TSL), Uppsala. The programme encompasses studies of elastic scattering, inelastic neutron production, i.e., (n, xn') reactions, light-ion production, fission and production of heavy residues. Recent results are presented and future program of development is outlined.

Keywords. Neutron; nuclear data; elastic scattering; light ion production; fission; residue production; accelerator driven system; waste transmutation.

PACS Nos

1. Introduction

One of the outstanding new developments in the field of partitioning and transmutation (P&T) concerns accelerator-driven systems (ADS), which consist of a combination of a high-power, high-energy accelerator, a spallation target for neutron production, and a sub-critical reactor core.

The development of the commercial critical reactors of today motivated a large effort on nuclear data up to about 20 MeV, and presently several million data points can be found in various data libraries. At higher energies, data are scarce or even non-existent. With the development of nuclear techniques based on neutrons at higher energies, nowadays there is need also for higher-energy nuclear data.

The nuclear data needed for transmutation in an ADS can roughly be divided into two main areas. First, the initial proton beam produces neutrons by spallation reactions. This means that data on proton-induced neutron production is needed. In addition, data on other reactions are needed to assess the residual radioactivity

of the target. Second, the produced neutrons can induce a wide range of nuclear reactions, and knowledge of these are useful in the design of ADS. Among these reactions, some cross-sections can be used directly. Examples are elastic scattering for neutron transport, proton and alpha production for assessment of the hydrogen and helium gas production in the target window or core, and fission for obvious reasons.

In most cases, however, direct data determination is not the ultimate goal. The global capacity for such measurements is insufficient to obtain complete coverage of important data. It is even impossible in theory to supply all relevant data. In a reactor core, large quantities of short-lived nuclides affect the performance of the core during operation, but measuring cross-sections for these nuclides is impossible because experiment targets cannot be made. This means that the experimental work must be focused on providing benchmark data for theory development [1], making it possible to use theoretical models for unmeasured parameters in a core environment.

An often overlooked aspect is the nuclear data that should be measured in the first place. Nuclear data are not needed for a demonstration of the principle of driving a sub-critical assembly with an external neutron source. The need for nuclear data becomes imminent when a realistic large-scale facility is the goal. With large uncertainties in the nuclear data, large safety margins have to be used, which results in excessive costs. Thus, the role of nuclear data is to reduce the cost for reaching a certain level of safety.

Another important aspect is the trade-off between general and particular information. Below 20 MeV, a single cross-section can be of paramount importance to the entire application. An example is the neutron capture resonance in ^{238}U that provides the Doppler effect so important for the stability of critical reactors. Moreover, some cross-sections are fundamentally inaccessible to theory, particularly in the resonance region. As a result, at low energies more or less complete data coverage for major elements is required. Above 20 MeV, the situation is fundamentally different. The cross-sections are smooth, and the behaviour of the total technical system is always dictated by the sum of a large number of reactions, neither of which strongly dominates the performance. Therefore, getting a grip on the overall picture is more important than precision data on a single reaction. For a review of nuclear data for ADS at high energies, see [2].

2. Activities at TSL, Uppsala

To meet the demand described above, a wide program on measurement of cross-sections of neutron-induced nuclear reactions is running at the Svedberg laboratory (TSL) in Uppsala, Sweden. The results presented here were all obtained at the old neutron beam facility, used between years 1990 and 2003. In the year 2003, a new facility was built and commissioned for joint use in nuclear data measurements and electronic testing (see Pomp *et al* [3]).

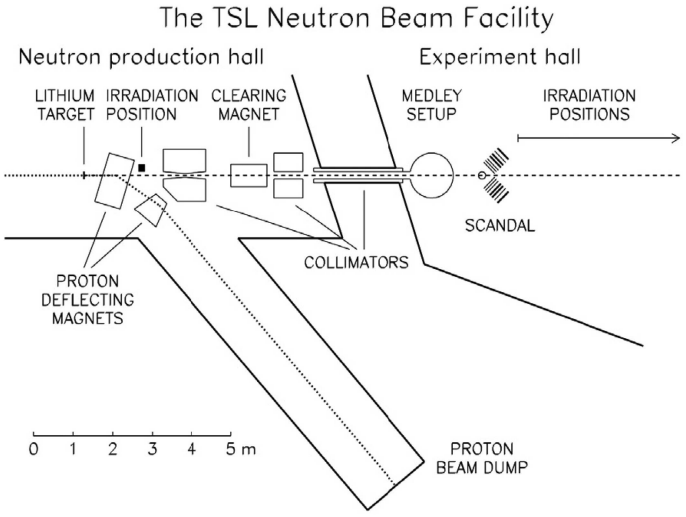

Figure 1. The old TSL neutron beam facility.

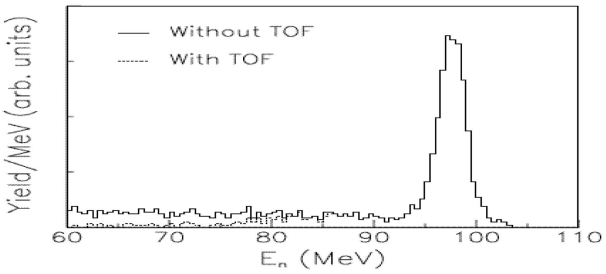

Figure 2. The neutron energy spectrum with and without TOF rejection of low-energy neutrons.

2.1 *Neutron production*

At the old neutron facility (see figure 1), quasi-mono-energetic neutrons are produced by the reaction ^{7}Li(p,n)^{7}Be in a target of 99.98% ^{7}Li. After the target, the proton beam is bent by two dipole magnets into a 8 m concrete tunnel, where it is focused and stopped in a well-shielded carbon beam-dump. A narrow neutron beam is formed in the forward direction by a system of three collimators, with a total thickness of more than 4 m. The energy spectrum of the neutron beam is shown in figure 2. About half of all the neutrons appear in the high-energy peak, while the rest are roughly equally distributed in energy, from the maximum energy and down to zero. The thermal contribution is small. The low-energy tail of the neutron beam can be reduced by time-of-flight measurements (see figure 2).

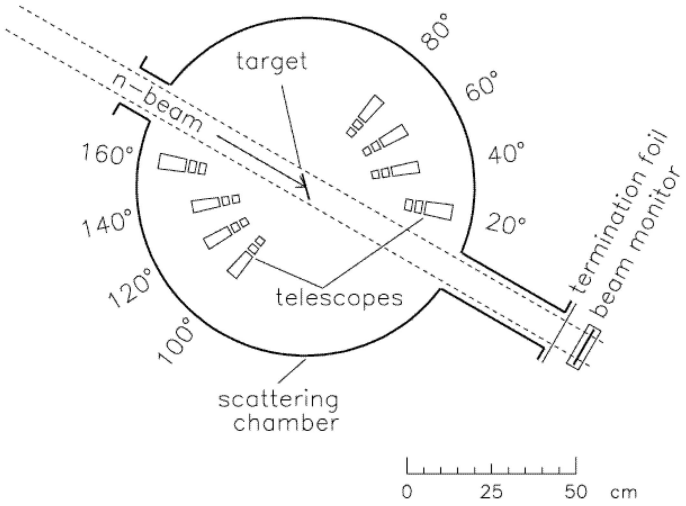

Figure 3. The MEDLEY set-up.

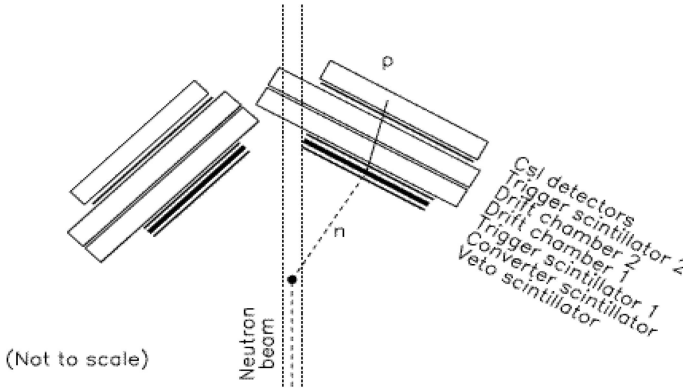

Figure 4. The SCANDAL set-up.

2.2 *Base equipment*

Two major experimental set-ups are semi-permanently installed. The MEDLEY detector telescope array (Dangtip *et al* 2000) is housed in a scattering chamber and operated in vacuum (see figure 3). At the exit of this chamber, a 0.1 mm stainless steel foil terminates the vacuum system, after which the neutrons travel in air. Immediately after MEDLEY follows SCANDAL (scattered nucleon detection assembLy), a set-up designed for large-acceptance neutron and proton detection [4].

The MEDLEY detector array consists of eight particle telescopes, placed at 20–160° with 20° separation. Each telescope is a ΔE-ΔE-E detector combination, with sufficient dynamic range to distinguish all light ions from a few MeV up to maximum

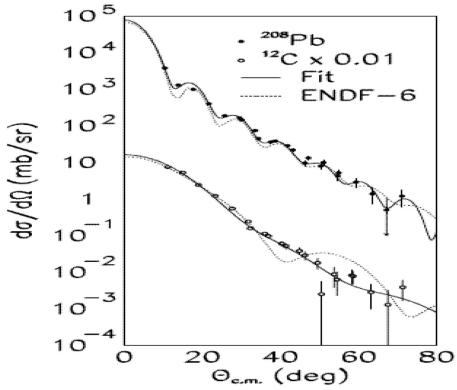

Figure 5. Elastic neutron scattering at 96 MeV from ^{208}Pb and ^{12}C.

energy, i.e., about 100 MeV. The ΔE detection is accomplished by fully depleted silicon surface barrier detectors, and CsI (Tl) crystals are used as E detectors. For some experiments, active collimators are used. These are plastic scintillators with a hole defining the solid angle. The equipment is housed in a 100 cm diameter scattering chamber, so that the charged particles can be transported in vacuum.

Recently, the facility has been used also for fission studies. In that case, the silicon detectors are used for fission fragment detection.

The SCANDAL set-up [4] has been designed for elastic neutron scattering studies. It consists of two identical systems, placed to cover 10–50 and 30–70°, respectively (see figure 4). The energy of the scattered neutron is determined by measuring the energy of proton recoils from a plastic scintillator and the angle is determined by tracking the recoil proton. In a typical neutron scattering experiment, each arm consists of a 2 mm thick veto scintillator for fast charged-particle rejection, a 10 mm thick neutron-to-proton converter scintillator, a 2 mm thick plastic scintillator for triggering, two drift chambers for proton tracking, a 2 mm thick ΔE- plastic scintillator which is also part of the trigger, and an array of CsI detectors for energy determination of recoil protons produced in the converter by n–p scattering. The trigger is provided by the coincidence of the two trigger scintillators, vetoed by the front scintillator. SCANDAL can also be used as proton or deuteron detector. In those cases, the veto and converter scintillators are removed.

3. Research programme

3.1 *Elastic neutron scattering*

Elastic neutron scattering is of utmost importance for a vast number of applications. Besides its fundamental importance as a laboratory for tests of isospin dependence in the nucleon–nucleon and nucleon–nucleus interactions, the optical potentials derived from elastic scattering come into play in virtually every application where a detailed understanding of nuclear processes is important. Elastic neutron scatter-

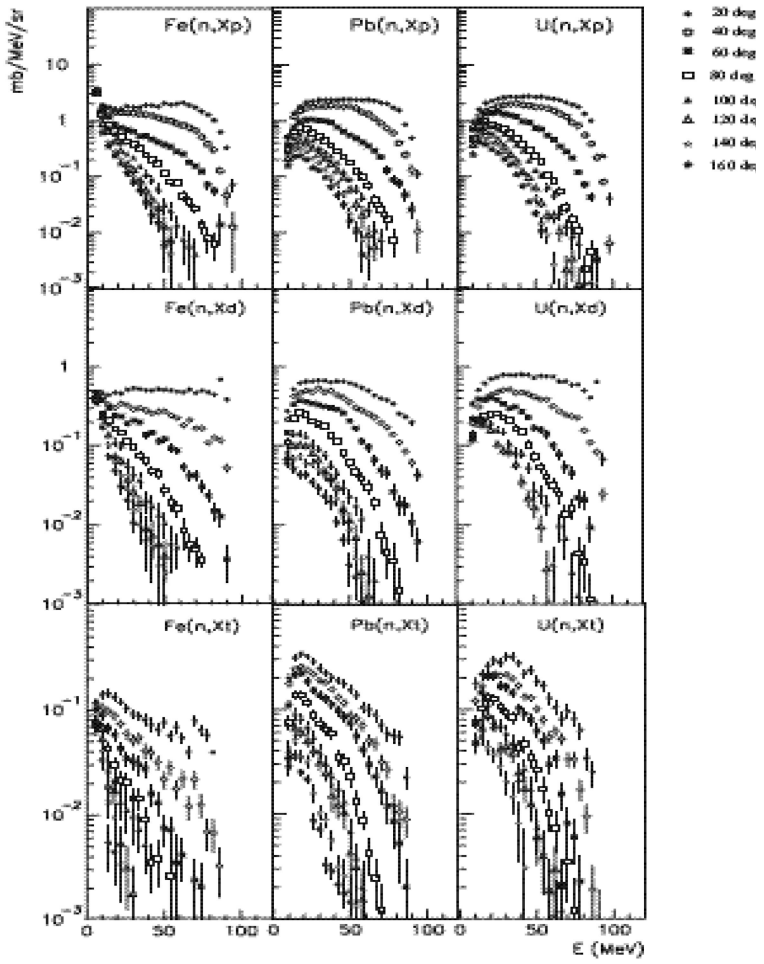

Figure 6. Neutron-induced light-ion production in iron, lead and uranium at 96 MeV.

ing is important also for fast-neutron cancer therapy, because the nuclear recoils account for 10–15% of the dose. Up to now, data on ^{12}C and ^{208}Pb at 96 MeV have been published by Klug *et al* [5] (see figure 5 also), and five other nuclei are under analysis.

A facility for studies of inelastic neutron scattering has recently been commissioned, and first data have been taken by Lecolley [6].

3.2 *Light-ion production*

Although the MEDLEY set-up was initially intended for medical purposes, the requirements from these led to a multipurpose detector design, which has turned out

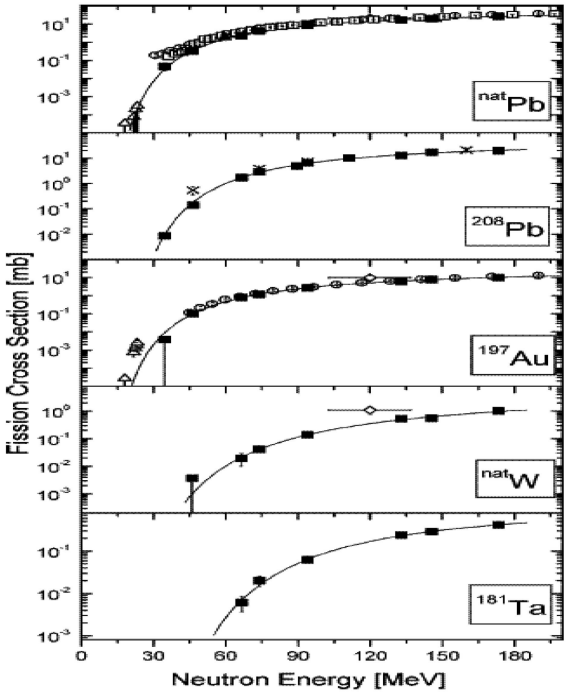

Figure 7. Cross-sections for neutron-induced fission.

to be useful for many different applications. One of these is hydrogen and helium production in ADS, exemplified with measurements on iron, lead and uranium (Blideanu *et al* [1], see figure 6 also).

3.3 *Fast-neutron fission*

Although the main fission effects in an ADS arise from neutrons at lower energies, the high-energy neutron fission gives significant contributions to the power released. Very little data exist on high-energy fission, but the situation is under rapid improvement. This can be exemplified by the ongoing work at the TSL neutron beam, manifested in a number of recent publications by Smirnov *et al* [7] and Ryzhov *et al* [8]. A new facility for studies of angular distributions is also under commissioning [9]. In figures 7 and 8 some of these measured data of fast-neutron fission cross-sections are displayed. For reference of parallel works, see ref. [10]. In figure 9 excitation function measurements carried out with existing facility has been shown with the intention that such future program is in developmental stage after increased beam intensity.

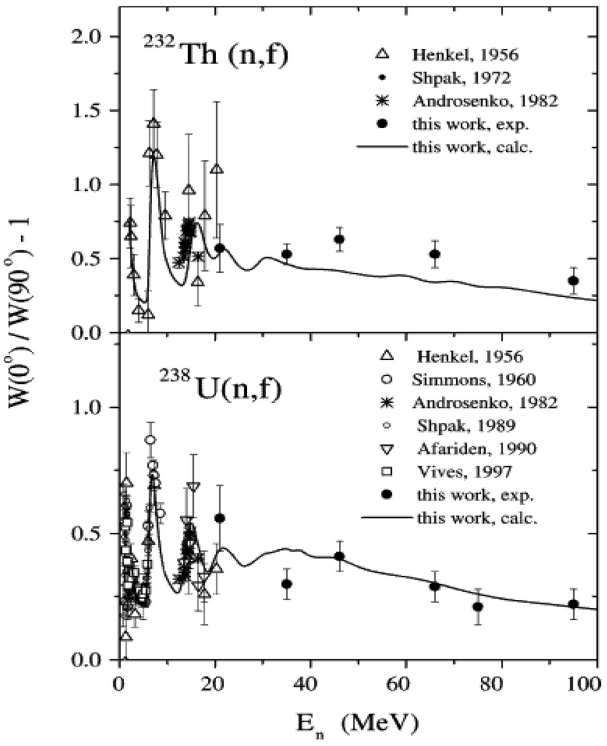

Figure 8. Anisotropies in neutron-induced fission.

3.4 *Residue production*

A series of studies of residue production has been carried out in parallel with the other experiments mentioned here, at an irradiation facility located just outside the primary neutron beam. For the short-lived residual radio-nuclides, cross-sections were determined using activation techniques. The production of long-lived radio-nuclides was studied by accelerator-mass spectroscopy (AMS) after chemical separation [11]. For another such study, see ref. [12] also.

4. Conclusions

The rapid growth in demand for neutrons has motivated the construction of a new 20–180 MeV neutron beam facility at TSL (see figure 10). The most important features of the new facility are, increased intensity by reduction of the distance from neutron production to experiments, availability of much larger beam diameters, increased versatility concerning various beam parameters, like the shape, and reserved space for a future pulse sweeping system.

For nuclear data research, the increased intensity will facilitate a large experimental program at 180 MeV, hitherto excluded by count rate limitations. For testing

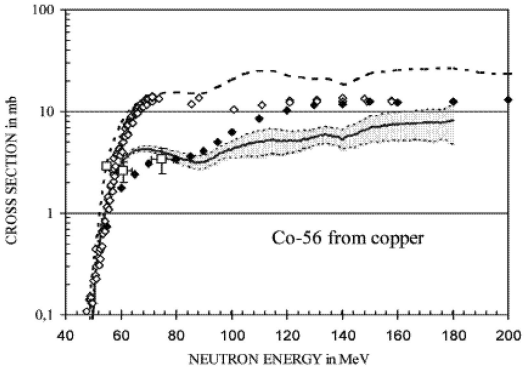

Figure 9. Excitation function for the production of ^{56}Co from natural copper by neutron-induced reactions.

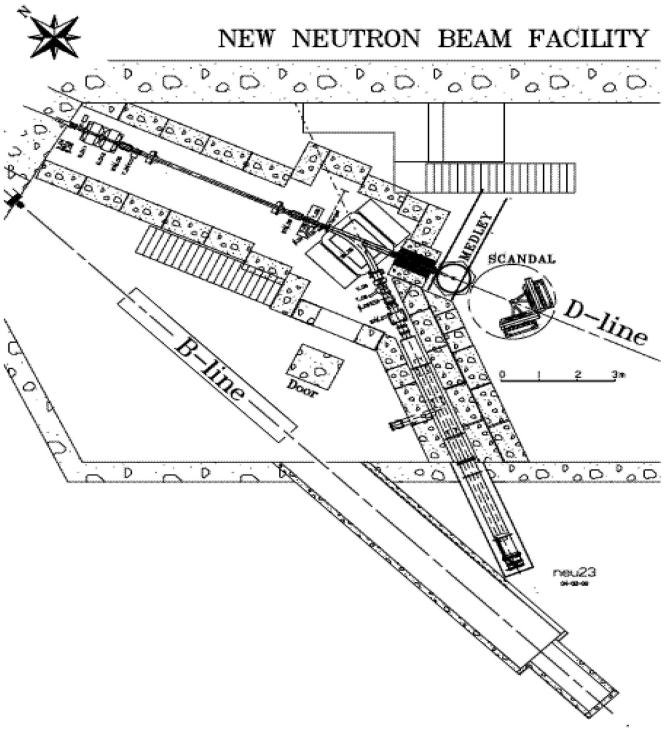

Figure 10. The new TSL neutron beam facility.

of electronics, the increased intensity in combination with a larger beam diameter, which facilitates testing a large number of components simultaneously, will provide a total failure rate of about a factor 300 larger than for the present facility. This means that the new TSL neutron beam facility can outperform any existing facility in the world. The facility being developed at TSL has wide application in the field

of medical sciences and its related data pool [13,14]. More such details are available at our web site www.tsl.uu.se.

Acknowledgments

This work was financially supported by Vattenfall AB, the Swedish Nuclear Fuel and Waste Management Company, the Swedish Nuclear Power Inspectorate, Ringhals AB, Barsebäck Power AB, Forsmarks Kraftgrupp AB, the Swedish Defence Research Agency, the Swedish Natural Science Research Council, the Swedish International Development Authority, the Swedish Nuclear Safety and Training Centre, and the European Union.

References

[1] V Blideanu, *et al*, *Phys. Rev.* **C70(01)**, 4607 (2004)
[2] J Blomgren, 'Experimental activities at high energies', *Workshop on Nuclear Data for Science and Technology: Accelerator Driven Waste Incineration*, Trieste, Italy, Sept. 10–21, 2001, edited by M Herman, N Paver and A Stanculescu, ICTP Lecture Notes **12**, 327 (2002)
[3] S Pomp *et al*, *AIP Conference Proceedings* **769**, 780 (2005)
[4] J Klug *et al*, *Nucl. Instrum. Methods* **A489**, 282 (2002)
[5] J Klug *et al*, *Phys. Rev.* **C68(06)**, 4605 (2003)
[6] F-R Lecolley, private communication (2004)
[7] A N Smirnov *et al*, *Phys. Rev.* **C70(05)**, 4603 (2004)
[8] I V Ryzhov *et al*, *Nucl. Phys.* **A76019**, 19 (2005)
[9] A V Prokofiev *et al*, *AIP Conference Proceedings* **769**, 800 (2005)
[10] H Condé *et al*, *Nucl. Instrum. Methods* **A292**, 121 (1990)
[11] R Michel *et al*, *AIP Conference Proceedings* **769**, 861 (2005)
[12] U Tippawan *et al*, 'Light-ion production in the interaction of 96 MeV neutrons with oxygen', *Phys. Rev. C* (2006) (accepted)
[13] J Blomgren and N Olsson, *Radiat. Prot. Dosim.* **103(4)**, 293 (2003)
[14] S Dangtip *et al*, *Nucl. Instrum. Methods* **A452**, 484 (2000)

Radiation Protection Dosimetry (2007), Vol. 126, No. 1–4, pp. 64–68
Advance Access publication 13 May 2007
doi:10.1093/rpd/ncm014

FAST NEUTRON BEAMS—PROSPECTS FOR THE COMING DECADE

J. Blomgren*
Department of Neutron Research, Uppsala University, Box 525, S-751 20 Uppsala, Sweden

The present status of neutron beam production techniques above 20 MeV is discussed. Presently, two main methods are used; white beams and quasi-monoenergetic beams. The performances of these two techniques are discussed, as well as the use of such facilities for measurements of nuclear data for fundamental and applied research. Recently, two novel ideas on how to produce extremely intense neuton beams in the 100–500 MeV range have been proposed. Decay in flight of beta delayed neutron-emitting nuclei could provide beam intensities five orders of magnitudes larger than present facilities. A typical neutron energy spectrum would be essentially monoenergetic, i.e., the energy spread is about 1 MeV with essentially no low-energy tail. A second option would be to produce beams of ^{6}He and dissociate the ^{6}He nuclei into α particles and neutrons. The basic features of these concepts are outlined, and the potential for improved nuclear data research is discussed.

INTRODUCTION

The interest in high-energy neutron data is rapidly growing since a number of potential large-scale applications involving fast neutrons are under development, or have been identified. This has motivated nuclear data research for neutron therapy of cancer tumours[1], transmutation of spent nuclear fuel[2–4], and upsets in electronics[5,6]. In the present paper, present and future techniques for nuclear data production for these applications are discussed.

PRESENT-DAY FACILITIES FOR NUCLEAR DATA MEASUREMENTS

At low energies (below 20 MeV or so), truly monoenergetic neutron beams can be produced. There are a few light-ion reactions, like D(d,n)^{3}He and T(d,n)^{4}He, which have positive Q-values and sizeable cross sections. Such beams are strictly monoenergetic up to about 2 MeV incident deuteron energy. Above this energy, there is a possibility that the deuteron breaks up into a proton and a neutron. In reality, this is not a major obstacle until about 30 MeV neutron energy is reached, because the T(d,n)^{4}He cross section is so large that the breakup neutrons form only a small low-energy tail. At even higher energies though, the T(d,n)^{4}He cross section is smaller, making the total yield too low for most measurements.

The largest neutron separation energy is about 20 MeV, making truly monoenergetic beams impossible to produce above that energy. The beams available at higher energies are quasi-monoenergetic beams, i.e., beams where a single energy dominates, but always accompanied by a low-energy tail.

*Corresponding author: Jan.Blomgren@tsl.uu.se

At energies of 50 MeV and above, three production reactions give reasonably monoenergetic beams. These are D(p,n), ^{6}Li(p,n) and ^{7}Li(p,n). The first has a large cross section, but the drawback that the energy resolution of the full-energy neutrons cannot be better than 3 MeV due to the Fermi motion of the neutron inside the deuteron. If a sharper energy definition is required, one of the two reactions using lithium is selected. They are almost equally good, but there is a major practical difference: ^{6}Li is used in hydrogen bombs and is therefore not easily obtained, whereas ^{7}Li is provided at low cost. As one could expect, ^{7}Li(p,n) is the most common production reaction for monoenergetic neutron beams. At 100 MeV, about 50% of the neutrons fall within 1 MeV at maximum energy, while the remaining half are distributed about equally from maximum energy down to zero. This is the closest to monoenergetic conditions nature provides. Effects due to the low-energy tail can, in some cases, be remedied on-line by the time-of-flight (TOF) rejection techniques. If that is unavailable, unfolding procedures are often used, in which cross sections at a few nominal energies have to be undertaken.

There is also a completely different approach; instead of trying to get the neutrons as well gathered in energy as possible, all energies are produced simultaneously. A high-energy proton beam hits a thick (in most cases stopping) target and lots of neutrons of all energies are produced, with typically a $1/E_n$ spectrum. If the incident proton beam is bunched and the experiment target is placed at a rather large distance from the neutron production target, TOF methods can be used to determine the energy of the incident neutron on an event-by-event basis.

The advantage of such so-called white beams is the total intensity produced, which is larger than for

monoenergetic beams, but instead the intensity per energy interval is much lower at high energies. This can partly be compensated for by summing data over limited energy intervals, but still the intensity per such interval is lower. The advantage of being able to measure at many energies simultaneously is not worth much if you get insufficient statistics everywhere. As a consequence, white beams are restricted to experiments at low energies, where the intensities are large, or to high-energy reactions with rather large cross sections. Another feature is that white sources require event-by-event measurements. Experiments of effects with an energy dependence, where the individual events cannot be distinguished, cannot be performed at white beams. For experiments fulfilling the above requirements, white sources can, however, provide large quantities of very valuable information. This is especially true when excitation functions, i.e., the energy dependence of a cross section, are of particular interest.

NUCLEAR DATA STATUS

Nuclear data status is a fairly limited class of reactions that are of interest for the further development of the applications under consideration. The most important are elastic scattering, inelastic neutron emission, light ion production, heavy ion production and fission. The most recent work in the field has been carried out at the The Svedberg Laboratory (TSL), Uppsala, Sweden. Below, an account of the recent research at TSL is given, and this is also a good indication on the present level of the field.

Elastic scattering has been studied at TSL on a range of nuclei up to 96 MeV. At present, ten nuclei have been studied and results are either published or underway[7]. An overall uncertainty of about 5% has been achieved. A novel normalisation method has been established that allows elastic scattering data to be absolutely normalised to about 3% uncertainty [8]. This method, however, works only for elastic scattering. Feasibility studies have shown that the technique as such works up to about 200 MeV, so these studies can be extended up in energy.

An experimental programme on inelastic neutron emission, i.e., (n,xn′) reactions is in progress[9]. Data have been taken on lead and iron, and the method as such seems to work. It is too early to quote a final uncertainty in the results, but 10% seems feasible.

Data on light-ion production has been acquired on about ten nuclei at 96 MeV, and analysis is in progress (10, 11). At present, about half the data set has been published. Normalisation has been obtained by simultaneous detection of *np* scattering at an angle where the cross section uncertainty can be estimated to about 5%, which is the dominating uncertatinty in the final light-ion production cross sections. These studies are presently being extended to 180 MeV.

Fission cross sections have been studied at many facilities up to about 200 MeV energy. The energy dependencies of the cross sections agree fairly well in shape, but the absolute scale differs by up to 15%. It is at present not clear what causes this. One possibility is the normalisations used. Another possible cause is that the sensitivity to low-energy neutrons is not under control for some of the experiments. Dedicated experiments to remedy this situation are underway.

In principle, fission cross sections can be measured up to several GeV using white beams with a very high initial proton energy, like at the CERN-nTOF facility[12]. The neutron beam intensity is very low, but the cross sections are large and it is possible to detect a major fraction of the fission fragments, resulting in reasonable statistical precision. A major problem, however, is normalisation, since the beam intensity is very difficult to monitor at these very high energies.

There are only a few examples of other fission data than cross sections. This means that important fission parameters, like angular distributions, yields etc., essentially remain to be investigated at high neutron energies.

POSSIBLE FUTURE FACILITIES

As was discussed in the previous section, the prospects for development in the near future, i.e., within ten years, can be summarised to extension to about 200 MeV of ongoing work on elastic scattering, inelastic neutron emission and light ion production at around 100 MeV, and fission studies of other parameters than the cross section.

If looking a bit further into the future, we can allow ourselves to be more visionary. To my opinion, the single most important problem to solve if we want a significant development of the field is normalisation. At present, we inevitably end up with an uncertainty of about 5%, because we have to normalise to a reference, typically *np* scattering, which is known to be—at best—5%, and it is difficult to see how this can be radically improved upon in a short term with the present techniques.

I consider energy resolution to be the second largest problem, with intensity being at the third place. These two are, however, to a large degree coupled. If one aims for a good neutron-beam energy resolution, one has to pay with poor intensity and vice versa. It is presently close to inconceivable to produce neutrons at high energies with a resolution better than 1 MeV with a reasonable intensity. The limited intensity puts severe constraints on the detection, in such a way that the detection often has to be performed with techniques that sacrifice resolution for efficiency, resulting in a final resolution of

a few MeV. This means that only in a few rare cases the final states can be resolved.

Recently, a way out of this dilemma has been proposed as a by-product of the CERN beta-beam facility[13], under consideration (Figure 1). The background is that neutrino physics has progressed rapidly in the last few years, with the discovery of neutrino oscillations as the most visible example. Up to now, essentially all accelerator-produced neutrinos have been muon neutrinos, being the final product of pion decay. Electron neutrinos are much more difficult to produce in large amounts, because they require a nuclear beta decay for their creation.

At the proposed CERN beta-beam facility, production of suitable beta-emitting nuclei should be undertaken in an ISOLDE-like facility, and the produced nuclei should be post-accelerated to very high energy and stored in a decay ring of race-track shape. At these very high energies, hundreds of GeV/A, there is a very strong Lorentz boost, which means that the neutrino is emitted very close to the beam direction in the laboratory system; in spite of that the emission is isotropic in its moving reference frame. Thereby, intense neutrino beams can be produced. The idea is to build the decay ring so that one straight section points towards a distant neutrino detector to allow studies of electron neutrino oscillations.

Intense neutron beams could be a spin-off from that facility. It has been proposed to use two production targets, one for nuclei suited for neutrino emission in the decay ring and one for beta-delayed neutron emitters[14]. Some neutron-rich nuclei beta decay to a nucleus that promptly emits a neutron, which typically has an energy of a few hundred keV in its rest frame. By accelerating the beta-delayed neutron emitters up to a few hundred MeV per nucleon, the Lorentz boost is sufficient to focus the beam to reasonable dimensions. For instance, at 100 MeV per nucleon, with a maximum transverse neutron energy of about 1 MeV (the maximum energy of a beta-delayed neutron), the maximum opening angle is about six degrees. The average divergence, however, is much smaller because the average neutron energy is smaller and since the decay is isotropic in the centre-of-momentum system, many decays take place close to the beam direction. Typically, a two degree divergence can be reached. All this can be done in parallel with the primary objective, since the accelerators for the neutrino emitters have a long cycle with a low duty factor.

The resulting neutron beam has an energy in the 100–500 MeV range with an energy resolution of about 1 MeV, and intensities of about 10^{11} n/s are estimated[14]. One example of a precursor nucleus is ^{137}I, for which the estimated production is $1 \cdot 10^{13}\ s^{-1}$, based on an expected fission rate of $1 \cdot 10^{15}\ s^{-1}$ with high-energy protons impinging on a UC_2 target. If the filling of a storage ring balances the decays, it means that the fraction of decays leading to delayed neutron emission determines the neutron intensity. In the present case, it is 7%, leading to $7 \cdot 10^{11}\ s^{-1}$ neutron intensity. Finally, only decays along the straight section of a racetrack storage ring would result in a beam. Assuming 15% of the circumference to act as a useful neutron source, the resulting neutron intensity would be $1 \cdot 10^{11}\ s^{-1}$. This should be compared with 10^6 for present-day technology, i.e., an improvement by a factor 100 000 (!). With such intensities, only imagination sets the limit for what can be achieved.

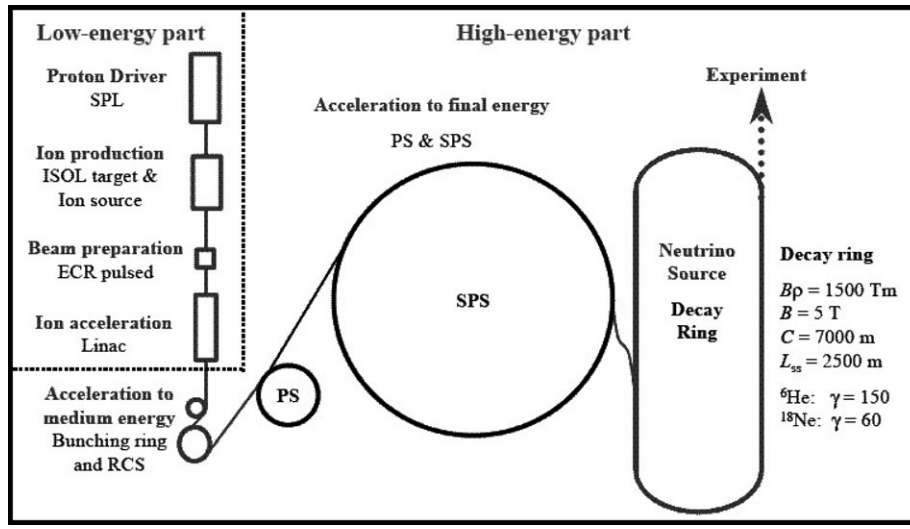

Figure 1. Overview of the proposed CERN beta-beam facility.

If we now restrict the discussion to nuclear data for applications and turn to my problem listed above, it seems feasible that we can address all of them through one experimental trick—tagging. If we use the neutron beam directly for experiments we have essentially only solved the intensity problem, but the other two remain; we end up in a 1 MeV resolution due to the inherent energy spread, and we are still plagued by the normalisation problem. Tagging means that we produce a secondary neutron beam of less intensity, but with much better known intensity. One candidate reaction is to let neutrons scatter from a hydrogen target, and the recoil proton is detected. Since this is a two-body final state, detection of the associated proton indicates that a neutron must have been scattered to the corresponding direction. Thereby, the normalisation problem can be circumvented, since we count the neutrons one by one through the associated particle. If high-resolution tagging is performed, we can also know the neutron energy event by event far better than the initial neutron beam energy resolution. If the tagging is performed with a magnetic spectrometer, the tagger can be made rather insensitive to the ambient background and a proton energy resolution of better than 100 keV can be obtained, resulting in a comparable neutron energy resolution.

With reasonable estimates on tagger parameters, 10^4 tagged neutrons with an energy resolution of 100 keV should be possible to reach, given the above beam intensity. This might sound like a poor intensity, but with such a resolution, final states can be well resolved, which means that a small number of events will result in a good precision. Moreover, since the intensity can be determined to about 1% in a typical tagger system, the accuracy is far better than what can be obtained today. In cases when the demands on energy resolution are not as stringent, a thicker tagger target can be used, resulting in increased intensity. This goes faster than linear, because with a worse resolution, the intensity at the tagger is increased, thicker secondary experimental targets can be used and the detection limitations are less severe. Therefore even with resolutions that are on the limit to be of possible untagged today, we might have tagged beams of intensities exceeding what is presently available as untagged in a not-too-distant future.

A second technique would be to use a similar production as above (1–2 GeV protons on a combined target-ion source) to produce ^{6}He, which in turn would be accelerated to hit a target[15]. Roughly, ^{6}He can be described as an α particle with two loosely attached neutrons. When hitting a target, the two neutrons are dissociated with a large probability, and continue along the direction of the incident beam with the incident velocity. The charged particles (the remaining ^{6}He and residual ^{4}He) are bent by a magnet system and a clean neutron beam is produced, with a divergence similar to that of a beta-delayed neutron beam. This latter technique does not have the potential to produce as intense fluxes as the beta-decay in flight, but on the other hand it requires much less advanced accelerators. This technique could possibly be installed at the existing CERN facilities after some upgrades. Initial estimates indicate a factor a hundred to a thousand larger neutron fluxes than for present facilities to be within reach.

ACKNOWLEDGEMENTS

The information from Mats Lindroos is gratefully acknowledged. This work was financially supported by the Swedish Nuclear Fuel and Waste Management Company, the Swedish Nuclear Power Inspectorate, Ringhals AB, Forsmarks Kraftgrupp AB, the Swedish Defense Research Agency, the Swedish Nuclear Safety and Training Centre, and the European Union.

REFERENCES

1. Koning, A., Beijers, H., Benlliure, J., Bersillon, O., Blomgren, J., Cugnon, J., Duijvestijn, M., Eudes, Ph., Filges, D., Haddad, F., Hilaire, S., Lebrun, C., Lecolley, F.-R., Leray, S., Meulders, J.-P., Michel, R., Neef, R.-D., Nolte, R., Olsson, N., Ostendorf, E., Ramström, E., Schmidt, K.-H., Schumacher, H., Slypen, I., Synal, H.-A. and Weinreich, R. HINDAS – *A European nuclear data program for accelerator-driven systems, International Conference on Nuclear Data for Science and Technology*, Tsukuba, Japan, 7–12 October 2001. J. Nucl. Sci. Tech. (Suppl. **2**) 1161 (2002).
2. Blomgren, J. In: Proceedings of Workshop on Nuclear Data for Science & Technology: Accelerator Driven Waste Incineration, Trieste, Italy, 10–21 September 2001, Herman, M., Paver, N. and Stanculescu, A. (eds.) ICTP lecture notes **12**, 327 (2002).
3. Blomgren, J. *Nuclear data for accelerator driven systems — Experiments above 20 MeV.* In: Proceedings of EU enlargement workshop on Neutron Measurements and Evaluations for Applications, Bucharest, Romania, October 20–23, 2004.
4. Blomgren, J. and Olsson, N. *Beyond KERMA – Neutron data for biomedical applications.* Radiat. Prot. Dosim. **103**(4), 293–304 (2003).
5. Blomgren, J., Granbom, B., Granlund, T. and Olsson, N. *Relations between basic nuclear data and single-event upsets phenomena*. Mat. Res. Soc. Bull. **28**, 121 (2003).
6. Blomgren, J. *Nuclear Data for Single-Event Effects.* In: Proceedings of EU enlargement workshop on Neutron Measurements and Evaluations for Applications, Budapest, Hungary, 5–8 November, 2003. EUR Report 21100 EN, Luxembourg: Office for Official Publications of the European Communities, ISBN 92-894-6041-5, European Communities, 2004.
7. Hildebrand, A., Blomgren, J., Bergenwall, B., Johansson, C., Klug, J., Mermod, P., Nilsson, L., Pomp, S., Tippawan, U., Olsson, N., Jonsson, O., Prokofiev, A. V., Nadel-Turonski, P., Österlund, M.,

Blideanu, V., Lecolley, J. F., Lecolley, F. R., Marie-Noury, N. and Haddad, F. Elastic neutron scattering at 96 MeV, Proceedings of International Conference on Nuclear Data for Science and Technology, Santa Fé, New Mexico, USA, September 26–October 1, 2004. AIPConference Proceedings **769**, 853 (2005).

8. Klug, J., Blomgren, J., Atąc, A., Bergenwall, B., Hildebrand, A., Johansson, C., Mermod, P., Nilsson, L., Pomp, S., Tippawan, U., Elmgren, K., Olsson, N., Jonsson, O., Prokofiev, A. V., Renberg, P.-U., Nadel-Turonski, P., Dangtip, S., Phansuke, P., Österlund, M., Le Brun, C., Lecolley, J. F., Lecolley, F. R., Louvel, M., Marie-Noury, N., Schweitzer, C., Eudes, Ph., Haddad, F., Lebrun, C., Koning, A.J. and Ledoux, X. *Elastic neutron scattering at 96 MeV from 12C and 208Pb*. Phys. Rev. C **68**, 064605 (2003).
9. Lecolley, F.-R. Private communication.
10. Blideanu, V., Lecolley, F. R., Lecolley, J. F., Lefort, T., Marie, N., Atąc, A., Ban, G., Bergenwall, B., Blomgren, J., Dangtip, S., Elmgren, K., Eudes, Ph., Foucher, Y., Guertin, A., Haddad, F., Hildebrand, A., Johansson, C., Jonsson, O., Kerveno, M., Kirchner, T., Klug, J., Le Brun, Ch., Lebrun, C., Louvel, M., Nadel-Turonski, P., Nilsson, L., Olsson, N., Pomp, S., Prokofiev, A. V., Renberg, P.-U., Riviére, G., Slypen, I., Stuttgé, L., Tippawan, U. and Österlund, M. *Nucleon-induced reactions at intermediate energies: New data at 96 MeV and theoretical status*. Phys. Rev. C. **70**, 014607 (2004).
11. Tippawan, U., Pomp, S., Atąc, A., Bergenwall, B., Blomgren, J., Dangtip, S.,, Hildebrand, A., Johansson, C., Klug, J., Mermod, P., Nilsson, L., Österlund, M., Olsson, N., Elmgren, K., Jonsson, O., Prokofiev, A. V., Renberg, P.-U., Nadel-Turonski, P., Corcalciuc, V., Watanabe, Y. and Koning, A. *Light-Ion Production in the Interaction of 96 MeV Neutrons with Silicon*. Phys. Rev. C **69**, 064609 (2004).
12. Tassan-Got, L. Private communication.
13. The CERN beta-beam working group, http://cern.ch/beta-beam.
14. Lindroos, M. Private communication.
15. Tanihata, I. and Nilsson, T. Private communication.

Radiation Protection Dosimetry (2007), Vol. 126, No. 1–4, pp. 1–2
Advance Access publication 25 May 2007
doi:10.1093/rpd/ncm139

Editorial

Progress in Dosimetry of Neutrons and Light Nuclei

TENTH INTERNATIONAL SYMPOSIUM ON NEUTRON DOSIMETRY

The Tenth International Symposium on Neutron Dosimetry (NEUDOS 10) took place in Uppsala, Sweden, 12–16, June 2006. The conference had the theme 'Progress in dosimetry of neutrons and light nuclei', reflecting the widening of the scope of the conference to include not only neutron dosimetry, but also all hadronic particles. This is also a recognition of the fact that the dose due to neutrons is delivered not by the neutron itself, but via secondary particles created in neutron-induced nuclear reactions, i.e. protons, deuterons, alpha particles and various other ions released in tissue. Thereby, the dosimetry of neutrons has a large scientific overlap with dosimetry in proton and heavy ion therapy.

This series of conferences started in 1972 and a historical view of these symposia provides testimony of the development of the field. In the first three meetings (1972–77), the programme was to ~90% composed of topics on dosimetry for radiotherapy ('beam dosimetry') and only ~10% on radiation protection dosimetry. The conferences were primarily motivated by the research needs for therapy with fast neutrons, and participants primarily came from EU and the USA. At these meetings, nuclear and atomic data, microdosimetry and facilities for fast neutron therapy were prevalent issues that later have decreased in importance.

In the 1980s, the programme had shifted to about equal fractions of beam dosimetry and radiation protection dosimetry. Radiation protection issues had at that time gained importance, influenced by new ICRU quantities. Increased attention was thus given to calibration aspects and calibration facilities, as well as microdosimetric principles for radiation protection. Also, the first papers using transport calculations appeared.

In the 1990s, the balance had moved even further, to 20% beam dosimetry and 80% radiation protection dosimetry, reflecting a decline of fast neutron therapy. New topics were BNCT and proton therapy, electronic dosemeters for neutrons and cosmic radiation and aircraft crew dosimetry.

There was an eight-year period without a conference of this series, but in 2003, the series was revived with NEUDOS9. Still the agenda comprised similar weights of beam dosimetry and radiation protection dosimetry, and this was the case also at NEUDOS10. At both symposia, many contributions have concerned aircraft crew dosimetry. Criticality and retrospective dosimetry have grown in importance. The attendance has increased and the age profile has changed dramatically; there were relatively many young participants, and participants new to the field. Europe provided the largest number of attendants with Japanese attendance now being larger than that of the USA. In total, 177 participants, whereof 20% women, from 26 countries participated in Uppsala. The number of participants was the same as at NEUDOS9.

The conference dealt with five sessions, A. Basic Aspects, B. Instrumentation and Techniques, C. Radiation Quality, D. Radiation Protection, and E. Radiotherapy. These sessions were rather unequal in size with B and D being slightly larger than A, and C and E being together about as large as A.

The number of oral presentations was rather limited, since no parallel sessions were organised. Therefore, a vast majority of the papers were presented in poster sessions. These poster sessions were opened with an overview report. The authors of poster contributions provided summaries of their papers in a one-page slide before the conference, and selected reporters gave an introduction to all papers of the entire poster session before the audience left the plenary hall and went out to the posters.

Eight invited talks were presented. Lars-Erik Holm, director of the Swedish Radiation Protection Authority, but invited in the role as chairman of the International Commission on Radiation Protection (ICRP), presented the new ICRP recommendations that had been issued in preliminary form shortly before the conference.

Arjan Koning, expert scientist at the Nuclear Research and consultancy Group (NRG), the Netherlands, reported on recent development in

nuclear theory of biomedical relevance. He and his group have developed user-friendly codes and nuclear data libraries that allow high-quality nuclear data handling without requiring wide expertise of the users.

Grady Hughes of the MCNP team at Los Alamos National Laboratory, USA, gave a talk, by himself depicted as anecdotal, on uncertainties in Monte Carlo calculations beyond statistics. This talk was motivated by the fact that numerical methods have now become a standard tool in the field, and it is important that reliability issues become identified. One particular example presented was that the exact composition of concrete can be of large importance in shielding of neutrons. Unfortunately, the composition is often poorly documented, and sometimes even impossible to know with sufficient precision, because the final porosity and water content can be beyond control in the casting process.

Werner Rühm of GSF, Germany, presented a recent re-evaluation of the biological information that can be extracted by judging the effects of the Hiroshima and Nagasaki nuclear bombs. Their conclusion is that it might be possible that the relative biological effectiveness of neutrons have been underestimated. Since the combined effect of neutrons and gamma rays is better known than the contribution from each type of radiation, this might simultaneously imply that gamma rays might be somewhat less severe than previously thought. If these results gain acceptance, they might influence recommendations for radiation protection. It should be pointed out, however, that the uncertainties in this type of research are large.

Takashi Nakamura of Tohoku University and National Institute of Radiological Sciences, Japan, presented recent progress in development of phoswich detectors for fast neutron detection. John Gueulette of Louvain-la-Neuve, Belgium, gave an overview of the present knowledge of biologic effects of high-LET radiation. Rick Tanner of the Health and Radiation Protection Authority, UK, presented lessons learned from EVIDOS, an EC sponsored project, which investigated the dosimetry of mixed neutron–photon fields in workplaces of nuclear industry.

Bengt Glimelius of the Academic Hospital, Uppsala, informed about the plans for a national facility for particle therapy to be built in Uppsala with first treatments planned for 2011. The decision to build the new centre was taken only a few days before the conference, so this invited talk was no doubt of the largest news value.

Selecting highlights from a conference is always a sensitive matter, because it can be interpreted as a grading of research quality. Instead of giving our subjective view, we here report the highlights from a media perspective. The re-evaluation of Hiroshima and Nagasaki attracted the most widespread attention from media, and was reported in newspapers and national scientific radio. The contributed presentations by Francis Cucinotta, Hooshang Nikjoo *et al.* on expected radiation doses to astronauts on future Mars missions were also reported in national radio. Newspaper articles on the neutron beam facility at The Svedberg Laboratory in Uppsala and the research carried out there were also prevalent, being of local importance.

The present proceedings have been prepared by a team of two joint guest editors, Jan Blomgren and Lennart Lindborg, assisted by five co-editors, one for each session: Helmut Schuhmacher for session A (Basic Aspects), Natalia Golnik for session B (Instrumentation and Techniques), Bo Stenerlöw for session C (Radiation Quality), Frantisek Spúrny for session D (Radiation Protection) and Dan Jones for session E (Radiotherapy).

The executive committee consisted of Jan Blomgren (chair), Lennart Lindborg, Hans Menzel, David Bartlett and Joe McDonald. We would like to thank all persons involved in the organisation, as well as all participants for having created a nice atmosphere during the conference. The NEUDOS10 conference was financially supported by the Swedish Research Council, the Swedish Foundation for Strategic Research, the Technical University Delft (organisers of NEUDOS9), the Swedish Cancer Society, the Swedish Radiation Protection Authority, the Swedish Nuclear Power Inspectorate, the Swedish Nuclear Technology Centre, the Forsmark Nuclear Power company, the Ringhals Nuclear Power company, Synodys Instruments, IBA, Gammadata and the council of Uppsala city.

The NEUDOS symposia are organised under the auspices of the European Radiation Dosimetry Group, EURADOS, which stimulates collaboration among European laboratories in the field of dosimetry of ionising radiation. Conferences with similar scope are not regularly organised outside Europe, and therefore the NEUDOS conferences have become of global importance, although with a European dominance. Recognising this feature, NEUDOS11, will be the first symposium in the series to be organised outside Europe. You are welcome to Cape Town, South Africa, in October 2009!

Jan Blomgren
Lennart Lindborg
Natalia Golnik
Dan Jones
Helmut Schuhmacher
František Spurný
Bo Stenerlöw

Radiation Protection Dosimetry (2007), Vol. 126, No. 1–4, pp. 109–112 doi:10.1093/rpd/ncm023
Advance Access publication 26 June 2007

PRECISION MEASUREMENTS OF THE *np* SCATTERING DIFFERENTIAL CROSS SECTION IN THE INTERMEDIATE ENERGY REGION

P. Mermod[1], J. Blomgren[1,*], L. Nilsson[1], S. Pomp[1], A. Öhrn[1], M. Österlund[1], A. Prokofiev[2] and U. Tippawan[3]
[1]Department of Neutron Research, Uppsala University, Box 525, S-75120 Uppsala, Sweden
[2]The Svedberg Laboratory, Uppsala University, Uppsala, Sweden
[3]Fast Neutron Research Facility, Chiang Mai University, Chiang Mai, Thailand

In fast neutron cancer therapy, ~50% of the cell damage is caused by recoil protons from neutron–proton (*np*) scattering. In the intermediate energy region, there is a need for unambiguous *np* scattering data with good precision in both the shape of the angular distribution and the absolute normalisation. The normalisation techniques have been reviewed for *np* scattering measurements as well as recent experimental results, particularly the data obtained at The Svedberg Laboratory at 96 and 162 MeV. In addition, to what extent systematic uncertainties in the *np* differential cross section might affect the determination of proton recoil kerma coefficients is investigated.

INTRODUCTION

Besides its crucial importance as a primary standard in neutron scattering measurements, the neutron–proton (*np*) differential cross section plays a major role in both fundamental nuclear physics and medical fast neutron applications. Precision measurements in two-nucleon systems allow to test the nucleon–nucleon potential models such as the CD-Bonn potential[(1)] and the AV18 potential[(2)], to cite two of the most recent ones. In particular, the *np* differential cross section at backward angles at intermediate energies can be used to extract the strength of the coupling of the pion to the nucleon in meson-exchange models, the π *NN* coupling constant.

In the present work, the authors are interested in fast neutron applications such as dosimetry and cancer treatment. Among the nuclei of interest for this application, the main components of human tissue and bones are identified, which are hydrogen, carbon, oxygen, nitrogen and calcium. The damage inflicted to the cells depends on cross sections for the neutron-induced reactions on these nuclei, as well as the energies and masses of the released ionising particles. A rough evaluation tells us that ~50% of the cell damage is due to recoil protons in *np* scattering, ~10% is due to elastic and inelastic scattering on other nuclei and the rest is due to neutron-induced emission of light ions[(3,4)]. The contribution from neutron scattering on carbon and oxygen is investigated in a separate paper[(5)], and lightion production at 96 MeV is discussed in articles by Tippawan *et al.* and Pomp *et al.* of this workshop[(6,7)]. In the present paper, the authors investigate how the evaluation of the 50% contribution from *np* scattering is affected by uncertainties in the *np* differential cross section.

*Corresponding author: jan.blomgren@tsl.uu.se

METHODS FOR *np* DIFFERENTIAL CROSS SECTION MEASUREMENTS

For the reasons mentioned earlier, one would like the *np* differential cross section at intermediate energies (typically between 65 and 250 MeV) to be known as precisely as possible, in both shape and absolute scale.

The *np* differential cross section at backward neutron angles can be obtained in a rather straightforward manner by detecting the recoil protons, usually from a CH2 target foil (and a graphite foil for carbon background subtraction), either with detector telescopes placed at different angles or with a magnetic spectrometer [see, e.g. the Rahm *et al.* experiments in Refs. (8,9)]. In the forward angular range, this method becomes impractical because the energy of the protons becomes too low, and the scattered neutrons must be detected instead. This can be done by converting the scattered neutrons into protons by a subsequent *np* reaction in a plastic scintillator and tracking the secondary protons through a detector setup [see, e.g. the Johansson *et al.* experiment in Ref. (10)].

A notorious problem is the absolute normalisation of the cross section, since the neutron beam fluence, when measured by means of fission-based monitors, is not known to a precision better than 10% in the intermediate energy region. There are two possible unambiguous methods to determine the *np* scattering cross section absolutely. One method is tagging,

i.e. the number of neutrons produced in the neutron production target are counted by detecting associated charged particles, for instance, proton recoils in the reaction $p + d \rightarrow n + 2p$. In that way, one sacrifices beam intensity for its exact knowledge. Recently, this method has been successfully applied at IUCF [see the Sarsour *et al.* experiment at 194 MeV in Ref. (11)]. The second method is to normalize the *np* differential cross section to the total *np* cross section, which in turn can be measured without knowledge of the beam intensity (a measurement of the relative beam attenuation in the target is sufficient) to a precision of ~1%. The drawback of this method is that it requires a large angular distribution coverage. In the Rahm *et al.*[8,9] experiments at 96 and 162 MeV, the lacking forward angular range was filled using nuclear models; it resulted in an absolute normalisation uncertainty of ~2%. Later on, data at 96 MeV were obtained in this angular range by Johansson *et al.*[10], which resulted in a renormalisation of the Rahm *et al.* data by 0.7%, and allowed to reduce the normalisation uncertainty to ~1%.

RECENT DATA AT 96 AND 162 MeV

The authors consider recent data of the *np* differential cross section obtained at 96 and 162 MeV, shown in the upper panels of Figures 1 and 2, respectively. The data shown at 96 MeV were taken at the Svedberg Laboratory(TSL) neutron beam facility in Uppsala, with the LISA (L) magnetic spectrometer [Rahm *et al.*[8]], the SCANDAL (S) setup [Johansson *et al.*[10], Blideanu *et al.*[12] and Mermod *et al.*[13]] and the MEDLEY (M) setup [Mermod *et al.*[14]]. The data at 162 MeV are from Rahm *et al.*[9]. The data from Sarsour *et al.*[11], obtained with a tagged neutron beam, were originally taken at 194 MeV. For comparison purposes, they are transformed to 162 MeV by multiplying each data point by the ratio of the differential cross section at 162 MeV to the differential cross section at 194 MeV (at the corresponding angle), using the Nijmegen partial wave analysis PWA93[15]. The PWA93 calculations and the prediction from the CD-Bonn *NN* potential (and, in Figure 1, also the AV18 potential) are plotted for comparison.

In the middle and bottom panels of the figures, one can follow in a comprehensive way how the probability to cause cell damage is obtained from the differential cross sections. The middle panels show the differential cross sections multiplied with the solid angle element $2\pi \sin\theta$ as functions of the neutron scattering angle in the laboratory system, θ; they illustrate the angular probability distributions for neutron scattering.As the solid angle vanishes at zero and 180°, these distributions are no longer forward and backward peaked. In the bottom panels, the distributions have been weighted with the energy of the recoil protons E_R, thus illustrating the angular probability distributions for the neutrons to

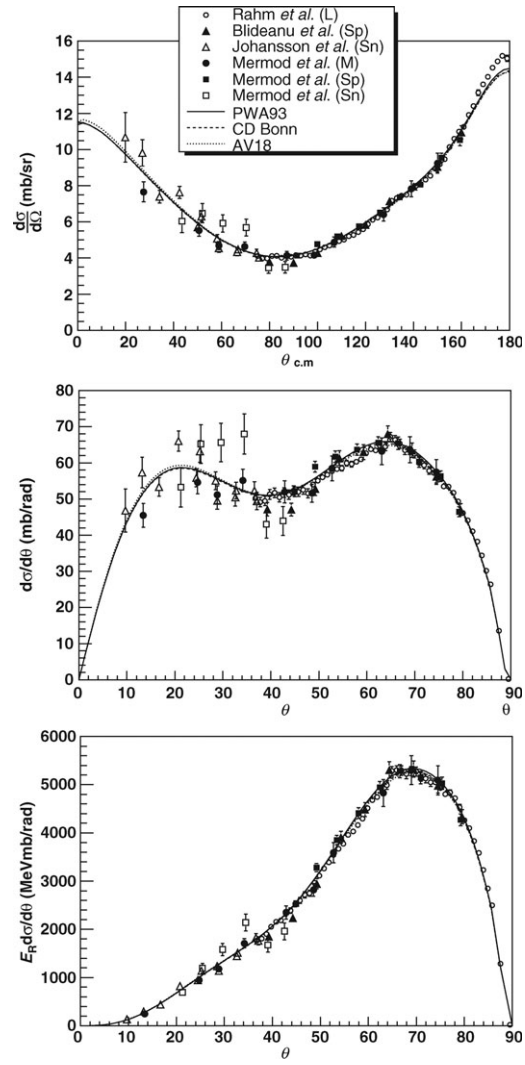

Figure 1. Elastic *np* scattering at 96 MeV. The angles $\theta_{c.m.}$ and θ are the neutron scattering angles in the c.m. and laboratory systems, respectively. The experimental data are from Uppsala, from Refs. (8,10,12–14): L is the LISA magnetic spectrometer, Sp and Sn are the SCANDAL setup where protons and neutrons are detected and M is the MEDLEY setup. The calculations are from the partial wave analysis PWA93[15] and the CD-Bonn[1] and AV18[2] *NN* potentials. Elastic scattering differential cross sections are shown in the top panels; in the middle panels, the differential cross sections were multiplied with the solid angle elements; in the bottom panels, they were further multiplied with the energy of the recoil protons. The areas under these last plots are proportional to the proton recoil kerma coefficients.

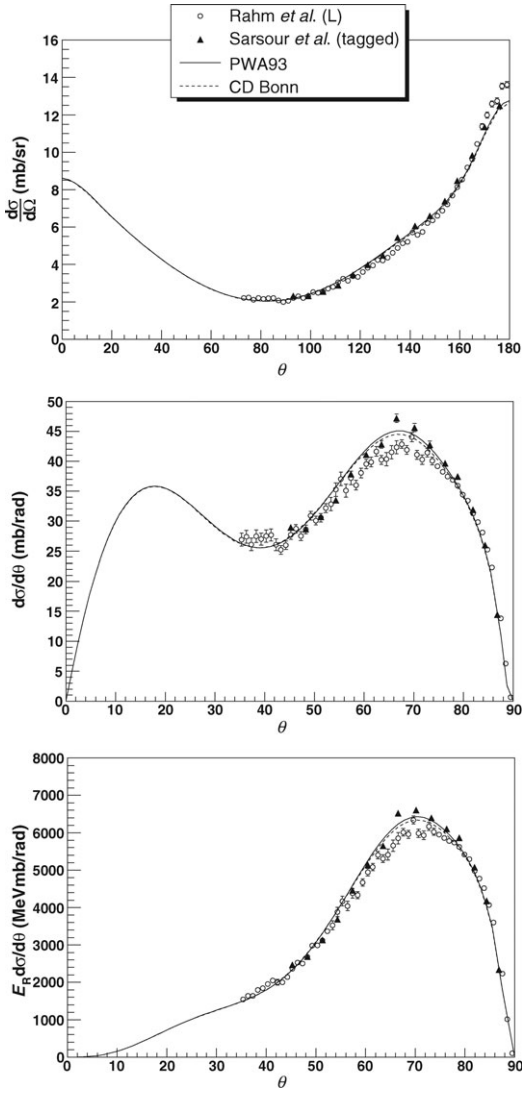

Figure 2. Elastic *np* scattering at 162 MeV. The angles $\theta_{\text{c.m.}}$ and θ are the neutron scattering angles in the c.m. and laboratory systems, respectively. The experimental data are from Rahm *et al.*[9] and Sarsour *et al.*[11]. The Sarsour *et al.* data, originally taken at 194 MeV, were transformed to 162 MeV using the PWA93 calculations. The curves are from PWA93[15] and the CD-Bonn[1] *NN* potential. Elastic scattering differential cross sections are shown in the top panels; in the middle panels, the differential cross sections were multiplied with the solid angle elements; in the bottom panels, they were further multiplied with the energy of the recoil protons. The areas under these last plots are proportional to the proton recoil kerma coefficients.

cause cell damage. Back-scattered neutrons transfer more energy to the protons than forward-scattered neutrons, and therefore the energy of the recoil nuclei increases with the neutron scattering angle. From these distributions, which peak at $\sim 70^\circ$, the authors deduce that most of the damage is caused by neutrons scattered between 50 and 85° (in the laboratory).

PROTON RECOIL KERMA COEFFICIENTS

The partial kerma coefficient k is the average kinetic energy of one type of charged particle produced in matter due to a certain reaction per unit mass divided by the neutron fluence. If the neutrons are propagating inside a living organism, the kerma coefficient is closely related to the probability to cause irreversible DNA damage through the considered reaction. In the case under consideration, the reaction is *np* scattering at 96 and 162 MeV incident neutron energy and the charged particle is the recoil proton. Thus, the proton recoil kerma coefficient is proportional to the integral of the differential cross section multiplied with the solid angle element and the energy of the recoil nucleus:

$$k = N \int E_{\text{R}} \frac{\text{d}\sigma}{\text{d}\Omega}(\theta) 2\pi \sin\theta \, \text{d}\theta$$

where N is the inverse nuclear mass of the recoil proton, E_{R} is its kinetic energy in the laboratory system and $2\pi \sin\theta$ is the solid angle element at the neutron laboratory angle θ. Note that the proton recoil kerma coefficients are proportional to the area under the distributions in the bottom panels of Figures 1 and 2.

The values of k are obtained for the Rahm *et al.*[8,9] data at the two energies under consideration as well as for the different theory predictions, and presented in Table 1. For the Rahm *et al.* data, in the forward region (where data are lacking) the curve from PWA93 was used for the extraction of k; this caused a negligible uncertainty since the contribution to k is small in this angular range. At 96 MeV, the ICRU value obtained from evaluated data[16] is also shown in the table.

Table 1. Proton recoil partial kerma coefficients at 96 and 162 MeV, for the Rahm *et al.*[8,9] data, the ICRU report from evaluated data[16], the Nijmegen partial-wave analysis PWA93[15] and the CD-Bonn and AV18 *NN* potentials[1,2].

k (fGy · m^{-2})	$E_n = 96$ MeV	$E_n = 162$ MeV
Rahm *et al.*	36.5 ± 0.4	40.6 ± 0.8
ICRU	36.6	—
PWA93	37.2	41.4
CD-Bonn	37.0	41.1
AV18	36.9	—

DISCUSSION AND CONCLUSION

By plotting the angular probability distribution for *np* scattering weighted with the recoil proton energy, it was identified that the most relevant angular range as far as the deposited dose is concerned is the region 50–85°. In this angular range, there exist high-precision *np* data from Uppsala at 96 and 162 MeV [the Rahm *et al.*[8,9] data], which were normalised to the total *np* cross section with an accuracy of 1–2%. The shape of the Rahm *et al.* data, however, do not match exactly with the shape of the PWA93 or *NN* potential calculations: the predictions tend to overestimate very slightly the data in the range 50–80°, which happens to be the sensitive region (and they tend to underestimate the data above 80°, but this has no consequences in the present discussion). Thus, this little mismatch is responsible for a difference of up to 2% in the proton recoil kerma coefficients between the data and calculations. However, the Sarsour *et al.*[11] data, obtained with a tagged neutron beam at 194 MeV, agree very well with the calculations in both the shape and the absolute scale, indicating that the effect might be due to systematic uncertainties in the Rahm *et al.* data affecting the shape of the angular distribution. This interpretation is supported by the observation that the shapes of the other sets of data at 96 MeV, measured with different techniques, tend to be in good agreement with PWA93.

ACKNOWLEDGEMENTS

The authors wish to thank the technical staff of the The Svedberg Laboratory for enthusiastic and skillful assistance. This work was supported by the Swedish Nuclear Fuel and Waste Management Company, the Swedish Nuclear Power Inspectorate, Ringhals AB, the Swedish Defence Research Agency and the Swedish Research Council.

REFERENCES

1. Machleidt, R. *High-precision, charge-dependent Bonn nucleon-nucleon potential*. Phys. Rev. **C63**, 024001 (2001).
2. Wiringa, R. B., Stoks, V. G. J. and Schiavilla, R. *Accurate nucleon-nucleon potential with charge independence breaking*. Phys. Rev. **C51**, 38 (1995).
3. Blomgren, J. and Olsson, N. *Beyond Kerma—neutron data for biomedical applications*. Radiat. Prot. Dosim. **103**, 293 (2003).
4. Chadwick, M. B., DeLuca, P. M. Jr. and Haight, R. C. *Nuclear data needs for neutron therapy and radiation protection*. Radiat. Prot. Dosim. **70**, 1 (1997).
5. Mermod, P., Blomgren, J., Nilsson, L., Pomp, S., Öhrn, A., Österlund, M., Prokofiev, A. and Tippawan, U., *Kerma coefficients for neutron scattering on 12C and 16O at 96 MeV.*
6. Tippawan, U., Dangtip, S., Pomp, S., Ataç, A., Bergenwall, B., Blomgren, J., Johansson, C., Klug, J., Mermod, P. and Nilsson, L. *et al. Light charged-particle production in 96 MeV neutron-induced reactions on carbon and oxygen*.
7. Pomp, S., Blomgren, J., Johansson, C., Klug, J., Öhrn, A., Österlund, M., Blideanu, V., Lecolley, F. R., Lecolley, J. F. and Lefort, T. *et al. Neutron-induced light-ion production from Fe, Pb and U at 96 MeV*, these proceedings.
8. Rahm, J. *et al. np scattering measurements at 96 MeV.* Phys. Rev. **C63**, 044001 (2001).
9. Rahm, J. *et al. np scattering measurements at 162 MeV and the π NN coupling constant*. Phys. Rev. **C57**, 1077 (1998).
10. Johansson, C. *et al. Forward-angle neutron-proton scattering at 96 MeV.* Phys. Rev. **C71**, 024002 (2005).
11. Sarsour, M. *et al. Measurement of the absolute np scattering differential cross section at 194 MeV.* Phys. Rev. Lett. **94**, 082303 (2005).
12. Blideanu, V. *et al. Nucleon-induced reactions at intermediate energies: New data at 96 MeV and theoretical status.* Phys. Rev. **C70**, 014607 (2004).
13. Mermod, P., Blomgren, J., Bergenwall, B., Hildebrand, A., Johansson, C., Klug, J., Nilsson, L., Olsson, N., Österlund, M. and Pomp, S. *et al. Evidence for three-body force effects in neutron-deuteron scattering at 95 MeV.* Phys. Rev. **C72**, (2005) 061002(R); Mermod, P., Blomgren, J., Johansson, C., Öhrn, A., Österlund, M., Pomp, S., Bergenwall, B., Klug, J., Nilsson, L., Olsson, N. *et al. 95 MeV neutron scattering on hydrogen, deuterium, carbon and oxygen*, submitted to Phys. Rev. C. **74** (2006) 054002.
14. Mermod, P. *et al. Search for three-body force effects in neutron-deuteron scattering at 95 MeV.* Phys. Lett. **B597**, 243 (2004).
15. Stoks, V. G. J., Klomp, R. A. M., Rentmeester, M. C. M. and de Swart, J. J. *Partial-wave analysis of all nucleon-nucleon scattering data below 350 MeV.* Phys. Rev. **C48**, 792 (1993).
16. ICRU Report 63, Nuclear Data for Neutron and Proton Radiotherapy and for Radiation Protection (International Commission on Radiation Units and Measurements, MD) (2000).

Radiation Protection Dosimetry (2007), Vol. 126, No. 1–4, pp. 113–118 doi:10.1093/rpd/ncm024
Advance Access publication 16 June 2007

KERMA COEFFICIENTS FOR NEUTRON SCATTERING ON ^{12}C AND ^{16}O AT 96 MeV

P. Mermod[1], J. Blomgren[1,*], L. Nilsson[1], S. Pomp[1], A. Öhrn[1], M. Österlund[1], A. Prokofiev[2] and U. Tippawan[3]
[1]Department of Neutron Research, Uppsala University, Box 525, S-75120 Uppsala, Sweden
[2]The Svedberg Laboratory, Uppsala University, Uppsala, Sweden
[3]Fast Neutron Research Facility, Chiang Mai University, Chiang Mai, Thailand

Recently, many new applications of fast neutrons are emerging or under development, like dose effects due to cosmic ray neutrons for airplane crew, fast neutron cancer therapy, studies of electronics failure induced by cosmic ray neutrons and accelerator-driven incineration of nuclear waste and energy production technologies. In radiation treatment, the kerma (Kinetic energy release in matter) coefficient, which describes the average energy transferred from neutrons to charged particles, is widely used. The kerma coefficient can be calculated from microscopic nuclear data. Nuclear data above 20 MeV are rather scarce, and more complete nuclear data libraries are needed in order to improve the understanding of the processes occurring on a cellular level. About half the dose in human tissue due to fast neutrons comes from proton recoils in neutron–proton (np) scattering, 10–15% from nuclear recoils due to elastic and inelastic neutron scattering and the remaining 35–40% from neutron-induced emission of light ions. Experimental data on elastic and inelastic neutron scattering at 96 MeV from ^{12}C and ^{16}O have been obtained recently at The Svedberg Laboratory in Uppsala, Sweden. These data are shown to be relevant for the determination of nuclear recoil kerma coefficients from elastic and inelastic neutron scattering at intermediate energies.

INTRODUCTION

Neutron cross sections at intermediate energies are relevant to applications such as transmutation of nuclear waste[1,2], medical treatment of tumours with fast neutrons[3], and the mitigation of single-event effects in electronics[4]. Experimental data for neutron-induced reactions on a wide range of nuclei are needed to improve data evaluations and nuclear models that are to be implemented in Monte-Carlo codes in relation to these applications.

Fast neutrons have a potential for efficient cancer therapy treatment. Among the nuclei of interest for this application, we identify the main components of human tissue and bones, which are hydrogen, carbon, oxygen, nitrogen and calcium. The damage inflicted to the cells depends on cross sections for the interactions of neutrons with these nuclei as well as the energies and masses of the released ionising particles. A rough evaluation tells us that ~50% of the cell damage is due to neutron–proton (np) scattering, ~10% is due to elastic and inelastic scattering on other nuclei and the rest is due to neutron-induced emission of light ions[3,5]. The contribution from np scattering is investigated in a separate paper[6], and light-ion production at 96 MeV is discussed in articles by Tippawan *et al.*[7] and Pomp *et al.*[8] of this workshop. In the present work, we focus on the ~10% contribution caused by elastic and inelastic neutron scattering on carbon and oxygen.

Using the SCANDAL multi-detector array at The Svedberg Laboratory in Uppsala (details about SCANDAL can be found in Ref.(9)), we performed neutron elastic scattering experiments at 96 MeV on a large variety of nuclei, such as ^{1}H, ^{2}H, ^{12}C, ^{14}N, ^{16}O, ^{28}Si, ^{40}Ca, ^{56}Fe, ^{89}Y and ^{208}Pb. In the present discussion, we concentrate on carbon and oxygen, and data on heavy nuclei are discussed in a separate contribution to this workshop by Österlund *et al.*[2]. Recently, in the context of a neutron–deuteron scattering experiment whose primary aim was to investigate three-nucleon force effects[10], (P. Mermod *et al.*, submitted for publication) high-precision differential cross sections were obtained for ^{12}C(n,n) and ^{16}O(n,n) scattering at 96 MeV. The measurement on carbon is an extension of the Klug *et al.* data obtained with the same technique[11]. In addition, inelastic scattering data were extracted. The new data on carbon and oxygen were reported in P. Mermod *et al.* (submitted for publication). In this publication, we pointed out that these data might be relevant for cancer treatment of tumours with fast neutrons and we identified angular regions where the accuracy of the theoretical calculations were not satisfying. In the present paper, we

*Corresponding author: jan.blomgren@tsl.uu.se

discuss further how the uncertainties in the elastic and inelastic differential cross sections on carbon and oxygen affect the estimation of the nuclear recoil kerma coefficients at intermediate energies.

DIFFERENTIAL CROSS SECTIONS AND KERMA COEFFICIENTS

The partial kerma coefficient k is the average kinetic energy of one type of charged particle produced in matter due to a certain process per unit mass divided by the neutron fluence. If the neutrons are propagating inside a living organism, the kerma coefficient is closely related to the probability to cause irreversible DNA damage through the considered process. In our case, the process is elastic or inelastic scattering at 96 MeV incident neutron energy and the charged particle is the carbon or oxygen recoil nucleus. Thus, the recoil kerma coefficient is proportional to the integral of the differential cross section multiplied with the solid angle element and the energy of the recoil nucleus:

$$k = N \int E_{\mathrm{R}} \frac{\mathrm{d}\sigma}{\mathrm{d}\Omega}(\theta) 2\pi \sin\theta \,\mathrm{d}\theta,$$

where N is the inverse nuclear mass of the recoil nucleus, E_{R}, its kinetic energy in the laboratory system and $2\pi \sin\theta$, the solid angle element at the neutron laboratory angle θ.

Figures 1 (carbon) and 2 (oxygen) illustrate how recoil kerma coefficients are obtained from the differential cross sections. The elastic neutron scattering data at 96 MeV are from P. Mermod *et al.* submitted for publication, Klug *et al.*[11], Salmon[12] and Osborne *et al.*[13]. The theoretical curves are predictions from the Koning and Delaroche global potential[14a,b], the Watson global potential[15], Amos *et al.*[16a], Karataglidis *et al.*[16b] and Crespo *et al.*[17] (see Refs. (11), P. Mermod *et al.* submitted for publication) for details). In the top panels of the figures, the differential cross sections (in logarithmic scale) are plotted as functions of the neutron scattering angle in the laboratory. In the bottom panels, the distributions have been multiplied with the solid angle element $2\pi \sin\theta$ and weighed with the energy of the recoil nuclei E_{R}, thus illustrating the angular probability distributions for the neutrons to cause cell damage. As the solid angle vanishes at 0°, these distributions are no longer forward-peaked. Back-scattered neutrons transfer more energy to the nuclei than forward-scattered neutrons, and therefore, the energy of the recoil nuclei increases with the neutron scattering angle. From these distributions, which peak at ~16°, we can deduce that most of the damage is caused by neutrons scattered between 10 and 30°, but there is still a significant contribution up to 60°. With this way of plotting, the recoil kerma coefficients are proportional to the areas under the distributions.

The data for inelastic scattering on carbon and oxygen at 96 MeV to excited states up to 12 MeV excitation energy (from P. Mermod *et al.*, submitted for publication) were treated the same way. The differential cross sections for inelastic scattering multiplied with the solid angle elements and the recoil nuclei energies are plotted in Figures 3 (carbon) and 4 (oxygen). Here we observe that the main contribution to the kerma from inelastic scattering is between 30 and 60° and tends to be significantly underestimated by the calculations.

The values of k for different data sets and different theoretical predictions were evaluated in Ref. (11) and P. Mermod *et al.* (submitted for publication), and are reported below in Table 1.

RESULTS

Differential cross sections for elastic and inelastic neutron scattering on carbon and oxygen must be well known for a precise evaluation of the damage caused by fast neutrons in human tissue. We have shown that a large angular coverage (up to 60°) was needed, due to the fact that the recoil nucleus energy increases with increasing scattering angle.

There are large variations in the evaluation of the recoil kerma coefficients k obtained with different models. For elastic scattering, the experimental uncertainty in the nuclear recoil kerma coefficients is ~5%, whereas it is at least 10% for the theoretical calculations or the values from evaluated data. The ICRU value obtained from evaluated data (18) agrees with the experimental values from Ref. (11) P. Mermod *et al.* (submitted for publication) within these uncertainties. Among the theoretical models, for elastic scattering on carbon, only Crespo *et al.* seems to give a reasonable prediction, and this is due to the fact that most models are inaccurate in the region 25–35°. For elastic scattering on oxygen, the prediction closest to the data is provided by the Koning and Delaroche potential. For inelastic scattering on both carbon and oxygen, all models underestimate significantly the data above 40°. As a consequence, the contribution to the kerma from inelastic scattering lies above the model predictions by ~50%. Although the contribution from inelastic scattering is small compared with elastic scattering, the disagreement between calculations and data for inelastic scattering is still responsible for a significant (~8%) discrepancy in the recoil kerma coefficient for the sum of elastic and inelastic scattering below 12 MeV excitation energy.

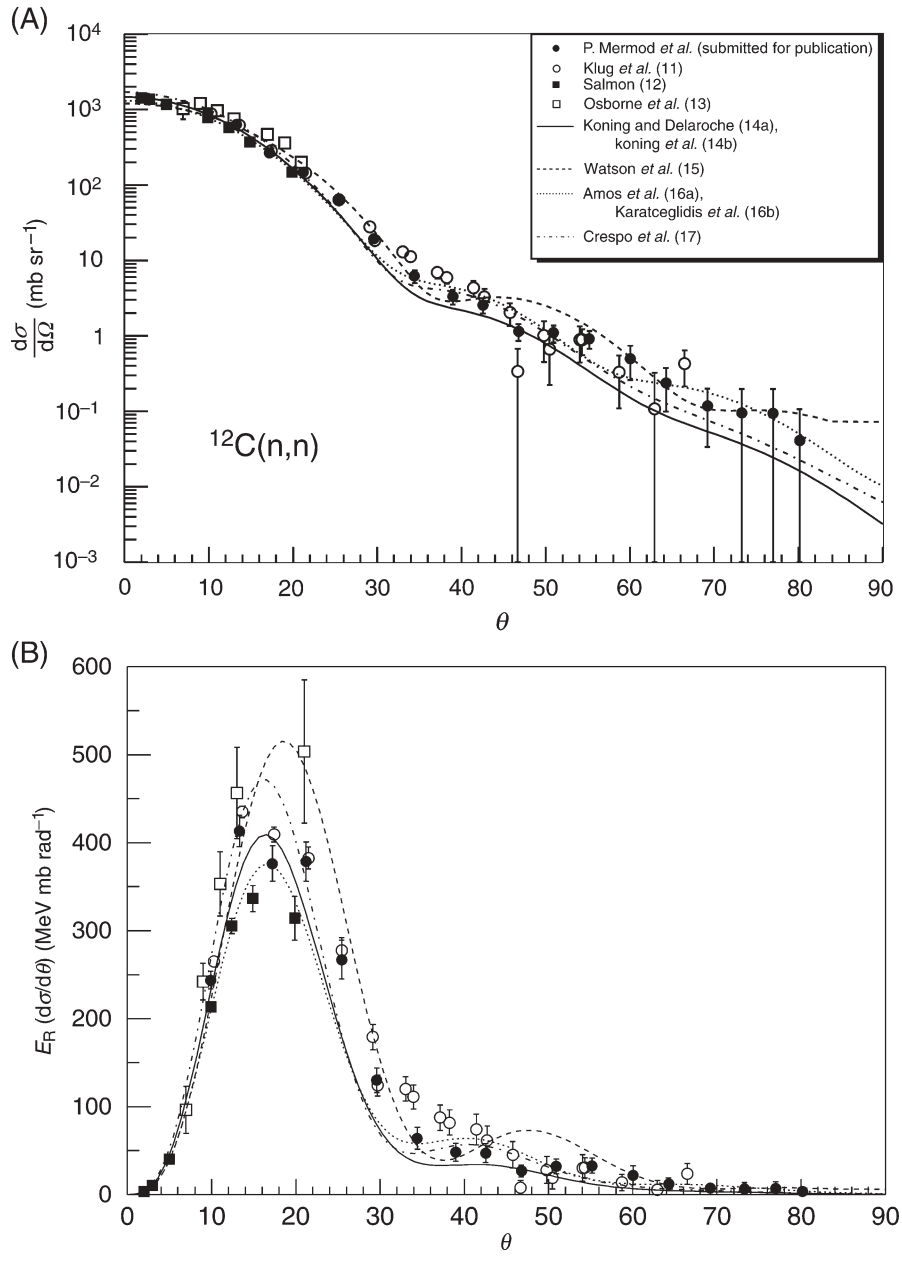

Figure 1. Elastic neutron scattering on carbon at 96 MeV. The angle θ is the neutron scattering angle in the laboratory. The experimental data are from Refs. (11, 12, 13), (P. Mermod *et al.*, submitted for publication). The elastic scattering differential cross section is shown in the top panel, and in the bottom panel, the differential cross section was multiplied with the solid angle element and with the energy of the recoil nucleus. The area under this plot is proportional to the nuclear recoil kerma coefficient for elastic scattering.

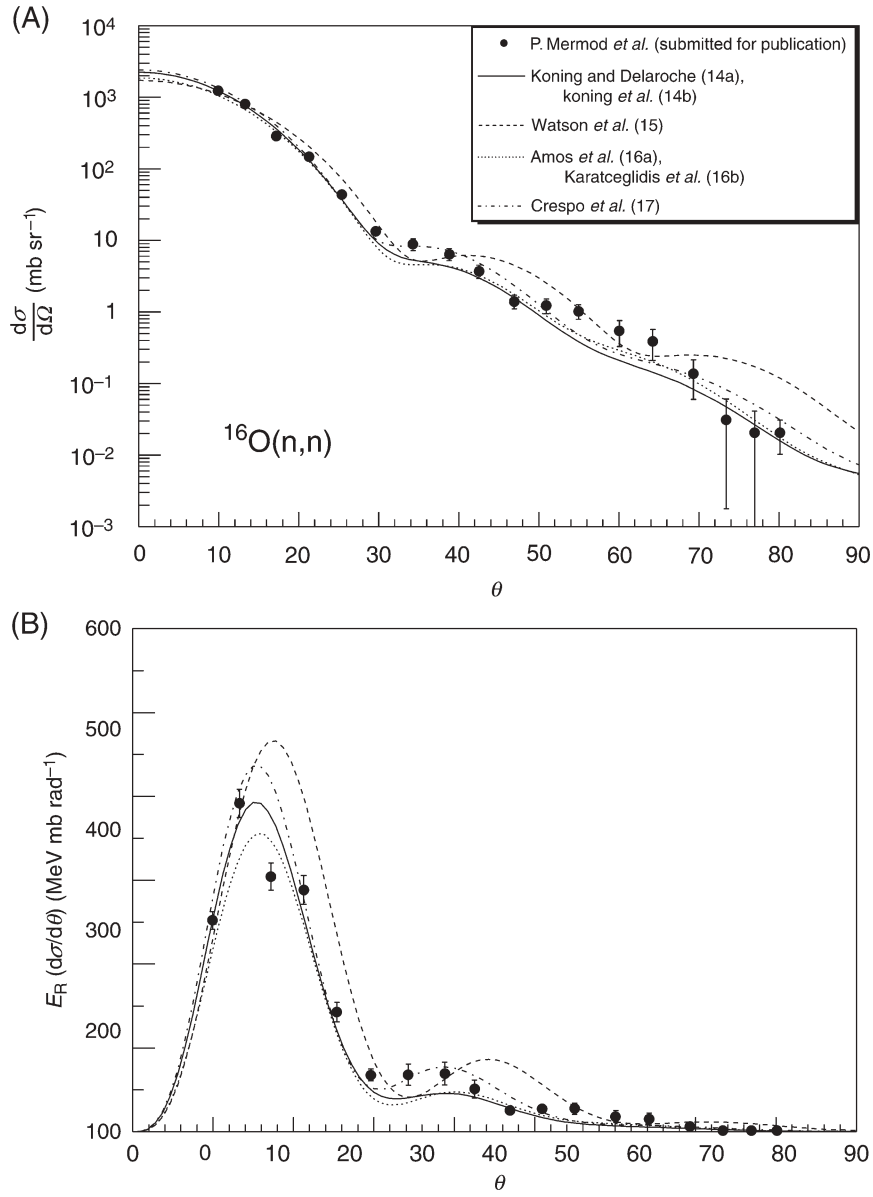

Figure 2. Elastic neutron scattering on oxygen at 96 Mev. The angle θ is the neutron scattering angle in the laboratory. The experimental data are from P. Mermod *et al.* (submitted for publication). The elastic scattering differential cross section is shown in the top panel, and in the bottom panel, the differential cross section was multiplied with the solid angle element and with the energy of the recoil nucleus. The area under this plot is proportional to the nuclear recoil kerma coefficient for elastic scattering.

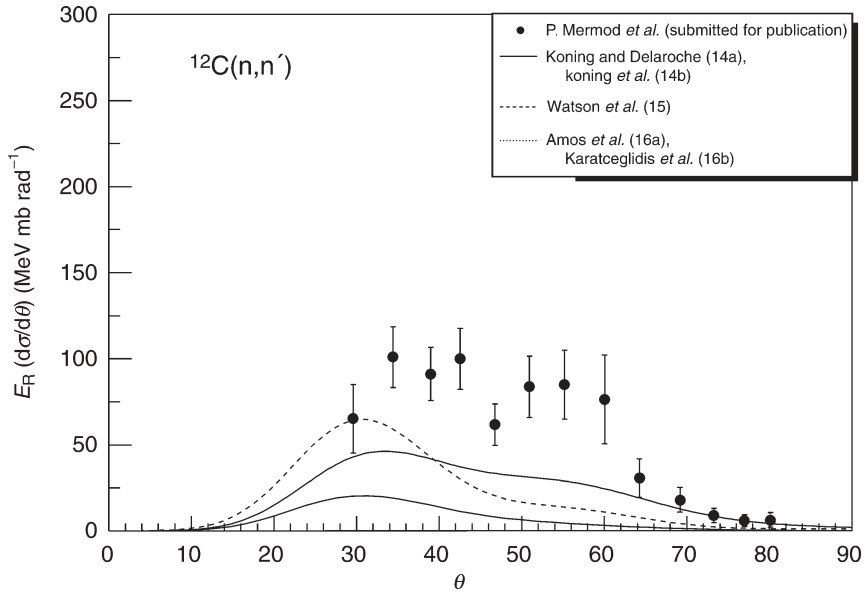

Figure 3. Differential cross section multiplied with the solid angle elements and the energy of the recoil nuclei for inelastic neutron scattering to excited states below 12 MeV on carbon at 96 MeV. The angle θ is the neutron scattering angle in the laboratory. The experimental data are from P. Mermod *et al.* (submitted for publication). The area under this plot is proportional to the nuclear recoil kerma coefficient for inelastic scattering.

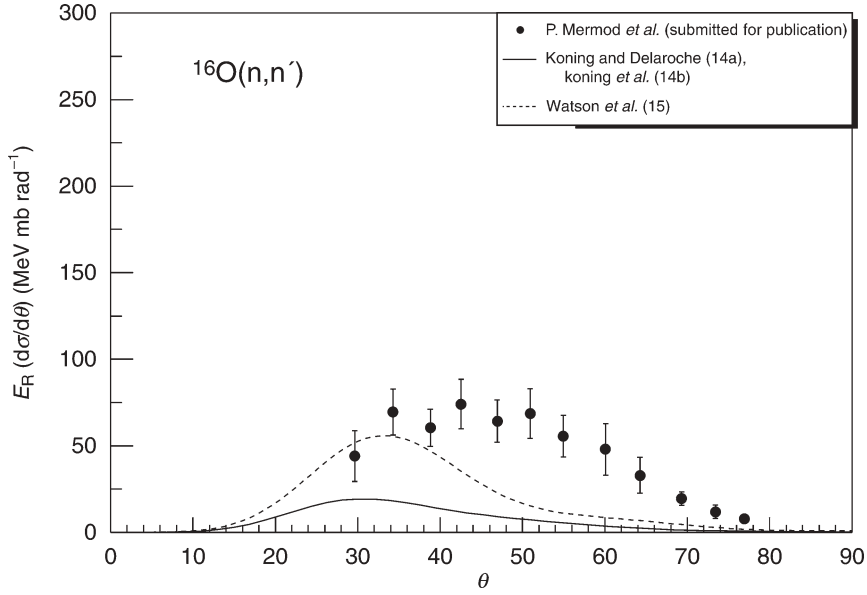

Figure 4. Differential cross section multiplied with the solid angle elements and the energy of the recoil nuclei for inelastic neutron scattering to excited states below 12 MeV on oxygen at 96 MeV. The angle θ is the neutron scattering angle in the laboratory. The experimental data are from P. Mermod *et al.* (submitted for publication). The are under this plot is proportional to the nuclear recoil kerma coefficient for inelastic scattering.

Table 1. Kerma coefficients for the recoil carbon (top) and oxygen (bottom) nuclei from elastic and inelastic neutron scattering at 96 MeV.

k (fGy m^2)	Elastic	Inelastic
^{12}C(n,n)		
p. Mermod *et al.* (submitted for publication)	0.120 ± 0.007	0.047 ± 0.029
Klug *et al.* (11)	0.126 ± 0.009	—
ICRU (18)	0.132 ± 0.013	—
Koning and Delaroche (14a), Koning *et al.* (14b)	0.102	0.007
Watson *et al.* (15)	0.145	0.023
Amos *et al.* (16a), Karataglidis *et al.* (16b)	0.105	0.026
Crespo *et al.* (17)	0.118	—
^{16}O(n,n)		
P. Mermod *et al.* (submitted for publication)	0.073 ± 0.004	0.028 ± 0.006
ICRU (18)	0.074 ± 0.007	—
Koning and Delaroche (14a), Koning *et al.* (15)	0.071	0.006
Watson *et al.* (15)	0.096	0.016
Amos *et al.* (16a), Karataglidis *et al.* (16b)	0.066	—
Crespo *et al.* (17)	0.082	—

Note: The inelastic scattering data corresponds to the sum of the excited states with excitation energies below 12 MeV.

ACKNOWLEDGEMENTS

We wish to thank the technical staff of the The Svedberg Laboratory for enthusiastic and skillful assistance. This work was supported by the Swedish Nuclear Fuel and Waste Management Company, the Swedish Nuclear Power Inspectorate, Ringhals AB, the Swedish Defence Research Agency and the Swedish Research Council.

REFERENCES

1. Blomgren, J. *Experimental Activities at High Energies*. Workshop on Nuclear Data for Science & Technology: Accelerator Driven Waste Incineration, Trieste, Italy, Sept. 10–21, 2001. Herman, M., Paver, N. and Stanculescu, A. Eds. ICTP lecture notes **12**, 327 (2002).
2. Blomgren, J. and Olsson, N. *Beyond kerma–neutron data for biomedical applications*. Radiat. Prot. Dosim. **103**, 293 (2003).
3. Blomgren, J., Granbom, B., Granlund, T. and Olsson, N. *Relations between basic nuclear data and single-event upsets phenomena*. Mat. Res. Soc. Bull. **28**, 121 (2003).
4. Chadwick, M. B., DeLuca, P. M. Jr. and Haight, R. C. *Nuclear data needs for neutron therapy and radiation protection*. Radiat. Prot. Dosim. **70**, 1 (1997).
5. Mermod, P. *et al.* Precision measurements of the np scattering differential cross section in the intermediate energy region, these proceedings.
6. Tippawan, U. *et al.* Light charged-particle production in 96 MeV neutron-induced reactions on carbon and oxygen, these proceedings.
7. Pomp, S. *et al.* Neutron-induced light-ion production from Fe, Pb and U at 96 MeV, these proceedings.
8. Klug, J. *et al. SCANDAL – a facility for elastic neutron scattering studies in the 50–130 MeV range*. Nucl. Instr. Method **A489**, 282 (2002).
9. Österlund, M. *et al.* Elastic neutron scattering studies on heavy nuclei at 96 MeV, these proceedings.
10. Mermod, P. *et al. Evidence of three-body force effects in neutron–deuteron scattering at 95 MeV*. Phys. Rev. **C72**, 061002 (2005).
11. Klug, J. *et al. Elastic neutron scattering at 96 MeV from ^{12}C and ^{208}Pb*. Phys. Rev. **C68**, 064605 (2003).
12. Salmon, G.L. *The elastic scattering of 96 MeV neutrons by nuclei.* Nucl. Phys. **21**, 15 (1960).
13. Osborne, J.H. *et al. Measurement of neutron elastic scattering cross sections for ^{12}C, ^{40}Ca, and ^{208}Pb at energies from 65 to 225 MeV*. Phys. Rev. **C70**, 054613 (2004).
14(a). Koning, A. J. and Delaroche, J. P. *Local and global nucleon optical models from 1 keV to 200 MeV*. Nucl. Phys. **A713**, 231 (2003).
(b). Koning, A.J., Hilaire, S. and Duijvestijn, M.C. *TALYS: comprehensive nuclear reaction modeling*. In: Proceedings of the International Conference on Nuclear Data for Science and Technology, Santa Fe, USA, Sep. 26–Oct. 1, 2004, CP769, 1154 (2005).
15. Watson, B. A., Singh, P. P. and Segel, R. E. *Optical-model analysis of nucleon scattering from 1p-Shell Nuclei between 10 and 50 MeV*. Phys. Rev. **182**, 977 (1969).
16(a). Amos, K., Dortmans, P. J., von Geramb, H. V., Karataglidis, S. and Raynal, J. *Nucleon-nucleus scatering: a microscopic nonrelativistic approach*. Adv. Nucl. Phys. **25**, 275 (2000).
(b). Karataglidis, S., Dortmans, P. J., Amos, K. and de Swiniarski, R. *Multi-ω and shell model analyses of elastic inelastic proton scattering from ^{14}N ^{16}O*. Phys. Rev. **C53**, 838 (1996).
17. Crespo, R., Johnson, R. C. and Tostevin, J. A. *Multiple scattering theory of proton elastic scattering at intermediate energies*. Phys. Rev. **C46**, 279 (1992).
18. International Commission on Radiation Units and Measurements. *Nuclear data for neutron and proton radiotherapy and for radiation protection*. (ICRU Report 63 MD:ICRU) (2000).

Radiation Protection Dosimetry (2007), Vol. 126, No. 1–4, pp. 119–122 doi:10.1093/rpd/ncm025
Advance Access publication 24 May 2007

ELASTIC NEUTRON SCATTERING STUDIES AT 96 MeV FOR TRANSMUTATION

M. Österlund[1,*], J. Blomgren[1], M. Hayashi[1,4], P. Mermod[1], L. Nilsson[1], S. Pomp[1], A. Öhrn[1], A. V. Prokofiev[2] and U. Tippawan[1,3]
[1]Department of Neutron Research, Uppsala University, Sweden
[2]The Svedberg Laboratory, Uppsala University, Sweden
[3]Fast Neutron Research Facility, Chiang Mai University, Thailand
[4]Department of Advanced Energy Engineering Science, Kyushu University, Japan

Elastic neutron scattering from ^{12}C, ^{14}N, ^{16}O, ^{28}Si, ^{40}Ca, ^{56}Fe, ^{89}Y and ^{208}Pb has been studied at 96 MeV in the10–70° interval, using the SCANDAL (SCAttered Nucleon Detection AssembLy) facility. The results for ^{12}C and ^{208}Pb have recently been published, while the data on the other nuclei are under analysis. The achieved energy resolution, 3.7 MeV, is about an order of magnitude better than for any previous experiment above 65 MeV incident energy. A novel method for normalisation of the absolute scale of the cross section has been used. The estimated normalisation uncertainty, 3%, is unprecedented for a neutron-induced differential cross section measurement on a nuclear target. Elastic neutron scattering is of utmost importance for a vast number of applications. Besides its fundamental importance as a laboratory for tests of isospin dependence in the nucleon–nucleon, and nucleon–nucleus, interaction, knowledge of the optical potentials derived from elastic scattering come into play in virtually every application where a detailed understanding of nuclear processes is important. Applications for these measurements are dose effects due to fast neutrons, including fast neutron therapy, as well as nuclear waste incineration and single event upsets in electronics. The results at light nuclei of medical relevance (^{12}C, ^{14}N and ^{16}O) are presented separately. In the present contribution, results on the heavier nuclei are presented, among which several are of relevance to shielding of fast neutrons.

INTRODUCTION

The interest in high-energy neutron data is rapidly growing, since a number of potential large-scale applications involving fast neutrons are under development, or at least have been identified. These applications primarily fall into three sectors—nuclear energy and waste, nuclear medicine and effects on electronics. For all these applications, an improved understanding of neutron interactions is needed for calculations of neutron transport and radiation effects. The nuclear data needed for this purpose come almost entirely from nuclear scattering and reaction-model calculations, which all depend heavily on the optical model, which in turn is determined by elastic scattering and total cross-section data.

The nuclear data needs for transmutation of nuclear waste, in general, and spent nuclear fuel, in particular, are outlined in Refs. (1–3), while the needs for neutron therapy of cancer tumours are reviewed in Ref. (4), and upsets in electronics are discussed in Refs. (5,6). In the present work, a programme on elastic neutron scattering at 96 MeV is presented, which deals with all these applications.

Neutron-scattering data are also important for a fundamental understanding of the nucleon–nucleus interaction, particularly for determining the isovector term[7]. Coulomb repulsion of protons creates a neutron excess in all stable nuclei with $A > 40$. Incident protons and neutrons interact differently with this neutron excess. The crucial part in these investigations has been neutron–nucleus elastic scattering data to complement the already existing proton–nucleus data. Above 50-MeV neutron energy, there has been only one previous measurement on neutron elastic scattering with an energy resolution adequate for resolving individual nuclear states, an experiment at UC Davis at 65 MeV on a few nuclei[8]. In addition, a few measurements in the 0–20° range are available, all with energy resolution of 20 MeV or more. This is, however, not crucial at such small angles because elastic scattering dominates heavily, but at larger angles such a resolution would make data very difficult to interpret. Recently, results on neutron scattering from ^{12}C, ^{40}Ca and ^{208}Pb in the 65–225 MeV range from Los Alamos have been published[9]. The energy resolution is comparable to the present work, but the angular range is limited to 7–23°.

EXPERIMENTAL SETUP

The neutron beam facility at The Svedberg Laboratory, Uppsala, Sweden, has recently been described in detail[10], and therefore only a brief description is given here. The 96 ± 0.5 MeV (1.2-MeV FWHM) neutrons were produced by

*Corresponding author: Michael.Osterlund@tsl.uu.se

the ^{7}Li(p,n) reaction by bombarding a 427 mg/cm^{2} disc of isotopically enriched (99.98%)^{7}Li with protons from the cyclotron. The low-energy tail of the source-neutron spectrum was suppressed by time-of-flight techniques. After the target, the proton beam was bent into a well-shielded beam dump. A system of three collimators defined a 9-cm diameter neutron beam at the scattering target.

Scattered neutrons were detected by the SCANDAL (SCAttered Nucleon Detection AssembLy) setup[10]. It consists of two identical systems, placed to cover 10–50° and 30–70°, respectively. The energy of the scattered neutrons is determined by measuring the energy of proton recoils from a plastic scintillator, and the angle is determined by tracking the recoil proton. In the present experiment, each arm consisted of a 2-mm-thick veto scintillator for fast charged-particle rejection, a 10-mm-thick neutron-to-proton converter scintillator, a 2-mm-thick plastic scintillator for triggering, two drift chambers for proton tracking, a 2-mm-thick ΔE plastic scintillator that was also part of the trigger and an array of CsI detectors for energy determination of recoil protons produced in the converter by *np* scattering. The trigger was provided by a coincidence of the two trigger scintillators, vetoed by the front scintillator. The total excitation energy resolution varies with CsI crystal, but is on average 3.7 MeV Full Width Half Maximum (FWHM). The angular resolution is in the 1.0–1.3° (rms) range.

RESULTS AND DISCUSSION

Angular distributions of elastic-neutron scattering from ^{12}C and ^{208}Pb at 96-MeV incident neutron energy[11,12] are presented in Figure 1. The data are compared with phenomenological and microscopic optical-model predictions in the left and right panels, respectively. The theoretical curves have all been folded with the experimental angular resolution to facilitate comparisons with data. The data by Salmon[13] at 96 MeV are also shown. The angular distributions presented have been corrected for reaction losses and multiple scattering in the target. The contribution from other isotopes than ^{208}Pb in the lead data has been corrected for, using cross-section ratios calculated with the global potential by Koning and Delaroche[14].

The absolute normalisation of the data has been obtained from knowledge of the total elastic cross section, which has been determined from the difference between the total cross section (σ_T)[15] and the reaction cross section (σ_R)[16,17]. This $\sigma_T - \sigma_R$ method, which is expected to have an uncertainty of ~3%, has been used to normalise the ^{12}C data [see Ref. (12) for details]. The ^{208}Pb(n,n) data have been normalised relative to the ^{12}C(n,n) data, knowing the relative neutron fluences, target masses, etc. The total elastic cross section of ^{208}Pb has previously been determined with the $\sigma_T - \sigma_R$ method. The accuracy of the present normalisation has been tested by comparing the total elastic cross-section ratio (^{208}Pb/^{12}C) obtained with the $\sigma_T - \sigma_R$ method above, and with the ratio determination of the present experiment, the latter being insensitive to the absolute scale. These two values differ by ~3%, i.e. they are in agreement within the expected uncertainty.

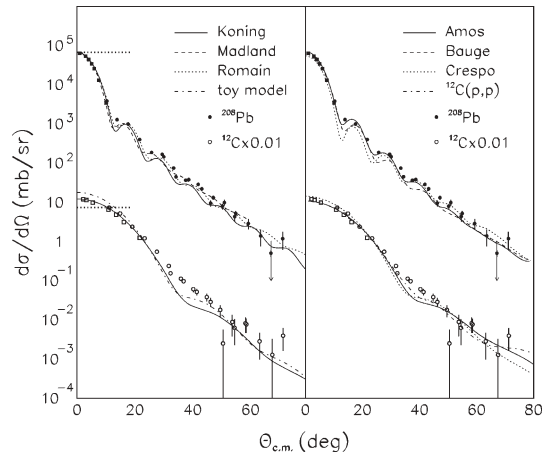

Figure 1. Angular distributions of elastic neutron scattering from ^{12}C (open circles) and ^{208}Pb (solid) at 96-MeV incident neutron energy. The ^{12}C data and calculations have been multiplied by 0.01. The data by Salmon(11) at 96 MeV are shown as squares. Left panel: predictions by phenomenological models. The thick dotted horizontal lines show Wick's limit for the two nuclei. Right panel: predictions by microscopic models, and data on elastic proton scattering from ^{12}C[25]. See the text for details, and Refs. (11,12) and references therein for a description of the theory models.

A novel technique for normalisation, which is based on relative measurements versus the *np* scattering cross section[18], has also been tested and was found to have an uncertainty of ~10%.

The data are compared with model predictions in Figure 1, where the left and right panels show phenomenological and microscopic models, respectively. The models are described in detail in Refs. (11,12).

When comparing these predictions with data, a few striking features are evident. First, all models are in reasonably good agreement with the ^{208}Pb data. It should be pointed out that none of the predictions contain parameters adjusted to the present experiment. In fact, they were all made before data were available. Even the absolute scale seems to be under good control, which is remarkable, given that the neutron beam intensities are notoriously difficult to establish. Second, all models fail to describe the ^{12}C data in the 30–50° range. The models predict a saddle structure, which is not evident from the data.

This mismatch has prompted a re-examination of the ^{12}C(n,n) cross section. Fortunately, this could be accomplished in combination with another experiment. Recently, the authors have studied *nd* scattering at the same energy to investigate three-nucleon interaction effects. These results show clear evidence of such 3*N* forces[19–21]. In these experiments, scattering from carbon was used for normalisation, as described above. The size of the target was, however, significantly larger than in the experiments above, resulting in far better statistics. This allowed more stringent analysis procedures to be used, and the results seem to indicate that the ^{12}C elastic scattering cross section is actually in agreement with the theory models. Thus, the main reason for the discrepancy above was probably contamination of the first excited state into the ground state in the analysis.

A basic feature of the optical model is that it establishes a lower limit on the differential elasticscattering cross section at 0° if the total cross section is known, often referred to as Wick's limit[22,23]. It has been observed in previous experiments at lower energies that for most nuclei, the 0° cross section falls very close to Wick's limit, although there is no *a priori* reason why the cross section cannot exceed the limit significantly. An interesting observation is that the present ^{208}Pb data are in good agreement with Wick's limit, while the ^{12}C 0° cross section lies ~70% above the limit. A similar behaviour has previously been observed in neutron-elastic scattering at 65 MeV[8], where the ^{12}C data overshoot Wick's limit by ~30%, whereas the ^{208}Pb data agree with the limit.

It has recently been shown by Dietrich *et al.*[24] that this makes sense. Using the Koning-Delaroche[12] potential, it has been shown that Wick's limit actually deviates <5% from an equality for ^{208}Pb over the entire 5–100 MeV interval. The lightest nucleus investigated was^{28}Si, but the systematics imply that large discrepancies for ^{12}C should be expected.

Preliminary data on ^{89}Y are presented in Figure 2, together with the Koning-Delaroche[12] potential. The data have been normalised to the model and it can be seen that it describes the shape of the data points reasonably well. The measurements on ^{16}O have been analysed and are presented in another contribution to this workshop. Measurements on ^{14}N, ^{28}Si, ^{40}Ca and ^{56}Fe have been completed and the data are under analysis.

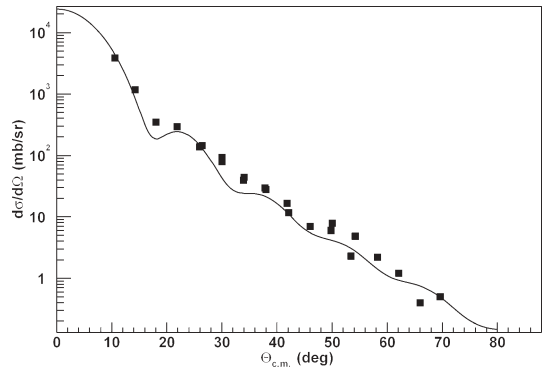

Figure 2. Preliminary angular distribution of elastic neutron scattering from ^{89}Y at 96-MeV incident neutron energy together with a prediction by the Koning-Delaroche[12] potential.

CONCLUSIONS AND OUTLOOK

In short, first results on elastic-neutron scattering from ^{12}C and ^{208}Pb at 96-MeV incident neutron energy are presented and compared with theory predictions. This experiment represents the highest neutron energy where the ground state has been resolved from the first excited state in neutron scattering. The measured cross sections span more than four orders of magnitude. Thereby, the experiment has met—and surpassed—the design specifications. The overall agreement with theory model predictions, both phenomenological and microscopic, is good. In particular, the agreement in the absolute cross-section scale is impressive.

Performance investigations have revealed that the method as such should work also at higher energies. Recently, the TSL neutron beam facility has been upgraded in intensity, making measurements at the highest energy, 180 MeV, feasible. An experimental campaign at 180 MeV does, however, require an upgrade of the CsI detectors of SCANDAL.

ACKNOWLEDGEMENTS

This work was financially supported by the Swedish Nuclear Fuel and Waste Management Company, the Swedish Nuclear Power Inspectorate, Ringhals AB, Forsmarks Kraftgrupp AB, the Swedish Defense Research Agency, the Swedish Nuclear Safety and Training Centre, and the European Union.

REFERENCES

1. Duijvestijn, M., Koning, A. and Hambsch, F.-J. *Nucleon-induced fission at intermediate energies.* J. Nucl. Sci. Tech. Suppl. **2**, 1161 (2002).
2. Blomgren, J. *Experimental activities at high energies*, In: Proceedings of Workshop on Nuclear Data for Science & Technology: Accelerator Driven Waste Incineration, Herman, M., Paver, N. and Stanculescu, A., Eds. Trieste, Italy, September 10–21, 2001, ICTP lecture notes **12**, 327 (2002).
3. Blomgren, J. *Nuclear data for accelerator-driven systems—Experiments above 20 MeV*, In: Proceedings of EU enlargement workshop on Neutron Measurements and Evaluations for Applications, Bucharest, Romania, October 20–23 (2004).

4. Blomgren, J. and Olsson, N. *Beyond kerma - neutron data for biomedical applications.* Radiat. Prot. Dosim. **103**(4), 293 (2003).
5. Blomgren, J., Granbom, B., Granlund, T. and Olsson, N. *Relations between basic nuclear data and single-event upsets.* Mat. Res. Soc. Bull. **28**, 121 (2003).
6. Blomgren, J. *Nuclear data for single-event effects.* In: Proceedings of EU Enlargement Workshop on Neutron Measurements and Evaluations for Applications, Budapest, Hungary, November 5–8 (2003). EUR Report 21100 EN, Luxembourg: Office for Official Publications of the European Communities, ISBN 92-894-6041-5, European Communities (2004).
7. See, e.g., Neutron–Nucleus Collisions: A probe of Nuclear Structure, AIP Conference Proceedings **124** (New York: AIP), (1985).
8. Hjort, E. L., Brady, F. P., Romero, J. L., Drummond, J. R., Sorenson, D. S., Osborne, J. H., McEachern, B. and Hansen, L. F. *Measurements and analysis of neutron elastic scattering at 65 MeV.* Phys. Rev. **C50**, 275 (1994).
9. Osborne, J. H., Brady, F. P., Romero, J. L., Ullmann, J. L., Sorenson, D. S., Ling, A., King, N. S. P., Haight, R. C., Rapaport, J., Finlay, R. W., Bauge, E., Delaroche, J. P. and Koning, A. J. *Measurement of neutron elastic scattering cross sections for ^{12}C, ^{40}Ca, and ^{208}Pb at energies from 65 to 225 MeV.* Phys. Rev. **C70**, 054613 (2004).
10. Klug, J., Blomgren, J., Ataç, A., Bergenwall, B., Dangtip, S., Elmgren, K., Johansson, C., Olsson, N., Pomp, S., Prokofiev, A. V., Rahm, J., Tippawan, U., Jonsson, O., Nilsson, L., Renberg, P. -U., Nadel-Turonski, P., Ringbom, A., Oberstedt, A., Tovesson, F., Blideanu, V., Le Brun, C., Lecolley, J. F., Lecolley, F. R., Louvel, M., Marie, N., Schweitzer, C., Varignon, C., Eudes, Ph., Haddad, F., Kerveno, M., Kirchner, T., Lebrun, C., Stuttgé, L., Slypen, I., Smirnov, A. N., Michel, R., Neumann, S. and Herpers, U. *SCANDAL-a facility for elastic neutron scattering studies in the 50-130 MeV range.* Nucl. Instr. Meth. **A489**, 282 (2002).
11. Klug, J., Blomgren, J., Ataç, A., Bergenwall, B., Hildebrand, A., Johansson, C., Mermod, P., Nilsson, L., Pomp, S., Tippawan, U., Elmgren, K., Olsson, N., Jonsson, O., Prokofiev, A. V., Renberg, P.-U., Nadel-Turonski, P., Dangtip, S., Phansuke, P., Österlund, M., Le Brun, C., Lecolley, J. F., Lecolley, F. R., Louvel, M., Marie-Noury, N., Schweitzer, C., Eudes, Ph., Haddad, F., Lebrun, C., Koning, A. J., Bauge, E., Delaroche, J. P., Girod, M., Ledoux, X., Romain, P., Madland, D. G., Amos, K., Deb, P. K., Karataglidis, S., Crespo, R. and Moro, A. M. *Elastic neutron scattering at 96 MeV from ^{12}C and ^{208}Pb.* Phys. Rev. **C67**, 031601(R) (2003).
12. Klug, J., Blomgren, J., Ataç, A., Bergenwall, B., Hildebrand, A., Johansson, C., Mermod, P., Nilsson, L., Pomp, S., Tippawan, U., Elmgren, K., Olsson, N., Jonsson, O., Prokofiev, A. V., Renberg, P.-U., Nadel-Turonski, P., Dangtip, S., Phansuke, P., Österlund, M., Le Brun, C., Lecolley, J. F., Lecolley, F. R., Louvel, M., Marie-Noury, N., Schweitzer, C., Eudes, Ph., Haddad, F., Lebrun, C., Koning, A. J. and Ledoux, X. *Elastic neutron scattering at 96 MeV from ^{12}C and ^{208}Pb.* Phys. Rev. **C68**, 064605 (2003).
13. Salmon, G. L. *The elastic scattering of 96 MeV neutrons by nuclei.* Nucl. Phys. **21**, 15 (1960).
14. Koning, A. J. and Delaroche, J. P. *Local and global nucleon optical models from 1 keV to 200 MeV.* Nucl. Phys. **A713**, 231 (2003).
15. Finlay, R. W., Abfalterer, W. P., Fink, G., Montei, E., Adami, T., Lisowski, P. W., Morgan, G. L. and Haight, R. C. *Neutron total cross sections at intermediate energies.* Phys. Rev. **C47**, 237 (1993).
16. DeJuren, J. and Knable, N. *Nuclear cross sections for 95-Mev neutrons*, Phys. Rev. **77**, 606 (1950).
17. Voss, R. G. P. and Wilson, R. *Neutron inelastic cross-section between 55 and 140 MeV.* Proc. Roy. Soc. **A236**, 41 (1956).
18. Johansson, C., Blomgren, J., Ataç, A., Bergenwall, B., Dangtip, S., Elmgren, K., Hildebrand, A., Jonsson, O., Klug, J., Mermod, P., Nadel-Turonski, P., Nilsson, L., Olsson, N., Pomp, S., Prokofiev, A. V., Renberg, P.-U., Tippawan, U. and Österlund, M. *Forward-angle neutron-proton scattering at 96 MeV.* Phys. Rev. **C71**, 024002 (2005).
19. Mermod, P., Blomgren, J., Bergenwall, B., Hildebrand, A., Johansson, C., Klug, J., Nilsson, L., Olsson, N., Osterlund, M., Pomp, S., Tippawan, U., Jonsson, O., Prokofiev, A., Renberg, P.-U., Nadel-Turonski, P., Maeda, Y., Sakai, H. and Tamii, A. *Search for three-body force effects in neutron-deuteron scattering at 95 MeV.* Phys. Lett. **B597**, 243 (2004).
20. Mermod, P., Blomgren, J., Hildebrand, A., Johansson, C., Klug, J., Österlund, M., Pomp, S., Tippawan, U., Bergenwall, B., Nilsson, L., Olsson, N., Jonsson, O., Prokofiev, A., Renberg, P.-U., Nadel-Turonski, P., Maeda, Y., Sakai, H. and Tamii, A. *Evidence of three-body force effects in neutron-deuteron scattering at 95 MeV.* Phys. Rev. **C72**, 061002(R) (2005).
21. Mermod, P., Blomgren, J., Johansson, C., Öhrn, A., Österlund, M., Pomp, S., Bergenwall, B., Klug, J., Nilsson, L., Olsson, N., Tippawan, U., Nadel-Turonski, P., Jonsson, O., Prokofiev, A., Renberg, P.-U., Maeda, Y., Sakai, H., Tamii, A., Amos, K., Crespo, R. and Moro, A. *95 MeV neutron scattering on hydrogen, deuterium, carbon, and oxygen*. Phys. Rev. C **74**, 054002 (2006).
22. Wick, G. C. *Sulla propagazione di un'onda di De Broglie in un mezzo materiale.* Atti. R. Accad. Naz. Lincei, Mem. Cl. Sci. Fis. Mat. Nat. **13**, 1203 (1943).
23. Wick, G. C. *On the space distribution of slow neutrons.* Phys. Rev. **75**, 738–756 (1949).
24. Dietrich, F. S., Anderson, J. D., Bauer, R. W. and Grimes, S. M. *Wick's limit and a new method for estimating neutron reaction cross sections.* Phys. Rev. **C68**, 064608 (2003).
25. Gerstein, G., Niederer, J. and Strauch, K. *Elastic scattering of 96-Mev protons.* Phys. Rev. **108**, 427 (1957).

Radiation Protection Dosimetry (2007), Vol. 126, No. 1–4, pp. 123–125 doi:10.1093/rpd/ncm026
Advance Access publication 17 May 2007

NEUTRON-INDUCED LIGHT-ION PRODUCTION FROM Fe, Pb AND U AT 96 MeV

S. Pomp[1,*], V. Blideanu[2], J. Blomgren[1], Ph. Eudes[3], A. Guertin[3], F. Haddad[3], C. Johansson[1], J. Klug[1], Ch. Le Brun[4], F. R. Lecolley[2], J. F. Lecolley[2], T. Lefort[2], M. Louvel[2], N. Marie[2], A. Prokofiev[5], U. Tippawan[6], A. Öhrn[1] and M. Österlund[1]
[1]Department of Neutron Research, Uppsala University, Sweden
[2]Laboratoire de Physique Corpusculaire, Caen, France
[3]SUBATECH, Nantes, France
[4]Laboratoire de Physique Subatomique et de Cosmologie, Grenoble, France
[5]The Svedberg Laboratory, Uppsala University, Sweden
[6]Fast Neutron Research Facility, Chiang Mai University, Thailand

Double-differential cross-sections for light-ion production (up to $A = 4$) induced by 96 MeV neutrons have been measured for Fe, Pb and U. The experiments have been performed at The Svedberg Laboratory in Uppsala, using two independent devices, MEDLEY and SCANDAL. The recorded data cover a wide angular range (20°–160°) with low energy thresholds. The data have been normalised to obtain cross-sections using np elastic scattering events. The latter have been recorded with the same setup, and results for this measurement are reported. The work was performed within the HINDAS collaboration with the primary aim of improving the database for three of the most important nuclei for incineration of nuclear waste with accelerator-driven systems. The obtained cross-section data are of particular interest for the understanding of the so-called pre-equilibrium stage in a nuclear reaction and will be compared with model calculations.

INTRODUCTION

To achieve a better understanding of nucleon-induced reactions in the 20–200 MeV range and develop improved models, detailed information on light-ion production in these reactions is needed. The need for such data comes also from a large number of applications. Incineration of nuclear waste using accelerator-driven systems is one example. For this reason, the interest in nucleon-induced reactions has been growing in the last few years. This interest has been manifested in part by extensive experimental campaigns, like the one carried out by several laboratories in Europe within the framework of HINDAS[(1)]. The results presented here are part of this program and concern double-differential cross-sections for light-ion emission (up to $A = 4$) induced by 96 MeV neutrons on ^{nat}Fe, ^{nat}Pb and ^{nat}U[(2)].

EXPERIMENTAL PROCEDURE

Experiments have been performed using the neutron beam available at The Svedberg Laboratory (TSL) in Uppsala, Sweden. The neutron beam characteristics (neutrons are not mono-energetic, large beam spot at the target position, and compared with proton beams of relatively low intensity) lead us to use two independent detection systems in order to obtain satisfactory count rate, keeping at the same time systematically uncertainties within reasonable limits.

The MEDLEY setup[(3)] is made of eight Si–Si–CsI telescopes, allowing detection of light-ions up to $A = 4$ with a low-energy threshold. The statistics accumulated using the MEDLEY setup is relatively poor, due to the thin targets used and to the small solid angles covered by the telescopes. The angular resolution is dictated by the target active area and by the opening angle of the telescopes. It was calculated using Monte Carlo simulations of the experiment, and the typical values found are of the order of 5° (FWHM).

In the case of the SCANDAL setup[(4)], the angular resolution is significantly improved by reconstructing proton trajectories using drift chambers. This device consists of two identical systems located on either side of the neutron beam. Each system uses two 2 mm thick plastic scintillators for triggering, two drift chambers for particle tracking and an array of 12 CsI detectors for energy determination. The emission angles of the particles are calculated using the trajectories in the drift chambers. The angular resolution achieved is of the order of 0.3°. A multi-target system (MTGT)[(5)] is used to increase the count rate without impairing the energy resolution. The MTGT allows up to seven targets to be mounted simultaneously, interspaced with multi-wire proportional counters. In this way, it is possible to study several reactions at the same time since we can determine from which target

*Corresponding author: Stephan.Pomp@tsl.uu.se

the particle has been emitted and apply corrections for energy losses in subsequent targets. In contrast to MEDLEY, SCANDAL has been used for proton detection only and with an energy threshold of $\sim$35 MeV, however, with a much higher count rate and better angular resolution.

Due to the difficulties encountered when monitoring neutron beam intensities, the absolute cross-section normalisation in neutron-induced reactions is a notorious problem. Therefore, the cross-sections are measured relative to the H(n,p) cross-section. For this reference cross-section, the most recent measurements[6] claim an absolute uncertainty of 2%. Values taken from Rahm *et al.*[6] have been used to calculate the absolute cross-sections presented in this work. Estimated systematic uncertainties affecting the experimental cross-sections reported are $<$5%.

RESULTS

The light-ion spectra have been measured for ^{nat}Fe, ^{nat}Pb and ^{nat}U over the 20–160° angular range. The low-energy threshold was 4 MeV for hydrogen isotopes, 12 MeV for ^{3}He and 8 MeV for alpha particles registered with MEDLEY and 35 MeV for proton detection in SCANDAL. The measurements were done up to the maximum possible energy. The energy bin has been fixed to 4 MeV, governed by the energy resolution of the detectors and the accumulated statistics. Figure 1a compares double-differential cross-sections for proton production from iron at 20°, independently measured by both the detection systems. Similar results have been obtained for all measured (n,xp) reactions and over the full angular range. The found good agreement, in the energy range covered by both measurements, shows that systematically uncertainties related to the cross-section normalisation are low. Figure 1b shows the Fe(n,xp) cross-section measured with MEDLEY at 20° together with data from Ronnqvist *et al.*[7], obtained using the magnetic spectrometer LISA. Also here, a good agreement is found between the two measurements in the common energy range. Similar agreement has been found for the Pb(n,xp) reaction.

The experimental double-differential cross-sections for the emission of hydrogen isotopes measured with MEDLEY are shown in Blideanu *et al.*[2].

Energy distributions are obtained from the double-differential cross-sections using the Kalbach systematics[8] to extrapolate the experimentally available angular range over the entire range. Experimental information on the energy-differential cross-sections is of great importance, since the agreement between calculations and experimental results for this observable is considered as a minimum condition to validate model predictions.

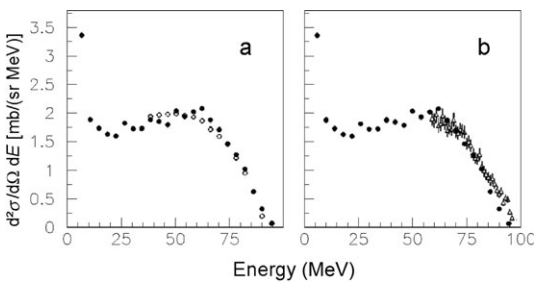

Figure 1. (a) Double-differential cross-sections for Fe(n,xp) at 20° measured by MEDLEY (filled circles) and SCANDAL (open circles). (b) Double-differential cross-sections for Fe(n,xp) at 20° measured by MEDLEY (filled circles) and data from Ronnqvist *et al.*[7] (open triangles).

COMPARISON WITH THEORETICAL CALCULATIONS

In Figures 2 and 3, the measured energy-differential cross-sections for p, d, t and alpha for 96 MeV neutrons on lead are compared with model calculations performed with the GNASH, TALYS and PREEQ codes. The GNASH code[9] describes the proton production rather well, while a strong underestimation is observed for the case of complex particles.

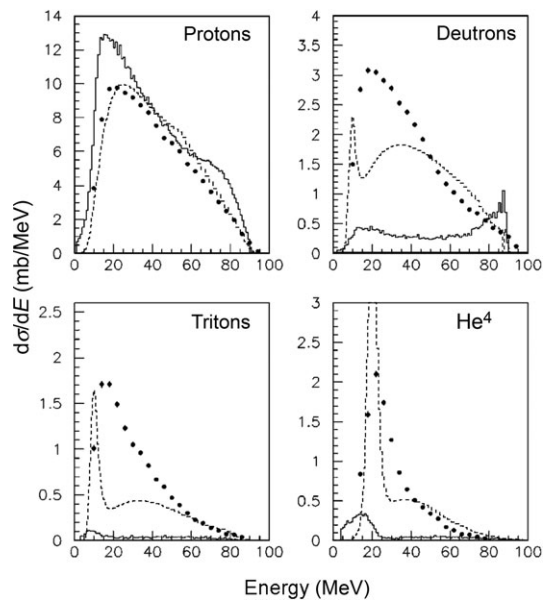

Figure 2. Energy-differential cross-sections calculated using the GNASH code (solid line) and the TALYS code (dashed line). The calculations have been done for 96 MeV neutrons on Pb. The experimentally obtained data are shown as points.

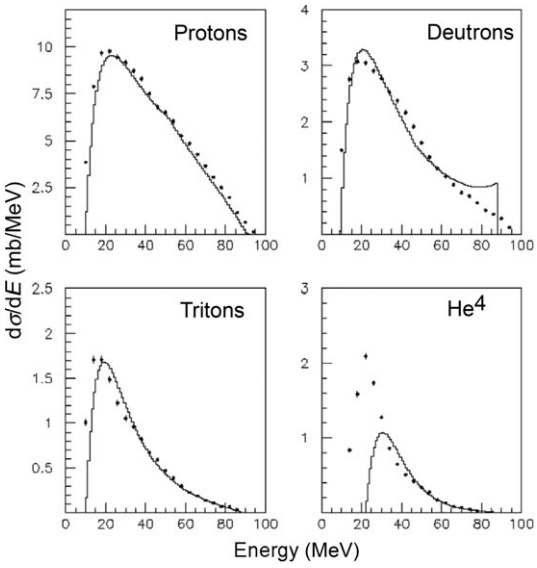

Figure 3. Same as Fig. 2, but for PREEQ calculations.

Improvements have recently been done with the TALYS code[10], taking into account the contribution of direct pick-up and knock-out reactions in the complex-particle emission spectra. Even if the agreement in the production rates for complex particles is significantly better, there are still important differences in the shape of the distributions.

A completely different approach takes into account the complex-particle formation probability in the pre-equilibrium stage. This process is treated in the framework of a coalescence model. The code PREEQ[11] uses this approach to calculate energy distributions for particle emission at pre-equilibrium. The results show a good agreement with the data in both shape and amplitude of the distributions.

SUMMARY

In this work, experimental double-differential cross-sections for light-ion production in 96 MeV neutron-induced reactions in iron, lead and uranium are reported. The extracted energy-differential cross-sections have been compared with model calculations by the GNASH, TALYS and PREEQ codes. The comparison of these calculations with the experimental data shows clearly that, despite the better agreement obtained with the TALYS code compared to the old version of the exciton model used in the GNASH code, improvements are still needed for a deep understanding of the reaction mechanisms leading to emission of complex-particles. An alternative is given by the PREEQ code, which takes the nucleon coalescence during the pre-equilibrium stage leading to cluster formation into account. This approach seems to give a better description of complex-particle emission in nucleon-induced reactions at intermediate energies.

ACKNOWLEDGEMENTS

This work was supported by the European Community under the HINDAS project (Contract No. FIKW-CT-2000-0031), the GDR GEDEON (Research Group CEA-CNRSEDF-FRAMATOME), Vattenfall AB, the Swedish Nuclear Fuel and Waste Management Company, the Swedish Nuclear Power Inspectorate, Barsebäck Power AB, Ringhals AB, the Swedish Defence Research Agency, and the Swedish Research Council. We would like to thank the TSL staff for assistance and quality of the neutron beam. The authors are also grateful to Dr. E. Betak for very useful discussions concerning calculations with the PREEQ code. Special thanks to Dr. C. Kalbach for her significant contributions to the progress of theory in nucleon-induced reactions.

REFERENCES

1. HINDAS: *High and Intermediate energy Nuclear Data for Accelerator-driven Systems.* (European Community). Contract No. FIKW-CT-2000-00031 (2000).
2. Blideanu, V. *et al. Nucleon-induced reactions at intermediate energies: new data at 96 MeV and theoretical status.* Phys. Rev. **C 70**, 014607 (2004).
3. Dangtip, S. *et al. A facility for measurements of nuclear cross sections for fast neutron cancer therapy.* Nucl. Instrum. Methods Phys. Res. **A 452**, 484 (2000).
4. Klug, J. *et al. SCANDAL—a facility for elastic neutron scattering studies in the 50–130 MeV range*, Nucl. Instrum. Methods Phys. Res. **A 489**, 282 (2002).
5. Condé, H. *et al. A facility for studies of neutron induced reactions in the 50–200 MeV range.* Nucl. Instrum. Methods Phys. Res. **A 292**, 121 (1990).
6. Rahm, J. *et al. np scattering measurements at 96 MeV.* Phys. Rev. **C 63** 044001 (2001).
7. Rönnqvist, T. *et al. The ^{54,56}Fe(n,p)^{54,56}Mn reactions at $E_n = 97$ MeV.* Nucl. Phys. **A 563,** 225 (1993).
8. Kalbach, C. *Systematics of continuum angular distributions: extensions to higher energies.* Phys. Rev. **C 37**, 2350 (1988).
9. Young, P. G., Arthur, E. D. and Chadwick, M. B. *Comprehensive nuclear model calculations: introduction to the theory and use of the GNASH Code.* Report No. LA-12343-MS (1992).
10. Koning, A. J., Hilaire, S. and Duijvestijn, M. C. *TALYS-0.64 user manual.* NRG Report rn21297/04.62741/P FAI/AK/AK (2004).
11. Betak, E. *Program for spectra and cross-section calculations with the pre-equilibrium model of nuclear reactions.* Comp. Phys. Comm. **9**, 92 (1975).

Radiation Protection Dosimetry (2007), Vol. 126, No. 1–4, pp. 35–39 doi:10.1093/rpd/ncm009
Advance Access publication 12 May 2007

LIGHT CHARGED-PARTICLE PRODUCTION IN 96 MeV NEUTRON-INDUCED REACTIONS ON CARBON AND OXYGEN

U. Tippawan[1,2], S. Pomp[2,*], J. Blomgren[2], S. Dangtip[1,2], C. Johansson[2], J. Klug[2], P. Mermod[2], L. Nilsson[2,4], A. Öhrn[2], M. Österlund[2], N. Olsson[2,3], A. V. Prokofiev[4], P. Nadel-Turonski[5], V. Corcalciuc[6], A. J. Koning[7] and Y. Watanabe[8]
[1]Fast Neutron Research Facility, Department of Physics, Chiang Mai University, Thailand
[2]Department of Neutron Research, Uppsala University, Sweden
[3]Swedish Defence Research Agency (FOI), Stockholm, Sweden
[4]The Svedberg Laboratory, Uppsala University, Sweden
[5]Department of Radiation Sciences, Uppsala University, Sweden
[6]Institute of Atomic Physics, Heavy Ion Department, Bucharest, Romania
[7]Nuclear Research and Consultancy Group NRG, Petten, The Netherlands
[8]Department of Advanced Energy Engineering Science, Kyushu University, Japan

In recent years, an increasing number of applications involving fast neutrons have been developed or are under consideration, e.g. radiation treatment of cancer, neutron dosimetry at commercial aircraft altitudes, soft-error effects in computer memories, accelerator-driven transmutation of nuclear waste and energy production and determination of the response of neutron detectors. Data on light-ion production in light nuclei such as carbon, nitrogen and oxygen are particularly important in calculations of dose distributions in human tissue for radiation therapy at neutron beams, and for dosimetry of high-energy neutrons produced by high-energy cosmic radiation interacting with nuclei (nitrogen and oxygen) in the atmosphere. When studying neutron dose effects, it is especially important to consider carbon and oxygen, since they are, by weight, the most abundant elements in human tissue. Preliminary experimental double-differential cross sections of inclusive light-ion (p, d, t, ^{3}He and α) production in carbon induced by 96-MeV neutrons have been presented. Energy spectra were measured at eight laboratory angles: 20, 40, 60, 80, 100, 120, 140 and 160°. Measurements were performed at The Svedberg Laboratory (TSL), Uppsala, using the dedicated MEDLEY experimental setup. The authors have earlier reported experimental double-differential cross sections of inclusive light-ion production in oxygen. In this paper, the deduced kerma coefficients for oxygen has been presented and compared with reaction model calculations.

INTRODUCTION

In the past few years, a number of applications involving fast neutrons have been developed or are under consideration, e.g. neutron dosimetry at commercial aircraft altitudes[1], fast-neutron cancer therapy[2,3], soft-error effects in computer memories induced by cosmic-ray neutrons[4], energy applications and determination of the response of neutron detectors. In fact, airplane personnel are the category that receives the largest doses in civil work, due to cosmic-ray neutrons. Cancer treatment with fast neutrons is performed routinely at about several facilities around the world, and today it represents the largest therapy modality besides the conventional treatments with photons and electrons. Data on light-ion production in light nuclei such as carbon, nitrogen and oxygen are particularly significant in calculations of dose distributions in human tissue for radiation therapy at neutron beams, and for dosimetry of high-energy neutrons produced by high-energy cosmic radiation interacting with nuclei (nitrogen and oxygen) in the upper atmosphere. When studying neutron dose effects in radiation therapy and at high altitude, it is particularly essential to consider carbon and oxygen, because they are the dominant elements (18 and 65% by weight, respectively) in average human tissue.

In this paper, experimental double-differential cross sections (inclusive yields) for protons, deuterons, tritons, ^{3}He and particles induced by 96-MeV neutrons incident on carbon are presented. Measurements have been performed at the cyclotron of The Svedberg Laboratory (TSL), Uppsala, using the dedicated MEDLEY experimental setup[5]. Spectra have been measured at eight laboratory angles, ranging from 20 to 160° in 20° steps. Partial kerma coefficients for oxygen are obtained directly from the measured microscopic cross sections for the five types of outgoing particles reported in Ref. (6).

EXPERIMENTAL METHODS

The neutron beam facility at TSL uses the ^{7}Li(p, n)^{7}Be reaction (Q = −1.64 MeV) to

*Corresponding author: stephan.pomp@tsl.uu.se

produce a quasi-monoenergetic neutron beam[7]. The 98.5 ± 0.3 MeV protons from the cyclotron impinge on the lithium target, producing a full energy peak of neutrons at 95.6 ± 0.5 MeV with a width of 3-MeV FWHM and containing 40% of the neutrons, and an almost constant low-energy tail containing 60% of the neutrons. The neutron beam is directly monitored by a thin-film breakdown counter (TFBC). Relative monitoring can be obtained by charge integration of the proton beam hitting the Faraday cup in the beam dump. The agreement between the two beam monitors was very good, deviating less than 2%, during the measurements.

The charged particles are detected by the MEDLEY setup. It consists of eight three-element telescopes mounted inside a 100-cm diameter evacuated reaction chamber. Each telescope has two fully depleted ΔE silicon surface barrier detectors. The thickness of the first ΔE detector (ΔE_1) is either 50 or 60 μm, whereas the second one (ΔE_2) is either 400 or 500 μm, and they are all 23.9 mm in diameter (nominal). In each telescope, a cylindrical CsI(Tl) crystal, 50-mm long and 40 mm in diameter, serves as the E detector.

A 22-mm diameter 500-μm-thick (cylindrical) disc of graphite is used as the carbon target and a same dimensional disk of fused quartz SiO_2 is used as the oxygen target. For the subtraction of the silicon contribution, measurements using a silicon wafer having a 32×32 mm^2 quadratic shape and a thickness of 303 μm are performed. For absolute cross section normalisation, a 25-mm diameter and 1.0-mm-thick polyethylene $(CH_2)_n$ target is used. The np cross section at 20° laboratory angle provides the reference cross section[8].

Background events, collected in target-out runs and analysed in the same way as target-in events, are subtracted from the corresponding target-in runs, with carbon, SiO_2 and silicon targets, after normalisation to the same neutron fluence.

The time-of-flight (TOF) obtained from the radio frequency of the cyclotron (stop signal for TDC) and the timing signal from each of the telescopes (start signal) is measured for each charged-particle event.

DATA REDUCTION PROCEDURES

The ΔE–E technique is used to identify light charged particles ranging from protons to lithium ions. Good separation of all particles is obtained over their entire energy range and therefore the particle identification procedure is straightforward.

Energy calibration of all detectors is obtained from the data itself[9,10]. Events in the ΔE–E bands are fitted with respect to the energy deposited in the two silicon detectors. This energy is determined from the detector thicknesses and calculations of energy loss in silicon. Supplementary calibration points are provided by the H(n, p) reaction, as well as transitions to the ground state and low-lying states in the ^{12}C(n, p)^{12}B and ^{12}C(n, d)^{11}B reactions. The energy of each particle type is obtained by adding the energy deposited in each element of the telescope.

Low-energy charged particles are stopped in the ΔE_1 detector, leading to a low-energy cutoff for particle identification of about 3 MeV for hydrogen isotopes and about 8 MeV for helium isotopes. The helium isotopes stopped in the ΔE_1 detector are nevertheless analysed and a remarkably low cutoff, ~4 MeV, can be achieved for the experimental alpha-particle spectra. These alpha-particle events could obviously not be separated from ^{3}He events in the same energy region, but the yield of ^{3}He is much smaller than the alpha-particle yield in the region just above 8 MeV, where the particle identification works properly. That the relative yield of ^{3}He is small is also supported by the theoretical calculations in the evaporation peak region. In conclusion, the ^{3}He yield is within the statistical uncertainties of the alpha-particle yield for alpha energies between 4 and 8 MeV. Knowing the energy calibration and the flight distances, the TOF for each charged particle from target to detector can be calculated and subtracted from the registered total TOF. The resulting neutron TOF is used for selection of charged-particle events induced by neutrons in the main peak of the incident neutron spectrum.

Absolute double-differential cross sections are obtained by normalising the target-in data to the number of recoil protons emerging from the CH_2 target. After selection of events in the main neutron peak and proper subtraction of the target-out and ^{12}C(n, px) background contributions, the cross section can be determined from the recoil proton peak, using *np* scattering data[8]. All data have been normalised using the *np* scattering peak in the 20° telescope.

Owing to the finite target thickness, corrections for energy loss and particle loss are applied to all targets individually. Details of the correction methods are described in Refs. (9,10). The cross sections for carbon are obtained directly after the thick target corrections, whereas the cross sections for oxygen are achieved after subtraction of the silicon data from the SiO_2 data with proper normalisation with respect to the number of silicon nuclei in the two targets.

RESULTS AND DISCUSSION

Preliminary double-differential cross sections for the ^{12}C(n, px), ^{12}C(n, dx) and ^{12}C(n, αx) reactions at laboratory angles of 20, 40, 100 and 140° are shown in Figures 1–3, respectively. The error bars represent statistical uncertainties only and the systematic

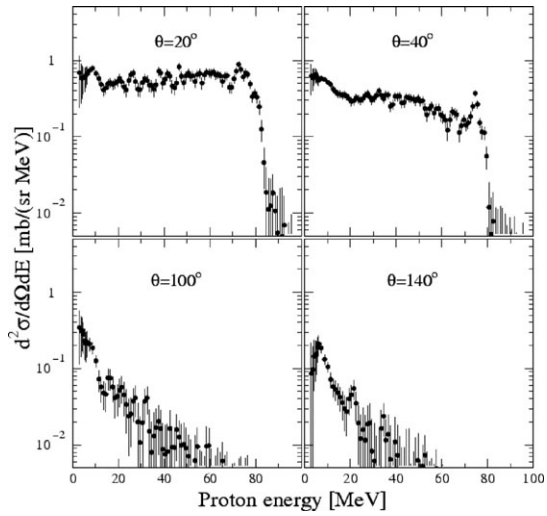

Figure 1. Preliminary double-differential cross sections (filled circles) of the C(n, px) reaction at 96 MeV at four laboratory angles.

uncertainty contributions are due to thick target correction (1–20%), collimator solid angle (5–9%), beam monitoring (2–3%), number of carbon nuclei (<5%), CsI(Tl) intrinsic efficiency (1%), particle identification (2%) and dead time (<0.1%).

The uncertainty in the absolute cross section normalisation is ~4%, which is due to uncertainties in the contribution from the low-energy continuum of the ^{7}Li(p, n) spectrum to the np scattering proton peak (3%), reference np cross sections (2%)[8], statistics in the np scattering proton peak (2%) and carbon contribution (0.1%).

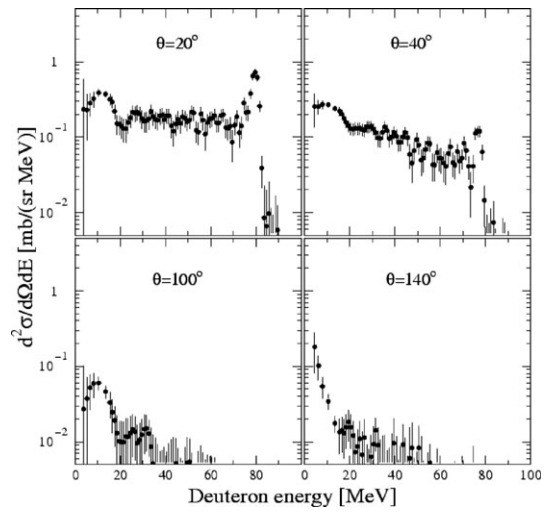

Figure 2. Same as Figure 1 for the C(n, dx) reactions.

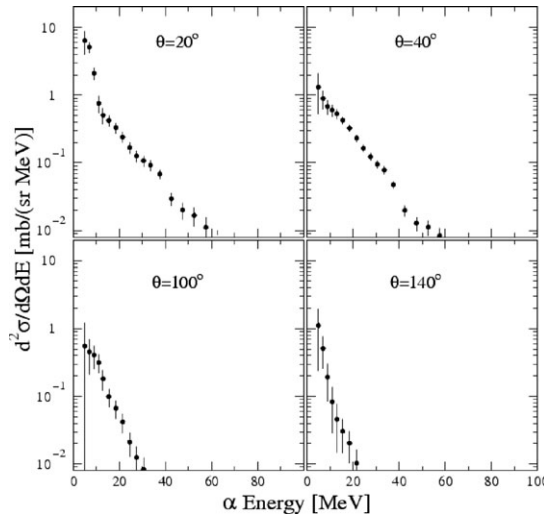

Figure 3. Same as Figure 1 for the C(n, α*x*) reactions.

All the particle spectra at forward angles show relatively large yields at medium-to-high energies. The emission of high-energy particles is strongly forward-peaked and hardly visible in the backward hemisphere. In addition to this broad distribution of emitted particles, the deuteron spectra at forward angles show narrow peaks corresponding to transitions to the ground state and low-lying states in the final nucleus, ^{11}B. These transitions are most likely due to pickup of weakly bound protons in the target nucleus, ^{12}C. A similar but less pronounced effect is observed in the proton spectra at forward angles.

Partial kerma coefficients were calculated from energy-differential cross sections[5] using

$$k_\phi = N \sum_i \left(\int \frac{\mathrm{d}^2\sigma}{\mathrm{d}\Omega\ \mathrm{d}E}(\theta,\ E_i)\mathrm{d}\Omega \right)_i E_i \Delta E_i = N \sum_i \left(\frac{\mathrm{d}\sigma}{\mathrm{d}E}(E_i) \right)_i E_i \Delta E_i \quad (1)$$

where N gives the number of nuclei in the target per unit mass, i denotes the energy bin number and E_i is the centroid of the energy bin with the width ΔE_i. For the oxygen data we have $N = 0.603225 \times 10^{-3}$. Table 1 presents the resulting experimental and theoretical partial kerma coefficients for the five types of outgoing particles in oxygen, induced by 96-MeV neutrons. The experimental values have to be corrected for the undetected particles below the low-energy cutoff to be compared with the calculated kerma.

The deduced kerma coefficients for protons, deuterons and a particles agree well with the calculated

Table 1. Partial kerma coefficients for protons, deuterons, tritons, ^{3}He and α particles in oxygen, induced by 96-MeV neutrons, from the present work.

k_ϕ	Experiment (fGy/m^2)	Cutoff corrected experiment		Theoretical calculation	
		GNASH	TALYS	GNASH	TALYS
(n, px)	3.99 ± 0.20	4.02	3.99	3.574	3.253
(n, dx)	1.31 ± 0.07	1.32	1.31	1.239	2.971
(n, tx)	0.24 ± 0.01	—	0.24	—	0.134
(n, ^{3}Hex)	0.11 ± 0.01	—	0.12	—	0.087
(n, αx)	0.80 ± 0.04	0.92	0.80	0.985	0.730

Theoretical values resulting from GNASH[11] and TALYS[12] calculations are given as well. The experimental data in the second column have been obtained with cutoff energies of 2.5, 3.0, 3.5, 8.0 and 4.0 MeV for p, d, t, ^{3}He and α particles, respectively. The third and forth columns show data corrected for these cutoffs, using the GNASH and the TALYS calculations, respectively.

kerma base on the GNASH[11] model. The TALYS[12] calculations overpredict the measured deuteron kerma coefficient by a factor of 2 or more. For the other types of particles, the TALYS calculations greatly underpredict the measured kerma coefficients.

CONCLUSION AND OUTLOOK

In the present paper, experimental data sets on light-ion production in carbon and oxygen induced by 96-MeV neutrons are reported. Experimental double-differential cross sections are measured at eight angles between 20 and 160°. The partial kerma coefficients for light-ion production for oxygen are presented and compared with the theoretical calculations based on the GNASH and the TALYS models. The carbon data are still preliminary and further minor corrections, such as the wraparound correction described in Refs. (9,10), have to be applied.

Because the use of kerma is widely spread in the dosimetry community, the authors report the derived kerma values. Nevertheless, we would like to emphasise the superior amount of information which is contained in microscopic data of the type presented here and which can be used directly in dosimetry applications[13].

ACKNOWLEDGEMENTS

This work was supported by the Swedish Natural Science Research Council, the Swedish Nuclear Fuel and Waste Management Company, the Swedish Nuclear Power Inspectorate, Ringhals AB and the Swedish Defence Research Agency. The authors wish to thank the The Svedberg Laboratory for excellent support.

REFERENCES

1. O'Sullivan, D., Zhou, D. and Flood, E. *Investigation of cosmic rays and their secondaries at aircraft altitudes*. Radiat. Meas. **34**, 277–280 (2001).
2. Orecchia, R., Zurlo, A., Loasses, A., Krengli, M., Tosi, G., Zurrida, S., Zucali, P. and Veronesi, U. *Particle beam therapy (Hadron therapy): Basis for interest and clinical experience*. Eur. J. Cancer **34**, 459 (1998).
3. Schwartz, D.L., Einck, J., Bellon, J. and Laramore, G.E. *Fast neutron radiotherapy for soft tissue and cartilaginous sarcomas at high risk for local recurrence*. Int. J. Radiat. Oncol. Biol. Phys. **50**, 449 (2001).
4. Tang, H.H.K. and Olsson, N. *Single-event upsets in microelectronics*, topical issue, Mat. Res. Soc. Bull. **28** (2003).
5. Dangtip, S. *et al. A facility for measurements of nuclear cross sections for fast neutron cancer therapy*. Nucl. Instr. Meth. Phys. Res. A **452**, 484 (2000).
6. Tippawan, U. *et al. Light-ion production in the interaction of 96 MeV neutrons with oxygen*. Phys. Rev. C **73**, 034611 (2006).
7. Klug, J. *et al. SCANDAL–a facility for elastic neutron scattering studies in the 50–130 MeV range*. Nucl. Instr. Meth. Phys. Res. A **489**, 282 (2002).
8. Rahm, J. *et al. np scattering measurements at 96 MeV*. Phys. Rev. C **63**, 044001 (2001).
9. Tippawan, U. *et al. Light-ion production in the interaction of 96 MeV neutrons with silicon*. Phys. Rev. C **69**, 064609 (2004).
10. Tippawan, U. Secondary Particle Spectra from Neutron Induced Nuclear Reaction in the 14–100 MeV Region, Doctoral thesis, Chiang Mai University (2004) (unpublished).

11. ICRU Report 63, International Commission on Radiation Units and Measurements, Bethesda, MD, March 2000.
12. Koning, A. J., Hilaire, S. and Duijvestijn, M. C. *TALYS-0.64 User Manual*, December 5, 2004, NRG Report 21297/04.62741/P FAI/AK/AK.
13. Blomgren, J. and Olsson, N. *Beyond kerma – neutron data for biomedical applications.* Radiat. Prot. Dosim. **103**, 293–304 (2003).

Radiation Protection Dosimetry (2007), Vol. 126, No. 1–4, pp. 394–397 doi:10.1093/rpd/ncm081
Advance Access publication 11 May 2007

A MONITOR FOR NEUTRON FLUX MEASUREMENTS UP TO 20 MeV

A. Öhrn,[1,*], J. Blomgren[1], H. Park[2], S. Khurana[3], R. Nolte[3], D. Schmidt[3] and K. Wilhelmsen[4]
[1]Department of Neutron Research, Uppsala University, Sweden
[2]Korean Research Institute of Standards and Science, Daejeon, Korea
[3]Physikalisch-Technische Bundesanstalt, Braunschweig, Germany
[4]Swedish Defense Research Agency, Stockholm, Sweden

A liquid scintillation detector aimed for neutron energy and fluence measurements in the energy region <20 MeV has been calibrated using monoenergetic and white spectrum neutron fields. Careful measurements of the proton light output function and the response matrix have been performed allowing for the application of unfolding techniques using existing codes. The response matrix is used to characterise monoenergetic neutron fields produced by the T(d,n) at a low-energy deuteron accelerator installed at the Swedish Defense Research Agency (FOI).

INTRODUCTION

The strongly expanding importance of fast neutrons in a number of applications requires steps to be taken to improve the technology for neutron fluence and energy measurements in various energy ranges. This requirement has been addressed and the current situation summarised at recent workshops[1,2].

For the application considered in this work—a monitor for fluence and energy measurements in the energy region from a few MeV to ~20 MeV—there are several options possible, but if resolution and detection efficiency are taken into consideration, the most attractive alternatives seem to be the organic scintillator with or without applying time-of-flight (TOF) techniques. In this application, the neutron source is continuous and therefore the TOF technique is out of question. The obvious choice is therefore to perform pulse-height spectrum measurements and to apply unfolding techniques.

In this paper, a calibration procedure for a liquid scintillator with pulse-shape discrimination possibilities is described. The method is based on the procedures developed at the Physikalisch-Technische Bundesanstalt (PTB), Braunschweig, Germany[3] and involves measurements of pulse-height spectra and unfolding of these spectra with existing computer codes using carefully recorded response functions at several energies in the region of interest. The procedure presented in this paper goes beyond the previously applied methods in that both the experimental and calculated response matrices are used with existing unfolding codes to determine the energy and fluence of monoenergetic neutron fields and make comparisons with TOF methods.

*Corresponding author: angelica.ohrn@tsl.uu.se

EXPERIMENTAL METHODS

For neutron energies <20 MeV, the response matrix of a scintillation detector can be calculated using Monte Carlo codes provided the specific light outputs for protons, deuterons and alpha particles are known for that particular detector. For energies above ~8 MeV, however, no available Monte Carlo code is capable of describing the response of a scintillation detector in full detail, because the required sufficiently detailed multidifferential emission cross-sections for alpha particles from the $^{12}C(n,n'3\alpha)$ reaction are not available. Hence, the characterisation of scintillation detectors always requires an experimental investigation of the detector response. The standard procedure developed at PTB for the characterisation of scintillation detectors uses monoenergetic and breakup neutrons produced with the D(d,n) reaction.

The standard procedure is satisfactory for the application of the TOF method. For the application of unfolding techniques, however, a proper description of the full response matrix is required since any deviation of the response matrix from the 'true' pulse-height response of the detector would cause spurious structures in the unfolded spectral fluence.

For this purpose, a method described by Dekempeneer *et al.*[4] has been adopted. A white neutron beam measurement is used to obtain a smooth light output function for protons and an experimental response matrix with sufficient resolution in neutron energy. This method has been tested on a liquid scintillator to be used as a neutron monitor for a DT neutron generator, i.e. a commercial cylindrical detector cell of the MAB-1F type filled with BC501 scintillator liquid.

The PTB standard procedure for the determination of the relevant properties of an organic

scintillation detector has been described in detail elsewhere[3]. Only the results obtained for the particular detector under study are summarised here.

Five neutron beams were produced by deuterons with energies of 5.01, 7.12, 9.06, 10.30 and 11.27 MeV using a deuterium gas target at the PTB neutron scattering facility. The energies of the monoenergetic neutrons were 7.95, 10.05, 11.93, 13.12 and 14.05 MeV. The maximum energy of the corresponding breakup continua was $\sim$6.5 MeV below that of the monoenergetic neutrons. About 30 narrow TOF windows were placed on the monoenergetic neutrons and the breakup continuum to produce pulse-height spectra, which were used to determine the proton light output and the efficiency of the detector.

The Monte Carlo code NRESP7[5] was used to calculate pulse-height spectra for comparison with experimental spectra obtained at the five energies where monoenergetic neutrons from the D(d,n)^{3}He reaction were available. By fitting these calculated spectra to the experimental ones, the light output function for protons, i.e. the pulse height corresponding to the recoil proton edge, was determined with an iterative procedure. The pulse height was measured using a calibration with photon sources.

The fluences of the monoenergetic neutrons were measured with the PTB $4'' \times 1''$ NE213 reference detector. This detector was repeatedly compared with the PTB recoil proton telescope. For a selected pulse-height threshold, the efficiency of the detector is known with an uncertainty of $\sim$1.5%[6]. The mean ratio of the fluence determined with the present BC501 detector and that measured with the PTB reference detector was 1.018 ± 0.009, which is within the range of results for other detectors[3].

A white neutron beam was produced at the PTB TOF facility by bombarding a thick Be target with a 19 MeV proton beam from the PTB isochronous cyclotron. The maximum energy of the neutron field at an emission angle of 0° is 17.15 MeV. The neutron field was collimated by one of the collimators of the PTB TOF facility. The scintillation detector was positioned at a distance of 27.39 m from the Be target.

Energy calibration of the pulse-height spectra was established using ^{137}Cs, ^{22}Na and ^{207}Bi photon sources. The calibration of the measured pulse height in the electron energies and the electronic offset were determined by fitting pulse-height spectra calculated with the PHRESP code[7] to the experimental spectra.

To establish an experimental response matrix, the PH spectra obtained with the white beam have to be normalised to unit fluence at the centre of the detector. This normalisation was carried out by fitting PH spectra calculated with NRESP7 to the experimental ones. The fit was restricted to the region extending from the beginning of the flat plateau to the recoil proton edge. This region is essentially determined by np scattering and can be accurately described by NRESP7.

TESTS OF RESPONSE MATRICES IN MONOENERGETIC NEUTRON FIELDS

In the present work, it was considered important to test the calculated and experimental response matrices in well-defined monoenergetic neutron fields in an energy region of relevance for the actual application. Such a test was regarded as particularly relevant, because of the observed deviations between the experimentally determined response matrix and the calculated one.

The experimental response matrix was tested in monoenergetic neutron fields with energies between 14 and 15.5 MeV. These fields were produced by the T(d,n)^{4}He reaction. Deuteron beams of 242, 412 and 643 keV were produced with the PTB 3.5 MeV van-de-Graaff accelerator. The spectral distributions of the neutron fields were calculated with the TARGET code[8]. The calculated average energies at 0° were 14.85, 14.99 and 15.60 MeV, respectively, and the corresponding calculated FWHM of the peaks amounted to 451, 699 and 644 keV. For the 412 keV deuteron beam, measurements were also carried out at a neutron emission angle of 98°. At this angle, the T(d,n)^{4}He reaction shows so-called kinematical focusing, i.e. the energy of the emitted neutrons is almost independent of the energy of the incident deuterons. Hence, broadening of the spectral distribution of the neutrons due to the energy loss of the deuterons in the Ti(T) layer is very small. In this particular case, the neutron field had a peak energy of 13.98 MeV and a FWHM of only 17 keV according to the TARGET calculations, which were carried out neglecting the angular straggling of the deuterons in the target.

The pulse-height spectra obtained during the present measurements were unfolded with the MAXED code[9] which is part of the UMG code package[10]. It was known from the TOF measurements that the spectral neutron distribution showed a D(d,n) background peak between 2 and 4 MeV in addition to the dominant T(d,n) peak at energies $>$14 MeV. Using this preinformation, the unfolding was carried out in two steps. First, a high PH threshold of 7 MeV corresponding to a neutron energy of a $\sim$11.2 MeV was used to select those events, which could not be caused by the low-energy background. The spectral fluence distribution obtained from this restricted unfolding exhibited a prominent peak and some background at intermediate energies. Second, this peak was used as preinformation for the next step of the unfolding procedure that comprised the pulse-height spectrum above a PH threshold of 280 keV.

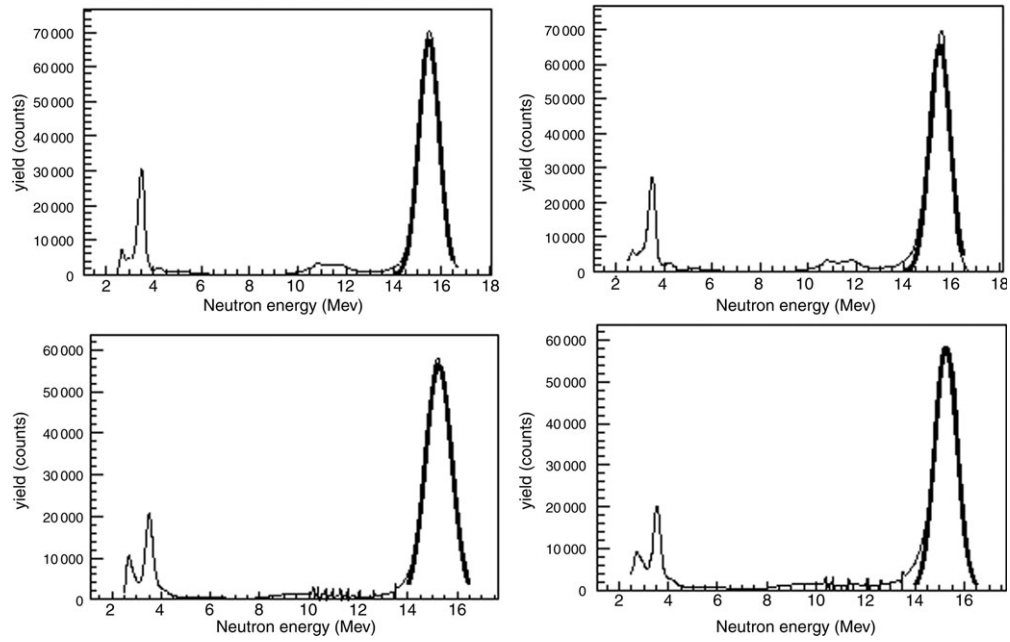

Figure 1. Results from the 15.60 MeV measurements. The unfolding in the left panels are performed with GRAVEL and those in the right panels with MAXED. In the upper panels, the experimental response is used and in the lower panels, the calculated one.

RESULTS AND DISCUSSION

The experimental and calculated response matrices were applied with unfolding codes available in the literature to determine the energy and fluence of monoenergetic neutron fields. Comparison with results from TOF measurements was performed.

Determination of the neutron energy has been performed from experiments performed with neutron energies of 13.98, 14.85 and 15.60 MeV. The pulse-height spectrum has been unfolded using MAXED as well as GRAVEL, the latter being another unfolding code in the UMG package[10]. Both codes give a good description of the neutron distribution. However, some spurious structures are generated especially in the low-energy region. A small structure $\sim$11 MeV can also be seen (Figure 1). There is no significant difference between GRAVEL and MAXED when determining the neutron energy (Table 1). The result from unfolding with the experimental response matrix is in better agreement with the result from the TOF measurements than the result from the calculated response matrix.

The absolute efficiency of the detector has been determined using the PTB proton recoil telescope. These measurements have verified that the efficiency, in terms of total number of counts in the detector above a threshold set at a low-pulse height, agrees with what can be expected with the used tagged neutron flux. This has been corroborated using the fact that the pulse height spectrum in the high-energy end is dominated by events due to np

Table 1. Results of the neutron energy measurements. Errors are statistical only.

Unfolding code	Response matrix	Neutron energy (MeV)
$E_n = 13.98$ MeV		
GRAVEL	Experimental	13.91 ± 0.02
GRAVEL	Calculated	13.67 ± 0.01
MAXED	Experimental	13.92 ± 0.03
MAXED	Calculated	13.70 ± 0.02
$E_n = 14.85$ MeV		
GRAVEL	Experimental	14.69 ± 0.02
GRAVEL	Calculated	14.43 ± 0.01
MAXED	Experimental	14.71 ± 0.03
MAXED	Calculated	14.47 ± 0.02
$E_n = 15.60$ MeV		
GRAVEL	Experimental	15.48 ± 0.01
GRAVEL	Calculated	15.26 ± 0.01
MAXED	Experimental	15.51 ± 0.03
MAXED	Calculated	15.26 ± 0.01

scattering, because the np scattering cross-section is well known at these energies.

The neutron fluence has been determined by integrating the T(d,n) peak from $E_0-\Gamma$ to $E_0+\Gamma$, where E_0 is the centroid and Γ is the FWHM (Figure 1). The intrinsic uncertainty of this method has been determined to 0.5% on the average with a worst case of 1.0%.

The fluence obtained from the TOF spectrum from the 15.60 MeV measurement agrees well with the fluence derived from unfolding with the experimental response matrix. The deviations are 0.7 (GRAVEL) and 1.9% (MAXED). The deviations are significantly larger in the unfolding with the calculated response matrix, 1.6% (GRAVEL) and 5.8% (MAXED). In all cases, the fluence obtained from unfolding is lower than that from the TOF information. On the basis of this information, it is concluded that the fluence can be determined with an uncertainty of 2% using this method.

CONCLUSIONS

The present work has shown that measurements in white neutrons beams can provide additional information for the specification of scintillation detectors, which cannot be obtained with monoenergetic neutron beams alone. In particular, smoother experimental light outputs can be obtained and the deficiencies of the present Monte Carlo codes used for the calculation of response matrices can be circumvented. On the other hand, the application of the TOF method for the determination of experimental response matrices with white neutron beams requires very careful experimental work to avoid artefacts like those observed in the present data for neutron energies >12 MeV. The application of the unfolding technique with experimentally determined response matrices provides a possibility for spectrometry in neutron beams over a large energy range. The present work has shown that even quite small spectral details can be resolved in the presence of other dominant structures.

ACKNOWLEDGEMENTS

The authors are indebted to A. Zimbal for guiding them through the technical pitfalls of the unfolding codes and for numerous discussions on this subject. The support of K. Tittelmeier, A. Toll and the staff of the PTB accelerator facility is gratefully acknowledged.

REFERENCES

1. Proceedings of the International Workshop on Neutron Field Spectrometry in Science, Technology and Radiation Protection, Pisa, Italy, June 4–8, 2000. In: Klein, H., Thomas, D., Menzel, H.G., Curzio, G. and d'Errico, F. Eds, Nucl. Instrum. Meth. Phys. Res. A, **476**, (1–2), 1 (2002).
2. Öhrn, A., Blomgren, J., Park, H., Khurana, S., Nolte, R., Schmidt, D. and Wilhelmsen, K. A monitor for neutron flux measurements up to 20 MeV, International workshop on Fast Neutron Detectors and Applications, Cape Town, South Africa, April 3–6, 2006. Proceedings of Science, PoS(FNDA2006)048.
3. Schmidt, D., Asselineau, B., Böttger, R., Klein, H., Lebreton, L., Neumann, S., Nolte, R. and Pichenot, G. *Characterization of liquid scintillation detectors.* Nucl. Instrum. Meth. Phys. Res. A, **476**, 186 (2002).
4. Dekempeneer, E., Liskien, H., Mewissen, L. and Poortmans, F. *A spectrometer for double-differential neutron-emission cross-section measurements in the energy range 1.6 to 16 MeV.* Nucl. Instrum. Meth. Phys. Res. A, **256**, 489 (1987).
5. Dietze, G. and Klein, H. *NRESP4 and NEFF4: Monte Carlo codes for the calculation of neutron response functions and detection efficiencies for the NE213 scintillation detectors.* PTB Report PTB-ND-22, (Braunschweig) (1982), (and an informal supplement describing the changes of version 7, 1991).
6. Schmidt, D. and Klein, H. *Precise time-of-flight spectrometry of fast neutrons—principles, methods and results.* PTB Report PTB-N-35 (Braunschweig), (1998).
7. Novotny, T. *Photon spectrometry in mixed neutron-photon fields using NE213 liquid scintillation detectors.* PTB Report PTB-N-28 (Braunschweig), (1997).
8. Schlegel, D. *TARGET user's manual*, PTB Laboratory Report PTB-6.41-98-1 (Braunschweig), (1998).
9. Reginatto, M., Goldhagen, P. and Neumann, S. Nucl. Instrum. Meth. Phys. Res. A, **476**, 242 (1989).
10. Reginatto, M., Wiegel, B. and Zimbal, A. *UMG-Code Package.* Available on Nuclear Energy Agency (NEA) Data Bank, http://www.nea.fr.

Radiation Protection Dosimetry (2007), Vol. 126, No. 1–4, pp. 491–496 doi:10.1093/rpd/ncm099
Advance Access publication 11 May 2007

THE PROBLEMS ASSOCIATED WITH THE MONITORING OF COMPLEX WORKPLACE RADIATION FIELDS AT EUROPEAN HIGH-ENERGY ACCELERATORS AND THERMONUCLEAR FUSION FACILITIES

P. Bilski[1], J. Blomgren[2], F. d'Errico[3], A. Esposito[4], G. Fehrenbacher[5], F. Fernàndez[6], A. Fuchs[7], N. Golnik[8], V. Lacoste[9], A. Leuschner[10], S. Sandri[11], M. Silari[12,*], F. Spurny[13], B. Wiegel[14] and P. Wright[15]
[1]IFJ, Krakow, Poland
[2]TSL/INF, Uppsala University, Sweden
[3]DIMNP, Pisa, Italy
[4]INFN, Frascati, Italy
[5]GSI, Darmstadt, Germany
[6]UAB, Barcelona, Spain
[7]PSI, Villigen, Switzerland
[8]IAE, Swierk, Poland
[9]IRSN, Cadarache, France
[10]DESY, Hamburg, Germany
[11]ENEA, Frascati, Italy
[12]CERN, Geneva, Switzerland
[13]NPI ASCR, Prague, Czech Republic
[14]PTB, Braunschweig, Germany
[15]RAL, Didcot, UK

The European Commission is funding within its Sixth Framework Programme a three-year project (2005–2007) called CONRAD, COordinated Network for RAdiation Dosimetry. The organisational framework for this project is provided by the European Radiation Dosimetry Group EURADOS. One task within the CONRAD project, Work Package 6 (WP6), was to provide a report outlining research needs and research activities within Europe to develop new and improved methods and techniques for the characterisation of complex radiation fields at workplaces around high-energy accelerators, but also at the next generation of thermonuclear fusion facilities. The paper provides an overview of the report, which will be available as CERN Yellow Report.

INTRODUCTION

Monitoring of ionising radiation around high-energy particle accelerators is a difficult task due to the complexity of the radiation field. The capability to distinguish between the high- (mostly neutrons) and the low-LET (Linear Energy Transfer) components of the radiation field at workplaces, and to correctly measure them, is of primary importance to evaluate the exposure of personnel. At proton machines, the dose equivalent outside a thick shield is mainly due to neutrons, with some contribution from photons and, to a minor extent, charged particles. At certain locations, the radiation field may contain neutrons with energies exceeding tens of MeV, which contribute 30 to 50% of the ambient dose equivalent outside the shielding. At high-energy electron accelerators, the dominant secondary radiations are high-energy neutrons, the shielding being thick enough to absorb most of the bremsstrahlung photons.

*Corresponding author: marco.silari@cern.ch

Similar high- and low-LET radiation components are present at experimental nuclear fusion facilities. The nuclear reactions employed—the deuterium–deuterium (D–D) and the deuterium–tritium (D–T)—produce high flux of fast neutrons. The plasma current in the toroidal vessels (tokamak) of fusion experiments based on magnetic confinement, the most practised fusion technology in Europe, generates bremsstrahlung X rays. Special system components of some fusion facilities, like neutral beam injectors, have their own radiation environment due to neutron and photon fields. Neutron activation for D–T based systems like JET is elevated in the in-vessel components and sometimes it is important also in the material of some associated devices, like in the water cooling system of the ITER project. The resulting radiation fields at workplaces, out of the concrete shielding that encase the main fusion facilities, are dominated by thermal neutrons but fast neutrons and photons are also present.

Neutron and photon dosimetry and spectrometry are thus essential tools in radiation protection

dosimetry around both high-energy particle accelerators and nuclear fusion facilities. There are some similarities between these radiation fields and those encountered at flight altitudes, and it is actually possible to partly 'simulate' the radiation field in the atmosphere with accelerator-produced radiation[1]. However, one important difference is that accelerators can operate in pulsed mode so that the radiation fields at workplaces can be pulsed. This is an important aspect to be taken into account for instrument response, and the measurements of average dose equivalent rates for radiation protection purposes in these fields present a challenge for instrumentation.

The European Commission is funding within its Sixth Framework Programme a three-year project (2005–2007) called CONRAD, COordinated Network for RAdiation Dosimetry. The organisational framework for this project is provided by the European Radiation Dosimetry Group EURADOS. One task within the CONRAD project, Work Package 6 (WP6), was to provide a report outlining research needs and research activities within Europe to develop new and improved methods and techniques for the characterisation of complex radiation fields at workplaces around high-energy accelerators, but also at the next generation of thermonuclear fusion facilities.

The CONRAD WP6 report[2] reviews the relevant techniques and instrumentation employed for monitoring neutron and photon fields around high-energy accelerators and fusion facilities (mainly JET and ITER), both in terms of dosimetry and spectrometry, emphasising some recent developments to improve the response of neutron measuring devices beyond 20 MeV. The report also reviews the major high-energy European accelerator facilities—both research accelerators and hospital-based hadron therapy centres—and the way workplace monitoring is organised at each of them. On-going research in radiation dosimetry and development work in passive dosimetry and active counting and spectrometric instrumentation at several European laboratories are discussed. Calibration problems are addressed, and the neutron calibration facilities available in Europe are listed. This paper provides a brief overview of the report, focusing in particular on some of the most important issues, such as the influence of the pulsed nature of the radiation field on the instrument and the calibration problems. For the review of the instrumentation and of the European facilities, the reader should refer to ref. (2).

MONITORING OF MIXED RADIATION FIELDS

Two types of dose quantities exist for radiological protection: body-related 'protection quantities' defined by the International Commission on Radiological Protection (ICRP)[3] and 'operational quantities' defined by the International Commission on Radiation Units and Measurements (ICRU)[4]. Although protection quantities serve to define dose limits that are not directly measurable, the exposure can be monitored by calculations or by measuring the operational quantities. Calculations of protection quantities require comprehensive knowledge of the energy and direction distribution of the particles in the radiation field and of their interaction with tissue.

One operational dose quantity suited to demonstrate compliance with the limits of the effective dose at workplaces is the ambient dose equivalent, $H^*(10)$, which is the dose equivalent, H, at a reference point at 10-mm depth in the ICRU sphere under defined irradiation conditions. Many radiation protection instruments used to measure $H^*(10)$ follow measurement principles other than those used in the definition and therefore require calibration with respect to this quantity. An alternative and, in general, more accurate procedure is to measure the spectral neutron fluence and fold this information with an appropriate set of fluence to dose equivalent conversion coefficients. In practice, monitoring instruments usually have a response function, which approximately follows $H^*(10)$ for a given type of radiation and over a given energy range. The approaches to the determination of ambient dose equivalent for neutrons are discussed in detail in ICRU Report 66[5].

Starting from the beam parameters of the accelerator important to radiation monitoring (type, energy, intensity and time structure of the accelerated particles) or from the characteristics of the radiation produced at nuclear fusion facilities, one can make predictions of the composition of the radiation field outside the shielding and then decide the type of area monitors to be employed (active and/or passive) and how to calibrate them.

PULSED FIELDS AND INSTRUMENT RESPONSE

Most accelerators operate in pulsed mode. Usually such sources deliver their output pulses in time intervals from nanoseconds to tens of microseconds spaced by at least a few milliseconds. This also concerns most of the conventional electron linacs used in radiotherapy, which are operated at 100–400 Hz with pulse widths of about 1–10 μs. In some accelerators, the microsecond output pulses consist of a series of separate 'bunches' each of duration of a few picoseconds, although the interval between bunches is generally less than one nanosecond. This time structure within the microsecond pulse can usually

be ignored for radiation field spectrometry and dosimetry.

Radiation protection at workplaces deals with stray radiation fields outside the shielding. At high-energy accelerators, such radiation fields comprise neutrons, photons and charged particles, with pulses that are usually shorter than 10 μs with high instantaneous fluence rates and dose rates. Measurements of the average dose equivalent (rate) for radiation protection purpose in these fields present a challenge for instrumentation and may become even more difficult at workplaces in the vicinity of new facilities with increasing particle energy.

At present, the time structure of the stray radiation fields is usually deduced from the design of the accelerator. Little or no experimental work has yet been reported concerning the pulsed structure of the radiation field modified by transport through the shield. It can be expected that thick shields of high-energy accelerators may seriously disturb the initial pulse structure because of e.g. different time of flight of the secondary particles through the material of the shield. The information about the real-time structure behind the shields can be important in order to decide whether a particular radiation field must be considered to be pulsed for a particular dosemeter. An important problem can also be represented by the time structure of high-energy neutron leakage from spallation targets.

The influence of pulsed radiation on the response of radiation detectors is considered in the literature first of all for dosimetry of the primary beam. The guidelines from such studies can be applied in radiation protection at workplaces, but lower dose rates at workplaces comparing with the beam conditions should be taken into account.

The most comprehensive source of information on the dosimetry of pulsed X ray or electron beams is ICRU Report 34[6]. Measurements using ionisation chambers, chemical dosemeters, calorimeters and solid-state devices are discussed. The report provides information on certain precautions to be taken and on the selection of calibration constants needed for dosimetry of pulsed low-LET radiation. High-LET radiation, mainly heavy charged particles and neutrons, is only shortly mentioned in ICRU 34, because there was not enough information about the influence of radiation pulsing on dosimetry in complex radiation fields at the time the report was issued (1982). Some up-to-date information and operational guidelines for radiation protection at particle accelerator facilities with energies from ~5 MeV up to the highest energies available can be found in NCRP Report No. 144[7], where the special problems of measurements in pulsed radiation fields are also addressed.

Workplace monitoring in complex radiation fields usually involves instruments based on the use of ionisation chambers, particle counting devices or solid-state detectors. The last two types of detectors are also often used in neutron and charge particle spectrometers. Tissue equivalent proportional counters (TEPC) and recombination ionisation chambers are used for microdosimetry and LET-spectrometry. The influence of the pulsed structure of the particle beam on the instrument response is different for the three classes of detectors.

RADIATION PROTECTION AND MONITORING AT EUROPEAN THERMONUCLEAR FUSION FACILITIES

Many radiation protection issues at experimental thermonuclear fusion machines and at associated facilities are similar to those arising around medium and low-energy accelerators. Radiation fields around these facilities are complex and mainly consist of neutrons and photons. Pulsed fields, short operation periods, complex operation scenarios and variable radiation energy spectrum are common situations at nuclear fusion facilities. The main difference to the radiation fields at particle accelerators is the lower maximum neutron energy: about 2.5 MeV for D–D plasmas and 14 MeV for D–T plasmas.

A specific radiation monitoring problem is related to the short time during which the so-called 'plasma burning' (or 'shot' or 'pulse') takes place. In this time period, that ranges from ~1 s to some tenths of seconds, plasma heating systems are activated and the thermonuclear conditions make the fusion reactions possible. Usually an intense, mixed neutron/photon radiation field is generated during the burning phase, and to collect the needed dosimetric information, the monitoring response during this interval has to be recorded. This is usually accomplished with active monitors and associated electronic devices suitable to activate the measurement for the time needed and to record the related dosimetric information. A discussion on the radiation monitoring system in use at JET and that planned for ITER is given in ref. (2).

CALIBRATION

Calibration is the process in which the calibration factor (quotient of the conventional true value by the value indicated) of a measuring device is determined in a reference radiation field of well-known ambient dose equivalent under well-specified calibration conditions[5]. Radioactive sources are frequently used, e.g. ^{60}Co or ^{137}Cs sources for photon dosemeters and ^{252}Cf or ^{241}Am(Be) sources for neutron dosemeters, since they can provide stable and reproducible calibration conditions. National standard laboratories, for example, provide such reference fields. Then, if used under conditions

identical to the calibration conditions, a calibrated instrument will measure $H^*(10)$ correctly. However, under different irradiation conditions, for example in fields of other particle compositions or with other particle energy distributions, deviations will occur since the dosemeters used in radiation protection practice usually do not have ideal response characteristics (e.g. the same energy dependence as the fluence-to-dose equivalent conversion function). In practical applications, these deviations are either small enough for the desired degree of accuracy or the user must apply field-specific correction factors to take the differences between calibration conditions and the conditions actually prevailing into account.

Since the radiation fields at workplaces around high-energy accelerators (but similar considerations apply for the cosmic radiation field in aircrafts responsible for aircrew exposure) differ strongly from those applied in standard calibration, the correction factors required can be large. In addition, since the field characteristics and the response of the instrument to all particles in the field are usually not well known, the correction factors cannot be calculated with the desired precision. The reliability and accuracy in personnel exposure monitoring can therefore be improved by performing the calibration in the field of interest or in a calibration field with similar characteristics. The direct *field calibration* of instruments in a given workplace requires a reference instrument that should be able to measure the (true value of) ambient dose equivalent (nearly) correctly for all radiation components and energies. The use of *reference fields* ('simulated workplace fields') produced under laboratory conditions requires particle compositions and spectral fluences similar to those in the workplace of interest. Those fields offer a good opportunity of investigating the dosemeter characteristics and of intercomparing different dosemeters under identical and reproducible conditions.

Photon dosemeters are conventionally calibrated with ^{137}Cs radionuclide sources emitting monoenergetic photon radiation with energy of 0.661 MeV. The reference quantity for the calibration is primarily the air kerma, K_a, which can be converted to $H^*(10)$ by applying appropriate conversion coefficients. Photon dosimetry is mostly understood for pure photon fields as well as low-energy photon spectrometry. In mixed fields, the situation is more complex, as is often not easy to take into account the response of a photon spectrometer or dosemeter to neutrons. On the other hand, photon spectrometry in the high-energy region still needs a lot of development work.

Reference neutron fields can be produced by radionuclide sources, nuclear reactors and nuclear reactions with charged particles from accelerators. A recent review of the subject can be found in ref. (8). Recommendations for producing reference neutron radiation fields are given by the International Organization for Standardization (ISO)[9–11]. The calibration of neutron instrumentation is discussed in more detail below.

NEUTRON CALIBRATION FIELDS

The calibration of instruments used for routine neutron monitoring, e.g. rem counters or personal dosemeters, is carried out using reference neutron fields with broad spectral distributions like those produced by radionuclide sources. The spectra encountered at workplaces, however, are usually significantly different from those used for the calibration. Hence, the fluence response $R_\Phi(E)$ of the instrument has to be determined as a function of the neutron energy E to enable the calculation of so-called 'field correction factors', which account for the dependence of the response on the neutron spectrum. The experimental determination of the response is carried out using reference fields in which the neutron fluence is concentrated at a single energy (monoenergetic fields) or, at least, the majority of the fluence is at a single energy with only a smaller contribution at other energies (quasi-monoenergetic fields). The basic quantity for the specification of reference fields is the spectral neutron fluence Φ_E. The neutron ambient dose equivalent $H^*(10)$ is obtained from Φ_E by folding the spectral distribution with recommended energy-dependent fluence-to-dose-equivalent conversion coefficients $h_\Phi(E)$.

Monoenergetic or quasi-monoenergetic reference fields are produced by bombarding low-Z targets (D, T, ^{7}Li) with light ions (protons or deuterons) accelerated with Van-de-Graaff accelerators or cyclotrons. In most cases, monoenergetic neutrons can be obtained only under ideal conditions. In reality, however, the effects of finite target thickness, neutron scattering in the target surroundings and the finite detector size as well as the break-up reactions at higher projectile energies cause deviations from the ideal situation; i.e. the fields are only quasi-monoenergetic with a high-energy peak of finite width and a low-energy continuum.

The response of a detector to high-energy neutrons ($E_n > 20$ MeV) is quite difficult to determine experimentally because of the low-energy tail in the spectrum provided by the available quasi-monoenergetic neutron facilities. Moreover, when measuring in the unshielded radiation fields, the contribution of high-energy hadrons also has to be taken into account (see for example, ref. (12)).

If both the energy and angular response characteristics of an instrument and the energy and direction distribution of the radiation field to be determined are well known—either experimentally or

theoretically—the response data can be folded with the field data to obtain a field correction factor. An alternative approach is to determine the response of the device either in the radiation field of interest (a field calibration) or in an experimental radiation field of sufficiently similar characteristics (a simulated workplace field). Modern Monte Carlo codes can help a lot in designing instrumentation and in understanding their performances and their response functions to various types of radiation. It is nonetheless important that the simulations are validated with calibration measurements in reference fields. A list of available calibration facilities providing monoenergetic or quasi-monoenergetic beams is given in ref. (2).

SIMULATED WORKPLACE FIELDS

When selecting a workplace neutron field (designed for calibrating and testing either personal dosemeters or area monitors), one has to consider the characteristics of the field to be simulated (such as its energy and direction distributions) and the response of the instruments or dosemeters used to determine the neutron distributions. Workplace neutron fields can be simulated using three types of irradiation facilities: radionuclide sources, nuclear reactors and particle accelerators[13]. Since we are interested in workplace fields around high-energy accelerators, the latter of the three methods is the only practicable one. Essentially only two facilities of this type are available in Europe: the CERF facility at CERN[1] and CANEL at Cadarache[14].

CONCLUSIONS

The CONRAD WP6 report has reviewed the principal techniques, based both on the active detectors and passive dosemeters, employed to monitor mixed radiation fields around high-energy particle accelerators and experimental thermonuclear fusion reactors. Neutron measuring devices include rem counters, Bonner sphere spectrometers, bubble detectors and etched track detectors. Techniques discussed for photon dosimetry and spectrometry are scintillation detectors, ionisation chambers, Geiger–Müller counters, TLDs (thermoluminescent dosimeters) and EPR (electron paramagnetic resonance) dosemeters. Instruments capable to distinguish between the low- and high-LET components of a field like TEPCs and recombination chambers are also discussed. Secondary (stray) radiation often keeps 'memory' of the original time structure of the primary beam, and if the beam is made up of very short bursts, the influence of such structure on active instruments has to be properly taken into account when selecting or designing a monitoring system. The characterisation of the neutron field produced at high-energy proton accelerators is quite a challenging task: developments occurred over the past few years to improve the response of neutron counters and spectrometers beyond 20 MeV are discussed.

Instruments and dosemeters used for workplace monitoring usually do not have ideal response characteristics, i.e. the same energy dependence as the fluence-to-dose equivalent conversion function. They are normally employed under irradiation conditions that are different from those in which they were calibrated. Thus deviations will occur and proper correction factors have to be applied.

The response of a device to the various components of a mixed radiation field can nowadays be determined quite precisely by means of Monte Carlo codes. It is nonetheless important that the simulations are validated with calibration measurements in monoenergetic or quasi-monoenergetic reference fields. It is also important to be able to calibrate a dosemeter in a simulated workplace field produced under laboratory conditions with particle compositions and spectral fluences similar to those encountered at the workplace of interest. Such a field offers the opportunity of investigating the dosemeter characteristics and of intercomparing different dosemeters under identical and reproducible conditions.

There are a number of issues that still need to be better understood, such as the problems arising from calibration for high-energy devices; for instance, rem counters with a lead insert, which are also sensitive to low-energy neutrons. For neutrons above 20 MeV only 'quasi-monoenergetic' fields are available, i.e. fields with a major component at one energy, but with an additional broad energy component, usually at lower energies, for which corrections have to be made. In addition, the quasi-monoenergetic neutron fields above 20 MeV are not regularly available for 'routine' calibrations. There is also a certain need of better estimating uncertainties in conversion coefficients.

The basic protection quantity is the effective dose E, but for purposes of radiation protection metrology the operational quantity ambient dose equivalent, $H^*(10)$, is used, which is meant to be a conservative approximation of E. Recent studies[15–17] have shown that in some circumstances, the operational quantities may not always provide an overestimate of protection quantities, so that future developments in instrumentation will have to take this fact into account.

ACKNOWLEDGEMENT

This work is funded in part by the European Commission under the auspices of the Euratom Sixth Framework Programme for research and training in nuclear energy, Contract No FI6R-012684.

REFERENCES

1. Mitaroff, A. and Silari, M. *The CERN–EU high-energy reference field (CERF) facility for dosimetry at commercial flight altitudes and in space*. Radiat. Prot. Dosim. **102**, 7–22 (2002).
2. Bilski, P. *et al. Complex workplace radiation fields at European high-energy accelerators and thermonuclear fusion facilities*. Yellow Report CERN-2006-007, Silari, M. editor (2006).
3. International Commission on Radiological Protection (ICRP). *1990 Recommendations of the International Commission on Radiological Protection*. Publication 60 (Oxford: Pergamon Press) (1991).
4. International Commission on Radiation Units and Measurements (ICRU). *Quantities and units in radiation protection dosimetry*. Report 51 (MD, USA: Bethesda) (1993).
5. International Commission on Radiation Units and Measurements (ICRU). *Determination of operational dose equivalent quantities for neutrons*. Report 66 (MD, USA: Bethesda) (2001).
6. International Commission on Radiation Units and Measurements (ICRU). *The dosimetry of pulsed radiation*. Report 34 (MD, USA: Bethesda) (1983).
7. National Council on Radiation Protection and Measurements (NCRP). *Radiation protection for particle accelerator facilities*. Report 144 (MD, USA: Bethesda) (2003).
8. Schuhmacher, H. *Neutron calibration facilities*. Radiat. Prot. Dosim. **110**, 33–42 (2004).
9. International Organization for Standardization (ISO). Reference neutron radiations–Part 1: characteristics and methods of production. ISO Standard 8529-1 (Geneva: ISO) (2001).
10. International Organization for Standardization (ISO). *Reference neutron radiations–Part 2: calibration fundamentals of radiation protection devices related to the basic quantities characterizing the radiation field*. ISO Standard 8529-2 (Geneva: ISO) (2000).
11. International Organization for Standardization (ISO). *Reference neutron radiations–Part 3: calibration of area and personal dosimeters and determination of their response as a function of neutron energy and angle of incidence*. ISO Standard 8529-3 (Geneva: ISO) (1998).
12. Agosteo, S., Dimovasili, E., Fassò, A. and Silari, M. *The response of a Bonner sphere spectrometer to charged hadrons*. Radiat. Prot. Dosim. **110**, 161–168 (2004).
13. International Organization for Standardization (ISO). *Reference neutron radiation–Characteristics and method of production of simulated workplace neutron fields*. ISO standard 12789-1 (Geneva: ISO) (2000).
14. Gressier, V. Les installations de l'IRSN dédiées à la métrologie des neutrons. IRSN Report DRPH/SDE 2005-012 (2005).
15. ICRP/ICRU Joint Publication. Conversion coefficients for use in radiological protection against external radiation. ICRP Publication 74 (Pergamon: Oxford) (1997) and ICRU Report 57 (MD, USA: Bethesda) (1998).
16. Ferrari, A., Pelliccioni, M. and Pillon, M. *Fluence to effective dose conversion coefficients for neutrons up to 10 TeV*. Radiat. Prot. Dosim. **71**, 165–173 (1997).
17. Bartlett, D.T., Drake, P., d'Errico, F., Luszik-Bhadra, M., Matzke, M. and Tanner, R.J. *The importance of the direction distribution of neutron fluence and methods of determination*. Nucl. Instrum. Meth. **A476**, 386–394 (2002).

Radiation Protection Dosimetry (2007), Vol. 126, No. 1–4, pp. 18–22 doi:10.1093/rpd/ncm006
Advance Access publication 17 May 2007

THE TSL NEUTRON BEAM FACILITY

A. V. Prokofiev[1,*], J. Blomgren[1], O. Byström[1], C. Ekström[1], S. Pomp[2], U. Tippawan[3], V. Ziemann[1] and M. Österlund[2]
[1]The Svedberg Laboratory, Uppsala University, Box 533, S-751 21 Uppsala, Sweden
[2]Department of Neutron Research, Uppsala University, Box 525, S-751 20 Uppsala, Sweden
[3]Fast Neutron Research Facility, Chiang Mai University, 50202 Chiang Mai, Thailand

A new quasi-monoenergetic neutron beam facility has been constructed at The Svedberg Laboratory (TSL) in Uppsala, Sweden. Key features include a neutron energy range of 11–175 MeV, high fluxes, user flux control, flexible neutron field size and shape, and spacious and easily accessible user area. The first results of the beam characterisation measurements are reported.

INTRODUCTION

The interest in high-energy neutrons is rapidly growing, since a number of potential large-scale applications involving fast neutrons are under development or have been identified. These applications primarily fall into four sectors: nuclear energy and waste[(1)], medicine[(2,3)], personnel dosimetry in aircraft[(4)] and spacecraft[(5)] and single-event effects (SEE) on electronics[(6,7)].

To satisfy the needs of these applications, monoenergetic neutron beams would be most suitable. In the energy region above ~20 MeV, a truly monoenergetic neutron beam is not feasible in a strict sense. For certain nuclear reactions, however, there is a strong dominance of neutrons in a narrow energy range. Therefore, such neutron sources are often called 'quasi-monoenergetic'. The most popular neutron production reaction above 20 MeV is ^{7}Li(p,n)^{7}Be. It is used, e.g. at quasi-monoenergetic neutron facilities in Cape Town[(8)], Davis[(9)], Louvain-la-Neuve[(10)], Saitama[(11)] and Takasaki[(12)].

There is a long-term experience in high-energy neutron production at The Svedberg Laboratory (TSL). The first neutron facility was built at TSL in the late 1980s[(13,14)] and remained in operation until 2003. In 2003–2004, a new facility was constructed. Emphasis was put on high neutron beam intensity in combination with flexibility in energy and neutron field shape.

TECHNICAL SPECIFICATION

The facility uses the ^{7}Li(p,n)^{7}Be reaction to produce a quasi-monoenergetic neutron beam. Two kinds of beams from the Gustaf Werner cyclotron are used for neutron production: (1) proton beam with energy variable in the 25–180 MeV range and (2) beam of H_2^+ ions with energy of ~13 MeV A^{-1}. The energy of the produced peak neutrons is controllable in the 11–175 MeV range.

A schematic plan view of the neutron beam facility is shown in Figure 1. The proton or H_2^+ beam is incident on a target of lithium, enriched to 99.99% in ^{7}Li. The available targets are 1, 2, 4, 8.5 and 23.5 mm thick. Proton energy loss in the target amounts to 2–6 MeV depending on the incident beam energy and target thickness. The targets are rectangular in shape, 20×32 mm^2, and are mounted in a remotely controlled water-cooled copper rig. An additional target position contains a fluorescent screen viewed by a TV camera, which is used for beam alignment and focusing. Downstream the target, the proton beam is deflected by a magnet into a 10-m long dumping line, where it is guided onto a heavily shielded water-cooled graphite beam dump.

The neutron beam is formed geometrically by a cylindrical shaped iron collimator block, 50 cm in diameter and 100-cm long, with an aperture of variable size and shape. The collimator is surrounded by concrete to form the end wall of the production line towards a user area. Thereby, shielding from the lithium target region is achieved that is sufficient for most experiments. A modular construction of the collimator allows the user to select the size and the shape of the neutron beam. At present, the following collimator apertures are available:

- cylindrical: 2, 3, 5.5, 10, 15, 20 and 30 cm in diameter,
- conical, with an entrance diameter of 3.66 cm and an exit diameter of 5.4 cm,
- with a quadratically shaped cross-section of 1 cm^2 area.

The last option is intended for irradiation of e.g. a separate electronic component without affecting the rest of an electronic board. Other collimator apertures in the 0–30 cm range can be provided upon

*Corresponding author: Alexander.Prokofiev@tsl.uu.se

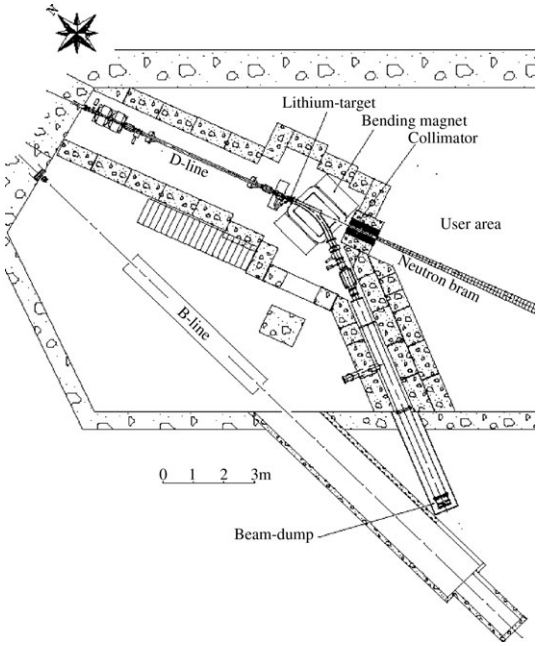

Figure 1. The schematic plan view of the neutron beam facility. The neutron beam, produced in the lithium target, continues along the D-line.

request. The time needed to change the aperture is typically ~30 min.

Non-uniformity of the neutron beam within the aperture was estimated on the basis of literature data on angular distributions of neutrons from the ^{7}Li(p,n)^{7}Be reaction. For the sharpest angular distribution, at the peak neutron energy of 175 MeV, the peak neutron flux near the periphery of the 10-cm aperture is expected to be 1.3% lower than at the beam axis. For the 30-cm aperture, the difference amounts to 12%.

The user area extends from 3 to 15 m downstream the lithium target. Positions located closest to the target are used for high-flux irradiation of compact objects, with achievable fluxes about an order of magnitude higher compared to the old TSL neutron facility[13,14], for the same target thickness, proton energy and current. Remote positions may be used to irradiate large objects, up to 1 m in diameter, e.g. entire computers or aircraft navigation systems. Proton beam currents of up to 10 μA can be used for energies below 100 MeV. Above 100 MeV, the achievable beam current is about a factor of 10 lower. The resulting reduction of the neutron flux can be partly compensated by using thicker lithium targets. The neutron flux can be varied by the user according to the needs of the specific experiment.

The time structure of the neutron beam is defined by the time structure of the proton beam from the cyclotron, which in turn depends on the energy and operation mode, as shown in Table 1.

The user area, situated at a level of 12 m below the ground, is connected by Ethernet and coaxial cables, ~100-m long, to counting rooms, which are located at the ground level. No time is required for 'cooling down' of the user area after irradiation because the dose rate from residual beta and gamma rays is then only slightly above the natural radiation level.

Two additional irradiation positions, which can be used parasitically with other experiments, are provided closer to the lithium target (Table 2). The increase of the neutron flux at these positions is reached at the expense of limited accessibility, limited size of irradiated objects, lack of standard monitors and more intense gamma ray background.

CHARACTERISATION OF THE FACILITY

Neutron spectra at 0° have been obtained by measuring elastic np-scattering with the Medley setup[15–17]. The scattered protons are registered at an angle of 20° relative to the neutron beam. The measured neutron spectra are shown in Figure 2 for peak energies of 21.8 (a), 46.5 (b), 94.7 (c) and 142.7 MeV (d). In all cases, the spectrum is dominated by a peak situated a few MeV below the energy of the primary protons and comprising ~40% of the total number of neutrons.

Table 1. Parameters of the time structure of the beam.

Type of the time structure	Repetition period	Beam pulse duration	Peak neutron energy (MeV)
Microstructure	45–80 ns[a]	~4 ns (FWHM)[b]	11–174
Macrostructure	≥5 ms[c]	~0.7 ms (FWHM)[b]	>100
Beam sharing mode[d]	~40 min[b]	~30 min[b]	174

[a]Dependent on the peak neutron energy.
[b]Typical value.
[c]May be increased up to 1 s upon user's request.
[d]This structure is present only if the accelerator beam time is shared between the neutron beam facility and the proton cancer therapy facility.

Table 2. Parasitic irradiation positions.

Position	Distance from the Li target (m)	Angle to the proton beam direction (°)	Gain in the peak neutron flux
PARTY	1.9	1.6	2.5
TUNIS	1.1	7.5	1.7–2.2[a]

[a]Dependent on the peak neutron energy.

Figure 2 includes a comparison of the measurements with model calculations of the neutron spectra folded with the function that describes the energy resolution in the present experiment. For the three higher energies (Figure 2b–d), the systematics of Prokofiev *et al.*[18] was employed. For the peak neutron energy of 21.8 MeV, the evaluation of Mashnik *et al.*[19] was used (Figure 2a). The differential cross-section for high-energy peak neutron production at 0° was obtained by multiplication of the angle-integrated cross-section of the ^{7}Li(p,n)^{7}Be reaction[19] to the 'index of forwardness' from the systematics of Uwamino *et al.*[20] The experimental data agree with the calculations except for the low-energy tail region in the 21.8-MeV spectrum where the model overpredicts the yield of neutrons with energies above 5 MeV by ~40%. This discrepancy may reflect difficulties in using statistical approach for description of nuclear reactions with such a light target nucleus as ^{7}Li (see Ref. (19) for further discussion). Further theoretical work is needed in order to achieve better description of the experimental neutron spectra.

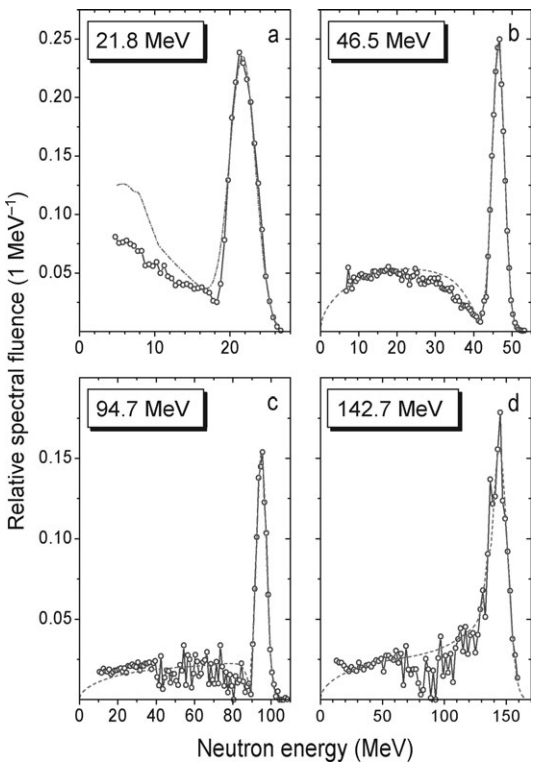

Figure 2. The neutron spectra at 0° for different peak neutron energies (see Table 3 for incident proton energies and ^{7}Li target thicknesses). Symbols connected by a solid line represent experimental data obtained in the present work. Predictions are shown as dashed lines (see text).

Table 3 summarises the main features of the measured spectra and the achieved neutron fluxes. The latter have been measured with a monitor based on a thin-film breakdown counter (TFBC)[21]. Another monitoring option is provided by an ionisation-chamber monitor (ICM). Both monitors utilise neutron-induced fission of ^{238}U with the cross-section adopted as neutron flux standard[22]. In addition, the neutron flux is indirectly monitored by a Faraday cup, which integrates the current of protons collected at the beam dump. In Table 3, gamma ray dose rate in the user area is given as well.

The measured contamination of the neutron beam at the user area, due to interactions of the primary protons with beam transport elements, typically does not exceed 0.05% for peak neutron energies up to 100 MeV and 0.3% for the 174-MeV energy. Such interactions lead to a minor surplus of neutrons in the user area, because charged particles produced near the lithium target and upstream are removed by the deflection magnet. The relative contamination of the neutron beam by protons with energies above 15 MeV is $\sim 10^{-5}$ for the peak neutron energy of 95 MeV.

Thermal neutrons were observed in the user area, using TFBCs with ^{235}U targets, shielded by a cadmium sheet during a part of the runs. Measurements of the relative thermal neutron flux were performed at the distance of ~11 m from the lithium target, for peak neutron energies from 22 to 174 MeV. The thermal neutron flux was estimated to be ~0.5–2% of the peak neutron flux, decreasing with the peak neutron energy. No statistically significant difference was found between the thermal neutron flux measured in-beam and out-of-beam. Thus, a rather uniform thermal neutron field was observed in the user area. These results come from an ongoing study of the low-energy part of the neutron spectra using TFBCs and different neutron-induced fission reactions[23].

Figure 3 shows a horizontal beam profile for 142.7-MeV neutrons, measured at a distance of 4.77 m from the lithium target. The measurement was performed by counting neutron-induced SEE in a set of memory chips positioned across the beam[24].

Table 3. Parameters of the available neutron beams.

Proton beam energy (MeV)	^{7}Li target thickness (mm)	Proton beam current (μA)	Average energy of peak neutrons (MeV)	Fraction of neutrons in the high-energy peak (%)		Peak neutron flux (10^5 cm^{-2} s^{-1})[a]	gamma ray dose rate (mSv h)$^{-2}$
				Measured	Calculated		
24.68 $\pm$ 0.04	2	10	21.8	$\sim$50	—	1.3	0.35
49.5 $\pm$ 0.2	4	10	46.5	39	36	2.9	1.7
97.9 $\pm$ 0.3	8.5	5	94.7	41	39	4.6	2.4
147.4 $\pm$ 0.6	23.5	0.6	142.7	55[c]	40	2.1	—

[a]At the entrance of the beam line to the user area.
[b]At the neutron beam path at the distance of 8 m from the lithium target.
[c]Upper limit due to poor energy resolution.

SUMMARY AND OUTLOOK

A new neutron beam facility has been constructed at TSL, and it is in frequent operation now (25 weeks during year 2005). The facility is capable of delivering neutrons in the 11–175 MeV range. This makes TSL the only laboratory in the world offering full quasi-monoenergetic neutron testing according to the JESD89 standard[7].

Recently, a neutron field with the peak energy of $\sim$11 MeV has been developed. Processing of neutron spectra at 11 and 174 MeV is in progress. A fast ionisation chamber for regular checks of the neutron spectrum is under development[25]. An additional neutron monitor based on counting of neutron-induced SEE is about to be installed[26]. Independent calibrations of neutron monitors are planned, using measurements of the ^{7}Be activity produced in the ^{7}Li target, following a technique suggested by Uwamino *et al.*[20] It is planned to rebuild the shielding wall around the collimator in order to diminish the flux of stray high-energy neutrons that lack through the wall and create unwanted background in e.g. experiments with the Medley setup[17].

A new upgrade of the facility is being launched in the framework of project ANITA (Atmospheric-like Neutrons from thick Target). The upgrade will allow us to deliver a neutron beam with a continuous 'white' spectrum and thus to reproduce the spectrum of neutrons in the atmosphere. Neutrons will be produced by irradiation of a thick tungsten target by high-energy protons. The possibility to deliver quasi-monoenergetic neutron beams will be kept.

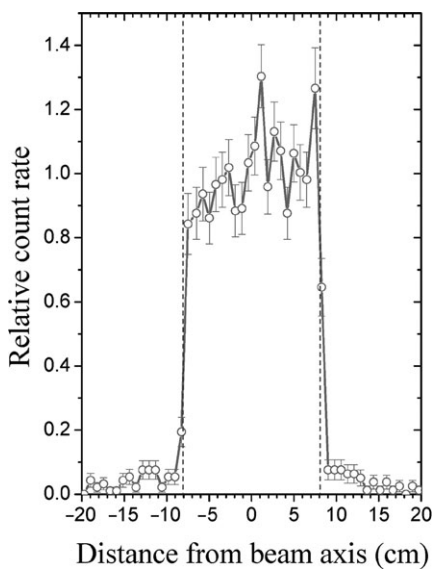

Figure 3. The horizontal beam profile for 142.7 MeV neutrons, measured at the distance of 4.77 m from the lithium target. Vertical dashed lines represent boundaries of the beam expected from the geometry of the collimator.

ACKNOWLEDGEMENTS

The authors would like to thank the staff at The Svedberg Laboratory for the excellent work in building this new facility. They are thankful to A. N. Smirnov and M. Olmos for providing us with the thermal neutron data and the beam profile data, respectively.

REFERENCES

1. Lecolley, F.-R. *et al. Neutron and light charged particle production in neutron or proton-induced reaction on iron, lead and uranium at intermediate energy (20 to 200 MeV) – the HINDAS collaboration*. In: Proceedings of International Conference on Nuclear Data for Science and Technology, Santa Fe, NM, September 26–October 1, 2004 (AIP Conf. Proc. **769**, 61–66 (2005)).

2. Orecchia, R., Zurlo, A., Loasses, A., Krengli, M., Tosi, G., Zurrida, S. and Zucali, P. U. Veronesi. *Particle beam therapy (hadrontherapy): basis for interest and clinical experience*. Eur. J. Cancer **34**, 459–468 (1998).
3. Schwartz, D. L., Einck, J., Bellon, J. and Laramore, G. E. *Fast neutron radiotherapy for soft tissue and cartilaginous sarcomas at high risk for local recurrence*. Int. J. Radiat. Oncol. Biol. Phys. **50**, 449–456 (2001).
4. Bartlett, D. T., Hager, L. G., Tanner, R. J. and Steele, J. D. *Measurements of the high energy neutron component of cosmic radiation fields in aircraft using etched track dosemeters*. Radiat. Meas. **33**, 243–253 (2001).
5. Bartlett, D. T., Hager, L. G. and Tanner, R. J. *Results of measurements on shuttle missions to the ISS of the neutron component of the radiation field*. Adv. Space Res. **37**, 1668–1671 (2006).
6. Tang, H. H. K. and Olsson, N. (eds) Single-Event Upsets in Microelectronics, topical issue, Mater. Res. Soc. Bull. 28 (2003).
7. JEDEC Standard. *Measurements and reporting of alpha particles and terrestrial cosmic ray-induced soft errors in semiconductor devices*. JESD89 (2001).
8. Nolte, R., Allie, M. S., Binns, P. J., Brooks, F., Buffler, A., Dangendorf, V., Meulders, J. P., Roos, F., Schuhmacher, H. and Wiegel, B. *High-energy neutron reference fields for the calibration of detectors used in neutron spectrometry*. Nucl. Instrum. Meth. Phys. Res. A **476**, 369–373 (2002).
9. Brady, F. P. *(n,p) studies at the University of California at Davis*. Can. J. Phys. **65**, 578–587 (1987).
10. Schuhmacher, H., Brede, H. J., Dangendorf, V., Kuhfuss, M., Meulders, J. P., Newhauser, W. D. and Nolte, R. *Quasi-monoenergetic neutron beams with energies from 25 to 70 MeV*. Nucl. Instrum. Meth. Phys. Res. A **421**, 284–295 (1999).
11. Nakao, N., Uwamino, Y., Nakamura, T., Shibata, T., Nakanishi, N., Takada, M., Kim, E. and Kurosawa, T. *Development of a quasi-monoenergetic neutron field using the ^{7}Li(p, n)^{7}Be reaction in the 70–210 MeV energy range at RIKEN*. Nucl. Instrum. Meth. Phys. Res. A **420**, 218–231 (1999).
12. Baba, M. *et al. Characterization of a 40–90 MeV ^{7}Li(p,n) neutron source at TIARA using a proton recoil telescope and a TOF method*. Nucl. Instrum. Meth. Phys. Res. A **428**, 454–465 (1999).
13. Condé, H. *et al. A facility for studies of neutron-induced reactions in the 50–200 MeV range*. Nucl. Instrum. Meth. Phys. Res. A **292**, 121–128 (1990).
14. Klug, J. *et al. SCANDAL – a facility for elastic neutron scattering studies in the 50–130 MeV range*. Nucl. Instrum. Meth. Phys. Res. A **489**, 282–303 (2002).
15. Dangtip, S. *et al. A facility for measurements of nuclear cross sections for fast neutron cancer therapy*. Nucl. Instrum. Meth. Phys. Res. A **452**, 484–504 (2000).
16. Pomp, S. *et al.* The New Uppsala Neutron Beam Facility. In: Proceedings of International Conference on Nuclear Data for Science and Technology, Santa Fe, NM, September 26–October 1, 2004; AIP (Conf. Proc. 769, 780–783 (2005)).
17. Tippawan, U. *et al. Light charged-particle production in 96 MeV neutron-induced reactions on carbon and oxygen*. These proceedings.
18. Prokofiev, A. V., Chadwick, M. B., Mashnik, S. G., Olsson, N. and Waters, L. S. *Development and validation of the ^{7}Li(p,n) nuclear data library and its application in monitoring of intermediate energy neutrons*. J. Nucl. Sci. Techn., **1** (Suppl 2), 112–115 (2002).
19. Mashnik, S. G., Chadwick, M. B., Young, P. G., MacFarlane, R. E. and Waters, L. S. *^{7}Li(p,n) nuclear data library for incident proton energies to 150 MeV*. LANL Report LA-UR-00–1067 (2000).
20. Uwamino, Y., Soewarsono, T. S., Sugita, H., Uno, Y., Nakamura, T., Shibata, T., Imamura, M. and Shibata, S. *High-energy p-Li neutron field for activation experiment*. Nucl. Instrum. Meth. Phys. Res. A **389**, 463–473 (1997).
21. Eismont, V. P., Prokofiev, A. V. and Smirnov, A. N. *Thin film breakdown counters and their applications (review)*. Radiat. Meas. **25**, 151–156 (1995).
22. Carlson, A. D., Chiba, S., Hambsch, F.-J., Olsson, N. and Smirnov, A. N. *Update to 'Nuclear Data Standards for Nuclear Measurements'*. In: Proceedings of International Conference on Nuclear Data for Science and Technology, Trieste, Italy, May 19–24, 1997, Part II, 1223–1229, Italian Physical Society (1997).
23. Smirnov, A. N. Private communication (2006); Smirnov, A. N. *et al.* to be published.
24. Olmos, M. Private communication (2004).
25. Ryzhov, I.V. private communication (2006).
26. Harboe-Sorensen, R. Private communication (2005).

200 and 300 MeV/nucleon nuclear reactions responsible for single-event effects in microelectronics

H. Jäderström,[1,*] Yu. Murin,[2,3] Yu. Babain,[2] M. Chubarov,[2] V. Pljuschev,[2] M. Zubkov,[2] P. Nomokonov,[3] N. Olsson,[4] J. Blomgren,[5] U. Tippawan,[5] L. Westerberg,[6] P. Golubev,[7] B. Jakobsson,[7] L. Gerén,[8] P.-E. Tegnér,[8] I. Zartova,[8] A. Budzanowski,[9] B. Czech,[9] I. Skwirczynska,[9] V. Kondratiev,[10] H. H. K. Tang,[11] J. Aichelin,[12] Y. Watanabe,[13] and K. K. Gudima[14]

[1]*Department of Nuclear and Particle Physics, Uppsala University, Box 531, S-751 21 Uppsala, Sweden*
[2]*V. G. Khlopin Radium Institute, 2nd Murinski prospect 28, RU-194021 Saint-Petersburg, Russia*
[3]*Joint Institute for Nuclear Research, JINR, RU-141980, Dubna, Russia*
[4]*Swedish Defence Research Agency (FOI), S-172 90 Stockholm, Sweden*
[5]*Department of Neutron Research, Uppsala University, Box 525, S-751 20 Uppsala, Sweden*
[6]*Department of Physics, Uppsala University, Box 530, S-751 21 Uppsala, Sweden*
[7]*Department of Physics, Lund University, Box 118, S-221 00 Lund, Sweden*
[8]*Department of Physics, Stockholm University, S-10691 Stockholm, Sweden*
[9]*H. Niewodniczanski Institute of Nuclear Physics, 31-342 Cracow, Poland*
[10]*St. Petersburg State University, RU-198504 St. Petersburg, Russia*
[11]*IBM, T. J. Watson Research Center, Yorktown Heights, New York 10598, USA*
[12]*IN2P3/CNRS, Ecole des Mines de Nantes, 4 rue Alfred Kastler, F-44072 Nantes cedex 03, France*
[13]*Department of Advanced Energy Engineering Science, Kyushu University, Kasuga, Fukuoka 816-8580, Japan*
[14]*Institute of Applied Physics, Moldova Academy of Sciences, MD-2028 Kishinev, Moldova*

(Received 27 November 2007; published 7 April 2008)

An experimental study of nuclear reactions between ^{28}Si nuclei at 200 and 300 MeV/nucleon and hydrogen or deuterium target nuclei was performed at the CELSIUS storage ring in Uppsala, Sweden, to collect information about the reactions responsible for single-event effects in microelectronics. Inclusive data on ^{28}Si fragmentation, as well as data on correlations between recoils and spectator protons or α particles are compared to predictions from the Dubna cascade model and the Japan Atomic Energy Research Institute version of the quantum molecular dynamics model. The comparison shows satisfactory agreement for inclusive data except for He fragments where low-energy sub-barrier fragments and recoiling fragments with very large momenta are produced much more frequently than predicted. The yield of exclusive data are also severely underestimated by the models whereas the charge distributions of recoils in these correlations compare well. The observed enhancement in He emission, which may well be important for the description of single-event effects, is most likely to be attributed to α clustering in ^{28}Si nuclei.

DOI: 10.1103/PhysRevC.77.044601 PACS number(s): 25.40.Sc, 25.45.−z, 27.30.+t, 34.50.Bw

I. INTRODUCTION

In this article we present the results of an experimental study of ^{28}Si+^{1}H and ^{28}Si+^{2}H reactions at 200 and 300 MeV/nucleon in inverse kinematics. The experiments were carried out at the CELSIUS storage ring of The Svedberg Laboratory, Uppsala, Sweden. The aim was twofold: to measure useful cross sections for the description of the single-event effects (SEEs) reactions and to describe such reactions with up-to-date models for p-nucleus collisions. The most prominent of all SEEs, the single-event upset (SEU) effect is manifested by the functional upsets of microelectronic memory devices primarily in space missions but also in aviation and even, to a lesser extent, at sea level [1,2].

Nuclear fragmentation of light nuclei induced by cosmic rays is related to the SEEs and other important applications, like optimizing microdosimetry for human tissue in radiation therapy. Theoretical "toolkits" have been developed but they are based on standard reaction models for heavy nuclei and may wash out important details in the topology of light nucleus fragmentation. The strong α clustering that we report on in this work may in fact be evidence for nuclear structure effects that are ignored in (multi-)fragmentation models. Another complication arises from the fact that in the energy domain of 50–500 MeV/nucleon, most interesting for the applications, the basic assumptions of the models are not valid. These energies are well above the Coulomb barrier but not high enough to assure that the quasi-classical approximation is fully satisfied or that all quantum effects can be neglected.

Theoretical models for intermediate energy p-nucleus and nucleus-nucleus collisions have been developed over the past four decades [3–5]. The uncertainties in the models and the lack of detailed experimental data motivated this experiment. At low altitudes the source of nuclear reactions producing upsets in chips made of Si is the neutron component of atmospheric cosmic rays. These neutrons have a broad energy range [6] that spreads from about 50 to 1000 MeV. The n+Si reaction is difficult to study and therefore measurements of the inverse kinematics, ^{28}Si+^{1}H, ^{2}H reactions are investigated in this work. In fact it is believed that the recoils, i.e., reaction products with charge $2 < Z \leqslant 14$, are to a large degree

*henrik.jaderstrom@tsl.uu.se

responsible for SEEs and therefore comprehensive data on light nucleus fragmentation at medium energy in general is important to collect. Typical ranges for these recoils are only a few microns in the detector. This is the major reason why there are so few recoil measurements. After pioneering work [7] on light ion production in p-nucleus reactions, one single experiment [8], bombarding 180-MeV protons on aluminum, reports on recoil production. The results of Ref. [9] are rather a good example of the crucial limitations in experiments on spallation of light target nuclei in normal kinematics. The basic idea of this project was to study fragmentation of silicon nuclei induced by medium-energy protons in the inverse kinematics scheme that gives much more favorable conditions to measure the heavy recoils with standard techniques [8–10].

Because it was not expected that one single model is able to describe the detailed data from this experiment, we choose to compare it with two well-known microscopic descriptions, the intranuclear cascade (INC) model and the quantum molecular dynamics (QMD) model. The mathematical formulation offered by the Dubna cascade model (DCM) [3,4] was utilized for the INC calculations. For calculations within the QMD framework, we used the model developed at the Japan Atomic Energy Research Institute (JAERI) in Japan (JQMD) [5]. DCM and JQMD are briefly described below. Both models are well known and have been reported to yield successful comparisons with experimental data on inclusive production of light particles (n, p, He) in hadron-nucleus and nucleus-nucleus collisions at intermediate energies [11], as well as at energies of several GeV. Both models are widely used for various practical applications [12–18]. The two approaches differ in their view of the recoils, where INC interprets them as the remnants of a long chain of individual emission of light nuclei from the highly excited source, whereas QMD generates recoils instantly through the cracking of an almost cold initial source with subsequent evaporative emission of light particles.

It is not at all obvious a priori that significant discrepancies between the recoil distributions from the two models should appear, especially because evaporation tends to smear out possible, initial differences. We will come back to this question in Sec. IV.

II. THE LAYOUT OF THE EXPERIMENT

The experiment was carried out at the cluster-jet target and the following quadrant of the CELSIUS ring. The experimental setup has been described in detail in Ref. [19] and only a brief description is given below. The layout of the experiment is shown in Fig. 1. The luminosity in the ^{28}Si+^{1}H reaction with an accelerated and cooled beam interacting with the hydrogen jet target was $\sim 5 \times 10^{27}$ cm^{-2} s^{-1}.

Secondary particles were registered simultaneously by four detector systems, the small angle detector (SAD), the forward wall detector (FWD), the zero angle detector (ZAD), and the spectator tagging detector (STD). FWD and STD (CHICSi) had been used in previous experiments at CELSIUS and are described elsewhere [20–25]. SAD and ZAD play a key role because they detect the product recoils, which are most important for the SEEs.

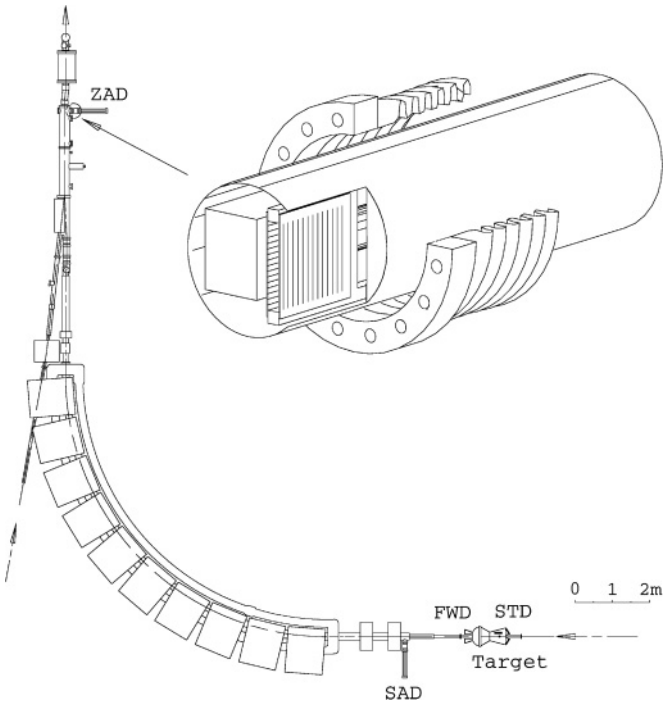

FIG. 1. Overview of the experimental setup.

SAD detects fragments from the ^{28}Si beam nuclei emitted at angles 0.6°–1.1°. It consists of two quadrants with 16 circular and 16 radial 300-μm Si strip detectors in front of an 8-mm plastic scintillator. Here, the unique properties of the cooled beam are fully exploited. During the injection and acceleration phases of the cycle, the beam occupies a large volume of the CELSIUS vacuum chamber but after the beam has been cooled, it shrinks to a diameter of 2 mm. To prevent the SAD detectors from radiation damage, they were moved out during injection/acceleration and returned to working position only after the beam reached maximum energy. The design of SAD is described in Ref. [19].

FWD [20] was used mainly for detection of light ($A \leqslant 4$) fragments emitted in the 3.9°–11.7° angular bin. In this experiment it consisted of twenty-four 750-μm Si detectors followed by 1-mm fast plastic scintillators glued on top of 80-mm-long CsI crystals. The main task for the FWD was to register He fragments in coincidence with recoils registered by SAD.

One Grand Motherboard (GMB) of the CHICSi detector [21–23] with 12 Si and 6 Si+GSO ΔE-ΔE-E telescopes mounted inside the ultrahigh vacuum chamber was used to tag events by spectator particles. Protons from the angular region 60°–120° identified as knocked-out free protons in the ^{28}Si+^{1}H and bound protons in the ^{28}Si+^{2}H reaction allowed us to extract Si+n data that represent the dominating source of SEEs in the atmosphere.

The ZAD is a telescope comprising two SSDs and a plastic scintillator similar to the one used in SAD. Here we make use of a technique developed at TSL [24,25] where the CELSIUS quadrant after the cluster-jet target is used as a magnetic spectrometer. ZAD is positioned at the focal plane of the spectrometer at a 22757-mm flight distance from the target.

In ZAD the strips make up a 32×32 rectangular net with a $60\times60\,\mathrm{mm}^2$ area. Vertical and horizontal strips of SSDs are used to detect projectile fragments, identify their charge, and determine the position of the hit point with respect to the nominal beam centerline. The electronic schemes of SAD and ZAD are identical [19].

At high recoil energy in the laboratory system the efficiency of the detectors approaches 100%. However, with the absence of detectors in the angular interval 1.1°–3.9° a significant fraction of the recoils, and especially the lighter ones, are not detected, which makes it impossible to measure the total cross sections directly.

III. THEORETICAL TOOLS

The basic idea of Serber [26], formulated in 1947, that p-nucleus (and heavy-ion) reactions at energies above 150 MeV/nucleon could be described as a superposition of binary nucleon-nucleon collisions, well separated in time and space, is still a common starting point for all models. The motivation for such a view is that the de Broglie wavelength of the bombarding nucleon(s) is getting smaller than the average intra nucleon distance. All INC models contain nucleon-nucleon collision chains as a first stage of the reaction, during which fast nucleons are ejected from the heavy nucleus. The INC is a rapid process that develops fully in approximately 10^{-22} s. It must, however, be supplemented with a statistical "after-burner" to describe the large yields of low-energy nucleons and light fragments observed in the experiments. Often evaporation from the excited remnants is introduced and this is a relatively slow process (10^{-21}–10^{-17} s) and it can therefore be regarded as the second stage of the reaction. The recoils are then considered as the "leftovers" of the two-stage process. Even if Serber's assumption is strictly not valid for collisions at lower energies, INC models have been reported to work well also for proton-induced reactions at energies as low as 60 MeV [15].

Several attempts to generalize the cascade-evaporation description have been made. Pre-equilibrium emission of particles between the first and the second stage of the reaction has been described within the Harp-Miller-Berne model [27], the Griffin exciton model [28], and its various later versions [29]. The Feshbach-Kerman-Koonin theory [30] was the first attempt to introduce quantum mechanics in the description of reactions at reasonably low energies. All these approaches have in fact mostly been used to describe low-energy reactions (20–150) MeV but even at much higher energies they do contain all necessary ingredients important for the description of the rescattered moderate-energy nucleons within the cascade. The modern INC models are in fact essentially based on the same ideas for building a three-stage sequence, i.e., INC, pre-equilibrium, and equilibrium evaporation as the driving mechanism of nuclear fragmentation.

QMD models appeared two decades ago to describe nuclear reactions. They consider the equations-of-motion of the nucleons in a concept borrowed from molecular physics. The molecular and nuclear versions differ in their most general formulation due to the difference of space and time scales. Nevertheless, in both cases QMD is the method to numerically solve the time-dependent Schrödinger equations for nucleons moving in a realistic potential and with a collision term similar to that used in transport theory [31]. A strong feature of the QMD approach is its natural inclusion of dynamics, which allows studies of collisions of large systems in real time.

QMD was first used for medium energy nucleus-nucleus collisions [32] and immediately a whole set of models [33,34] was developed to exploit the QMD method for all kinds of reactions. Often assumptions and parameters are borrowed in these models from the INC model to such an extent that final results from the models of the two types discussed also come out similarly and it is difficult to refine the differences between the two conceptually different theoretical approaches. In this work we confronted our experimental data with versions of the two models, each representing the two different approaches to the problem. Microscopic calculations have been performed within the time-dependent version of the Dubna intranuclear cascade model (DCM) (see Refs. [3,4] and references therein). The QMD model that we use, JQMD, has been developed at JAERI in Japan [5].

DCM divides the collision into three stages, well separated in time. During the first initial stage INC develops, primary particles can scatter and secondary particles can re-scatter several times prior to their absorption or escape from the nucleus. At the end of this step the coalescence model is used to localize d, t, ^{3}He, and ^{4}He particles from nucleons found inside spheres with well-defined radii in configuration space and momentum space. The emission of cascade particles determines a particle-hole configuration, i.e., Z, A, and excitation energy that is taken as the starting point for the second, pre-equilibrium stage of the reaction, described according to the standard Gudima-Toneev prescription, CEM [3] in its latest version CEM03.01 [35]. Some pre-equilibrium particles may be emitted and this leads to a lower excitation of the thermalized residual nuclei. In the third, final evaporation/fission stage of the reaction, the de-excitation of the residue is described with the generalized evaporation model (GEM) of Furihata [36]. All components contribute normally to the final spectra of particles and light fragments. If, however, the residual nuclei after the INC have atomic numbers $A < 12$, the Fermi breakup model [37] is used instead to describe their further disintegration instead of GEM. For relativistic energies the INC part of DCM is replaced by the refined cascade model, which is a version of the quark-gluon string model (QGSM) developed in Ref. [38] and extended to intermediate energies in Ref. [39].

The description of the mean-field evolution is simplified in the DCM in the sense that the scalar nuclear potential, defined by the local Thomas-Fermi approximation, remains the same throughout the collision. Only the potential depth changes in time according to the number of knocked-out nucleons. This "frozen mean-field" approximation allows us to take into account the nuclear binding energies and the Pauli exclusion principle, as well as to estimate the excitation energy of the residual nucleus by counting the excited particle-hole states (excitons). This approximation is usually considered to work particularly well for hadron-nucleus collisions.

The well-documented JQMD code in its standard version [5] is our second choice of model. This is also a hybrid

model with a first QMD step and the statistical decay model (SDM) [40] as second step. This code introduces relativistic kinematics and relativistic corrections for the interaction term, the Lorentz boost of the initial and final states, realistic momentum distributions in the ground state, and a comprehensive nucleon-nucleon collision term [5]. The model works well for pre-equilibrium emission of particles in proton induced collisions [4,5]. In medium-energy nucleus-nucleus collisions [41] the emission of light fragments requires some minor refinements in the code. For reactions close to those studied in this work, JQMD successfully describes fragment production in p+^{56}Fe and ^{27}Al [42] in a wide energy range, from 50 MeV to 5 GeV. It could also be mentioned that JQMD has recently been used for generating a nuclear database on neutron-induced fragmentation of Si [43].

IV. EXPERIMENTAL RESULTS CONFRONTED WITH DCM AND JQMD MODELS

In this experiment the charge (Z), azimuthal (ϕ), and polar (θ) angles of the recoils were measured, whereas no energy was determined because the detector systems did not stop the recoils. By calculating the flight trajectories in the magnetic field of the CELSIUS fourth quadrant from the collision point to ZAD [19], the momenta could be obtained for 0° recoils with $A/Z = 2$. Whereas all recoils with $Z \geqslant 6$ registered in SAD provide good statistics, only a small number of heavier fragments was observed and measured by the FWD. This allows only the determination of inclusive production rates for FWD recoils, whereas recoil-He correlations can be exploited.

The technique to use inverse kinematics reactions in storage rings has the advantages of high luminosity, reduced background, etc., but leads to difficulty in measuring absolute cross sections. Because we used Monte Carlo simulations with complete experimental filters, we chose to normalize the experimental data on He fragments registered in the first ring of FWD at an angle of 4.9° by the corresponding predictions of the DCM model. Table I shows the value of differential cross section used for the normalization. This is justified, first because DCM is quite well established for the emission of He with energies 5–40 MeV and angles 30°–160°, corresponding to the region of phase space explored with FWD when the kinematics are reversed. Second, such an approach provides high statistics for He fragments in FWD and this minimizes the statistical uncertainties of the procedure. The results of the JQMD calculations were taken as they came out but they were not used for the normalization of the experimental data. DCM shows a better agreement of the shape of the angular distribution in Fig. 2 that justifies the choice of DCM for normalization. We estimate the accuracy of the absolute normalization of the experimental data to be within 20–25% [19].

TABLE I. The differential cross section for He at 4.9° used for the normalization.

Reaction	Energy (MeV/nucleon)	$\frac{d\sigma}{d\Omega}$ (b/sr)
^{28}Si+^{1}H	200	2.9
^{28}Si+^{1}H	300	2.3
^{28}Si+^{2}H	200	5.9
^{28}Si+^{2}H	300	4.9

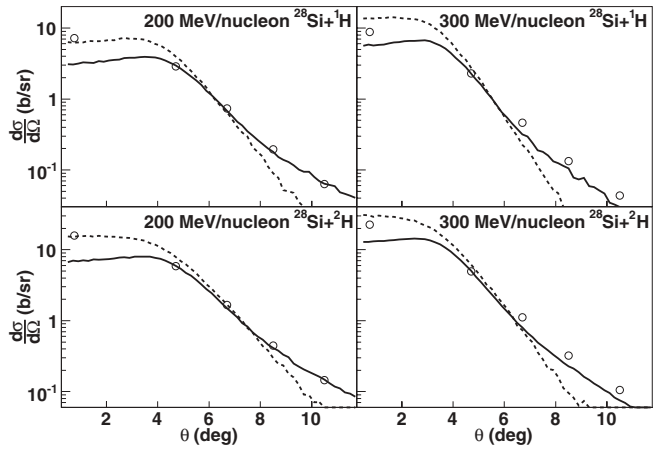

FIG. 2. Angular distribution of He fragments observed with FWD and SAD (open points) for 200 and 300 MeV/nucleon ^{28}Si+^{1}H(^{2}H) reactions confronted to the prescription of DCM (solid curves) and JQMD (dashed curves). Statistical error bars fall within the point size.

A. Inclusive production of α particles and recoils

Figure 2 shows the angular distributions of He nuclei registered by SAD, the very first point, and by FWD with four points corresponding to polar angles of the four FWD rings. DCM reproduces the shape of the angular distributions for all reactions in the region of FWD but fails quite severely to predict the yield in SAD. The JQMD version of Ref. [5], however, does not reproduce the overall shape of the distributions at all until the improvements, discussed below, are introduced.

Two improvements of the standard JQMD version have been proposed [44,45]. The first one introduces GEM [36] instead of SDM as the evaporation stage. This allows evaporation of heavy fragments. The second improvement is connected with the assumption of coalescence of light particles on the surface of the excited nucleus. This was first introduced to explain the high-energy part of the He particles measured in Ref. [46]. Introducing these two improvements may very well improve the agreement in Fig. 2 for JQMD. However, it is important to remember that the QMD approach meets principal difficulties in describing α particles [47] due to their specific properties. With this in mind, the better agreement between JQMD and the experimental values for He registered by SAD in Fig. 2 could be accidental and therefore should be taken with caution.

The systematic failure of DCM to describe the production of He nuclei within the SAD angular region is unexpected. These He fragments are almost at rest in the frame of the fragmenting source, which may be the reason why they have never been measured before in conventional experiments with stationary

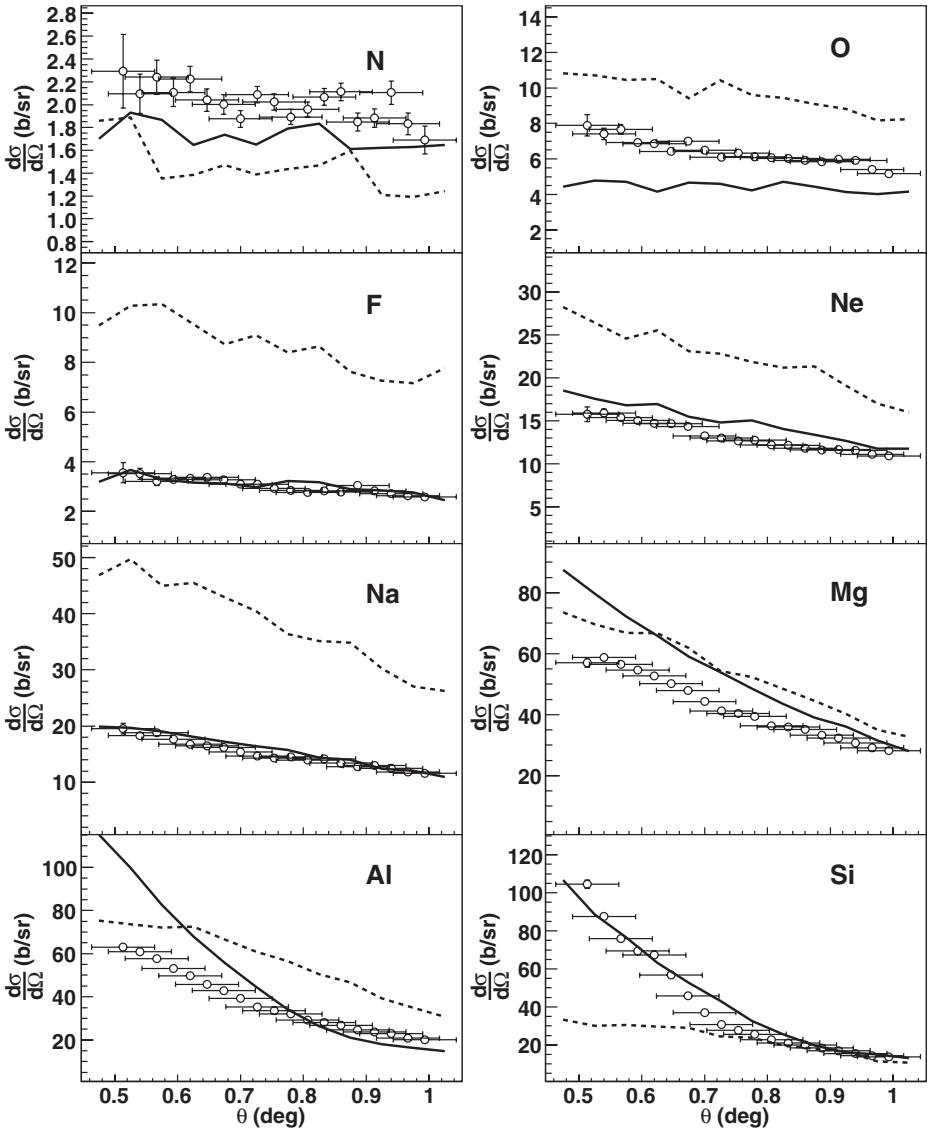

FIG. 3. Angular distribution of recoils in 200 MeV/nucleon ^{28}Si+^{1}H reactions (open points) compared with predictions of DCM (solid curves) and JQMD (dashed curves).

targets. Here, we demonstrate that there is an additional process that is strongly populating the very edge of the phase space of the statistical after-burner. Quasi-elastic scattering of α clusters preformed in the ^{28}Si nucleus could be the origin of the observed deviation from theory.

The DCM model was originally constructed for the interpretation of inclusive production of light particles and it was consequently tuned mostly by data of this kind. Therefore, it is especially interesting to check the consistency of this model for both light and heavy fragment production, measured in the same experiment. Figures 3 and 4 show the angular distributions of all recoils for ^{28}Si+^{1}H reactions at 200 and 300 MeV/nucleon. The corresponding angular distributions of recoils in ^{28}Si+^{2}H reactions, not shown for brevity, are very similar.

The experimental data are again shown together with the results of computer simulations based on the prescriptions of DCM (solid curves) and JQMD (dashed curves). Both models predict the general trend in the evolution of the shape with recoil charge rather well. These distributions are quite broad and structureless. The general tendencies to have broader distributions with decreasing fragment charge and with increasing beam energy are noticeable. Such behavior is qualitatively understood by simple phase-space arguments. The increase of the number of nucleons that are not tied up in the recoil opens up the available phase space of the recoil and so does the increased energy of the beam nucleus.

Yet, it appears from Figs. 3 and 4 that the predicting power of both models is limited to the qualitative angular dependences. The proper absolute levels are achieved only for few fragments without systematic trends. In general the DCM depicts a slightly better predictive power than JQMD for the shape of the angular distributions of the heaviest recoils. The absolute values of cross sections for production of lighter fragments, i.e., O, F, and Na, seem to be grossly overestimated by the JQMD, even if one takes into account the above mentioned uncertainties in absolute normalization of the data.

As mentioned above the experimental information on production of recoils from medium-energy reactions with light

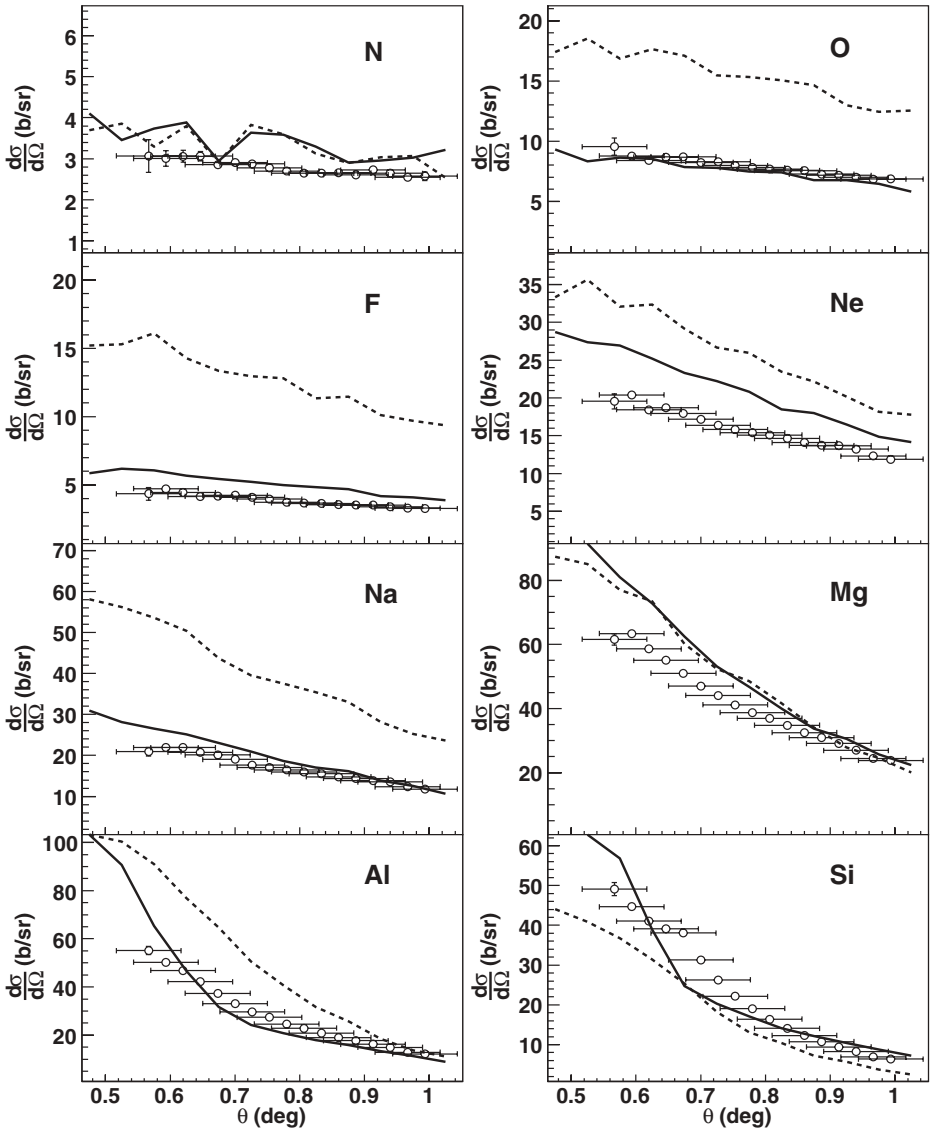

FIG. 4. Angular distribution of recoils in 200 MeV/nucleon ^{28}Si+^{1}H reactions (open points) compared with predictions of DCM (solid curves) and JQMD (dashed curves).

nuclei is quite scarce. Since the 1960s a vast amount of experimental data has been accumulated for the production of radioactive recoils, e.g., ^{18}F, ^{22}Na, and ^{24}Na in interactions of medium-energy protons with light nuclei [48]. The unique results of Ref. [8] report on mass, energy, and angular distributions of all products in the p+Al reaction at 180 MeV. No similar data exist for other reactions for energies below 500 MeV/nucleon. Figure 5 summarizes the cross sections of recoils detected by SAD in 200- and 300-MeV/nucleon ^{28}Si+^{1}H and ^{28}Si+^{2}H reactions. The results are again confronted with the DCM and JQMD theoretical cross sections filtered through the constraints of the experimental setup. The following remarks can be made.

The predictions from the two models follow in general the experimental distributions. In particular the DCM predictions are impressive with absolute yields within 10% of the measured ones with some exceptions, an overestimation of the Mg production in 200-MeV/nucleon ^{28}Si+^{2}H reactions by 20% and underestimation of Al by 20% in the 300-MeV/nucleon reactions.

The production cross sections of fragments emitted at angles close to 0°, capable of reaching ZAD, show a different behavior (Fig. 6). Although both models predict correctly the increase of the yields with increasing Z except for $Z = 14$, they both overestimate considerably the yields for all Z at angles close to 0° by factors of 5 to 10. However, a systematic difference is seen between the DCM and JQMD, especially for high Z values. This will be discussed below.

Figure 7 shows the experimental fragment momentum distributions of $A/Z = 2$ fragments emitted close to 0° from the 300-MeV/nucleon ^{28}Si+^{2}H reaction compared with the predictions from DCM. It should be noted that the theoretical distributions have been divided by 50 to get the same order of magnitude of the spectra. The model cannot reproduce the shape of the distributions at least for the heavy fragments (Al, Mg, Na, and Ne). If the model overestimates, the low- or high-momentum part is indeterminable because of the large difference in the absolute values. For the lighter fragments it is not that evident due to poor statistics in the theoretical distributions.

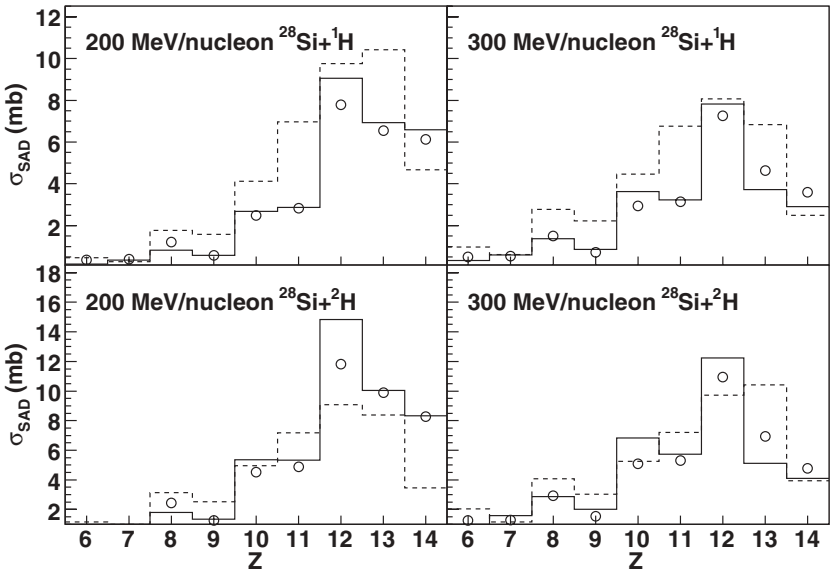

FIG. 5. The cross section for recoils of different charge detected by SAD (open points) compared with the predictions of DCM (solid histograms) and JQMD (dashed histograms).

B. Recoil-He correlations

Reactions producing $Z = 6$–13 recoils within the angular interval 0.6°–1.1°, accompanied by He nuclei, emitted at angles between 3.9° and 11.7° were analyzed through the events with coincidences between SAD and FWD. Figure 8 shows the coincidence yield as a function of the relative azimuthal angle, $\Delta\phi = \phi_{\text{recoil}} - \phi_{\text{He}}$, between the recoil and the He fragment. The experimental data are compared with theoretical prescriptions from JQMD and DCM.

The observed distributions are rather broad with centers located around $\Delta\phi$ values close to 180°. These registered recoils are the heaviest fragments emitted in each collision and normally carry away a substantial part of the total momentum of the decaying system. Momentum conservation in the decaying system prefers that the transverse-momentum components of the two most important fragments are directed back to back. All particles not registered in the setup smear out such an ideal picture. The overall power of the theory to predict these features could be confirmed only by the shapes of the distributions, whereas the yields are overestimated. The analysis of the rates for the recoil-He correlations registered by SAD and FWD for all reactions is depicted in Fig. 9. Points at $Z = 13$ and 14 are kept to demonstrate the level of the background for this experiment.

A closer look into the experimental data shows that both theories fail to explain correlations of recoils and He in cases of large relative momentum. This is shown in Fig. 10, which demonstrates the dependence of the cross sections for the discussed correlations on the scattering angle of He fragment registered in different rings of the FWD.

The intensity of He-recoil coincidences measured for larger scattering angles of He is considerably higher than that predicted by DCM and JQMD. Again, as in case of low-energy inclusive emission (Fig. 2) a possibility of direct knock-out of α clusters from the ^{28}Si nuclei could be discussed with regard to the observed discrepancies between theory and experiment.

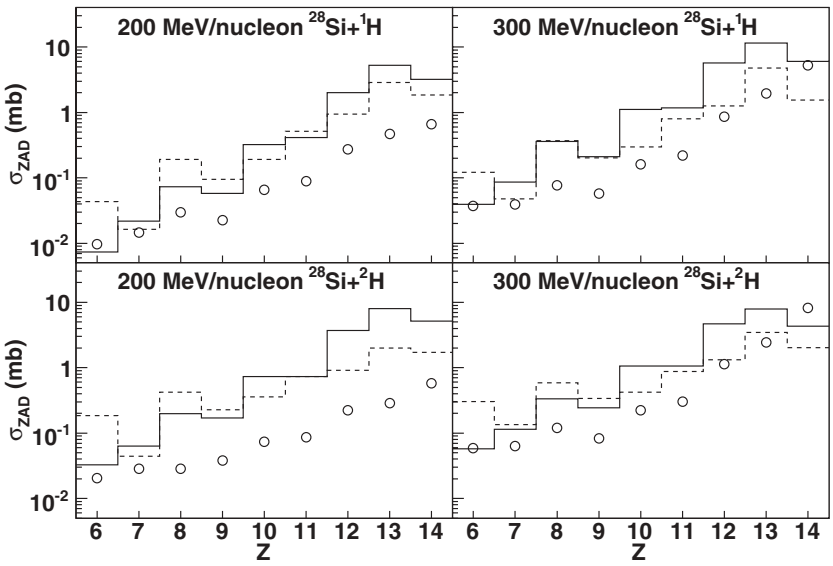

FIG. 6. Measured (open circles) and theoretically predicted DCM (solid histogram) and JQMD (dashed histogram) cross sections for ^{12}C, ^{14}N, ^{16}O, ^{18}F, ^{20}Ne, ^{22}Na, ^{24}Mg, ^{26}Al, and ^{28}Si reaching ZAD.

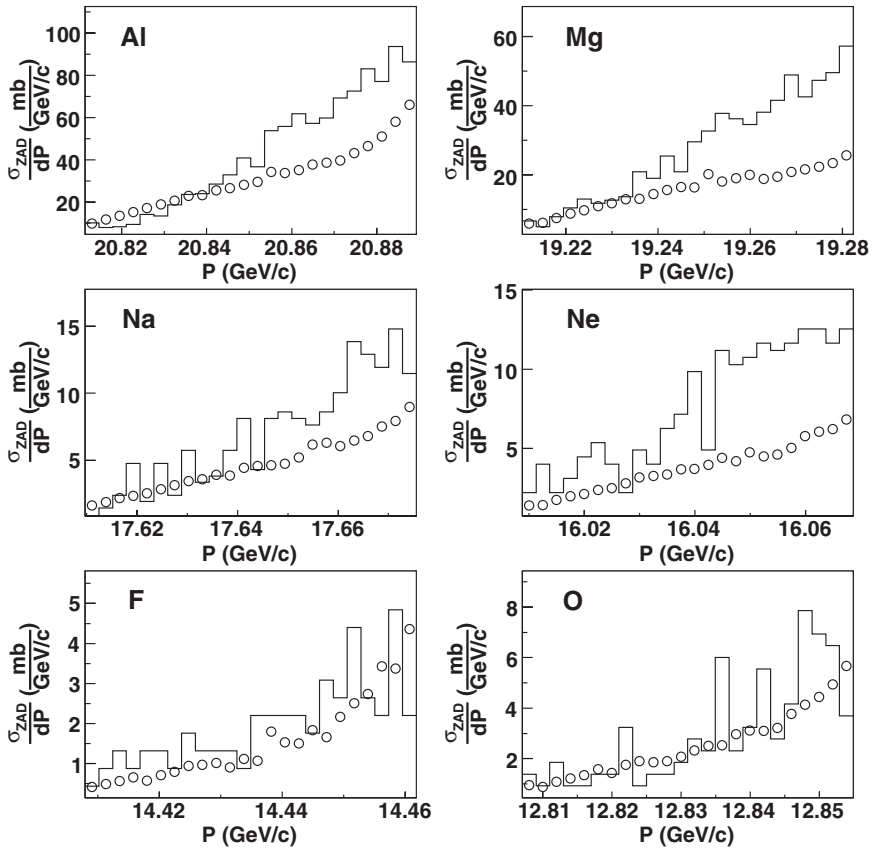

FIG. 7. Momentum distributions of recoils with $A/Z = 2$ emitted close to 0° in 300 MeV/nucleon ^{28}Si+^{2}H (open points) reactions compared to DCM predictions (histograms). The cross sections for DCM have been divided by 50 to make the comparison of the shapes easier.

C. Recoil-spectator proton correlations in ^{28}Si+^{2}H reactions

The relative cross section for the reaction channel where a recoil in SAD is registered in coincidence with a targetlike spectator, mostly protons, in STD with emission angle between 60° and 120° is shown in Fig. 11. The total cross section for this reaction channel is overestimated in JQMD, whereas it is better reproduced by DCM. The Z dependence is also better described by DCM although discrepancies still exist. Si and Al are underestimated, whereas O and Ne are overestimated.

The coincidence cross sections show many similarities with the inclusive cross sections in Fig. 5, such as the maximum of the recoil cross sections at $Z = 12$ and the local minimum for $Z = 9$. DCM also shows the same underestimation in producing the heaviest recoils. The increase of the cross section with increasing Z up to 13 (Al), predicted by JQMD, is observed neither in the data nor in the same model without coincidence. However, it would be dangerous to state that the depicted distributions are tagged by spectator-like protons only. The observed angular distributions of the tagging protons are broad and a large admixture of coincidence events where the registered proton is coming from another source than the target deuteron is possible. This possibly explains the depicted failure of JQMD to describe the experimental data and in any case it calls for additional experimental refinement.

V. DISCUSSION AND ANALYSIS

The experimental inclusive data on recoil production exhibit a satisfactory overall agreement with both DCM and JQMD models. This may, however, reflect the ability of both models to describe well the phase space that is available for the products. Both models also predict the Z dependence quite well of the fragmentation cross section in semiexclusive events with recoil-He correlations. The absolute yields of such events are overestimated by as much as 50–75%.

The two models differ, particularly in their predictions of the yields of the heaviest recoils in favor of DCM, but it should be mentioned that further development of the standard JQMD is already undertaken [44,45]. It is important to note that the situation is quite the opposite when reaction channels with small momentum transfer are addressed. The obvious preference of JQMD, with its built-in ability to describe the dynamical features of reactions, is revealed very distinctly. Figure 6 illustrates also the failure of the DCM to describe the yields of recoils emitted at very small angles due to the dynamical effects that that model totally ignores. Although not influencing the predictive power of the DCM, this reflects the limitation of the "frozen mean-field" approximation of that model. On the contrary, the ability of JQMD to describe the same data better than DCM could be explained by its ability, at least qualitatively, to describe collective "bounce-off" attributed to the dynamics of the reaction.

The ability of any of these theories to prescribe the reaction channels generating He seems questionable. An overall agreement between theory and experiment on inclusive production of He is observed only for the DCM and only if the deep sub-barrier component is not considered. JQMD fails to prescribe the slopes of the He spectra and the QMD approach is known to meet principle difficulties in

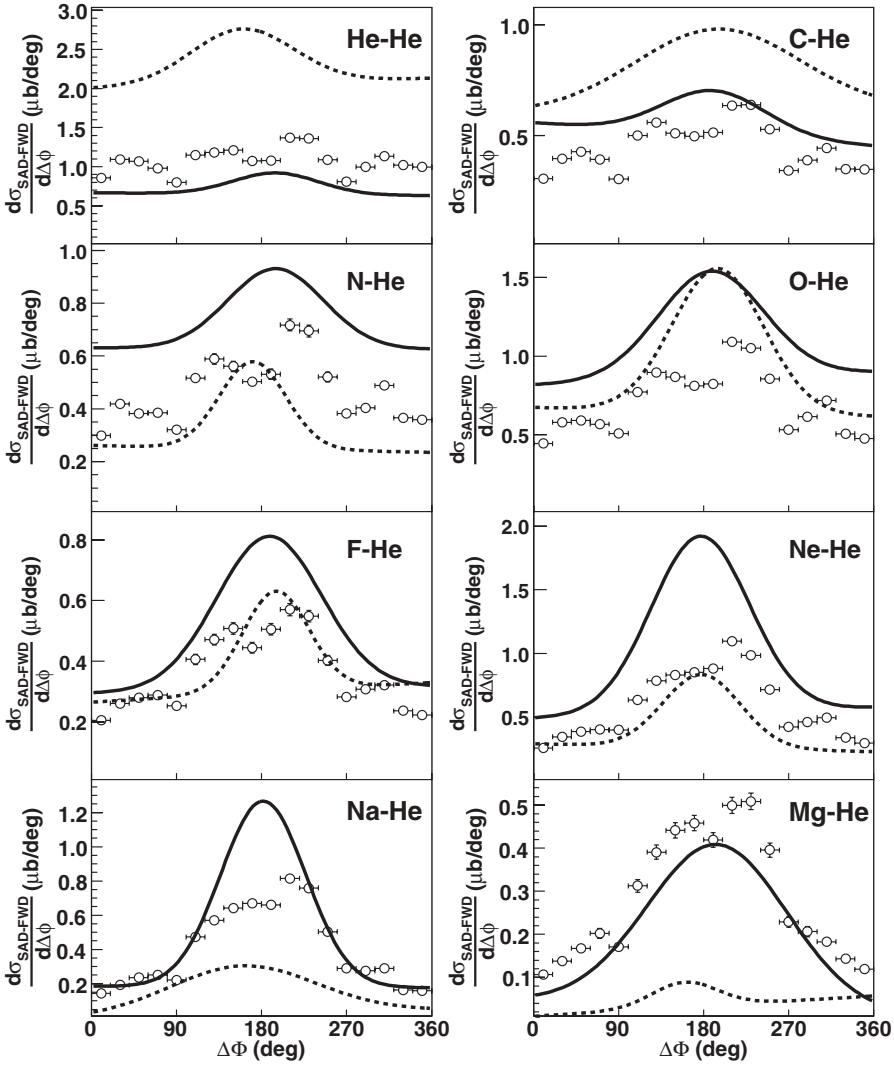

FIG. 8. Azimuthal correlations between recoils and He fragments registered by SAD and FWD. Experimental results on 300 MeV/nucleon ^{28}Si+^{2}H reactions (open points) are compared with predictions from DCM (solid lines) and JQMD (dashed lines).

describing α particles [47] due to their specific properties. The improvements of JQMD discussed in Sec. IV A could improve the inclusive angular distribution of He but we believe that these improvements will not alter our basic conclusions.

The experiment revealed two specific features of the reactions that neither DCM nor JQMD can handle. Both features are of greatest importance for the further development of the models and they could probably lead to substantial

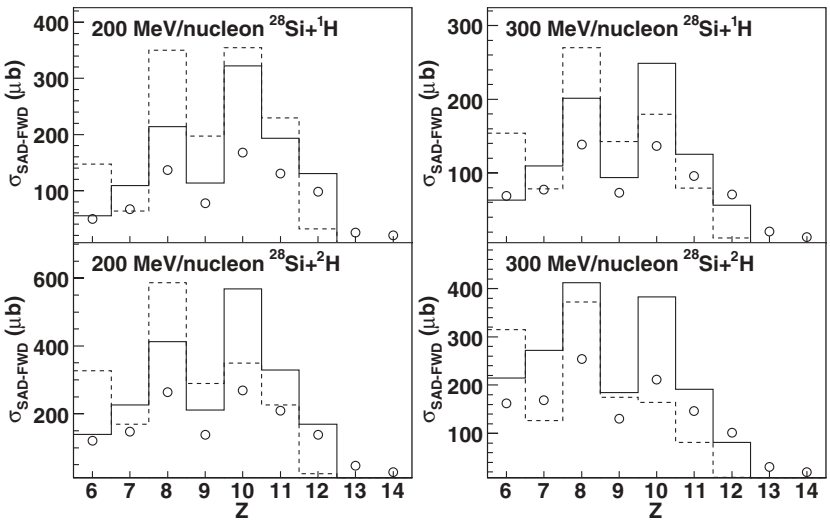

FIG. 9. Charge dependence of the cross section for correlations between recoils measured by SAD and He fragments registered by FWD (open points) compared with predictions of DCM (solid histograms) and JQMD (dashed histograms).

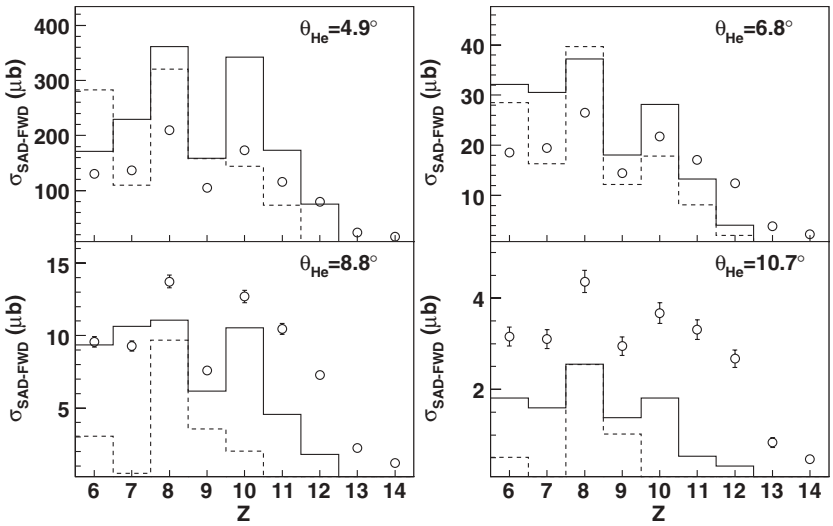

FIG. 10. Recoil-He correlation cross sections for different charge of the recoil in 300-MeV/nucleon ^{28}Si+^{2}H reactions. The emission angle ranges from 4.9° (upper left) to 10.7° (lower right). Data (open points) and predictions by DCM (solid lines) and JQMD (dashed lines).

improvement of their prediction power. First, although the total cross section for the recoil-He correlation is described well by both models the cross section for such correlations at larger scattering angle (relative momentum) is much larger in the experiment. There exists a number of predictions of preformed α clustering in light nuclei [49]. It seems obvious that future modifications of models like DCM and JQMD should address this problem specifically for light nuclei. Second, a considerable excess of He products within the acceptance of SAD has been observed for which DCM seems to have no definite explanation. SAD has an extremely low detection threshold of 100 keV for He fragments in their production system. These He nuclei could not be measured in conventional experiments. A reasonable explanation is again to be found in α clustering in ^{28}Si.

The apparent difference between the cross sections for production of recoils from the data of Figs. 5 and 6 and the results reported in Ref. [8] is misleading due to the following reasons. First, no direct comparison is possible for the data of this article to that previously reported for the 180-MeV p+Al reaction summarized in Ref. [8], our article focused on charge distributions, whereas that of the authors of Ref. [8] focused on mass distributions. To link the two sets of data, one needs to know the isotopic distributions of the reaction products, which, in fact, turn out to be strongly model dependent. Second, one should be aware that, due to the experimental setup, the recoil charge distributions demonstrated in Figs. 5 and 6 refer to recoil yields integrated within the angular acceptance of SAD or ZAD and essentially differ from the total recoil cross sections, especially in case of lighter recoils.

The similarity in the differential cross sections in Figs. 3 and 4 for all recoils except Si might indicate that saturation of the fragmentation cross sections has been reached at 200 MeV/nucleon. However, data in Fig. 6 show that this statement is not valid for recoils emitted at very small angles. As mentioned above, our experimental setup covered only a part of the available phase space and therefore, direct measurements of the total cross sections are needed before definite conclusions on the energy threshold for limiting fragmentation of Si can be made.

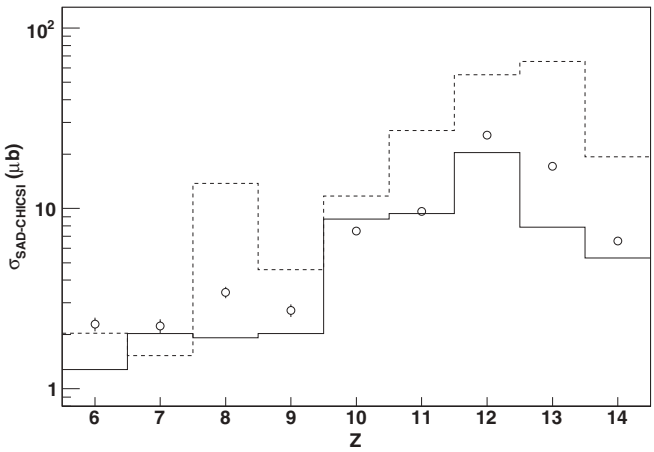

FIG. 11. Charge dependence of the cross section in 300-MeV/nucleon ^{28}Si+^{2}H reactions for a recoil in SAD in coincidence with a low-energy proton in STD. Notations are the same as described in the caption to Fig. 10.

VI. SUMMARY

We measured the relative production cross sections of recoils from 200- and 300-MeV/nucleon proton and deuteron-induced reactions with ^{28}Si nuclei. The data, obtained in the inverse kinematics scheme, were compared with predictions from the hybrid DCM and JQMD models.

It was found that in general both models describe reasonably well the overall charge and angular distributions of the fragmentation cross sections but the absolute yields differ by as much as 50–75%. The number of recoils emitted at very small angles is described reasonably well only within the frame of the JQMD model, which we attributed to the "bounce-off" of the source of recoils, which cannot be described by the DCM. These experimental observations call for improvements of the models before using them for SEEs predictions.

Two features of the studied reactions are not described at all by the models: first, the growing excess of the experimental cross sections for the recoil-He correlation over standard theory with increasing scattering angle between the recoil and He. This may be linked to the knock-out process of He from ^{28}Si, usually explained in terms of preformed α clustering. Second, we observe a large excess of low-energy He fragments that could also be explained qualitatively by α clustering in ^{28}Si nuclei.

These observations call for additional experimental and theoretical study of fragmenting nuclear systems with large initial admixture of α clusters that in turn could lead to a considerable improvement of the reaction models of primary importance for the SEEs application.

ACKNOWLEDGMENTS

We are grateful for all help that the staff of TSL provided and especially for the extraordinary efforts made by the TSL accelerator team, headed by Dag Reistad. This project has been funded by the US Party of the International Science and Technology Center (ISTC) [50], for which we are deeply grateful. Our thanks go also to the FOI, Sweden, providing funds to support stays of the international team at TSL.

[1] H. H. K. Tang, IBM J. Res. Dev. **40(1)**, 91 (1996).
[2] H. H. K. Tang and N. Olsson, MRS Bull. **28(2)** (2003).
[3] V. D. Toneev and K. K. Gudima, Nucl. Phys. **A400**, 173 (1983).
[4] K. K. Gudima, S. G. Mashnik, and V. D. Toneev, Nucl. Phys. **A401**, 329 (1983).
[5] K. Niita, S. Chiba, T. Maruyama, T. Maruyama, H. Takada, T. Fukahori, Y. Nakahara, and A. Iwamoto, Phys. Rev. C **52**, 2620 (1995).
[6] P. Goldhagen, MRS Bull. **28**, 131 (2003).
[7] F. E. Bertrand and R. W. Peelle, Phys. Rev. C **8**, 1045 (1973).
[8] K. Kwiatkowski, S. H. Zhou, T. E. Ward, V. E. Viola, H. Breuer, G. J. Mathews, A. Gökmen, and A. C. Mignerey, Phys. Rev. Lett. **50**, 1648 (1983).
[9] H. Machner, D. G. Aschman, K. Baruth-Ram, J. Carter, A. A. Cowley, F. Goldenbaum, B. M. Nangu, J. V. Pilcher, E. Sideras-Haddad, J. P. F. Sellschop *et al*., Phys. Rev. C **73**, 044606 (2006).
[10] L. W. Woo, K. Kwiatkowski, W. G. Wilson, V. E. Viola, H. Breuer, and G. J. Mathews, Phys. Rev. C **47**, 267 (1993).
[11] M. B. Chadwick, S. Chiba, K. Niita, T. Maruyama, and A. Iwamoto, Phys. Rev. C **52**, 2800 (1995).
[12] S. Chiba, M. B. Chadwick, K. Niita, T. Maruyama, T. Maruyama, and A. Iwamoto, Phys. Rev. C **53**, 1824 (1996).
[13] H. H. K. Tang, G. R. Srinivasan, and N. Azziz, Phys. Rev. C **42**, 1598 (1990).
[14] J. Cugnon and J. Vandermeulen, Ann. Phys. (Paris) **17**, 49 (1989).
[15] J. Cugnon and P. Henrotte, Eur. Phys. J. A **16**, 393 (2003).
[16] Y. Murin *et al*., *STORI 05, Schriften des Forschungszentrums Jülich. Reihe Materie und Material/Matter and Materials 30*, edited by David Chiladze, Andro Kacharava, Hans Ströher (Forschungszentrum Jülich, Zentralbibliothek, Verlag, Jülich, 2005), p. 153.
[17] J. Aichelin, C. Bargholtz, J. Blomgren, A. Budzanowski, M. Chubarov, B. Czech, C. Ekström, L. Gerén, B. Jakobsson, A. Kolozhvari *et al*., in *Proceedings of International Conference on Nuclear Data for Science and Technology*, Santa Fe, NM, September 26–October 1, 2004, AIP Conf. Proc. No. 769, edited by Robert C. Haight, Mark B. Chadwick, Toshihiko Kawano, and Patrick Talou (AIP, New York, 2005), p. 1624.
[18] C. C. Foster, P. M. O'Neill, and C. K. Kouba, IEEE Trans. Nucl. Sci. **53**, 3494 (2006).
[19] Y. Murin, Y. Babain, M. Chubarov, Y. Tuboltsev, V. Pljuschev, M. Zubkov, P. Nomokonov, A. Voronin, M. Merkin, V. Kondratiev *et al*., Nucl. Instrum. Methods A **578**, 385 (2007).
[20] A. Budzanowski, B. Czech, A. Siwek, I. Skwirczynska, and P. Staszel, Nucl. Instrum. Methods A **482**, 528 (2002).
[21] L. Westerberg, V. Avdeichikov, L. Carlén, P. Golubev, B. Jakobsson, C. Rouki, A. Siwek, E. J. van Veldhuizen, and H. J. Whitlow, Nucl. Instrum. Methods A **500**, 84 (2003).
[22] P. Golubev, V. Avdeichikov, L. Carlén, B. Jakobsson, A. Siwek, E. J. van Veldhuizen, L. Westerberg, and H. J. Whitlow, Nucl. Instrum. Methods A **500**, 96 (2003).
[23] L. Carlén, G. Førre, P. Golubev, B. Jakobsson, A. Kolozhvari, P. Marciniewski, A. Siwek, E. J. van Veldhuizen, L. Westerberg, H. J. Whitlow *et al*., Nucl. Instrum. Methods A **516**, 327 (2004).
[24] C. Bargholtz, K. Lindh, D. Protic, N. Ruus, P.-E. Tegnér, P. T. Engblom, and K. W. Rolander, Nucl. Instrum. Methods A **390**, 160 (1997).
[25] A. Ringbom, G. Tibell, R. Zorro, J. Blomgren, H. Condé, K. Elmgren, S. Hultqvist, J. Nilsson, N. Olsson, C. Fahlander *et al*., Nucl. Instrum. Methods A **373**, 57 (1996).
[26] R. Serber, Phys. Rev. **72**, 1114 (1947).
[27] G. D. Harp and J. M. Miller, Phys. Rev. C **3**, 1847 (1971).
[28] J. J. Griffin, Phys. Lett. **B24**, 5 (1967).
[29] M. Blann and M. B. Chadwick, Phys. Rev. C **57**, 233 (1998).
[30] H. Feshback, A. Kerman, and S. Koonin, Ann. Phys. (NY) **125**, 429 (1980).
[31] G. F. Bertch and S. Das Gupta, Phys. Rep. **160**, 189 (1988), and references therein.
[32] J. Aichelin, Phys. Rep. **202**, 233 (1991), and references therein.
[33] H. Feldmeier, Nucl. Phys. **A515**, 147 (1990).

[34] A. Ono, H. Horiuchi, T. Maruyama, and A. Ohnishi, Prog. Theor. Phys. **87**, 1185 (1992).
[35] S. G. Mashnik, K. K. Gudima, A. J. Sierk, M. I. Baznat, and N. V. Mokhov, Los Alamos National Laboratory Report LA-UR-05-7321.
[36] S. Furihata, Nucl. Instrum. Methods B **171**, 251 (2000).
[37] E. Fermi, Prog. Theor. Phys. **5**, 570 (1950).
[38] V. D. Toneev, N. S. Amelin, K. K. Gudima, and S. Y. Sivoklokov, Nucl. Phys. **A519**, 493 (1990).
[39] N. S. Amelin, K. K. Gudima, and V. D. Toneev, Sov. J. Nucl. Phys. **50**, 172 (1990), and references therein.
[40] R. J. Charity, Nucl. Phys. **A483**, 371 (1988).
[41] S. Chiba, O. Iwamoto, T. Fukahori, K. Niita, T. Maruyama, T. Maruyama, and A. Iwamoto, Phys. Rev. C **54**, 285 (1996).
[42] T. Maruyama, K. Niita, and A. Iwamoto, Phys. Rev. C **53**, 297 (1996).
[43] Y. Watanabe, A. Kodama, Y. Tukamoto, and H. Nakashima, in *Proceedings of International Conference on Nuclear Data for Science and Technology*, Santa Fe, NM, September 26–October 1, 2004, AIP Conf. Proc. No. 769, edited by Robert C. Haight, Mark B. Chadwick, Toshihiko Kawano, and Patrick Talou (AIP, New York, 2005), p. 1646.
[44] Y. Watanabe and D. N. Kadrev, Radiation Protection Dosimetry, **126**, 1 (2007).
[45] H. Iwase, K. Niita, and T. Nakamura, J. Nucl. Sci. Technol. **39**, 1142 (2002).
[46] U. Tippawan, S. Pomp, A. Ataç, B. Bergenwall, J. Blomgren, S. Dangtip, A. Hildebrand, C. Johansson, J. Klug, P. Mermod *et al*., Phys. Rev. C **69**, 064609 (2004).
[47] A. Ono (private communication).
[48] R. G. Korteling and A. A. Caretto, Phys. Rev. C **1**, 193 (1970).
[49] J. A. Maruhn, M. Kimura, S. Schramm, P.-G. Reinhard, H. Horiuchi, and A. Tohsaki, Phys. Rev. C **74**, 044311 (2006).
[50] Http://www.istc.ru.

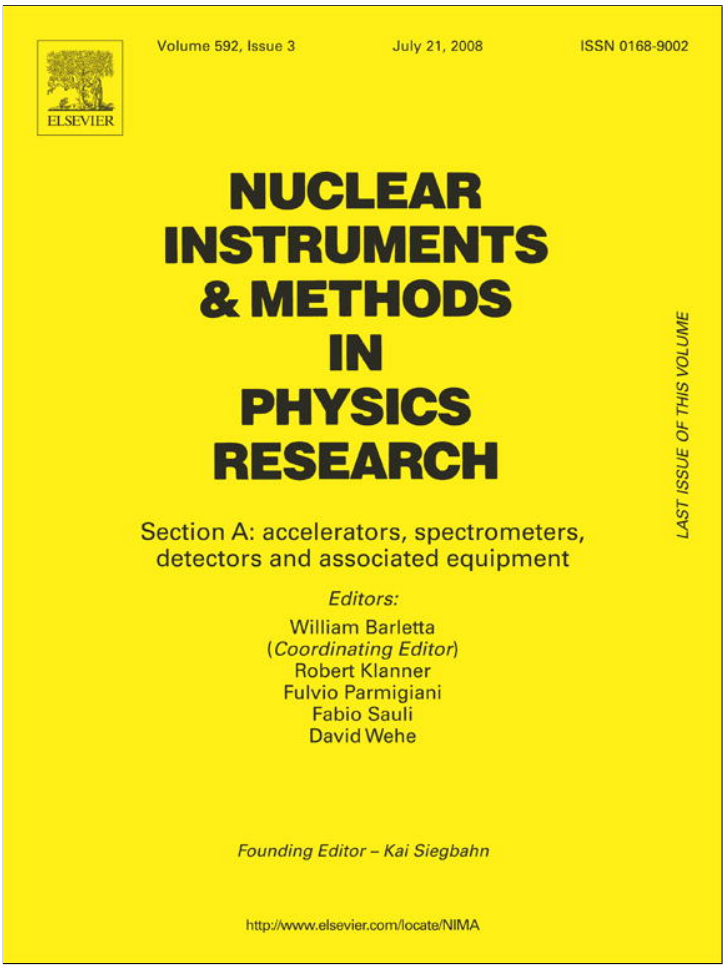

Nuclear Instruments and Methods in Physics Research A 592 (2008) 405–413

Contents lists available at ScienceDirect

Nuclear Instruments and Methods in Physics Research A

journal homepage: www.elsevier.com/locate/nima

Calibration procedure for a neutron monitor at energies below 20 MeV

A. Öhrn [a,*], J. Blomgren [a], H. Park [b], S. Khurana [c], R. Nolte [c], D. Schmidt [c], K. Wilhelmsen [d]

[a] Department of Neutron Research, Uppsala University, Uppsala, Sweden
[b] Korean Research Institute of Standards and Science, Daejeon, Korea
[c] Physikalisch-Technische Bundesanstalt, Braunschweig, Germany
[d] Swedish Defense Research Agency, Stockholm, Sweden

ARTICLE INFO

Article history:
Received 26 October 2007
Received in revised form
27 March 2008
Accepted 17 April 2008
Available online 6 May 2008

Keywords:
Neutron
Detector response
Unfolding
Flux measurements
Liquid scintillator

ABSTRACT

A liquid scintillation detector aimed for neutron energy and fluence measurements in the energy region below 20 MeV has been calibrated using monoenergetic and white spectrum neutron fields. Careful measurements of the proton light output function and the response matrix have been performed allowing for the application of unfolding techniques using existing codes. The response matrix is used to characterize monoenergetic neutron fields produced by the T(d,n) reaction at low deuteron energies.

1. Introduction

During the last few decades, it has become possible to produce sufficiently intense beams of fast neutrons with quasi-monoenergetic as well as white spectra [1,2] to perform studies of nuclear structure phenomena and to investigate various biological (radiation protection) [3] and technical (single-event effects) [4,5] consequences of environmental fast neutrons. Fast neutrons are also utilized for tumor treatment in radiation therapy [3,6]. Other research fields where fast neutrons are expected to play an important role are within the energy sector, i.e., for transmutation of nuclear waste from fission reactors [7,8] and for plasma diagnostics in fusion research [9]. The strongly expanding importance of fast neutrons in these applications requires steps to be taken to improve the technology for neutron fluence and energy measurements in various energy ranges. This requirement was addressed and the current situation summarized at a recent workshop, the International Workshop on Neutron Field Spectroscopy in Science held in Pisa, Italy, June 4–8, 2000 [10]. In a review talk [11] at this conference the development within the neutron spectroscopy field during the last two decades of the previous century and the present status were summarized. The talk gives an overview of the breadth of the technology of the field and suggests that it is advisable to consider the various options before choosing a particular technique for a certain application in a certain neutron energy region.

In the application considered in this work—a monitor for fluence and energy measurements in the energy region from a few MeV to about 20 MeV—there are several options possible, but if resolution and detection efficiency are taken into consideration, the most attractive alternatives seem to be the organic scintillator with or without applying time-of-flight (TOF) techniques. In the present application the neutron source is continuous and therefore the TOF technique is out of question. The obvious choice is therefore to perform pulse-height (PH) spectrum measurements and to apply unfolding techniques. An attractive feature of some organic scintillators is that pulse-shape discrimination (PSD) techniques can be used to distinguish neutron radiation from gamma rays. Another advantage in using an organic scintillator is that the technique is relatively user friendly once the detector assembly has been properly characterized.

In the present paper, a method is described which goes beyond the procedure developed in the past at Physikalisch-Technische Bundesanstalt (PTB) for the determination of response matrices for liquid scintillation detectors [13,14]. The earlier method involved measurements of the light output function and the PH resolution of the detector [12]. These quantities were used as input for the calculation of the response matrix using the Monte Carlo method. In the new approach, the response matrix is established using experimental PH spectra. Monte Carlo simulations are only required for the normalization of the experimental spectra. In the present work, both approaches were used to obtain

* Corresponding author.
E-mail address: angelica@tsl.uu.se (A. Öhrn).

0168-9002/$ - see front matter © 2008 Elsevier B.V. All rights reserved.
doi:10.1016/j.nima.2008.04.030

response matrices which were used to determine spectral neutron fluence distributions by unfolding of PH spectra. The results from the unfolding procedures were compared with those obtained using the TOF to measure the spectral fluence. They have been presented at a conference [15].

The experimental methods and the basic data analysis are described in Section 2. Tests of calculated and experimental response matrices are presented in Section 3. Conclusions from the present work are given in Section 4.

2. Experimental methods

2.1. Basic detector requirements and measuring procedure

Organic scintillation detectors are frequently employed to determine the spectral distribution of neutrons fields. Depending on the source properties, either the TOF method or unfolding of PH spectra is used to obtain spectrometric information. As a prerequisite, the two methods require a detailed description of the detector properties.

For neutron energies below 20 MeV, the response matrix of a scintillation detector can be calculated using Monte Carlo codes provided the specific light outputs for protons, deuterons and alpha particles are known for a particular detector. For energies above about 8 MeV, however, no available Monte Carlo code is capable of describing the response of a scintillation detector in full detail, because the required sufficient detailed multi-differential emission cross-sections for alpha particles from the $^{12}C(n, n'3\alpha)$ reaction are not available. Hence, the characterization of scintillation detectors always requires an experimental investigation of the detector response.

The standard procedure developed at PTB for the characterization of scintillation detectors uses monoenergetic and breakup neutrons produced with the D(d,n) reaction. It provides the light output functions for protons and alpha particles as well as empirical corrections for the efficiencies calculated with a Monte Carlo code for selected detection thresholds [16].

The standard procedure is satisfactory for the application of the TOF method. For the application of unfolding techniques, however, a proper description of the full response matrix is required since any deviation of the response matrix from the 'true' PH response of the detector would cause spurious structures in the unfolded spectral fluence. This is of particular importance if unfolding techniques are to be applied to neutron fields covering a broad energy range since low detection thresholds have to be used in this case.

For this purpose, a method described by Dekempeneer et al. [17] has been adopted. A white neutron beam measurement is used to obtain a smooth light output function for protons and an experimental response matrix with sufficient resolution in neutron energy. This method has been tested on a liquid scintillator that will be used as a neutron monitor for a DT neutron generator recently installed at the Swedish Defense Research Agency (FOI) [18]. The detector will be employed to measure the spectral neutron fluence over the energy range from about 1 to 15 MeV, primarily to distinguish unscattered neutrons produced by the T(d,n) reaction from scattered neutrons and to exclude neutrons produced by the D(d,n) reaction with implanted deuterium. Because the neutron generator runs in DC mode, the only applicable spectrometric technique is unfolding of PH spectra.

2.2. The scintillation detector

The scintillation detector consists of a commercial cylindrical detector cell of the MAB-1F type filled with BC501 scintillator liquid. The inner length and diameter of the cell is 5.08 cm. The cell is coupled to the photocathode of an XP2020 photomultiplier tube by a conical PMMA light guide which is partially coated with white reflective paint to reduce the effect of the spatially inhomogeneous light collection efficiency on the PH resolution [19]. The detector is equipped with a standard PTB gain stabilization system [20] which regulates the high voltages in such a way that the maximum change of the gain due to count-rate and temperature effects is smaller than 0.5%. Standard NIM modules are used to derive a pulse-height (PH) signal from the ninth dynode as well as a pulse-shape (PS) signal for n/γ discrimination and a time-of-flight (TOF) signal from the anode of the photomultiplier. The three signals are registered by a multi-parameter data acquisition system.

2.3. Detector characterization using the standard PTB procedure

The PTB standard procedure for the determination of the relevant properties of an organic scintillation detector has been described in detail elsewhere [12]. Only the results obtained for the particular detector under study are summarized here.

Five neutron beams were produced by deuterons with energies of 5.01, 7.12, 9.06, 10.30, and 11.27 MeV using a deuterium gas target at the PTB neutron scattering facility. The energies of the monoenergetic neutrons were 7.95, 10.05, 11.93, 13.12, and 14.05 MeV. The maximum energy of the corresponding breakup continua was about 6.5 MeV below that of the monoenergetic neutrons. About 30 narrow TOF windows were placed on the monoenergetic neutrons and the breakup continuum to produce PH spectra which were used to determine the proton light output and the efficiency of the detector.

The Monte Carlo code NRESP7 [21] was used to calculate PH spectra for comparison with experimental spectra obtained at the five energies where monoenergetic neutrons from the D(d,n)^{3}He reaction were available. By fitting these calculated spectra to the experimental ones, the light output function for protons, i.e., the pulse height corresponding to the recoil proton edge, was determined with an iterative procedure. The pulse height was measured using a calibration with photon sources. The deviation of the experimentally determined light output for protons from the arbitrary reference light output [21], which was used for the calculation of spectra in the first iteration, is 3–4% at maximum. The reference light output function depends linearly on the proton energy above 8 MeV. It has to be noted that only the five data points from monoenergetic neutrons are available above 8 MeV. Hence, a smooth interpolating curve through the scattered data points below 8 MeV had to be matched continuously to a linear fit to the five data points above 8 MeV to arrive at an improved smooth light output curve for use in further Monte Carlo calculations.

The experimentally determined PH resolution $\Delta L/L$ is shown in Fig. 1. A fit of the standard parametrization [12]

$$\left(\frac{\Delta L}{L}\right)^2 = A^2 + \frac{B^2}{L} + \left(\frac{C}{L}\right)^2 \quad (1)$$

showed an unexpectedly large value of the parameter A which describes the effect of spatial inhomogeneties in the light collection efficiency. The observed value $A = 7.2 \pm 0.6\%$ for this particular detector has to be compared with $A \approx 3\%$ usually obtained for detectors of the same size and construction. The parameter B for the present detector was $10.5 \pm 0.5\%$ which is within the range observed for other comparable detectors. The parameter C accounts for the effect of electronic noise and yields a negligible contribution to the resolution, except at very low pulse height. For this parameter a value of 0.5% was assumed. Despite

several efforts, no definitive reason for the unexpectedly large value of parameter A has been found. Possible explanations, however, could be an inhomogeneous sensitivity of the cathode of the photomultiplier or deficiencies in the optical coupling of the scintillator cell to the photomultiplier.

The fluences of the monoenergetic neutrons were measured with the PTB 4 in. $\times$ 1 in. NE213 reference detector. This detector was repeatedly compared with the PTB recoil proton telescope. For a selected PH threshold, the efficiency of the detector is known with an uncertainty of about 1.5% [16]. The fluence was also determined with the FOI detector by normalizing calculated PH spectra to corresponding experimental spectra in the flat part of the response function which is essentially determined by np scattering. The calculated spectra were obtained with NRESP7 using the nominal detector data for the density and elemental composition of the liquid scintillator and the dimensions of the detector cell. The mean ratio of the fluence determined with the FOI detector and that measured with the PTB reference detector was 1.018 ± 0.009 which is within the range of results for other detectors [12]. This is illustrated in Fig. 2 which shows comparisons of the measured and calculated PH spectra for the five energies where monoenergetic neutrons were available. These figures also illustrate the insufficient description of the structures in the PH response caused by the $^{12}C(n, \alpha x)$ channels, in particular at neutron energies above 10 MeV. The deviations visible near the edge of the PH spectra for monoenergetic 13.12 MeV and the 14.05 MeV neutrons were also observed for other detectors with similar diameter and lengths of 2 in. as well as 4 in. They can only partly be explained by the angular dependence of the differential (np) scattering cross-sections which was taken from ENDF/B-V or by deficiencies of the gaussian model used to describe the PH resolution. This is why an alternative method for a completely experimental determination of the response function is of importance.

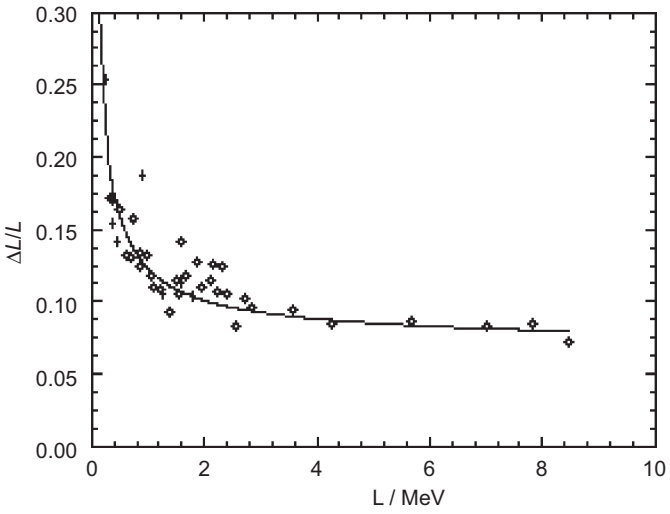

Fig. 1. Experimental PH resolution of the detector.

2.4. Determination of the experimental response matrix

A white neutron beam was produced at the PTB TOF facility by bombarding a 3 mm thick Be target with a 19 MeV proton beam from the PTB isochronous cyclotron. The maximum energy of the neutron field at an emission angle of 0° is 17.15 MeV. The spectral fluence in this neutron field extends to neutron energies below 1 MeV and varies by about one order of magnitude over this energy range. The relative spectral fluence distribution at the position of the scintillation detector is shown in Fig. 3. More details on this neutron field can be found in the literature [22].

The neutron field was collimated by one of the collimators of the PTB TOF facility. The scintillation detector was positioned at a distance of 27.39 m from the Be target. At this position the beam had a diameter of about 45 cm. The repetition frequency was reduced to 243.37 kHz by the internal beam pulse selector system of the cyclotron. Hence, the neutron energy threshold for time-frame overlap was 0.23 MeV. This neutron energy corresponds to a

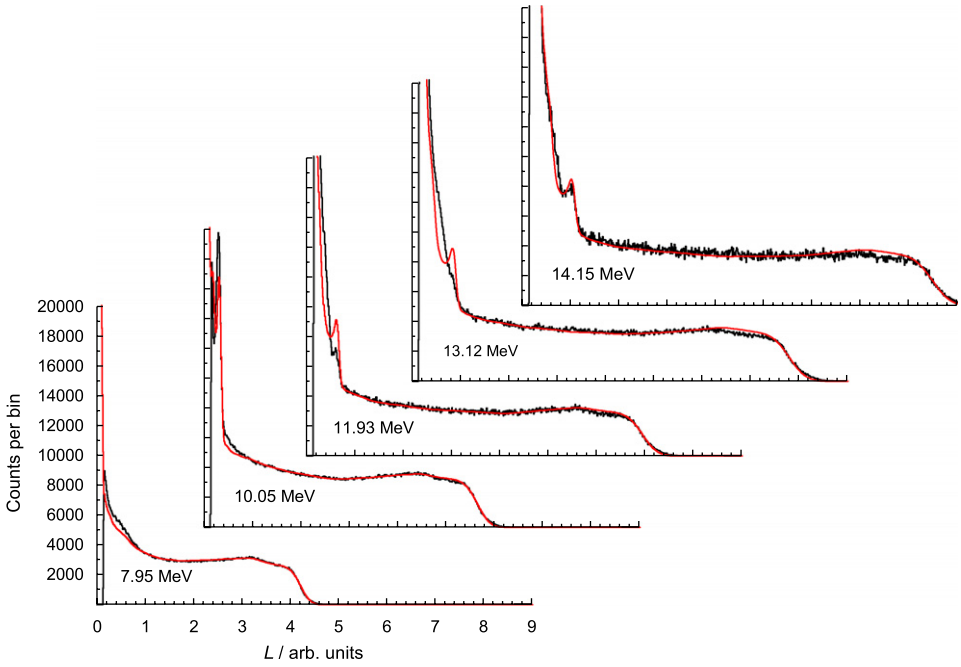

Fig. 2. Experimental (black histogram) and calculated (red line) pulse height spectra for monoenergetic neutrons from the D(d,n) reaction. The calculated spectra were produced with the NRESP7 code using the proton light output function determined for the FOI detector.

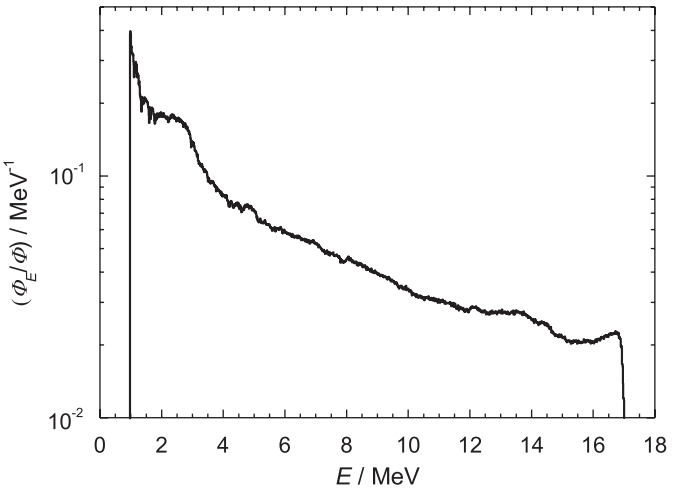

Fig. 3. Spectral neutron distribution of the ^{9}Be(p,n) field produced with a 19 MeV proton beam incident on a thick Be target.

PH of about 23 keV, which is far below the hardware PH threshold of about 200 keV. The proton current was about 150 nA which results in about 4.5×10^3 neutrons/s on the detector front face. The average zero-threshold detection efficiency for neutrons from the white beam spectrum is about 25%. The probability for multiple neutron interactions during one beam pulse was therefore less than 0.5%. Hence, a correction for the distortion of PH spectra by multiple neutron interactions was not necessary.

Energy calibration of the PH spectra was established using ^{137}Cs, ^{22}Na and ^{207}Bi photon sources. The calibration of the measured PH in electron energies and the electronic offset were determined by fitting PH spectra calculated with the PHRESP code [23] to the experimental spectra. The stability of the PH calibration and the electronic offset was investigated by repeated measurements with a ^{22}Na source. The energy per channel was found to vary no more than a few per mille throughout the experiment.

The differential non-linearity of the time-to-amplitude converter (TAC) was measured using the anode signal produced by photons from a radioactive source as the start signal and the output of an 100 kHz oscillator as the stop signal. Non-statistical relative deviations from the mean of the flat TOF spectrum were less than 10^{-3}. The deviating structures extended over less than 50 ns. Hence, the uncertainty of the TOF measurement due to TAC non-linearities was smaller than 50 ps. For comparison, the width of a channel in the TOF spectrum was 0.6 ns.

The registered events were sorted into two two-dimensional matrices. The PH vs. PS matrix served to establish the condition for the separation of events caused by interaction of photons generated in the neutron production target (prompt photons) or by inelastic scattering of neutrons in the detector (neutron-induced photons) from those caused by light charged particles (LCP), i.e., hydrogen and helium isotopes, resulting from interactions of neutrons with hydrogen and carbon nuclei. Events of the latter kind were stored in the PH vs. TOF matrix.

The time structure of the proton beam showed satellite pulses, i.e., proton bunches which were not completely deflected by the internal beam pulse selector system. This manifests itself in spurious shifted neutron distributions in the PH vs. TOF matrix. The separation of these distributions from the main distribution are multiples of the repetition time of the unpulsed proton beam. It can be assumed that the spectral distribution of the satellite neutrons are identical to that of the neutrons resulting from the main proton bunch. Therefore, the PH vs. TOF matrix was corrected by subtracting shifted TOF spectra. These spectra were normalized by the ratio of the integral number of events in the main and satellite TOF spectra for high PH thresholds for which a complete separation of main and satellite peaks is obtained. The number of satellite events were always less than 1% of the main peak, see Fig. 6 in Ref. [24].

The full TOF range was subdivided into narrow adjacent windows which covered the neutron energy range from 1 to 17 MeV. The width $\Delta E_i = E_i - E_{i-1}$ of window i was small compared with the width of the energy interval corresponding to the PH resolution ΔL_{p_i} at the proton energy E_i,

$$\Delta E_i \approx \frac{1}{5}\left(\frac{\mathrm{d}L_p}{\mathrm{d}E}\right)^{-1} \Delta L_{p_i}. \quad (2)$$

Fig. 4 shows the width of the TOF windows as a function of neutron energy. The PH spectra produced for these small energy windows should be essentially identical to that of monoenergetic neutrons if distortions of the spectra caused by the selection of events via TOF conditions can be excluded.

The most important effect to be considered in this respect is the residual dependence of the measured TOF on PH, i.e. the time-walk of the constant fraction discriminator (CFD) used to provide the start signal for the TOF measurement. This is most clearly visible in the dependence of the position of the high-energy edge of the neutron TOF spectrum on PH. Fig. 5 shows the variation of the position of this structure when small PH windows are used to produce TOF spectra. The maximum deviation is about 0.4 ns which corresponds to less than one channel in the TOF spectrum and to about 15% of the width of the smallest TOF window used to produce PH spectra. In principle, a correction of the walk effect could be carried out by applying a transformation to the PH vs. TOF matrices which depends on the PH. However, such a transformation could result in new artefacts due to the binned structure of the data, in particular when strong spectral gradients are present. Therefore, such a correction was not attempted in the present analysis.

Distortions of the PH spectra obtained from the measurements in the white beam could be detected by a comparison of these spectra with those measured using monoenergetic neutrons for energies above 10 MeV. This comparison is depicted in Fig. 6 for neutron energies above 8 MeV. Fig. 7 shows the ratio of the integral number of events above a lower integration threshold L_0. For neutron energies above 10 MeV deviations are visible in the flat part of the PH spectra. The relative deviation in the flat part amounts to 4% at maximum which is larger than expected from

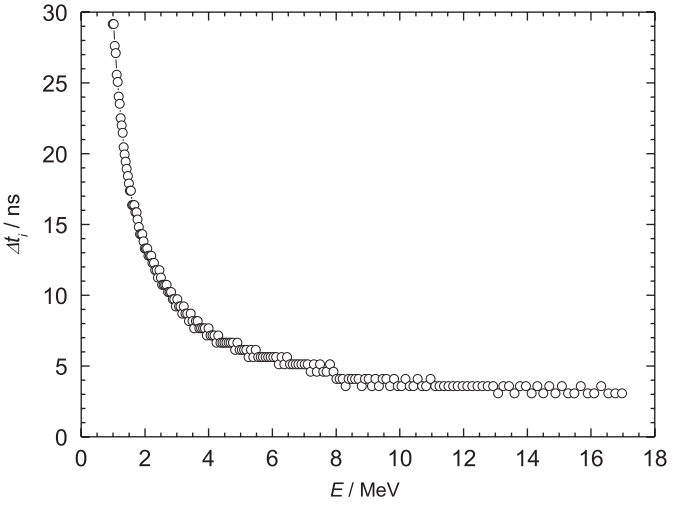

Fig. 4. Width of the TOF windows used for producing the PH spectra for the experimental response matrix. The widths were calculated using Eq. (1) and Eq. (2).

the time-walk effect discussed above. At lower neutron energies, the agreement of the shape of the PH spectra measured in the white ^{9}Be(p,n) beam and the D(d,nx) breakup continuum was much better. At these energies, the time-walk effect discussed above would have a less important influence because the width of the TOF windows is larger. So far, the origin of these discrepancies remains unexplained but an electronic artefact seems to be the most likely reason. The influence of the deviations on the application of the response matrix has therefore to be investigated. Such an investigation has been performed and will be described below.

To establish an experimental response matrix, the PH spectra obtained with the white beam have to be normalized to unit fluence at the centre of the detector. This normalization was carried out by fitting PH spectra calculated with NRESP7 to the experimental ones. The fit was restricted to the region extending from the beginning of the flat plateau to the recoil proton edge. This region is essentially determined by np scattering and can be accurately described by NRESP7.

At the same time, this fitting procedure yields more data points for the determination of the proton light output function than is

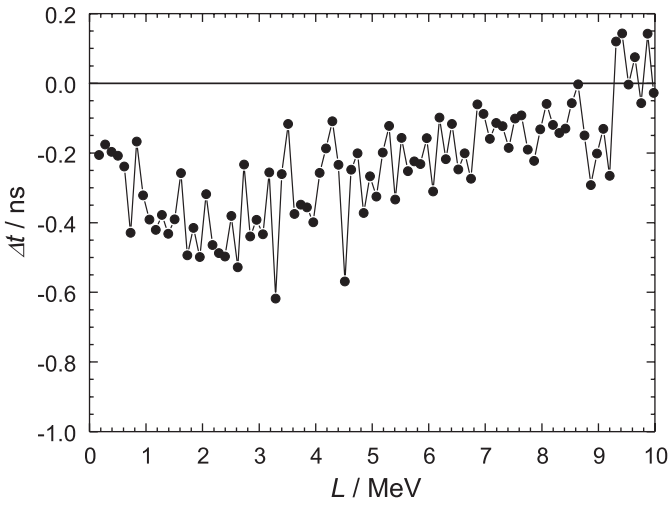

Fig. 5. Variation of the position of the high-energy edge of the neutron TOF spectrum as a function of the centroid of small PH windows used for producing the TOF spectra. The position of the edge was determined by a reference step function folded with a gaussian. The scatter of the data reflects the uncertainty of this fitting process.

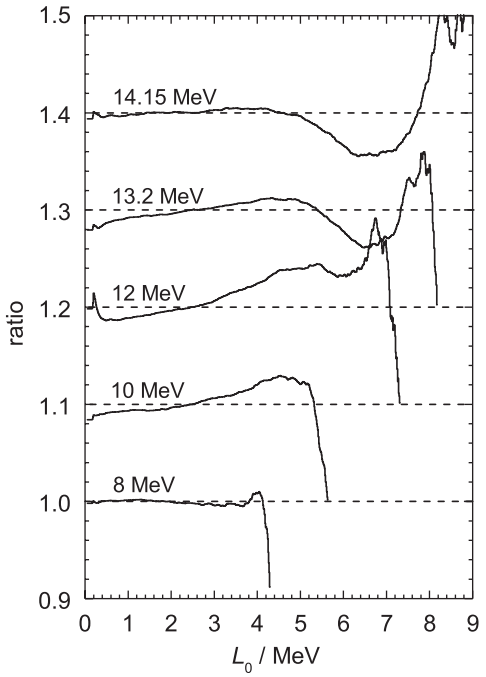

Fig. 7. Ratio of the integral number of events above a lower integration threshold L_0 for the PH spectra shown in a. The curves obtained for the different neutron energies are offset by 0.1.

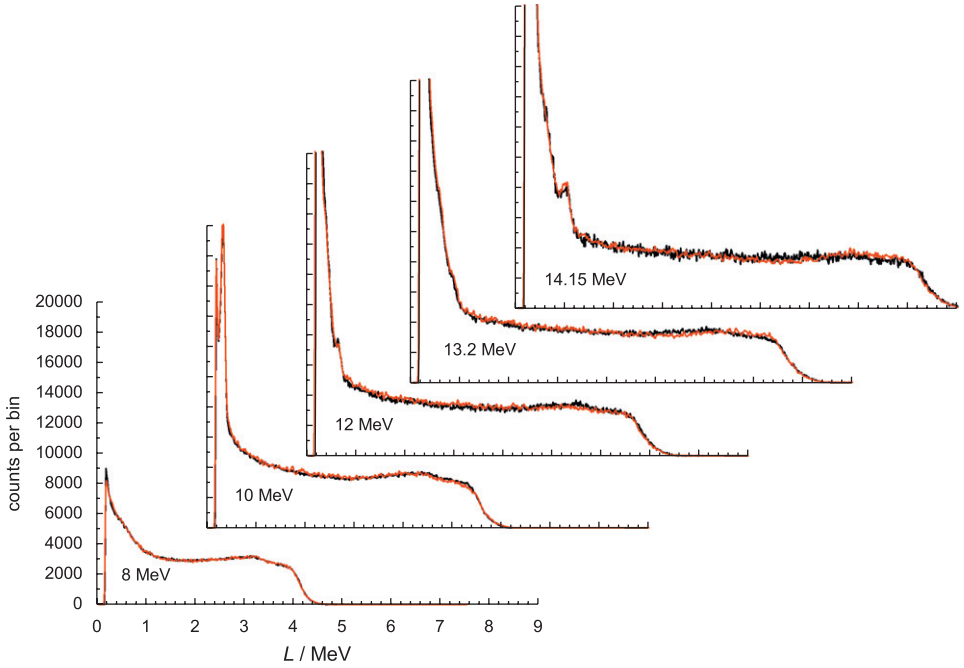

Fig. 6. Comparison of PH spectra measured with the white neutron beam (open line) and with monoenergetic neutrons from the D(d,n) reaction (black histogram). The width of the TOF window used to obtain the spectra for the measurements with the white beam corresponds to the calculated FWHM of the spectral distribution of the monoenergetic neutrons. The deviations in the flat part of the PH spectra are less than 4%.

available with the standard PTB procedure. The light output obtained with the white beam deviates by up to about 3% from the reference light output. This light output function exhibits a non-linearity between 8 and 10 MeV. Above 10 MeV the slope is slightly different from that determined with monoenergetic neutrons. The experimentally determined light output function was employed to calculate the PH spectra which were used to normalize the experimental response matrix. The results obtained with the D(d,n) source are in agreement with those obtained with the polyenergetic beam after multiplication with a factor of 0.98. The energy dependences are similar, but the shift of 2% remains to be explained.

3. Test of calculated and experimental response matrices in monoenergetic neutron fields

In the present work, it was considered important to test the calculated and experimental response matrices in well-defined monoenergetic neutron fields in an energy region of relevance for the actual application. Such a test was regarded as particularly relevant, because of the observed deviations between the experimentally determined response matrix and the calculated one.

3.1. Characterization of the neutron fields by TOF measurements

The experimental response matrix was tested in monoenergetic neutron fields with energies between 14 and 15.5 MeV. These fields were produced by the T(d,n)^{4}He reaction. The target consisted of a Ti(T) layer with an areal mass density of 1.07 mg/cm^2 which was deposited on an Al backing. The target contained about 0.96 T atoms per Ti atom. Deuteron beams with energies of 242, 412 and 643 keV were produced with the PTB 3.5 MV van-de-Graaff accelerator. At the two lower energies, the deuterons were stopped in the Ti(T) layer; only the 643 keV deuterons reached the Al backing of the target. The spectral distributions of the neutron fields were calculated with the TARGET code [25]. The calculated average energies at 0° were 14.85, 14.99 and 15.60 MeV, respectively, and the corresponding calculated FWHM of the peaks amounted to 451, 699 and 644 keV.

For the 412 keV deuteron beam, measurements were also carried out at a neutron emission angle of 98°. At this angle, the T(d,n)^{4}He reaction shows so-called kinematical focusing, i.e., the energy of the emitted neutrons is almost independent of the energy of the incident deuterons. Hence, broadening of the spectral distribution of the neutrons due to the energy loss of the deuterons in the Ti(T) layer is very small. In this particular case, the neutron field had a peak energy of 13.98 MeV and a FWHM of only 17 keV according to the TARGET calculations which were carried out neglecting the angular straggling of the deuterons in the target.

With the exception of the field produced with the 242 keV beam, all measurements were performed with a pulsed deuteron beam. The spectral distribution could therefore be measured using the TOF technique. The time resolution of the chopper and buncher system of the van-de-Graaff accelerator is limited to about 5 ns at the low beam energies used for the present measurements. The flight distance was 6.342 m for the 0° and 4.382 m for the 98° measurements. Hence, the energy resolution is about 10% and 14% for 0° and 98°, respectively. The contributions from neutrons scattered from structures in the PTB low-scattering experimental hall were removed by measurements with a shadow cone positioned halfway between the target and the detector.

The experimental TOF spectra were compared with spectra using the spectral neutron distribution calculated with the TARGET code. The time structure of the deuteron beam was determined by fitting an analytical parametrization to the TOF peak produced by prompt photons. The calculated spectra were folded with this time distribution and multiplied with the detection efficiency for comparison with the measured TOF spectra. The efficiency of the detector for a 300 keV threshold was calculated with the NEFF7 code [21] using the light output function determined from the measurements in the white neutron beam.

Fig. 8 shows a comparison of experimental and calculated TOF spectra. The calculated spectra were normalized to the experimental ones in the region of the prominent peak caused by monoenergetic neutrons from the T(d,n) reaction. The second peak in the experimental spectra corresponds to neutrons produced by the D(d,n)^{3}He reaction with deuterium impurities present in the target. This background reaction is not included in the TARGET simulation.

At 14 MeV, good agreement is obtained while the experimental spectra for 15 and 15.5 MeV neutrons exhibit a shift by about 0.39 ns corresponding to an energy deviation of about 90 keV. An investigation of possible disturbing influences, like uncertainty of the position of the prompt photon peak, TAC non-linearity or uncertainty of the flight distance revealed that the combined effect of these uncertainty contributions resulted in a standard measurement uncertainty of the experimental TOF of about 0.3 ns for a neutron with a given energy from the monoenergetic T(d,n) peak. The uncertainty of the neutron energy is close to the experimentally observed deviation. The main contribution to this uncertainty is the uncertainty of the centroid of the prompt photon peak.

An important quantity for the spectral neutron distribution not studied so far is the distribution of the T in the Ti(T) layer. An inhomogeneous T distribution would cause a shift in the spectral distributions for the 0° measurements while it would have virtually no effect on the 98° results, which is in line with the experimental finding. The observed shift of the experimental spectra for 15 and 15.5 MeV to higher energies would require a T profile which decreases in direction from the target surface to the backing.

3.2. Spectrometry by unfolding of PH spectra

The PH spectra obtained during the present measurements were unfolded with the MAXED code [26], which is part of the UMG code package [27]. It was known from the TOF measurements that the spectral neutron distribution showed a D(d,n) background peak between 2 and 4 MeV in addition to the

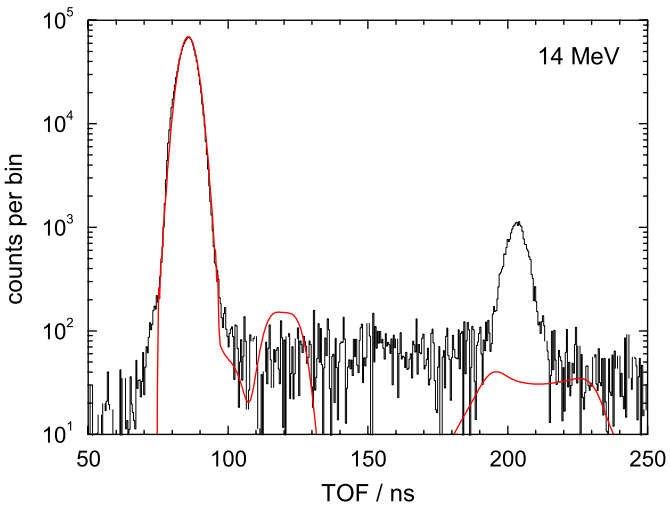

Fig. 8. Experimental (black histogram) and calculated (red line) TOF spectra. The neutron field was produced with the T(d,n) reaction. See text for details.

dominant T(d,n) peak at energies above 14 MeV. Using this preinformation, the unfolding was carried out in two steps. First, a high PH threshold of 7 MeV corresponding to a neutron energy of a about 11.2 MeV was used to select those events which could not be caused by the low-energy background. The spectral fluence distribution obtained from this restricted unfolding exhibited a prominent peak and some background at intermediate energies. Second, this peak was used as preinformation for the next step of the unfolding procedure which comprised the PH spectrum above a PH threshold of 280 keV.

Figs. 9–11 show a comparison of spectra obtained by unfolding and TOF spectrometry. In addition, the spectral fluences calculated with the TARGET code for the nominal target parameters are depicted. The TARGET calculations were normalized to the spectra obtained with the TOF method in the energy region of the T(d,n) peak. In this region, the resolution achieved with the TOF method is inferior to that obtained with the unfolding technique. The spectrum depicted in Fig. 9 was measured at 98° where the intrinsic width of the neutron distribution was very small. Thus, this figure shows the energy resolution achievable with the unfolding technique for the present detector. The two spectra shown in Figs. 10 and 11 were measured at 0°. Here the width and shape of the unfolded T(d,n) peak are very close to the calculated peaks with only minor differences between the results obtained with the experimental and the calculated response matrix. At 15.6 MeV the unfolded spectra show a tail on the low-energy side of the T(d,n) peak which is not present in the TARGET calculations. This tail could be caused by diffusion of T into the Al backing since the deuterons are not stopped in the Ti(T) layer at this energy. In contrast to the spectral fluence distributions obtained by unfolding, the width of the T(d,n) peak obtained with the TOF method is much larger due to the insufficient time resolution of the accelerator and the small flight distance. The correction of this broadening effect would require an unfolding of the TOF spectra using the temporal distribution of the proton beam pulse as determined from the shape of the prompt photon peak. The fluences in the regions of the T(d,n) peaks of the spectra obtained with the different spectrometric methods deviate by only 2.5% at maximum which shows the proper normalization of

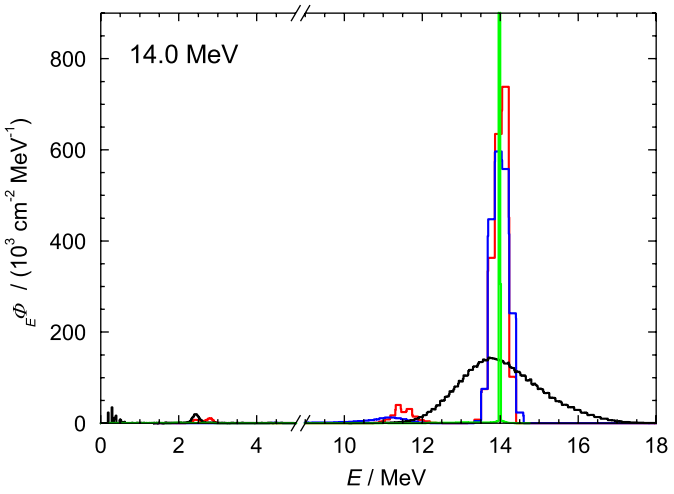

Fig. 9. Comparison of the spectral fluences unfolded from the PH spectra using the experimental (red histogram) and the calculated (blue histogram) response matrix. The spectral fluence measured with the TOF method is shown by the black histogram. In addition, the spectral fluence as calculated with TARGET [25] for the nominal target properties is depicted by the green histogram. The TARGET calculation was normalized to the TOF measurement in the energy region of the T(d,n) peak. The deuteron energies and neutron emission angles were 412 keV and 98° (above), 412 keV and 0° (Fig. 10), 643 keV and 0° (Fig. 11).

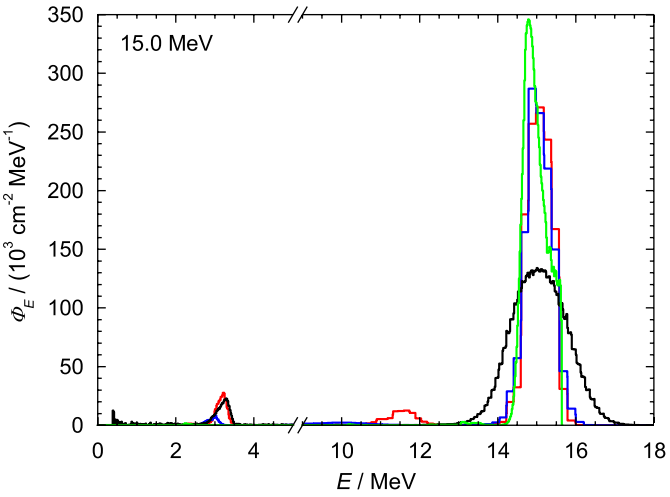

Fig. 10. See Fig. 9 for details.

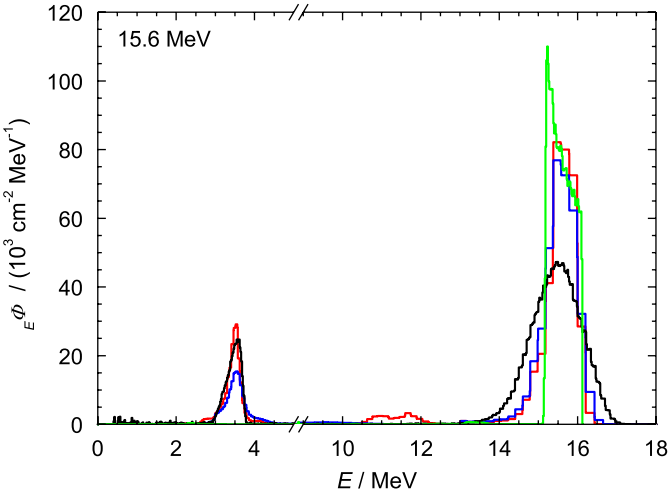

Fig. 11. See Fig. 9 for details.

the experimental response matrix. The mono-energetic peak contains about 75%, 85% and 90% of the total neutron fluence for the 15.6, 14.85 and 13.98 MeV measurements, respectively.

Discrepancies between the spectra become visible in the energy region between 10 and 12 MeV. Here the distortions observed in the experimental response matrix cause spurious structures in the unfolded spectral distributions, which are absent in the spectral distributions obtained with the TOF method. However, also the spectra obtained with the calculated response matrix show smaller spurious structures in this energy range which are caused by mismatches between the calculated and the experimental response due, for example, to imperfections in the light output functions used for the Monte Carlo calculation. This finding emphasizes the importance of proper response functions for the application of the unfolding technique. The discrepancies observed in the energy region below the T(d,n) peak were enhanced considerably when a flat default spectrum was used as pre-information and the unfolding procedure carried out in one step.

The strongest differences are visible in Figs. 10 and 11 in the energy region of the D(d,n) background peak between 2 and 3 MeV. Here the experimental response matrix gives by far better results than the calculated one. This finding is not unexpected since neutrons in this energy range produce maximum pulse

heights in the 200 keV to 1 MeV range. In this PH range, events caused by $^{12}C(n,\alpha x)$ reactions of neutrons from the prominent high-energy peak make a dominant contribution. Hence, any deficiency of the calculated response function due to an insufficient description of the $^{12}C(n,\alpha x)$ channels affects the unfolded spectral neutron distribution in the 1–3 MeV range. Fig. 12 shows a comparison of the unfolded spectral distributions and that calculated with TARGET for a deuteron energy of 242 keV where TOF measurements were impossible. As expected from the strong decrease of the D(d,n) cross-section with decreasing deuteron energy, the unfolded spectra do not exhibit a significant contamination with a D(d,n) background.

3.3. Determination of the neutron energy and neutron fluence

A sensitive method to study the qualities of the unfolding method is to determine the neutron energy and the neutron fluence from the unfolding of the mono-energetic neutron fields. The extracted neutron energy is compared with the value obtained from kinematic calculations for the neutron production reaction, T(d,n)^{4}He, and with results from the TOF measurements. The neutron fluence is compared with the number obtained by integrating the corresponding peak in the TOF distribution.

In this study, the unfolding code MAXED is used together with the experimentally determined response matrix. The determination of neutron energy and fluence is performed at three neutron energies used in the characterization of the neutron fields (see Section 3.1), namely 15.60, 14.85 and 13.98 MeV. The first two of these are obtained at 0° with deuteron energies of 643 and 242 keV, respectively, whereas the third one is produced by 412 keV deuterons at an angle of 98° relative to the deuteron beam. At this deuteron energy and neutron emission angle the T(d,n) reaction displays kinematical focusing as discussed in Section 3.1.

The results of the neutron energy measurements with statistical errors are displayed in Table 1. As a rule the energies obtained in the TOF measurements and from the unfolding procedure are in agreement, but slightly lower than those from the kinematic calculations. The TARGET calculations were carried out using the nominal areal mass of Ti and a T/Ti ratio which was adapted to experimental results. Hence, deviations of the target properties from the nominal values would also influence the comparison with the experimental results. It should be pointed out that the widths of the neutron energy distributions determined in the unfolding procedure are much narrower than those from the TOF measurements. In addition to the statistical errors in the neutron energies obtained in the unfolding procedure and given in the last row of Table 1, there are systematic errors of the order of 100 keV related to the energy calibration of the PH spectra.

As discussed already in Section 2.3 above, the normalization of the response matrix was verified by the measurements relative to the PTB reference detector using monoenergetic neutrons from the D(d,n)^{3}He reaction.

For the final application, however, another issue has to be studied. Even if the total number of counts is correct, the unfolding procedure could in principle distort the information, i.e., if part of the neutron flux is misidentified in energy in the unfolding procedure, this can result in an incorrect fluence determination. This could be studied using the TOF information.

The neutron fluence has been determined by integrating the T(d,n) peak from $E_0 - \Gamma$ to $E_0 + \Gamma$, where E_0 is the centroid and Γ is the FWHM. The intrinsic uncertainty of this method has been determined to 0.5% on the average with a worst case of 1.0%.

The fluences of the T(d,n) peak obtained from the time-of-flight spectrum from the 13.98 and 15.6 MeV measurements agree well with the fluence derived from unfolding with the MAXED code and the experimental response matrix, see Table 2. The results obtained from unfolding are 2.4% and 1.9% lower than that given by the TOF information. Based on this and other information, it is concluded that the fluence can be determined with an uncertainty of 2.5% using this method. This small deviation of the fluences obtained with different spectrometric methods show the proper normalization of the experimental response matrix. Since the fluence study has only been carried out in the 14–16 MeV region, the performance of the detector is limited to this energy range.

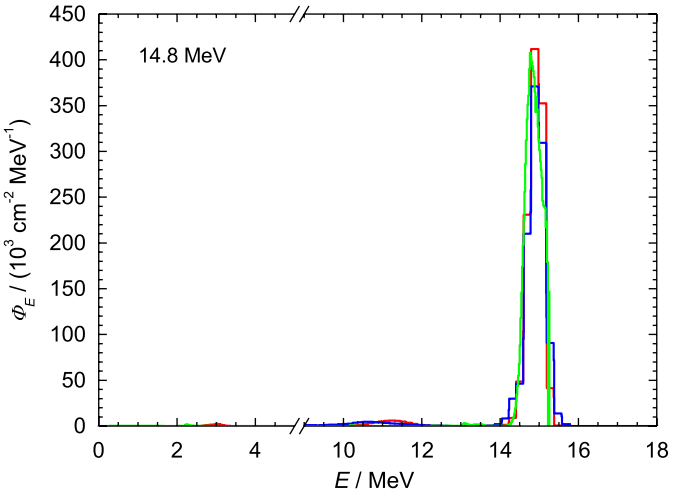

Fig. 12. Comparison of the spectral fluences unfolded from the PH spectra using the experimental (blue histogram) and the calculated (red histogram) response matrix. The spectral fluence as calculated with TARGET for the nominal target properties is depicted by the green histogram. The TARGET calculation was normalized to the spectral fluence obtained with experimental response matrix in the energy region of the T(d,n) peak. The deuteron energy and neutron emission angle were 242 keV and 0°, respectively.

Table 1
Neutron energies determined by kinematic calculations using the TARGET code [25], time-of-flight (TOF) measurements and unfolding using the MAXED code [26] in the study of the properties of the unfolding procedure for mono-energetic neutron fields produced by the T(d,n)^{4}He reaction

E_d (keV) θ (°)	643 keV 0°	242 keV 0°	412 keV 98°
E_n TARGET code (MeV)	15.60	14.85	13.98
E_n TOF (MeV)	15.50 ± 0.09	–	13.94 ± 0.09
E_n MAXED (MeV)	15.51 ± 0.03	14.71 ± 0.02	13.92 ± 0.03

At the lowest deuteron energy of 242 keV it was not possible to produce a decent pulsed beam. The errors are statistical only.

Table 2
Neutron fluences determined by time-of-flight (TOF) measurements and unfolding using the MAXED code [26] in the study of the properties of the unfolding procedure for mono-energetic neutron fields produced by the T(d,n)^{4}He reaction

E_d (keV) θ (°)	643 keV 0°	412 keV 98°
Φ_n TOF (counts)	73370 ± 730	110300 ± 1100
Φ_n MAXED (counts)	71980 ± 720	107700 ± 1080

The errors are statistical only.

4. Conclusions

The present work has shown that measurements in white neutrons beams can provide additional information for the specification of scintillation detectors which cannot be obtained with monoenergetic neutron beams alone. In particular, smoother experimental light outputs can be obtained and the deficiencies of the present Monte Carlo codes used for the calculation of response matrices can be circumvented. On the other hand, the application of the TOF method for the determination of experimental response matrices with white neutron beams requires very careful experimental work to avoid artefacts like those observed in the present data for neutron energies above 12 MeV. The application of the unfolding technique with experimentally determined response matrices provides a possibility for spectrometry in neutron beams over a large energy range. The present work has shown that even quite small spectral details can be resolved in the presence of other dominant structures.

Acknowledgements

The authors are indebted to A. Zimbal for guiding them through the technical pitfalls of the unfolding codes and for numerous discussions on this subject. The support of K. Tittelmeier, A. Toll and the staff of the PTB accelerator facility is gratefully acknowledged.

References

[1] J. Klug, et al., Nucl. Instr. and Meth. Phys. Res. A 489 (2002) 282.
[2] P.W. Lisowski, C.D. Bowman, G.J. Russell, S.A. Wender, Nucl. Sci. Eng. 106 (1990) 208.
[3] ICRU Report 63, Nuclear Data for Neutron and Proton Radiotherapy and for Radiation Protection, International Commission on Radiation Units and Measurements, Bethesda, MD, 2000.
[4] H.H.K. Tang, N. Olsson (Eds.), Single-Event Upsets in Microelectronics topical issue, Mater. Res. Soc. Bull. 28 (2003).
[5] J. Blomgren, Nuclear data for single-event effects, in: Proceedings of EU Enlargement Workshop on Neutron Measurements and Evaluations for Applications, Budapest, Hungary, November 5–8, 2003, EUR Report 21100 EN, Luxembourg: Office for Official Publications of the European Communities, ISBN 92-894-6041-5, European Communities, 2004.
[6] J. Blomgren, N. Olsson, Radiat. Prot. Dosim. 103 (4) (2003) 293.
[7] J. Blomgren, in: M. Herman, N. Paver, A. Stanculescu (Eds.), Proceedings of Workshop on Nuclear Data for Science and Technology: Accelerator Driven Waste Incineration, Trieste, Italy, September 10–21, 2001, ICTP Lecture Notes 12 (2002) 327.
[8] J. Blomgren, Nuclear data for accelerator-driven systems—experiments above 20 MeV, in: Proceedings of EU Enlargement Workshop on Neutron Measurements and Evaluations for Applications, Bucharest, Romania, October 20–23, 2004.
[9] O.N. Jarvis, Plasma Phys. Control. Fusion 12 (1994) 209.
[10] H. Klein, D. Thomas, H.G. Menzel, G. Curzio, F. d'Errico (Eds.), Proceedings of the International Workshop on Neutron Field Spectrometry in Science, Technology and Radiation Protection, Pisa, Italy, June 4–8, 2000; Nucl. Instr. and Meth. Phys. Res. A 476 (1 and 2) (2002) 1.
[11] F.D. Brooks, H. Klein, Nucl. Instr. and Meth. Phys. Res. A 476 (2002) 1.
[12] D. Schmidt, B. Asselineau, R. Böttger, H. Klein, L. Lebreton, S. Neumann, R. Nolte, G. Pichenot, Nucl. Instr. and Meth. Phys. Res. A 476 (2002) 186.
[13] A. Zimbal, H. Klein, M. Reginatto, H. Schumacher, L. Bertalot, A. Murari, and JET-EFDA Contributors, in: Proceedings of International Workshop on Fast Neutron Detectors and Applications, Cape Town, South Africa, 2006; Proceedings of Science, PoS(FNDA2006)035 ⟨http://pos.sissa.it/⟩.
[14] A. Zimbal, Radiation Protections Dosimetry, Advance Access published May 11, 2007, doi:10.1093/rpd/ncm085.
[15] A.Ohrn, J. Blomgren, H. Park, S. Khurana, R. Nolte, D. Schmidt, K. Wilhelmsen, Radiation Protections Dosimetry, Advance Access published May 11, 2007, doi:10.1093/rpd/ncm081.
[16] D. Schmidt, H. Klein, Precise time-of-flight spectrometry of fast neutrons—principles, methods and results. PTB Report PTB-N-35, Physikalisch-Technische Bundesanstalt, Braunschweig, 1998.
[17] E. Dekempeneer, H. Liskien, L. Mewissen, F. Poortmans, Nucl. Instr. and Meth. Phys. Res. A 256 (1987) 489.
[18] A. Axelsson, P. Andersson, K. Elmgren, N. Olsson, A. Ringbom, K. Wilhelmsen-Rolander, in: H. Schubert, A. Kuznetsov (Eds.), Proceedings of the NATO Advanced Research Workshop on Detection of Bulk Explosives; Advanced Techniques against Terrorism, St. Petersburg, Russia, June 2003.
[19] H. Klein, H. Schölermann, IEEE Trans. Nucl. Sci. NS-26 (1) (1979) 373.
[20] K. Tittelmeier, H.J. Barrenscheen, Stabilisierung von Szintillationsdetektoren, PTB Laboratory Report PTB-6.42-03-2, Physikalisch-Technische Bundesanstalt, Braunschweig, 2003 (in German).
[21] G. Dietze, H. Klein, NRESP4 and NEFF4: Monte Carlo codes for the calculation of neutron response functions and detection efficiencies for the NE213 scintillation detectors, PTB Report PTB-ND-22, Physikalisch-Technische Bundesanstalt Braunschweig, 1982 (and an informal supplement describing the changes of version 7, 1991).
[22] H.J. Brede, G. Dietze, K. Kudo, U.J. Schrewe, F. Tancu, C. Wen, Nucl. Instr. and Meth. Phys. Res. A 274 (1989) 332.
[23] T. Novotny, Photon spectrometry in mixed neutron–photon fields using NE213 liquid scintillation detectors, PTB Report PTB-N-28, Physikalisch-Technische Bundesanstalt, Braunschweig, 1997.
[24] A. Hildebrand, H. Park, S. Khurana, R. Nolte, D. Schmidt, Experimental determination of the response matrix of a BC501 scintillation detector using a wide neutron spectrum: a status report, PTB Report PTB-6.42-05-1, Physikalisch-Technische Bundesanstalt, Braunschweig, 2005.
[25] D. Schlegel, TARGET Users Manual, PTB Laboratory Report PTB-6.41-98-1, Physikalisch-Technische Bundesanstalt, Braunschweig, 1998.
[26] M. Reginatto, P. Goldhagen, S. Neumann, Nucl. Instr. and Meth. Phys. Res. A 476 (1989) 242.
[27] M. Reginatto, B. Wiegel, A. Zimbal, UMG-Code Package, available from the Nuclear Energy Agency (NEA) Data Bank ⟨http://www.nea.fr⟩.

International Conference on Nuclear Data for Science and Technology 2007
DOI: 10.1051/ndata:07369

CANDIDE – Coordination Action on Nuclear Data for Industrial Development in Europe

J. Blomgren[1,a], E. Bauge[2], D. Cano Ott[9], S. Csifrus[5], K. Dahlbacka[6], I. Gonçalves[13], E. Gonzalez[9], H. Henriksson[15], R. Jacqmin[2], A. Koning[4], D. Lecarpentier[12], E. Malambu[8], A. Mengoni[14], R. Mills[11], A. Plompen[3], G. Rimpault[2], V. Starý[7], C. Trakas[10], P. Vaz[13], and C. Zimmerman[11]

[1] Uppsala University, Dept of Neutron Research, Box 525, 75120 Uppsala, Sweden
[2] Commissariat à l'Énergie Atomique, France
[3] Joint Research Centre – Institute for Reference Materials and Measurements, EU
[4] Nuclear Research and consultancy Group, The Netherlands
[5] Budapest University of Technology and Economics, Hungary
[6] Teollisuuden Voima Oy, Finland
[7] Nuclear Research Institute Řež, Czech Republic
[8] Studiecentrum voor Kernenergie – Centre d'étude de l'Energie Nucléaire, Belgium
[9] Centro de Investigaciones Energéticas, Medioambientales y Tecnológicas, Spain
[10] AREVA, France
[11] Nexia Solutions Ltd., UK
[12] Électricité de France, France
[13] Instituto Tecnológico e Nuclear, Portugal
[14] International Atomic Energy Agency, Austria
[15] Nuclear Energy Agency, OECD

Abstract. A Co-ordinated Action has been launched with the ambition to establish a durable network on nuclear data efforts that are important in the context of minimising the high-level waste stream of nuclear energy. This implies optimal incineration of all actinides that nowadays constitute spent nuclear fuel, in critical and sub-critical reactors. As a consequence, the scope of the CA encompasses transmutation in fast critical reactors as well as sub-critical systems (ADS). The purpose is to identify the needs for improved nuclear data, assess the present status of knowledge, and to estimate what accuracy can be reached with state-of-the-art techniques.

1 Introduction

The EC-supported Coordination Action (CA) CANDIDE, Co-ordination Action on Nuclear Data for Industry Development in Europe, addresses the following two objectives:

- Establishment of better links between academia, research centres and industry end users of nuclear data. This is reflected in the project name.
- Assessment of nuclear data needs for advanced nuclear reactors. The emphasis is on the radioactive waste issue, i.e., either waste transmutation in critical or sub-critical devices or minimizing the production of nuclear waste in future nuclear reactors, as envisaged in some fast critical systems.

For a long time activities concerning all aspects of nuclear data for commercial nuclear power reactors, i.e., nuclear data production, theory, evaluation, validation and industrial use, have been part of a well-organized international community, monitored by large international organizations, like OECD. Recently, a new nuclear data community has been formed around the production of nuclear data for accelerator-driven systems, while the other ingredients of traditional nuclear data work (e.g., evaluation and validation) have to a large degree been missing up to now. The present project aims at establishing links for this new community to the existing structure of coordinated nuclear data activities in general, and to provide links to industry in particular.

Another recent development in Europe has been the enlargement of the EU, which opens new possibilities in the realm of nuclear data. Integration – both of different research communities and between new and previous member states – is an important objective of the CANDIDE project. Moreover, improved training and integration are essential parts of the CA, exemplified by the development of a European course on nuclear data to be part of the project.

In the public literature, the concept of transmutation is quite often used in a restricted sense, synonymous to accelerator-driven systems for incineration of spent nuclear fuel. CANDIDE has been designed with the intention to consider transmutation in a broader, more general sense, i.e., incineration of spent nuclear fuel by changing the nature of the elements through nuclear reactions. As a consequence, the scope of the proposed CA will encompass transmutation in fast critical reactors as well as sub-critical systems (ADS). The purpose of CANDIDE is not to produce new experimental data or evaluations, but to review the current modes of nuclear data production, assess the present status of our knowledge, estimate what accuracy can be reached with state-of-the-art numerical simulation techniques, identify the needs for improved

[a] Presenting author, e-mail: jan.blomgren@tsl.uu.se

nuclear data, and suggest appropriate actions to be taken to meet those needs. A large fraction of the existing data were obtained far back in time, and it might be beneficial to identify cases where new experiments on already measured reactions could exploit technology improvements. Key input is expected from industrial partners, since they are closely involved in application of nuclear data libraries and their performance.

The final result of the CA will be a report describing the state-of-the-art and giving recommendations to EC outlining how nuclear data research should be organized in FP7 and beyond. Moreover, the organisation of workshops and a training course will lead to broader European involvement in the subject.

2 Nuclear data for transmutation of spent nuclear fuel

In the public debate of today, the concept of *transmutation* has often become synonymous with accelerator-driven systems (ADS) for incineration of nuclear waste. This is not surprising, because ADS represents a very innovative option, while the use of critical reactors represent a more conventional alternative. In CANDIDE, however, we will consider transmutation in a very broad sense, not restricted to a particular system or scenario. Presently, nuclear waste transmutation options are investigated as part of reactor and fuel cycle studies for existing reactor types (PWR, BWR, CANDU), i.e., GEN-III, for evolutionary designs of existing reactors, GEN-III+ (EPR, AP600, etc.), for GEN-IV reactors (SFR, GFR, LFR, MSR, SCWR, VHTR) or for dedicated transmuters (such as ADS). All these activities generate a significant amount of nuclear data needs either for the feasibility phase of these studies or for the performance phase.

Up to now, there has been a very large research volume spent on data on neutron-induced nuclear reactions up to 20 MeV. This was carried out from around 1950 until today, and was motivated by the needs in the development of civil nuclear power, as well as weapons applications and fusion technology. During the last decade, nuclear data at higher energies have been in the limelight due to the discussions about ADS.

The approaches in these two disciplines differ significantly. This is neither a surprise nor a bad choice, because the underlying physics differs significantly, resulting in different research strategies. Below 20 MeV, a single cross section can be of paramount importance to the entire application. An example is the neutron capture resonance at 6.7 eV in ^{238}U that provides the Doppler effect so important for the stability of critical reactors. Moreover, some cross sections are fundamentally inaccessible to theory, in particular in the resonance region. As a result, at low energies more or less complete data coverage for major elements is required. Above 20 MeV, the situation is fundamentally different. The cross sections are slowly varying in energy, and the behaviour of the system is always dictated by the sum of a large number of reactions, none of which strongly dominates the performance. Therefore, getting a grip on the overall picture has been a more natural ambition in an initial stage, rather than providing precision data on a single reaction.

Thanks to the nuclear data campaigns for ADS in FP5 and FP6, we have now reached a stage where such an overall picture, although fairly rough in many respects, is appearing. As a consequence, the uncertainty in modelling of various ADS concepts due to nuclear data uncertainties have decreased significantly during the last few years. There is, however, still plenty of room for improvement of ADS-relevant nuclear data, only part of which will be fulfilled by IP-EUROTRANS [1].

Up to now, nuclear data at the energies of critical reactors (less than 10 MeV) and accelerator-driven systems (up to 1 GeV) have not been systematically treated on an equal basis. The importance of this aspect was recently highlighted at the International Workshop on Nuclear Data Needs for Generation IV Nuclear Energy Systems [2], after which a WPEC subgroup was established to investigate the nuclear data needs for advanced reactor systems [3]. We find it important for the further development of nuclear data activities for transmutation, and even for the entire research on transmutation, that the nuclear data from these very different regimes can be compared and used in a consistent manner. This is a major underlying theme of CANDIDE.

In general, the safe, economical, and reliable operation of a nuclear reactor depends on the use of nuclear data to predict several important characteristics of plant operation. In the case of transmutation in general, the major benefit of accurate nuclear data relates specifically to avoiding unnecessary conservatism in design and operation such as shielding requirements, power coefficients for a core loaded with minor actinides, and the related power requirements of the proton accelerator for ADS systems.

Another important difference between a dedicated transmutation system – critical or sub-critical – and a conventional critical power reactor is that for the latter, deficiencies in detailed nuclear data can partly be overcome through normalizing calculations to existing reactor measurements or experience from the operation of prototypes and test rigs. The desire to pursue new designs (Gen-IV as well as ADS concepts) without performing extensive reactor experiments dictates using nuclear data that will support reactor calculations that give dependable results even without experimental re-normalization.

On a (very) broad level, the nuclear data requirements for transmutation of waste fall into two classes: (1) resonance and fast neutron reactions for materials that are specific to transmutation: unconventional structural materials, coolants and (in the case of ADS) targets, and minor actinides, whose abundance in the core is much larger than in a conventional reactor, (2) energy regimes that extend beyond the fast neutron region (up to hundreds of MeV) for the above materials and conventional materials. The first class applies to any transmutation method, i.e., including critical reactors, whereas the second class exclusively applies to ADS. In this project, we will consider both classes. Although the motivation for the present project arises from waste minimization using novel reactor types, conventional power reactors can still benefit from the outcome of the CA. Indeed, nuclear data needs that apply to a critical power system, in general also apply to transmutation systems, critical as well as sub-critical. For example, the important interplay between ^{238}U fission, capture and inelastic scattering, is crucial for a precise determination

of criticality. Minimizing the uncertainties in these data is also important for transmutation systems. One interest of the CA is to identify needs that are common to various applications.

3 Training and networking

CANDIDE is not limited to involvement of existing activities, but will also promote growth for the future. Therefore, an important part of the project is the development of a dedicated training course on nuclear data for young professionals, the European course on EXperiment, Theory and Evaluation of Nuclear Data (EXTEND) to be held in Budapest. The target group of this course are young professionals, primarily recently employed staff in industry and at research centres, as well as Ph.D. students in the field.

Summer schools in nuclear engineering (e.g., the Eugene Wigner School on Reactor Physics [4] within the ENEN [5] association or the Frederic Joliot-Otto Hahn summer school [6]) are regularly organized, and there are relatively frequent summer schools on fundamental nuclear physics. Up to now, however, there have been few initiatives to bridge these two communities. EXTEND has been designed to fill this gap.

Besides the development of EXTEND, other activities on training and mobility of young industry professionals and researches, as well as European integration are also foreseen. The most visible example is the planned extension of NEMEA workshops [7], organized by IRMM, which are included in the CA. The previous NEMEA workshops have been targeting nuclear data research in Eastern Europe, but will now be enlarged to be open to all Europe. Our intention is to make these workshops meeting places for all European scientists in the field, including the nuclear industry, which has previously not been the case. The outcomes of two previous such workshops have been beneficial for the present proposal, in so far that they have promoted valuable links between old and new member states in general, and scientists from these in particular.

4 Project strategy

As has been described above, we have identified possibilities to enlarge the nuclear data activities in Europe by integrating the new research communities (ADS research, new member and candidate states) into the already existing structures for nuclear data work, and CANDIDE will address these issues by organizing open workshops intended for bridging gaps between these communities. Moreover, the project itself has been designed to make industry a more visible player in the research-related activities via the top-down approach of CANDIDE. Last but not least, the development of a new course for young professionals is in line with these goals, but it is also intended to foster closer links between nuclear physics and reactor physics.

The project involves a wide range of industry partners. Three reactor construction or manufacturing organizations are represented. AREVA (France) is a leading manufacturer of nuclear reactors in Western Europe, having received widespread attention recently with the two EPRs under construction in Finland and France. The BNFL group (UK) has a wide range of reactors on its repertoire, gas-cooled reactors in the UK as well as light-water reactors (LWR) manufactured by Westinghouse. The Skoda corporation in the Czech Republic is constructing heavy structural parts to nuclear reactors, like reactor vessels, and are represented in the present CA via their technical support organization, NRI Řež.

Two power utilities, TVO (Finland) and EdF (France), participate in the project, representing light water reactor technology. Fuel manufacturing is represented by Nexia/BNFL and AREVA, while reprocessing is represented by Nexia/BNFL. Design of future ADS-related facilities is represented by SCK·CEN (Belgium) and CIEMAT (Spain).

The validation (CEA Cadarache, NRG Petten) and evaluation (CEA Cadarache, CEA Bruyères-le-Châtel, NRG Petten) teams of the proposed CA represent leading European competence in the field. ITN (Portugal) contributes expertise in nuclear data related to spallation targets. The current-day computer power enables sophisticated nuclear reaction modelling and validation against integral experiments with both deterministic and Monte Carlo software.

On the experimental side, IRMM Geel is the dedicated EU lab for reactor-relevant nuclear data (0–20 MeV), while TSL Uppsala is the primary European facility for neutrons above 20 MeV (up to 200 MeV), which will cover important input for ADS neutronics.

With these partners, we cover the entire chain from industry to experiments, with a top-down approach. The industry partners define the needs from the end-users perspective, and their participation guarantees that the work is application-oriented. The role of the non-industry partners is to assess the possibilities to provide data of sufficient quality to meet the application needs. As a consequence, the issue of which data is required or need to be improved is primarily an industry concern, while the question of how to reach those goals is mostly dealt with by the non-industry partners. Efficient dissemination is guaranteed by the involvement of the IAEA and OECD/NEA Data Banks.

Improved training, as well as integration of new member states, are important issues for the CA. Improvement of training on nuclear data is undertaken in close collaboration with European Nuclear Education Network (ENEN) [5], and it brings educational resources in old and new member states together. Additional integration is provided by the strong involvement of industry throughout Europe. Close contacts with the EFNUDAT [8] integrated infrastructure initiative have been established.

5 Project scientific content

As outlined above, the project concerns the integration of nuclear data efforts for all types of transmutation-relevant nuclear systems, i.e., critical thermal and fast reactors, as well as accelerator-driven systems. Up to now, various nuclear-data projects have concentrated on different sub-sets of the global issue. In the present CA, we attempt to unify important aspects of these activities, with the ambition to provide a consistent basis for comparisons of various waste transmutation options.

A general approach to nuclear data for waste management would imply a very large project. To keep the task limited

to a reasonable size, but still with the potential to provide results of relevance to the assessment of various transmutation strategies, the work has to be concentrated to a few issues that are of key importance to both fast critical reactors and ADS.

Up to now, the nuclear data research at classical reactor energies, up to 20 MeV, and the ADS-motivated research above 20 MeV have been conducted with very different approaches. This has made sense, because the pre-conditions have been very different. With the recent development in nuclear data for ADS, resulting from FP5 and FP6 projects, we believe it is now possible to conduct research on what is common to critical reactors and ADS. A major unifying aspect is the role of neutrons. In both concepts, the major incineration is due to neutron-induced fission. Moreover, other neutron-induced reactions, like capture and scattering, play significant roles in all these techniques. Another common aspect is that the core will contain large amounts of minor actinides, although the composition differs among various systems. Furthermore, the design studies around GEN-IV type systems encompass not only the core but also the full fuel cycle. One important GEN-IV criterion is the reduction of radioactive waste that is competing against other criteria such as sustainability (full use of Uranium or Thorium ores), economics, safety and reliability, proliferation resistance and physical protection.

As a natural consequence of this, a study that could cover only the transmutation aspect of a core would not be complete. We therefore envisage the project to cover all nuclear data that have some relation to the reactors and their associated fuel cycles, whether they are dedicated specifically to transmutation (just like ADS) or if transmutation is only one of their key features.

In the present CA, we intend to assess the data situation for all neutron energies, from thermal and up to the highest available (200 MeV), both experimentally and theoretically. In the first instance, the focus of the CA should be on cores of fast reactors and ADS. Nuclear data are of great relevance also for irradiation effects on materials, radiation protection and a number of other issues. A possible list of data to be studied is given below:

- General purpose files that include (1) cross sections induced by neutrons, protons and gammas, (2) secondary particle energy distributions, and (3) fission spectra and energy release.
- Gamma production induced by different reaction types.
- Fuel cycle data (fission yields, spallation yields, decay heat).
- Activation files.

Participants from nuclear industry should give guidance on the proper parameters to be investigated and optimised. These needs should be translated into data evaluation and measurement requests, to be carried out in FP7 and beyond. Part of the effort in this CA consists of a critical assessment of major and minor actinide data in the latest nuclear data libraries and an assessment of the corresponding uncertainties. This should in a natural way lead to well-focused measurement requests.

As has been emphasized, the industrial needs will drive the assessment within the CA. It is worthwhile to point at the close connection of the present collaboration with the OECD-NEA High Priority Request List for nuclear data, where such well-defined requests are collected and reviewed to mobilise the community for their resolution. CANDIDE will serve to identify and propagate the EU interests in this domain and to provide the focus for future EU research on nuclear data. Also in the area of follow up on the formulated requests, CANDIDE is well connected to running EC projects, especially the JEFF project, as mentioned previously.

This work was financially supported by the European Union, contract 036397.

References

1. EUROTRANS – European Research Programme for the Transmutation of High-Level Nuclear Waste in an Accelerator-Driven System. http://nuklear-server.ka.fzk.de/eurotrans/.
2. *Proceedings of the International Workshop on Nuclear Data Needs for Generation IV Nuclear Energy Systems*, *Antwerpen, Belgium, 5–7 April 2005*, edited by P. Rullhusen, http://www.jrc.cec.eu.int/gen4-workshop/main.html.
3. M. Salvatores et al. (these proceedings).
4. The Eugene Wigner School on Reactor Physics. http://www.reak.bme.hu.
5. The European Nuclear Education Network. http://www.sckcen.be/ENEN.
6. The Frédéric Joliot & Otto Hahn Summer School on Nuclear Reactors. http://www-cadarache.cea.fr/fr/cadarache/ecoles/fjohss2007.htm.
7. The most recent event in this series was NEMEA-3, *3rd Workshop on Neutron Measurements, Evaluations and Applications*, *Oct. 25–28, 2006, Borovets, Bulgaria*, http://www.irmm.jrc.be/html/events/events/nemea-3.htm.
8. G. Barreau on behalf of the EFNUDAT consortium (these proceedings), www.efnudat.eu.

International Conference on Nuclear Data for Science and Technology 2007
DOI: 10.1051/ndata:07372

Elastic neutron scattering at 96 MeV

Angelica Öhrn[1,a], Joakim Klug[1], Jan Blomgren[1], Cecilia Gustavsson[1], Philippe Mermod[1], Leif Nilsson[1], Stephan Pomp[1], Michael Österlund[1], Udomrat Tippawan[2], Alexander Prokofiev[3], and Gennady Tutin[4]

[1] Department of Neutron Research, Uppsala University, P.O. Box 525, 75120 Uppsala, Sweden
[2] Fast Neutron Research Facility, Chiang Mai University, Thailand
[3] The Svedberg Laboratory, Uppsala University, Sweden
[4] Khlopin Radium Institute, St. Petersburg, Russia

Abstract. A facility for detection of scattered neutrons in the energy interval 50–130 MeV, SCANDAL (SCAttered Nucleon Detection AssembLy), has recently been installed at the 20–180 MeV neutron beam line of the The Svedberg Laboratory, Uppsala. Elastic neutron scattering from ^{12}C, ^{56}Fe, ^{89}Y and ^{208}Pb has been studied at 96 MeV in the 10–70° interval. The results from ^{12}C and ^{208}Pb have recently been published, while the data from ^{56}Fe and ^{89}Y are under analysis. The achieved energy resolution, 3.7 MeV, is about an order of magnitude better than for any previous experiment above 65 MeV incident energy. The present experiment represents the highest neutron energy where the ground state has been resolved from the first excited state in neutron scattering. A novel method for normalization of the absolute scale of the cross section has been used. The estimated normalization uncertainty, 3%, is unprecedented for a neutron-induced differential cross section measure ment on a nuclear target. The results are compared with modern optical model predictions, based on phenomenology or microscopic theory. Applications for these measurements are nuclear waste incineration, single event upsets in electronics, dosimetry and fast neutron therapy.

1 Introduction

The interest in high-energy neutron data is rapidly growing, since a number of potential large-scale applications involving fast neutrons are under development, or at least have been identified. These applications primarily fall into three sectors; nuclear energy and waste, effects on electronics and nuclear medicine.

For all these applications, an improved understanding of neutron interactions is needed for calculations of neutron transport and radiation effects. The nuclear data needed for this purpose come almost entirely from nuclear scattering and reaction model calculations, which all depend heavily on the optical model, which in turn is determined by elastic scattering and total cross section data.

Neutron scattering data are also important for a fundamental understanding of the nucleon-nucleus interaction, in particular for determining the isovector term [1]. Coulomb repulsion of protons creates a neutron excess in all stable nuclei with A > 40. Incident protons and neutrons interact differently with this neutron excess. The crucial part in these investigations has been neutron-nucleus elastic scattering data to complement the already existing proton-nucleus data.

Above 50 MeV neutron energy, there has been only one measurement on neutron elastic scattering with an energy resolution adequate for resolving individual nuclear states, an experiment at UC Davis at 65 MeV on a few nuclei [2]. In addition, a few measurements in the 0–20° range are available, all with energy resolution of 20 MeV or more. This is, however, not crucial at such small angles because elastic scattering dominates heavily, but at larger angles such a resolution would make data very difficult to interpret.

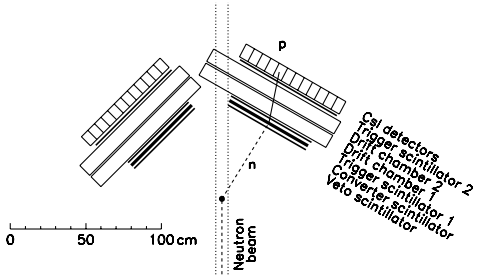

Fig. 1. A schematic layout of the SCANDAL setup. A typical event is indicated.

2 Experimental setup

The neutron beam facility at the The Svedberg Laboratory, Uppsala, Sweden, has recently been described in detail [3], and therefore only a brief description is given here. The 96 ± 0.5 MeV (1.2 MeV FWHM) neutrons were produced by the ^{7}Li(p,n) reaction by bombarding a 427 mg/cm^2 disc of isotopically enriched (99.98%) ^{7}Li with protons from the cyclotron. The low-energy tail of the source neutron spectrum was suppressed by time-of-flight techniques. After the target, the proton beam was bent into a well-shielded beam dump. A system of three collimators defined a 9 cm diameter neutron beam at the scattering target.

Scattered neutrons were detected by the SCANDAL (SCAttered Nucleon Detection AssembLy) setup [3]. (see fig. 1). It consists of two identical systems, placed to cover

[a] Presenting author, e-mail: angelica.ohrn@tsl.uu.se

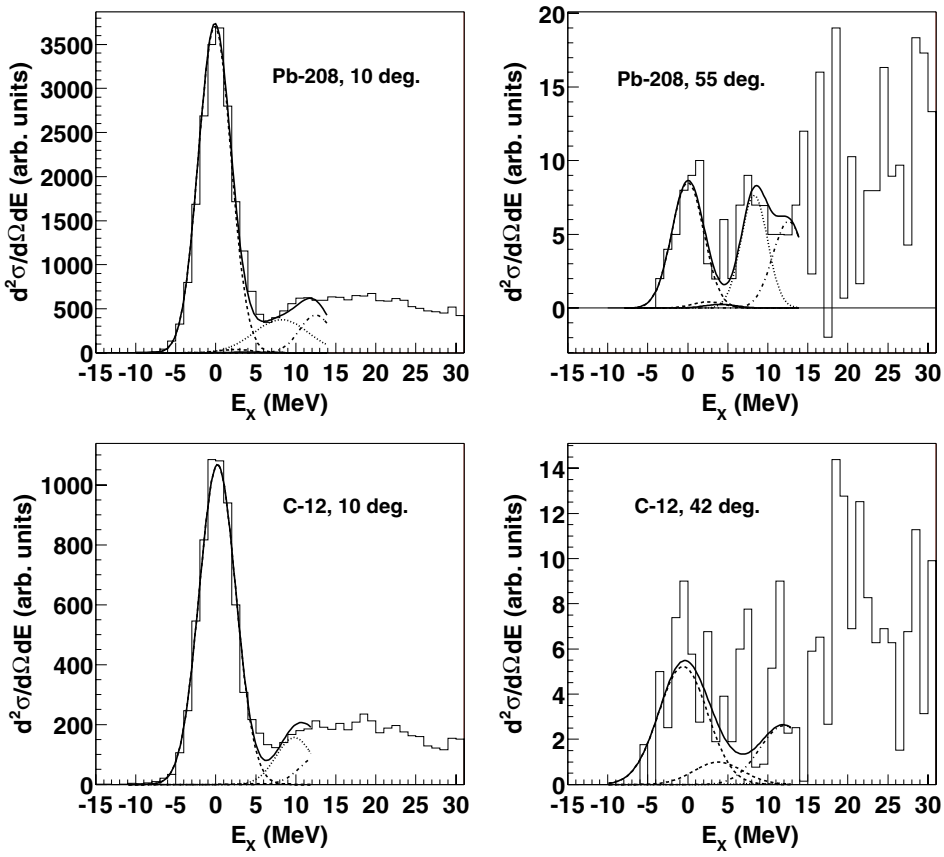

Fig. 2. Excitation energy spectra for elastic neutron scattering from ^{12}C and ^{208}Pb at 96 MeV incident neutron energy, together with gaussians representing known excited states. See the text for details.

10–50° and 30–70°, resp. The energy of the scattered neutrons is determined by measuring the energy of proton recoils from a plastic scintillator, and the angle is determined by tracking the recoil proton. In the present experiment, each arm consisted of a 2 mm thick veto scintillator for fast charged-particle rejection, a 10 mm thick neutron-to-proton converter scintillator, a 2 mm thick plastic scintillator for triggering, two drift chambers for proton tracking, a 2 mm thick ΔE plastic scintillator which was also part of the trigger, and an array of CsI detectors for energy determination of recoil protons produced in the converter by np scattering. The trigger was provided by a coincidence of the two trigger scintillators, vetoed by the front scintillator. The total excitation energy resolution varies with CsI crystal, but is on average 3.7 MeV (FWHM). The angular resolution is in the 1.0–1.3° (rms) range.

3 Results and discussion

3.1 Data on ^{12}C and ^{208}Pb

Excitation energy spectra are presented in figure 2. In these spectra, gaussians representing known states are indicated. For ^{12}C, the ground state (0^+) and the two collective states at 4.4 MeV (2^+) and 9.6 MeV (3^-) are shown. In the case of ^{208}Pb, the ground state (0^+) and the two collective states at 2.6 MeV (3^-) and 4.1 MeV (2^+) are shown, as well as a gaussian at 8.3 MeV representing a cluster of weak states. For both nuclei, a gaussian at 12.6 MeV represents the opening of conversions due to ^{12}C(n,p) reactions in the converter scintillator, i.e., an instrument background. As can be seen, in no case the population of excited states seriously affects the determination of the ground state cross section. Angular distributions of elastic neutron scattering from ^{12}C and ^{208}Pb at 96 MeV incident neutron energy are presented in figure 3. The data are compared with phenomenological and microscopic optical model predictions in the upper and lower panels, respectively. The theoretical curves have all been folded with the experimental angular resolution to facilitate comparisons with data. The data by Salmon at 96 MeV [4] are also shown.

The angular distributions presented have been corrected for reaction losses and multiple scattering in the target. The contribution from other isotopes than ^{208}Pb in the lead data has been corrected for, using cross section ratios calculated with the global potential by Koning and Delaroche [5]. The absolute normalization of the data has been obtained from knowledge of the total elastic cross section, which has been determined from the difference between the total cross section (σ_T) [6] and the reaction cross section (σ_R) [7,8]. This σ_T - σ_R method, which is expected to have an uncertainty of about 3%, has been used to normalize the ^{12}C data. The present ^{208}Pb(n,n) data have been normalized relative to the present ^{12}C(n,n) data,

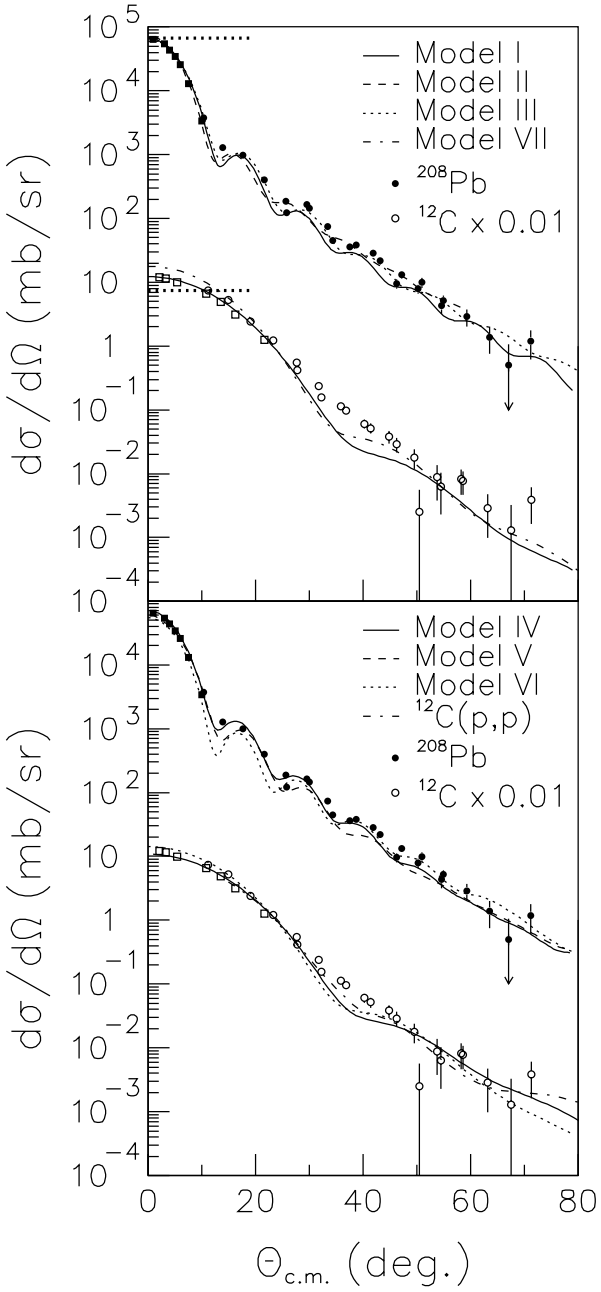

Fig. 3. Angular distributions of elastic neutron scattering from ^{12}C (open circles) and ^{208}Pb (solid) at 96 MeV incident neutron energy. The ^{12}C data and calculations have been multiplied by 0.01. The data by Salmon at 96 MeV [4] are shown as squares. Upper panel: predictions by phenomenological models (I–III, VII). The thick dotted horizontal lines show Wick's limit for the two nuclei. Lower panel: predictions by microscopic models (IV–VI), and data on elastic proton scattering from ^{12}C [12]. See the text for details.

knowing the relative neutron fluences, target masses, etc. The total elastic cross section of ^{208}Pb has previously been determined with the σ_T - σ_R method. The accuracy of the present normalization has been tested by comparing the total elastic cross section ratio (^{208}Pb/^{12}C) obtained with the σ_T - σ_R method above, and with the ratio determination of the present experiment, the latter being insensitive to the

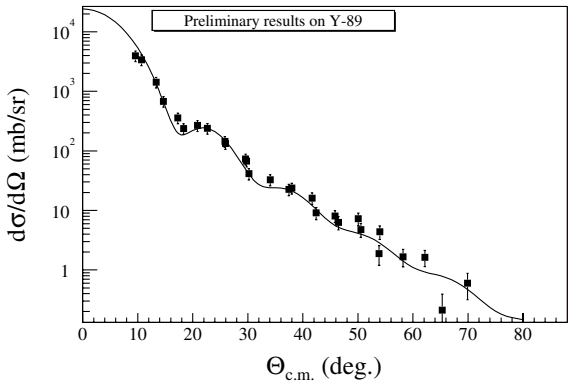

Fig. 4. Preliminary angular distribution of elastic neutron scattering from ^{89}Y at 96 MeV incident neutron energy together with a prediction by a phenomenological model [5].

absolute scale. These two values differ by about 3%, i.e., they are in agreement within the expected uncertainty.

The data are compared with model predictions in figure 3, where the upper and lower panels show phenomenological (I–III, VII) and microscopic (IV–VI) models, respectively. The models are described in detail in refs. [9] and [10].

All models are in reasonably good agreement with the ^{208}Pb data. It should be pointed out that none of the predictions contain parameters adjusted to the present experiment. In fact, they were all made before data were available. Even the absolute scale seems to be under good control, which is remarkable, given that neutron beam intensities are notoriously difficult to establish.

A new measurement on ^{12}C has recently been performed. The results show good agreement with the models used above, see ref. [11].

A basic feature of the optical model is that it establishes a lower limit on the differential elastic scattering cross section at 0° if the total cross section is known, often referred to as Wick's limit. It has been observed in previous experiments at lower energies that for most nuclei, the 0° cross section falls very close to Wick's limit, although there is no a priori reason why the cross section cannot exceed the limit significantly. An interesting observation is that the present ^{208}Pb data are in good agreement with Wick's limit, while the ^{12}C 0° cross section lies about 70% above the limit. A similar behaviour has previously been observed in neutron elastic scattering at 65 MeV [2], where the ^{12}C data overshoot Wick's limit by about 30%, whilst the ^{208}Pb data agree with the limit.

3.2 Other nuclei

Preliminary data on ^{89}Y [14] are presented in figure 4, together with Model I [5]. Corrections for multiple scattering remain. The model describes the shape of the data points reasonably well. Preliminary data on ^{56}Fe [15] are presented in figure 5, together with Model I [5]. All corrections as well as the subtraction of the contribution of inelastic scattering events remain to be performed, which are the most likely reasons why the model does not describe the shape of the data points better. For normalization, both ^{89}Y and ^{56}Fe have been measured relative to ^{12}Ca.

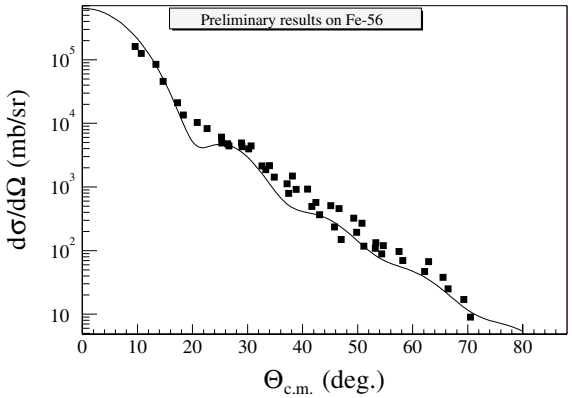

Fig. 5. Preliminary angular distribution of elastic neutron scattering from ^{56}Fe at 96 MeV incident neutron energy together with a prediction by a phenomenological model [5].

4 Summary, conclusion and outlook

In short, first results on elastic neutron scattering from ^{12}C and ^{208}Pb at 96 MeV incident neutron energy are presented, and compared with theory predictions. This experiment represents the highest neutron energy where the ground state has been resolved from the first excited state in neutron scattering. The measured cross sections span more than four orders of magnitude. Thereby, the experiment has met – and surpassed – the design specifications. The overall agreement with theory model predictions, both phenomenological and microscopic, is good. In particular, the agreement in absolute cross section scale is impressive.

The SCANDAL setup will be upgraded with thicker CsI crystals which will allow elastic scattering measurements at higher energies.

We wish to thank the technical staff of The Svedberg Laboratory for enthusiastic and skillful assistance. This work was supported by the HINDAS project of the 5th EU framework programme, as well as by Vattenfall AB, Swedish Nuclear Fuel and Waste Management Company, Swedish Nuclear Power Inspectorate, Barsebäck Power AB, Forsmark AB, Ringhals AB, Swedish Defence Research Agency and the Swedish Research Council.

References

1. See, e.g., *Neutron-Nucleus Collisions: A probe of Nuclear Structure*, AIP Conf. Proc. **124** (AIP, New York, 1985).
2. E.L. Hjort et al., Phys. Rev. C **50**, 275 (1994).
3. J. Klug et al., Nucl. Instrum. Meth. A **489**, 282 (2002).
4. G.L. Salmon, Nucl. Phys. **21**, 15 (1960).
5. A.J. Koning, J.P. Delaroche, Nucl. Phys. A **713**, 231 (2003)
6. R.W. Finlay et al., Phys. Rev. C **47**, 237 (1993).
7. J. DeJuren, N. Knable, Phys. Rev. **77**, 606 (1950).
8. R.G.P. Voss, R. Wilson, Proc. Roy. Soc. A **236**, 41 (1956).
9. J. Klug et al., Phys. Rev. C **68**, 064605 (2003).
10. J. Klug et al., Phys. Rev. C **67**, 031601(R) (2003).
11. P. Mermod et al., Phys. Rev. C **74**, 054002 (2006).
12. G. Gerstein, J. Niederer, K. Strauch, Phys. Rev. **108**, 427 (1957).
13. J. Matero, Z. Phys. A **351**, 29 (1995).
14. A. Öhrn et al. (to be published).
15. M. Österlund et al. (to be published).

International Conference on Nuclear Data for Science and Technology 2007
DOI: 10.1051/ndata:07435

95 MeV neutron scattering on hydrogen, deuterium, carbon and oxygen

P. Mermod[1], J. Blomgren[1,a], C. Johansson[1], A. Öhrn[1], M. Österlund[1], S. Pomp[1], B. Bergenwall[2], J. Klug[1], L. Nilsson[1], N. Olsson[3], U. Tippawan[4], P. Nadel-Turonski[5], O. Jonsson[6], A. Prokofiev[6], P.-U. Renberg[6], Y. Maeda[7], H. Sakai[7], A. Tamii[7], K. Amos[8], and R. Crespo[9]

[1] Department of Neutron Research, Uppsala University, P.O. Box 525, 75120 Uppsala, Sweden
[2] Department of Nuclear and Particle physics, Uppsala University, Sweden
[3] Swedish Defence Research Agency, Stockholm, Sweden
[4] Fast Neutron Research Facility, Chiang Mai University, Thailand
[5] The George Washington University, Washington, DC, USA
[6] The Svedberg Laboratory, Uppsala University, Sweden
[7] Department of Physics, University of Tokyo, Japan
[8] School of Physics, University of Melbourne, Australia
[9] Departamento de Fisica, Instituto Superior Técnico, Lisboa, Portugal

Abstract. Three neutron-deuteron scattering experiments at 95 MeV have been performed recently at The Svedberg Laboratory in Uppsala. Subsets of the results of these experiments have been reported in two short articles, showing clear evidence for three-nucleon force effects. In this paper, we present further discussion of the results. We obtained excellent precision in the angular range of the nd cross section minimum. The data are in good agreement with Faddeev calculations using modern *NN* potentials and including 3*N* forces from a 2π-exchange model, while the calculations without 3*N* forces fail to describe the data. CHPT calculations at next-to-next-to-leading order represent an improvement compared to calculations with *NN* forces only, but still underestimate the data in the minimum region. In addition to neutron-deuteron scattering data, neutron-proton and ^{12}C(n,n) elastic scattering data have been measured for normalization purposes, and ^{16}O(n,n) data have been obtained for the first time at this energy. It was possible to extract ^{12}C(n,n') and ^{16}O(n,n') inelastic scattering cross sections to excited states below 12 MeV excitation energy. These data are shown to have a significant impact on the determination of nuclear recoil kerma coefficients.

1 Introduction

Nuclear properties and interactions can be understood ab initio from the basic knowledge of the nucleon-nucleon (*NN*) interaction. For this purpose, *NN* potentials, which are based on meson-exchange theories, have been developed: the most widely used ones are the Argonne AV18 potential [1], the CD-Bonn potential [2,3] and the Nijmegen potentials [4]. After proper adjustment of the free parameters, these models are able to describe very well a restricted pp and np data base below 350 MeV [5].

In three-nucleon (3*N*) systems, quantitative descriptions can be provided rigorously by using *NN* potentials in the Faddeev equations [6]. However, theoretical considerations indicate that the description of systems made of more than two nucleons is not complete if three-body forces are not taken into account: 3*N* forces can be represented by introducing a 3*N* potential in the Faddeev equations. As a first experimental evidence, the ^{3}H and ^{3}He binding energies can be reproduced model-independently taking 3*N* forces into account [7], while calculations using only *NN* interactions underestimate them by typically half an MeV [2]. The ^{4}He binding energy can also be described correctly with combined *NN* and 3*N* forces [8], indicating that the role of four-nucleon forces is not significant.

The ultimate goal of nuclear physics would be to have a single consistent theory that could describe both nucleon and nuclear properties and dynamics. Chiral symmetry breaking can be analyzed in terms of an effective field theory, chiral perturbation theory (CHPT). This model can be applied to describe consistently the interaction between pions and nucleons, as well as the pion-pion interaction. Calculations made within the CHPT framework at next-to-next-to-leading order implicitly include 3*N* forces [9,10]. Calculations at the next higher order were made recently [11,12], allowing for instance an excellent description of *NN* phase shifts.

Besides the ^{3}H and ^{3}He binding energies, a number of observables that may reveal the effects of 3*N* forces have been identified. We will concentrate our discussion to nucleon-deuteron scattering in the energy range 65–250 MeV. At these energies, significant 3*N*-force contributions are expected in the elastic scattering angular distribution [13, 14] as well as for various spin-transfer observables in elastic scattering [6] and observables in the break-up process in various kinematical configurations [15,16]. In particular, for elastic nucleon-deuteron scattering, Faddeev calculations including a 3*N* potential with parameters adjusted to the triton binding energy predict that 3*N* forces affect substancially the differential cross section in the minimum region of the angular distribution [13]. Around 100 MeV, this effect is of the order of 30% in the minimum region.

Thus, a robust way to investigate 3*N* forces is to measure the proton-deuteron (pd) and neutron-deuteron (nd) elastic scattering differential cross sections. Numerous pd elastic scattering experiments have been performed [18–26].

[a] Corresponding author, e-mail: jan.blomgren@tsl.uu.se

A coulomb-free signal can be obtained by performing nd scattering experiments [27–31]. In general, for both pd and nd scattering, in the energy range 65–150 MeV the data show the expected effects of 3*N* forces in the cross section minimum, while at higher energies, the effects tend to be too large to be accounted for by present theories. This might be due to the lack of a full relativistic treatment in the calculations [32,33]. At 95 MeV, the energy of the present work, relativistic effects are not expected to contribute significantly.

In the context of the nd scattering experiments, we obtained elastic scattering angular distributions for carbon and oxygen at 95 MeV. Differential cross sections for neutron inelastic scattering on carbon and oxygen to excited states below 12 MeV excitation energy could also be extracted [34]. These data are relevant for medical treatment of tumors with fast neutrons as well as in dosimetry, since the human body contains significant amounts of carbon and oxygen. Recoil nuclei from elastic and inelastic scattering are expected to account for more than 10% of the cell damage, the rest being mainly due to neutron-proton (np) scattering and neutron-induced emission of light ions [35,36]. The oxygen data may also be relevant for future incineration of nuclear waste in subcritical reactors fed by a proton accelerator, where the nuclear fuel might be in oxide form.

2 Results for np and nd scattering

By detecting either the scattered neutron or the recoil proton/deuteron, we were able to cover the angular range from 15 to 160 degrees in the c.m. system. By using two different detector setups, MEDLEY [37] and SCANDAL [38] in various configurations, we could keep the systematic uncertainties under control. Additionally, by measuring the np scattering differential cross section and, in the case where scattered neutrons were detected, also elastic scattering in carbon (i.e., the ^{12}C(n,n) reaction), the systematic error due to uncertainties in the normalization factors was minimized.

The np data are shown in figure 1. The absolute scale was adjusted to the Rahm et al. data [39] (filled triangles) which were in turn normalized to the well-known total np cross section [40]. The excellent agreement with both previous data and calculations based on *NN* potentials allows us to validate the quality of the nd data since the np and nd differential cross sections were measured under essentially the same conditions. Besides, the np data give supplementary information about the np angular distribution at 95 MeV (for previous data, see, e.g., refs. [39,40]). In many experiments, neutron cross sections are measured relative to the np cross section [40], i.e., it is used as a cross section standard. Neutron-proton scattering plays an important role in nuclear physics, since it can be used to validate *NN* potentials and to derive a value of the absolute strength of the strong interaction. The extensive database of np differential cross sections is not always consistent and, not unrelated, there are still problems with the determination of a precise value of the πNN coupling constant [5,41,42].

The nd results at 95 MeV in the minimum region ($80° < \theta_{\mathrm{c.m.}} < 160°$) are shown in figure 2, and are compared with theoretical predictions based on Faddeev calculations [13] using the AV18 *NN* potential [1] combined with two different

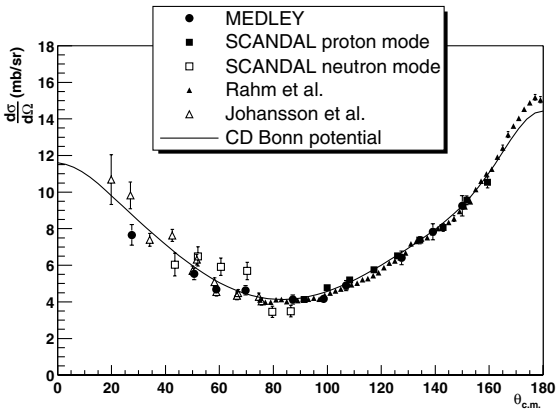

Fig. 1. The present and previous Uppsala data for np elastic scattering at 95 MeV. The dots and squares are the results of our nd experiments [28,29], and the triangles were obtained from previous np experiments by Rahm et al. [39] and Johansson et al. [40]. The data are compared with a calculation using the CD-Bonn *NN* potential [2].

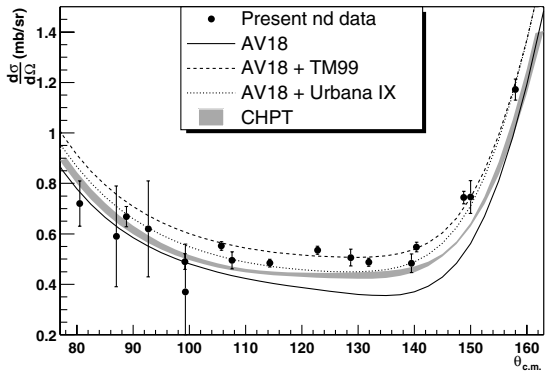

Fig. 2. The present nd data (filled dots) in the angular range $80° < \theta_{\mathrm{c.m.}} < 160°$. The solid, dashed, and dotted curves were obtained from Faddeev calculations with the Argonne AV18 potential [1] without 3*N* forces, with the Tucson-Melbourne (TM99) 3*N* potential [43], and with the Urbana IX 3*N* potential [44], respectively. The gray band was obtained from chiral perturbation theory at next-to-next-to-leading order [9].

3*N* potentials (Tucson-Melbourne [43] and Urbana IX [44]), as well as predictions from CHPT [9]. It is quantitatively illustrative to compute the reduced χ^2 between our data and the calculations for the nd differential cross section in the minimum, i.e., all data points shown in the figure. When no 3*N* forces are included, the χ^2 is larger than 18. The best description is given by the CD-Bonn potential (version 1996) with the TM99 3*N* force, with a χ^2 of 2.1. With the AV18 potential (shown in the figure), the nd differential cross section is slightly better described with the TM99 3*N* potential (χ^2 = 2.3) than with the Urbana IX potential (χ^2 = 3.5). The CHPT prediction gives a χ^2 of 6.5. Note that the deviations from one may be partly due to the normalization uncertainties in the data [29,34].

3 Results for ^{12}C(n,n) and ^{16}O(n,n) scattering

Differential cross sections for elastic and inelastic neutron scattering on carbon and oxygen must be well known for a

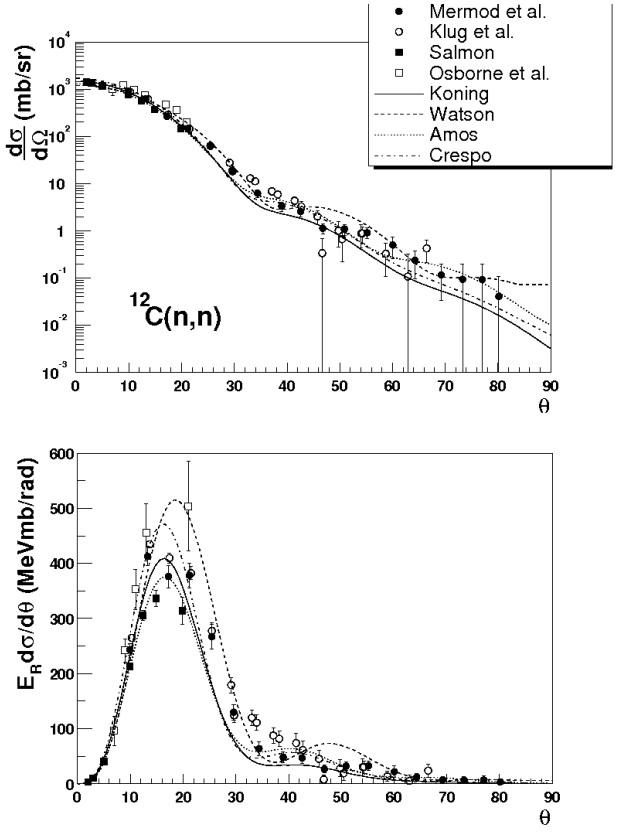

Fig. 3. Elastic neutron scattering on carbon at 96 MeV. The angle θ is the neutron scattering angle in the laboratory. The experimental data are from refs. [34,45–47]. The elastic scattering differential cross section is shown in the top panel, and in the bottom panel, the differential cross section was multiplied with the solid angle element and with the energy of the recoil nucleus. The area under this plot is proportional to the nuclear recoil kerma coefficient for elastic scattering.

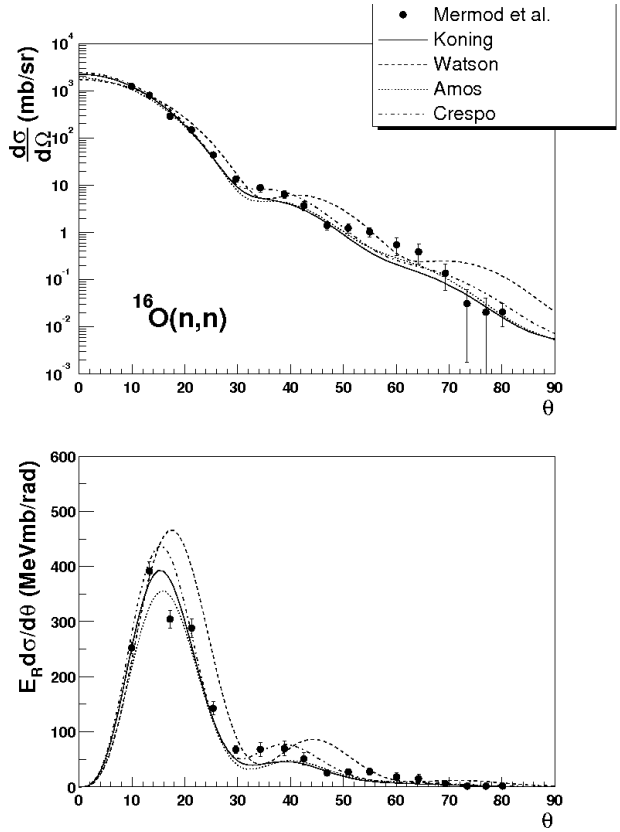

Fig. 4. Elastic neutron scattering on oxygen at 96 MeV. The angle θ is the neutron scattering angle in the laboratory. The experimental data are from ref. [34]. The elastic scattering differential cross section is shown in the top panel, and in the bottom panel, the differential cross section was multiplied with the solid angle element and with the energy of the recoil nucleus. The area under this plot is proportional to the nuclear recoil kerma coefficient for elastic scattering.

precise evaluation of the damage caused by fast neutrons in human tissue. Figures 3 (carbon) and 4 (oxygen) illustrate how recoil kerma coefficients are obtained from the differential cross sections. The elastic neutron scattering data at 96 MeV are from Mermod et al. [34], Klug et al. [45], Salmon [46] and Osborne et al. [47]. The theoretical curves are predictions from the Koning and Delaroche global potential [48], the Watson global potential [49], Amos et al. [50], and Crespo et al. [51] (see refs. [34,45] for details). In the top panels of the figures, the differential cross sections (in logarithmic scale) are plotted as functions of the neutron scattering angle in the laboratory. In the bottom panels, the distributions have been multiplied with the solid angle element $2\pi \sin\theta$ and weighed with the energy of the recoil nuclei E_R, thus illustrating the angular probability distributions for the neutrons to cause cell damage. As the solid angle vanishes at zero degrees, these distributions are no longer forward-peaked. Back-scattered neutrons transfer more energy to the nuclei than forward-scattered neutrons, and therefore the energy of the recoil nuclei increases with the neutron scattering angle. From these distributions, which peak at about 16°, we can deduce that, for elastic scattering, most of the damage is caused by neutrons scattered between 10 and 30°, but there is still a significant contribution up to 60°. With this way of plotting, the recoil kerma coefficient (and the cell damage due to elastic scattering) is proportional to the area under the distribution [34]. There are large variations among the different models, it leads to an uncertainty in the the recoil kerma coefficients of at least 10% for the theoretical calculations, while the experimental uncertainty reached with the present data is about 5%. For elastic scattering on carbon, most models are inaccurate in the region 25–35°. For oxygen, the prediction closest to the data is provided by the Koning and Delaroche potential. For inelastic scattering on carbon and oxygen at 96 MeV to collective states up to 12 MeV excitation energy, the main contribution to the kerma from inelastic scattering is between 30 and 60°. The data obtained in this angular range (not shown in the figures) tend to be significantly underestimated (by about 50%) by the calculations [34]. Although the contribution from inelastic scattering is small compared to other processes, the disagreement between calculations and data for inelastic scattering is still responsible for a significant (about 8%) discrepancy in the recoil kerma coefficient for the sum of elastic and inelastic reactions below 12 MeV excitation energy.

4 Conclusions

The np and nd elastic scattering differential cross sections at 95 MeV have been extensively and accurately measured. The data agree well with predictions based on *NN* and 3*N* potentials, provided that 3*N* forces are taken into account for nd scattering. This represents an important step to validate the approach in which *NN* and 3*N* potentials or effective field theories are used in ab initio models, which can be applied in systems of more than three nucleons.

As by-products of the nd experiments, elastic and inelastic neutron scattering differential cross sections on carbon and oxygen have been measured at 95 MeV. Experimental recoil kerma coefficients were obtained and shown to be quite sensitive to the differential cross sections in the angular range $25 - 70°$. This is relevant for the evaluation of deposited doses for applications such as dosimetry and fast neutron cancer therapy.

This work was supported by the Swedish Nuclear Fuel and Waste Management Company, the Swedish Nuclear Power Inspectorate, Ringhals AB, the Swedish Defence Research Agency and the Swedish Research Council.

References

1. R.B. Wiringa, V.G.J. Stoks, R. Schiavilla, Phys. Rev. C **51**, 38 (1995).
2. R. Machleidt, F. Sammarruca, Y. Song, Phys. Rev. C **53**, R1483 (1996).
3. R. Machleidt, Phys. Rev. C **63**, 024001 (2001).
4. V.G.J. Stoks, R.A.M. Klomp, C.P.F. Terheggen, J.J. de Swart, Phys. Rev. C **49**, 2950 (1994).
5. R. Machleidt, I. Slaus, J. Phys. G **27**, R69 (2001).
6. W. Glöckle, H. Witała, D. Hüber, H. Kamada, J. Golak, Phys. Rep. **274**, 107 (1996).
7. A. Nogga, A. Kievsky, H. Kamada, W. Glöckle, L.E. Marcucci, S. Rosati, M. Viviani, Phys. Rev. C **67**, 034004 (2003).
8. A. Nogga, H. Kamada, W. Glöckle, B.R. Barrett, Phys. Rev. C **65**, 054003 (2002).
9. E. Epelbaum, A. Nogga, W. Glöckle, H. Kamada, U.-G. Meissner, H. Witała, Phys. Rev. C **66**, 064001 (2002).
10. P.F. Bedaque, U. van Kolck, Annu. Rev. Nucl. Part. Sci. **52**, 339 (2002).
11. D.R. Entem, R. Machleidt, Phys. Rev. C **68**, 041001(R) (2003).
12. E. Epelbaum, W. Glöckle, U.-G. Meissner, Nucl Phys. **A747**, 362 (2005).
13. H. Witała, W. Glöckle, D. Hüber, J. Golak, H. Kamada, Phys. Rev. Lett. **81**, 1183 (1998).
14. S. Nemoto, K. Chmielewski, S. Oryu, P.U. Sauer, Phys. Rev. C **58**, 2599 (1998).
15. L.D. Knutson, Phys. Rev. Lett. **73**, 3062 (1994).
16. J. Kuroś-Żołnierczuk, H. Witała, J. Golak, H. Kamada, A. Nogga, R. Skibiński, W. Glöckle, Phys. Rev. C **66**, 024003 (2002).
17. S.A. Coon, M.D. Scadron, P.C. McNamee, B.R. Barrett, D.W.E. Blatt, B.H.J. McKellar, Nucl. Phys. **A317**, 242 (1979); S.A. Coon, W. Glöckle, Phys. Rev. C **23**, 1790 (1981).
18. O. Chamberlain, M.O. Stern, Phys. Rev. **94**, 666 (1954).
19. H. Postma, R. Wilson, Phys. Rev. **121**, 1229 (1961).
20. K. Kuroda, A. Michalowicz, M. Poulet, Nucl. Phys. **88**, 33 (1966).
21. G. Igo, J.C. Fong, S.L. Verbeck, M. Goitein, D.L. Hendrie, J.C. Carroll, B. McDonald, A. Stetz, M.C. Makino, Nucl. Phys. A **195**, 33 (1972).
22. R.E. Adelberger, C.N. Brown, Phys. Rev. D **5**, 2139 (1972).
23. H. Shimizu, K. Imai, N. Tamura, K. Nisimura, K. Hatanaka, T. Saito, Y. Koike, Y. Taniguchi, Nucl. Phys. A **382**, 242 (1982).
24. H. Sakai et al., Phys. Rev. Lett. **84**, 5288 (2000).
25. K. Hatanaka et al., Phys. Rev. C **66**, 044002 (2002).
26. K. Ermisch et al., Phys. Rev. C **68**, 051001(R) (2003).
27. H. Rühl et al., Nucl. Phys. A **524**, 377 (1991).
28. P. Mermod et al., Phys. Lett. B **597**, 243 (2004).
29. P. Mermod et al., Phys. Rev. C **72**, 061002(R) (2005).
30. J.N. Palmieri, Nucl. Phys. A **188**, 72 (1972).
31. Y. Maeda et al. (submitted to Phys. Rev. C).
32. H. Witała, J. Golak, W. Glöckle, H. Kamada, Phys. Rev. C **71**, 054001 (2005).
33. K. Sekiguchi et al., Phys. Rev. Lett. **95**, 162301 (2005).
34. P. Mermod et al., Phys. Rev. C **74**, 054002 (2006).
35. M.B. Chadwick, P.M. DeLuca Jr., R.C. Haight, Radiat. Prot. Dosim. **70**, 1 (1997).
36. J. Blomgren, N. Olsson, Radiat. Prot. Dosim. **103**, 293 (2003).
37. S. Dangtip et al., Nucl. Instrum. Meth. A **452**, 484 (2000).
38. J. Klug et al., Nucl. Instrum. Meth. A **489**, 282 (2002).
39. J. Rahm et al., Phys. Rev. C **63**, 044001 (2001).
40. C. Johansson et al., Phys. Rev. C **71**, 024002 (2005).
41. J. Blomgren, N. Olsson, J. Rahm, Phys. Scr. T **87**, 33 (2000).
42. M. Sarsour et al., Phys. Rev. Lett. **94**, 082303 (2005).
43. J.L. Friar, D. Hüber, U. van Kolck, Phys. Rev. C **59**, 53 (1999); S.A. Coon, H.K. Han, Few-Body Syst. **30**, 131 (2001).
44. B.S. Pudliner, V.R. Pandharipande, J. Carlson, S.C. Pieper, R.B. Wiringa, Phys. Rev. C **56**, 1720 (1997).
45. J. Klug et al., Phys. Rev. C **68**, 064605 (2003).
46. G.L. Salmon, Nucl. Phys. **21**, 14 (1960).
47. J.H. Osborne et al., Phys. Rev. C **70**, 054613 (2004).
48. A.J. Koning, J.P. Delaroche, Nucl. Phys. A **713**, 231 (2003).
49. B.A. Watson, P.P. Singh, R.E. Segel, Phys. Rev. **182**, 977 (1969).
50. K. Amos, P.J. Dortmans, H.V. von Geramb, S. Karataglidis, J. Raynal, Adv. Nucl. Phys. **25**, 275 (2000).
51. R. Crespo, R.C. Johnson, J.A. Tostevin, Phys. Rev. C **46**, 279 (1992).

International Conference on Nuclear Data for Science and Technology 2007
DOI: 10.1051/ndata:07734

Mono-energy neutron testing of Single Event Effects

J. Blomgren[1,a], S. Pomp[1], J.-C. Bourselier[1], M. Österlund[1], A. Prokofiev[2], and A. Koning[3]

[1] Uppsala University, Dept of Neutron Research, Box 525, 75120 Uppsala, Sweden
[2] Uppsala University, The Svedberg Laboratory, Box 535, 75121 Uppsala, Sweden
[3] Nuclear Research and consultancy Group, P.O. Box 25, Petten, The Netherlands

Abstract. The role of mono-energy neutron testing for Single Event Effects (SEE) is outlined. Recent improvements in nuclear reaction theory of relevance to computation of single-event effects from fundamental physics is reported. Older data, as well as recent results obtained with mono-energy neutron testing are well described. Future options of extremely intense mono-energy neutron sources are discussed.

1 Introduction

Neutron testing of SEEs in memory devices is performed with two major methods. White beam testing, performed at spallation neutron sources, has the advantage of simplicity, in that the facility spectrum resembles the spectrum of atmospheric neutrons, and only a single measurement is needed. A drawback is that these two spectra are not identical. Moreover, different test sites provide different neutron spectra. Thus, corrections have to be estimated if precise results are required, or if data from different white beam facilities should be compared. Unfortunately, accurate corrections are in general very difficult to determine, because the fundamental requirement for such a correction to be determined is knowledge about not only the neutron spectra involved, but also the energy dependence of the SEE sensitivity. The latter cannot even in principle be determined in a white beam, and therefore the corrections have to be estimated from very crude assumptions, resulting in limited precision in the results.

Mono-energy testing has the advantage of being able to overcome these obstacles. By measuring the energy dependence of the SEE sensitivity (i.e., the SEE cross section) at a number of energies, the total SEE sensitivity can be obtained by simply multiplying the SEE sensitivity and the neutron flux versus energy. In principle, this method allows more precise data to be produced than with white beam testing, but with the drawback that measurements have to be performed at several energies (which often is time-consuming). Moreover, the term *mono-energy* is a truth with qualification. Typically, about half the neutrons are found in a narrow energy interval at maximum neutron energy, while the remaining 50% constitute a structure-less tail from maximum down to zero energy. The effects of this tail can, however, be corrected for.

A major advantage of using mono-energy testing is that the energy dependence of the SEE sensitivity can provide deep insights into the nuclear reaction mechanisms ultimately causing these effects. This is of great value for the development of computational tools allowing the SEE sensitivity to be estimated already before a new circuit design is taken into production.

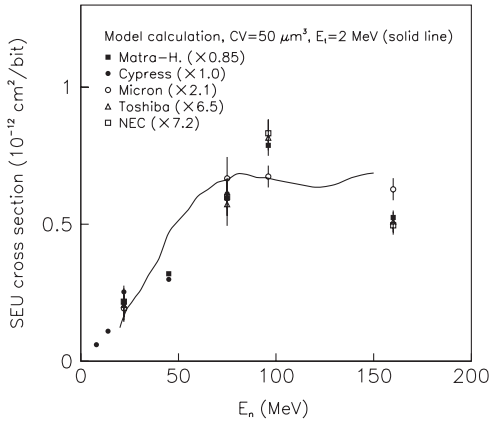

Fig. 1. The SEU cross section for a few memory devices produced in the late 1990s versus neutron energy, reprinted from ref. [5]. The line refers to a model calculation of the SEU cross section using the GNASH code [7] with a similar methodology as TALYS, described elsewhere in the present paper.

The present paper gives a few examples of how previous and recent measurements of the energy dependence of the SEE sensitivity can shed light on the underlying nuclear physics. Recent advances in relevant nuclear theory are described, and the possibilities to develop computational tools for pre-manufacturing SEE sensitivity estimations are outlined.

2 Fundamentals on neutron testing

The ultimate goal of all neutron SEE testing is to establish the sensitivity to the natural neutron flux. In principle, devices could be tested by subjecting them to the natural flux, but this is so time-consuming that it is generally not a realistic option [1]. Naively, one might assume that the ideal testing method would be to have a neutron flux with an energy spectrum identical to the natural flux, but with significantly larger intensity.

In reality, this is difficult to achieve. This is not just a problem related to testing methods, but also to the natural flux itself. The latter is not constant, but depends on a variety

[a] Presenting author, e-mail: jan.blomgren@tsl.uu.se

of natural parameters, like altitude, latitude or weather. In addition, man-made effects play a role. For instance, the presence of shielding material, like buildings or ship hulls, can modify the flux of cosmic particles. Thus, testing in one single neutron field supposed to be identical with the "natural flux" is ultimately impossible. There is no single "natural flux", but many.

If demands on accuracy are modest, white beam testing can be employed. In such facilities, neutrons are created by protons impinging on (most often also stopping in) a target of heavy nuclei, resulting in a strong neutron flux. The energy distribution resembles natural fluxes, but far from perfectly. If normalizing a given artificial and a given natural flux at a single energy to each other, the neutron flux can differ by a factor two in another energy region.

This is also true when comparing different white beam facilities. Different production techniques (i.e., different energy of the incoming beam and different target construction) can result in fairly different energy distributions. Thus, results obtained at two different white beam facilities can be significantly different, up to about a factor two. The standard approach in physics would be to establish correction factors to allow comparisons from, e.g., different facilities, but this is impossible unless information is available on the energy distribution both on the neutron fluxes involved and the energy dependence of the device sensitivity. Since the latter cannot be obtained at white beams, mono-energy testing is required. It should be pointed out that when it comes to correction factors to correlate testing of two different white beam facilities, the correction factors are unique to each component, because the energy dependence of their sensitivity is individual. The sensitivity depends on technical parameters, like critical charge and cell dimensions. Moreover, a correction factor established for a certain device to correlate, e.g., single-bit upset rate, does not apply to other effects in the same device, like multi-bit upsets or latch-ups. This is because the energy dependences of the sensitivities to different types of errors are different.

It can be concluded that if the result should be reliable to about a factor two, white beams can be used, but for better accuracy, mono-energy testing has to be used. Thus, the first added value of mono-energy testing is the potential to reach better accuracy. As will be discussed below, this is not the only reason.

3 Mono-energy neutron testing

If accuracy better than what can be obtained at facilities resembling the natural flux (i.e., white beams) is desired, mono-energy testing is the only alternative. Mono-energy testing is presently based on techniques in which a beam of charged particles hit a stationary target. Only a small fraction of the incident beam causes neutron production, and the remaining beam is bent and dumped in a way not to create unmanageable background. The neutrons are primarily produced in the forward direction, but the angular distribution is rather wide, and therefore collimators are required. Due to the fact that neutrons are very penetrating, these collimators have to be thick, of the order of meters, which is one unavoidable limitation of any neutron production technique.

The ideal production reaction should have a large probability (cross section) and as good mono-energy character as possible, i.e., a large fraction of the neutrons should appear in a narrow energy interval. Moreover, the incoming charged particle should preferably be easily accelerated, which in reality means protons. Three suitable reactions are available, proton-induced neutron production on deuterium (^{2}H) and the two stable lithium isotopes, ^{6}Li and ^{7}Li. Deuterium produces a nice spectrum, but requires expensive handling of liquid deuterium. The two lithium isotopes give comparable performance, but ^{6}Li is of strategic importance (it is an important ingredient in thermonuclear weapons) making it difficult to obtain. Thus, ^{7}Li has become the choice at essentially all present mono-energy neutron facilities.

The presence of a low-energy tail is unavoidable with neutron production on a fixed target for neutron energies above about 25 MeV, the limit determined by the maximum binding energy difference between the initial and final nuclear systems involved. Since testing has to be performed at higher energies, methods to correct for these tails have to be developed. Such corrections are routinely used in, e.g., nuclear physics research, and a large number of de-convolution codes exist. The most important limiting factors in the final result is a combination of the statistical uncertainty in the raw data, knowledge of the neutron energy spectra, systematic errors in the de-convolution methods (de-convolution is a poorly conditioned mathematical problem, with no single unique solution), and assumptions about the energy dependence of the real cross section.

The latter deserves a special discussion. For a higher nominal neutron energy, a larger fraction of the neutrons are found in the tail. If the real SEE cross section rises with energy all the way to the highest energy point, the correction factors become smaller than if the cross section peaks at a relatively low energy and then decreases. In the latter case, a smaller fraction of the events at the highest nominal energy are due to the full-energy peak, resulting in a larger correction factor, with a correspondingly larger uncertainty.

Thus, the final uncertainty is different for different cases. In general, a final uncertainty of the order of 10% should be possible to reach with state-of-the-art methods. It is not likely that the final uncertainty can be significantly reduced in a foreseeable future. One ultimately limiting factor is monitoring of the neutron beam flux, which is very difficult to perform to better than 5% uncertainty in these types of measurements.

4 Added value of mono-energy testing

As has been discussed above, the first added value of mono-energy testing is the possibility to suppress the final uncertainty from about a factor two to about 10%. In the discussion of neutron testing, one important aspect often overlooked is the usefulness of large intensity at high energies. White beams can in principle be designed to yield a larger total number of neutrons, but the large majority of the neutrons have low energy. The spectrum typically peaks around one or a few MeV, and falls off approximately as 1/E. This means that the intensity at high energies is much lower than at mono-energy

facilities. In fact, the low-energy tail of the high-energy fields at intense mono-energy facilities contains more neutrons than the presently most intense white beam. A consequence of this is that testing of effects caused only by high-energy neutrons becomes very time-consuming at white beams. For instance, latch-up effects seems to require at least about 100 MeV in recent devices, and their sensitivity increases rapidly with neutron energy. This means that the testing to reach the same accuracy in the results would require at least an order of magnitude longer irradiation at LAMPF than at TSL (180 MeV field).

This is also needed when considering other types of effects more complex than standard single-bit SEU in memory devices. Multi-bit upsets (SMU) have been shown to have different energy dependence than single-bit SEU [2], with SMUs becoming more important at high energies. No measurement of energy-resolved SMU cross sections has been published recently, but the general trend of the pioneering paper in 1999 could be well described using fundamental nuclear physics theory, and using the same nuclear theory and modern device parameters results in a similar picture.

Testing is presently often carried out until a preset total number of upsets have been logged. If this is carried out at a white beam, this means that the risk – or chance – that complex errors appear is smaller than in mono-energy testing. Obviously, there is then a risk that the device later shows effects not observed in the testing. Up to now, the discussion has focused on commercial testing. Another advantage of mono-energy beams is their usefulness for research. For instance, mono-energy neutron beam results can in some cases be directly compared with proton beam results (which are inherently of mono-energy character), allowing improved insight into the underlying reaction mechanisms.

5 Results and discussion

In the present work, computations with TALYS [3] have been used to calculate energy and angular distributions of all ions created in neutron-induced nuclear reactions on silicon. For reasons described below, not all released reaction products induce upsets. Therefore, a separate post-analysis program has been developed that uses the output from TALYS and converts it to SEE probability, taking only relevant emitted ions into account [4].

In figure 1, the results of the first energy-resolved measurement of neutron-induced single-event upsets (SEU), published in 1998 [5], are presented. Five different memory devices were tested, and it was found that the energy dependence was very similar for all of them, but the absolute sensitivity differed by up to almost an order of magnitude. The oldest components showed lower sensitivity than more recent ones. As can be seen, the sensitivity showed a slow rise from low energy up to about 100 MeV, where it saturated or possibly even decreased.

In figure 2, the results of a recent similar test, published in 2005 [6], are shown, however for one device only. It can be seen that the uncorrected result, i.e., raw data before correction for the low-energy neutron tail, partly resembles the results in figure 1, but with a maximum at a much lower energy and a significant decrease of the SEU cross section at high energies.

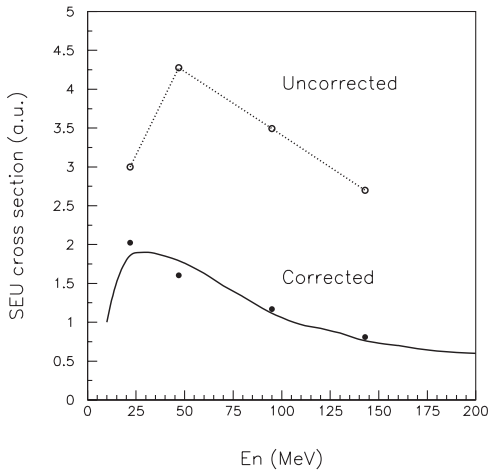

Fig. 2. The SEU cross section for a recent memory devices versus neutron energy, reprinted from ref. [6]. The two data sets are before and after correction for the low-energy tail. The figure is modified by the inclusion of a prediction by the nuclear reaction code TALYS of the cross section. The cross section scale is arbitrary. See the text for details.

The corrected result, however, shows a steady decrease already from the first datum point at 22 MeV.

All these results can be understood from fundamental nuclear physics point of view. These effects are caused by neutrons that induce nuclear reactions, releasing charge via emitted ions. (The neutron itself makes no effect, neither do emitted gamma rays.) Whether the released ions cause an upset or not primarily depends on the total charge released, that has to be larger than the critical charge of the component, and on the specific energy loss (dE/dx), i.e., the amount of energy transferred to the critical volume per length unit of the ion propagation. The latter is important because even if a large total energy in the form of a specific ion is released, but that particular ion does not deposit sufficient energy in a single bit, no upset will result.

All components shown in figure 1 required a rather large critical charge for a bit flip. This had the consequence that relatively exotic nuclear reactions were primarily responsible for the upsets. The cross section for those reactions has a threshold around 10–20 MeV and it increases slowly with energy up to about 50–150 MeV (depending of ion) after which it begins to decrease. Thus, the dependence in figure 1 is in line with expectations from well-known nuclear physics.

Recent components have a much smaller critical charge, but also smaller dimensions of the critical volume. These two effects go in opposite directions when it comes to sensitivity, but it seems as the leading effect is the former, i.e., modern devices require less specific energy loss to cause an SEU. This opens the possibility that other, more common, reaction channels come into play. The dominating neutron-induced nuclear reaction is always elastic scattering. In fact, it is a fundamental quantum mechanics property that elastic scattering must constitute at least half the total neutron cross section. In elastic scattering, the neutron is deflected, leaving the nucleus in its ground state, but with a recoil due to the transferred momentum. This recoiling nucleus has a low energy, resulting

in a large specific energy loss. Elastic scattering has no energy threshold, so the lowest energy in which it can induce an SEU is primarily determined by the critical charge of the device. As soon as the neutron energy is large enough to cause an upset via the recoils of elastic scattering, this can be expected to be the dominant mechanism, because the cross section is large. In addition, the effect can be expected to peak rather near to the threshold, and then the cross section should slowly decrease with energy.

This is in agreement with the dependence in figure 2. The solid line shows the prediction by TALYS, presuming reasonable dimensions of the critical volume and charge. The line and the data are normalized to each other, i.e., TALYS describes the trends well, but to get the absolute scale right, also unavailable detailed information on device parameters is needed.

6 Future facilities

Until recently, it has been an implicit truth that mono-energy facilities always has a low-energy tail, and that white beams in principle can be made more intense (although at present the leading mono-energy and white facilities actually produce about the same total number of neutrons per second). These presumptions are based on the boundary condition of neutron production on fixed targets. Recently, completely different neutron production techniques have been proposed, in which very intense mono-energy neutron beams can be envisioned.

Two production techniques have been proposed. The first is to use a proton beam of about 1–2 GeV impinging on a combined target and ion source to produce beta-decaying nuclei, which in turn are accelerated and inserted into a storage ring of race-track geometry [8]. Some beta-decaying nuclei emit neutrons immediately after the beta decay[1]. This neutron has a low energy relative to the decaying nucleus. This means that if the nucleus decays in flight, the neutron will be emitted along the direction of motion of the decaying nucleus, with the same velocity. As a consequence, intense mono-energy fluxes will be produced along the straight sections.

It has been estimated that fluxes of 10^{11} n/s could be achieved, compared with 10^6 today, i.e., a factor 100 000 (!) more intense than today. Even if the technique would be a factor 100 less efficient than the design implies, it would still be a factor 1000 more neutrons than presently. Moreover, with such a technique all neutrons would appear in a narrow (few MeV) energy range with no low-energy tail. This concept is a spin-off from a conceptual program at the particle physics laboratory CERN, in which similar techniques would be used to produce intense neutrino fluxes for particle physics and cosmology research. The proposed scheme requires infrastructure of the type only CERN can provide, e.g., several coupled high-energy accelerators. Thus, the realization of this technique depends on the realization of the proposed neutrino facility.

A second technique would be to use a similar production as above (1–2 GeV protons on a combined target-ion source) to produce the radioactive nuclide ^{6}He, which in turn would be accelerated to hit a target [9]. Roughly, ^{6}He can be described as an alpha particle with two loosely attached neutrons. When hitting a target, the two neutrons are dissociated with a large probability, and continue along the direction of the incident beam with the incident velocity. The charged particles (the remaining ^{6}He and residual ^{4}He) is bent by a magnet system and a clean neutron beam is produced. This latter technique does not have the potential to produce as intensive fluxes as the beta-decay in flight, but on the other hand it requires much less advanced accelerators. This technique could possibly be installed at existing CERN facilities after some upgrades. Initial estimates indicate a factor a hundred to a thousand larger neutron fluxes than for present facilities to be within reach.

This work was financially supported by the Swedish Nuclear Fuel and Waste Management Company, the Swedish Nuclear Power Inspectorate, Ringhals AB, Barsebäck Power AB, Forsmark Power AB, the Swedish Defense Research Agency, the Swedish Natural Science Research Council, the Swedish Nuclear Safety and Training Centre, and the European Union.

References

1. J.F. Ziegler, H. Puchner, *SER–History, Trends and Challenges* (Cypress, 2004).
2. K. Johansson, M. Ohlsson, N. Olsson, J. Blomgren, P.-U. Renberg, IEEE Trans. Nucl. Sci. **46**, 1427 (1999).
3. A.J. Koning, S. Hilaire, M.C. Duijvestijn, AIP Conf. Proc. **769**, 154 (2005).
4. J.-C. Bourselier, Uppsala University Neutron Physics report 05/07, 2005.
5. K. Johansson, P. Dyreklev, B. Granbom, N. Olsson, J. Blomgren, P.-U. Renberg, IEEE Trans. Nucl. Sci. **45**, 2519 (1998).
6. M. Olmos, A.V. Prokofiev, R. Gaillard, *2005 IEEE International Reliability Physics Symposium Proceedings, 43rd Annual, San Jose, California, April 17–21, 2005*, pp. 696–697.
7. M.B. Chadwick, H.H. Barschall, R.S. Caswell, P.M. DeLuca Jr., G.M. Hale, D.T.L. Jones, R.E. MacFarlane, J.P. Meulders, H. Schuhmacher, U.J. Schrewe, A. Wambersie, P.G. Young, Med. Phys. **26**, 974 (1999) ; and ICRU Report **63** (International Commission on Radiation Units and Measurements, Bethseda, MD, 2000).
8. CERN beta beam project, http://beta-beam.web.cern.ch/beta-beam/.
9. I. Tanihata, M. Lindroos (private communication).

[1] This effect is of major importance for the stability of nuclear power reactors.

International Conference on Nuclear Data for Science and Technology 2007
DOI: 10.1051/ndata:07483

Angular anisotropy of intermediate energy nucleon-induced fission of actinide and subactinide nuclei

V.P. Eismont[1,a], N.P. Filatov[1], A.N. Smirnov[1], and J. Blomgren[2]

[1] V.G. Khlopin Radium Institute, 2oi Murinskiy Prospect 28, Saint-Petersburg 194021, Russia
[2] Department of Neutron Research, Uppsala University, Box 525, 75120 Uppsala, Sweden

Abstract. New results of measurements of the angular distributions of proton-induced fission fragments of ^{182,183,184,186}W in the proton energy region 50–180 MeV are presented. The results are discussed together with earlier data, obtained for subactinide nuclei ^{204,206,207,208}Pb and ^{209}Bi and actinide nuclei ^{232}Th and ^{233,235,238}U, for both proton- and neutron-induced fission. Similarity is noted of values and energy dependences of angular anisotropy of fission induced by protons and neutrons (taking into account a trivial effect of Coulomb factor) as well as influence on the anisotropy value of the emission character of fission of actinide nuclei and its connection with parameter of fissionability Z^2/A.

1 Introduction

Studies of fission fragment angular anisotropies is a way to determine the state of a fissioning nucleus at the saddle point – shape, angular momentum and temperature. For the understanding of dynamics of fission process the knowledge of these key characteristics is necessary in wide range of fissioning nuclei, their excitation energies and angular momenta. With this goal, in framework of ISTC projects measurements have carried out of the angular anisotropies in neutron-induced fission of ^{232}Th and ^{238}U in the 20–160 MeV energy region and ^{209}Bi at 75 MeV [1], and in proton-induced fission of ^{204,206,207,208}Pb and ^{209}Bi in the 50–180 MeV energy region [2]. The results have been analyzed together with compiled data on angular anisotropies in proton-induced fission of ^{232}Th and ^{233,235,238}U [3] and subactinides [4]. Analysis of the experimental data for actinides have shown that the value of the anisotropy depends on ratio of neutron and fission widths, Γ_n/Γ_f, of fissioning nuclei which determine the multi-chance structure of fission of these nuclei (its dependence on the fissionability of nucleus).

In the present work new results of measurements of the angular distributions of proton-induced fission fragments of ^{182,183,184,186}W in the energy range 50–180 MeV are presented and compared with compiled data for adjacent nuclei, ^{185}Re and ^{181}Ta, and for subactinides in lead-bismuth region. The discussion is carried out in frame of the standard statistical (transition state) model taking into account the characteristics of the intermediate compound nuclei formed in process of interaction of nucleons with target nuclei.

2 Experimental results

Fission fragment angular distributions for intermediate energy proton-induced fission of ^{182,183,184,186}W have been measured at the proton beam of the Gustaf Verner cyclotron of the The Svedberg Laboratory of the Uppsala University, Sweden. The measurements were carried out using a vacuum chamber with thin-film breakdown counters (TFBC) for fission fragment detection placed in the angular ranges of about 0°–90° and 90°–180° relatively to the proton beam direction. The targets were prepared from enriched mixtures of tungsten isotopes ^{182}W (99.1%), ^{183}W (99.8%), ^{184}W (99.2%) and ^{186}W (99.9%) in the WO_3 chemical form. The target layer thicknesses were about 2 mg/cm^2. Measurements were carried out at proton energies 49.5, 137.4 and 177.3 MeV. Experimental angular distributions obtained were fitted by computer code based on standard kinematics expressions for nuclear reactions as well as parameters of fission targets, mass and energy distributions of fission fragments and detection properties of the TFBC.

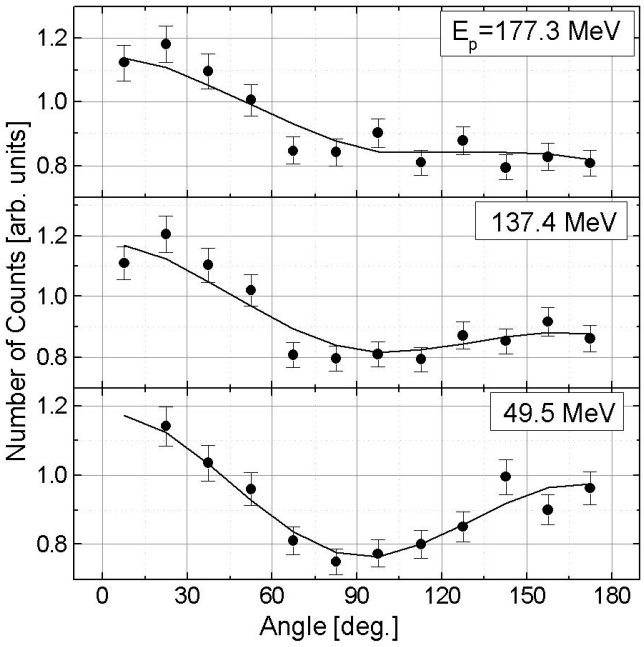

Fig. 1. Angular distributions of the ^{184}W fission fragments at the proton energies 49.5, 137.4, and 177.3 MeV in the laboratory frame. Curves are the model calculations.

[a] Presenting author, e-mail: 105@atom.nw.ru

Table 1. Anisotropy factor for proton-induced fission fragments.

Isotope	Proton energy, MeV		
	49.5 ± 0.1	137.4 ± 1.0	177.3 ± 1.2
^{186}W	0.30 ± 0.06	0.25 ± 0.05	0.14 ± 0.05
^{184}W	0.40 ± 0.06	0.25 ± 0.07	0.14 ± 0.05
^{183}W	0.40 ± 0.06	-	0.14 ± 0.03
^{182}W	0.40 ± 0.06	0.25 ± 0.12	0.14 ± 0.03

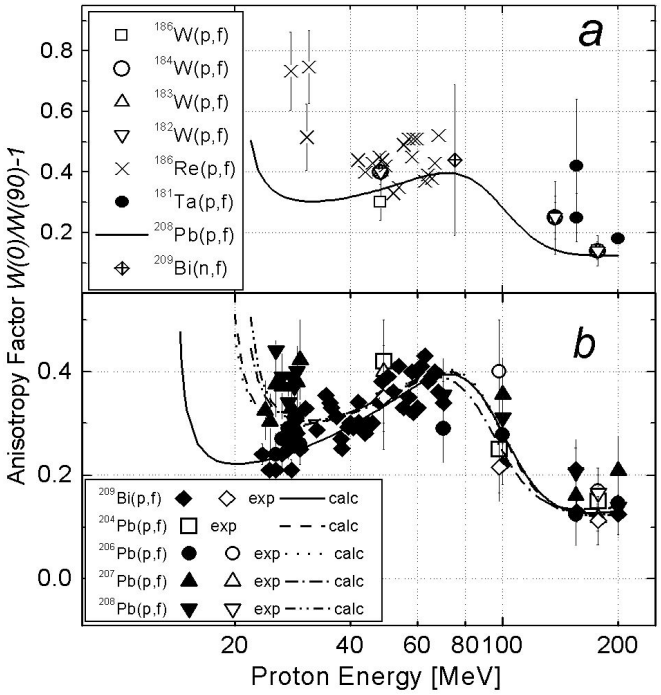

Fig. 2. Energy dependence of the anisotropy factor for proton-induced fission.

The experimental setup, measurement conditions and procedure of process of experimental results are described in details in our reports [2,5].

In figure 1 the experimental angular distributions of the ^{184}W fission fragments in the laboratory frame are presented for three energies of incident protons. The anisotropy factors, C = W'(0°)/W'(90°)-1, for ^{182,183,184,186}W are given in table 1 and shown in figure 2a together with compiled data for adjacent nuclei, ^{185}Re and ^{181}Ta [6].

3 Angular anisotropy for subactinides

In our previous study [4] we have performed semi-empirical analysis of energy dependence of angular anisotropy for subactinide nuclei in the lead-bismuth region. Experimental data on proton-induced fission for separated lead isotopes and bismuth were taken from compilation [6] and supplemented by our measurements [2]. The analysis has been carried out in the frame of transition state model [7], where the anisotropy factor C is merely connected with the mean square of the angular momentum of a nucleus at the saddle point, $\langle I^2\rangle$, and the dispersion of the momentum projection on the axis of fissioning nucleus, K_o^2: $C = \langle I^2\rangle/K_0^2$, where $K_o^2 = (I/\hbar^2)J_{eff}T$, where J_{eff} is the effective moment of inertia, and T is the temperature of a nucleus in this state. Because of complexity of quantitative consideration of cascade and pre-equilibrium particle emission resulting in formation of a broad set of residual nuclei, for subacinide region we applied an "integral" description where $\langle I^2\rangle$ and $\tilde{E}_0^2$ are averaged over the states of fissioning nuclei. The results of these calculations are summarized in figure 2b.

It is seen from figure 2 that experimental data sets for lead-bismuth and tungsten regions are very similar. In particular, despite of considerable widening of range of average parameter Z^2/A of composite system (incident particle + target nucleus) relatively to ref. [4] – from 33.60 (for ^{209}Bi+p) and 32.96 (for ^{208}Pb+p) to 30.08 (for ^{186}W+p) – the maximal values of the anisotropy factor practically did not change. This testifies about independence $K_o^2 \sim J_{eff}T$, and probably I (as far as approximate constancy of J_{eff} for these nuclei is predicted by liquid drop model [8]) on Z^2/A for subactinide nuclei having weak fissionability and accordingly low probability of emission fission. Thus the calculated energy dependences of the anisotropy factors for lead isotopes can be used for all tungsten isotopes. In figure 2a the curve calculated for ^{208}Pb is used as for nucleus with closest fission barrier. It is seen from figure 2 that the calculated curve satisfactorily describe experimental results.

Measurements of angular anisotropy in neutron-induced fission in intermediate energy region have been started in ref. [1]. One of the first results was measurement of angular distribution of fission fragments and anisotropy factor for the ^{209}Bi(n,f) reaction at neutron energy 75 MeV using a Frish gridded ionization chamber [9].

A physical base for comparison of data obtained at neutrons and protons can be found in hypothesis of quasi-compound nucleus formed in interaction of heavy nuclei with intermediate energy particles [10]. The "compound nucleus" effect is manifested in similarity of number of observed characteristics for composite systems with the same charge Z, mass A and excitation energy E^*, independently on incident particle (proton or neutron), but taking into account trivial factor of Coulomb barrier for protons. This effect, probably, reflects closeness of parameters of interim compound nuclei formed as a result of intra-nuclear cascade and preliminary emission. For two reactions ^{208}Pb+p and ^{209}Bi+n the average values $\langle Z\rangle$, $\langle A\rangle$ and $\langle E^*\rangle$, versus the incident nucleon energy as well as the shapes of their distributions for three values of the projectile energy are shown in figure 3. The data are extracted from calculations by CEM03.01 event generator [11]. Similarity of average values of the above mentioned parameters have been established earlier in ref. [12] as results of calculations by the TALYS code [13].

In case of angular anisotropy account of Coulomb barrier results in change of introduced angular momentum, thus it appears that $C_n = (E/(E-V))C_p$. Experimental value of C_n for ^{209}Bi(n,f) – 0.52 ± 0.20 corrected to this factor is compared with C_p for the ^{208}Pb(p,f) in figure 2a. It is seen that the values do not contradict each other although they have large uncertainties.

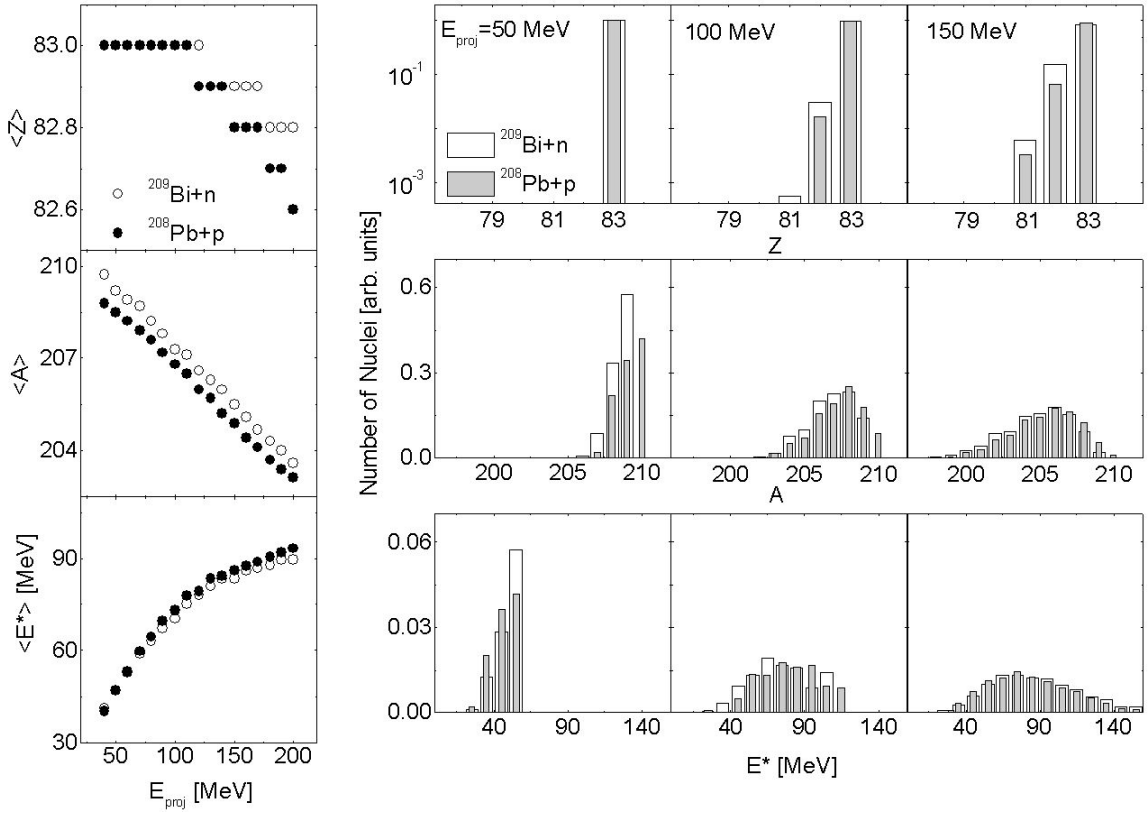

Fig. 3. Average charge, mass and excitation energy and their distributions vs projectile energy for reactions ^{209}Bi+n and ^{208}Pb+p calculated by the code CEM03.

4 Angular anisotropy for actinides

Measurements of angular anisotropies for neutron-induced fission of ^{232}Th and ^{238}U in the neutron energy region 20–160 MeV [1,14] have contributed in more detailed comparison of values and energy dependences of the anisotropy for protons and neutrons as well as in determination of physical factors affecting the anisotropy for actinide nuclei. In ref. [3] all compiled experimental data on angular anisotropies for proton-induced fission of ^{232}Th, ^{238}U, ^{233}U and ^{235}U have been analyzed. The best agreement of calculated in frame of transition state model (like for subactinide nuclei) and experimental values of anisotropy factors has been obtained for excitation energy at a saddle point for ^{238}U approximately to about 8 MeV more than for ^{232}Th that has been connected with difference in fissionability for these nuclei.

The dependence of anisotropy on the fissility parameter Z^2/A in fission induced by low-energy neutrons but at energies higher than the threshold of the emission fission was discussed in refs. [15,16]. It is interesting that parameter Z^2/A of the composite systems plays the same role at higher energies when the mechanism of the reaction becomes more complex and the excitation energy of fissioning nuclei becomes higher. It has been assumed that, as in the case of subactinide nuclei, the anisotropy factor for actinides in neutron-induced fission can be calculated using the anisotropy factor for the same energy protons and the composite system with the same parameter Z^2/A, taking into account the difference of introduced momenta: $Cn = (E/(E - V))Cp$. In our case the energy dependence of anisotropy for the reaction ^{238}U + n(Z^2/A = $92^2/239$ = 35.41) was calculated using the reaction ^{232}Th + p(Z^2/A = $91^2/233$ = 35.54). The positive result of this approach for converting data for protons to neutron ones has made it possible to apply the reverse procedure to the case of the ^{232}Th(n,f) reaction and thus to obtain the data on the anisotropy for the hypothetical case of proton fission of the composite nucleus with Z^2/A = 34.76. Thus the use of neutron data allowed to expanding the analyzed range of fissilities.

Data on anisotropy factors for 40 MeV proton-induced fission (including converted from data on neutron-induced ones) and all known data on anisotropy of fission induced by deuterons and alpha-particles have been compared with data on ratio of neutron and fission widths, Γ_n/Γ_f (determining fissionability of nuclei $P_f = (1 + \Gamma_n/\Gamma_f)^{-1}$ in the range of parameter of fissionability Z^2/A about $35 \div 38$ (see fig. 4). It has been concluded that similarity of behavior of the anisotropy and the probability of neutron emission before the saddle point which is determined by Γ_n/Γ_f shows that the temperature at the saddle point remains to be an important factor influencing the anisotropy of fission heavy nuclei induced by intermediate energy nucleons as at low energies.

5 Conclusion

Experimental studies of angular anisotropies of intermediate energy nucleon-induced fission in the wide range of parameter

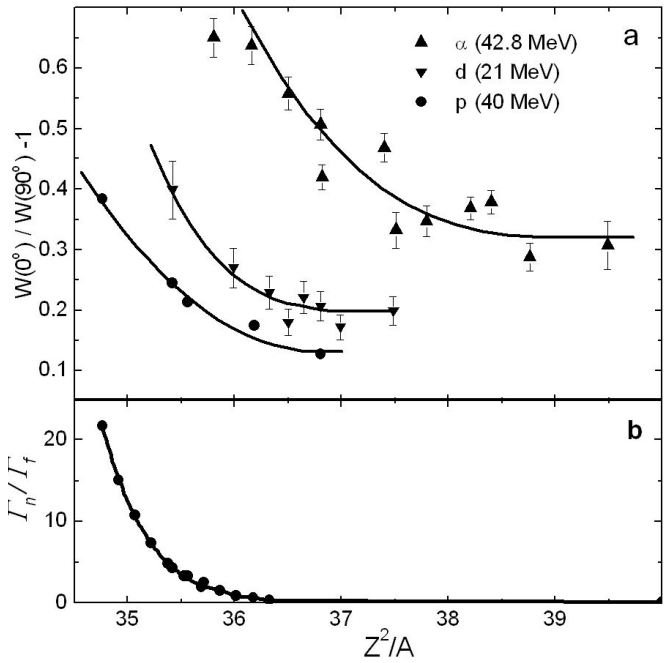

Fig. 4. The dependence of anisotropy coefficient for fission induced by p, d and α-particles (the experimental data on d and α-particles are from the ref. [17], the curves are ours) on composite nucleus fissility parameter (a), the dependence of the ratio of neutron and fission widths at $E^* \approx 10$ MeV on composite nucleus fissility parameter (b).

of fissionability of nuclei has shown a major similarity of values and energy dependencies of the anisotropy for protons and neutrons. Observed difference in the projectile energy region below 50–60 MeV is connected with effect of Coulomb factor diminishing the angular momentum introduced by protons and reducing the anisotropy factor. It reflects the effect of "compound nucleus" being manifested in similarity of characteristics of fission reaction for composite systems of equal nucleon composition and excitation energy. Such similarity is seen from calculations of parameters of interim compound nuclei carried out in frame of modern model codes CEM03 and TALYS. At the same time a significant difference takes place between actinides and subactinides in dependence of the anisotropy of fission by both charged particles and neutrons on parameter Z^2/A. The value of the anisotropy coefficient for subactinides practically does not depend on this parameter, while for actinides it drops strongly with the parameter increase. It is connected with strong dependence of fissionability on Z^2/A resulting in difference of excitation energies in saddle point, determining the value of anisotropy in transition state model.

The authors are thankful to Dr A.V. Prokofiev for active participation in the experimental part of the study and Dr S.G. Mashnik for providing model calculation by the CEM03.01 code. This work was performed in framework of the ISTC project 2213.

References

1. V.P. Eismont (Project Manager), Final Project Technical Report of ISTC 540-97, V.G. Khlopin Radium Institute, St.-Petersburg, 1999.
2. V.P. Eismont (Project Manager), Final Project Technical Report of ISTC 1309-99, V.G. Khlopin Radium Institute, St.-Petersburg, 2002.
3. V.P. Eismont et al., J. Nucl. Sci. Technol., Suppl. 2, 299 (2002).
4. V.P. Eismont et al., in *Proc. Int. Conf. on Nuclear Data for Science and Technology*, *Santa Fe, NM*, *Sept. 26–Oct. 1, 2004*, AIP Conf. Proc. **769** (2005), p. 633.
5. V.P. Eismont (Project Manager), Final Project Technical Report of ISTC 2213-03, V.G. Khlopin Radium Institute, St.-Petersburg, 2006.
6. A. I. Obukhov, Phys. Part. Nuclei **32**, 162 (2001).
7. H. Halpern, V.M. Strutinskiy, *Proc. of the Second United Nations Int. Conf. on Peaceful Uses of Atomic Energy*, *Geneva*, *Switzerland, 1958* (United Nations, Geneva, Switzerland, 1958), p. 408; R. Vandenbosch, R. Huizenga, *Nuclear Fission* (Academic Press, New York, 1973).
8. V.M. Strutinskiy, Sov. J. Nucl. Phys. **1**, 821 (1965) (in Russian).
9. V.P. Eismont et al., in *Proc. Int. Conf. on Nuclear Data for Science and Technology*, *May 19-24, 1997, Trieste, Italy*, p. 658
10. A.N. Smirnov et al. (these proceedings).
11. S.G. Mashnik et al., LANL Report LA-UR-05-2686, Los Alamos, 2005; E-prints: nucl-th/0502019; nucl-th/0503061.
12. A.N. Smirnov et al., in *Proc. Int. Conf. on Nuclear Data for Science and Technology, Santa Fe, NM*, *Sept. 26–Oct. 1, 2004*, AIP Conf. Proc. **769** (2005), p. 780.
13. A.J. Koning et al., in *Proc. Int. Conf. on Nuclear Data for Science and Technology, Santa Fe, NM*, *Sept. 26 – Oct. 1, 2004*, AIP Conf. Proc. **769** (2005), p. 1154.
14. G.A. Tutin et al., Nucl. Instrum. Meth. Phys. Res. A **457**, 646 (2001).
15. R.L. Henkel, J.E. Brolley, Phys. Rev. **103**, 1292 (1956).
16. A.N. Protopopov, V.P. Eismont, JETP **34**, 250 (1958) (in Russian).
17. T. Datta et al., Z. Phys. A **351**, 305 (1995).

International Conference on Nuclear Data for Science and Technology 2007
DOI: 10.1051/ndata:07749

Nucleon-induced fission cross sections of tantalum and separated tungsten isotopes and "compound nucleus" effect in intermediate energy region

A.N. Smirnov[1,a], O.I. Batenkov[1], V.P. Eismont[1], N.P. Filatov[1], J. Blomgren[2], H. Condé[2], A.V. Prokofiev[3], and S.G. Mashnik[4]

[1] V.G. Khlopin Radium Institute, 2-nd Murinskiy prospect 28, Saint-Petersburg 194021, Russia
[2] Department of Neutron Research, Uppsala University, Box 525, 751 20 Uppsala, Sweden
[3] The Svedberg Laboratory, Uppsala University, Box 533, 751 21 Uppsala, Sweden
[4] Los Alamos National Laboratory, Los Alamos, NM 87545, USA

Abstract. Neutron- and proton-induced fission cross sections of separated isotopes of tungsten (^{182}W, ^{183}W,^{184}W, and ^{186}W) and ^{181}Ta relative to ^{209}Bi have been measured in the incident nucleon energy region 50–200 MeV using fission chambers based on thin-film breakdown counters (TFBC) using quasi-monoenergetic neutrons from the ^{7}Li(p,n) reaction and at the proton beams of The Svedberg Laboratory (TSL), Uppsala University (Uppsala, Sweden). The results are compared with predictions by the CEM03.01 event generator, as well as with the recent data for nuclei in the lead-bismuth region. The effect of "compound nucleus" in the intermediate energy region is discussed, displaying in exponential dependence of nucleon-induced fission cross sections on the parameter Z^2/A of the composite system (projectile+target nucleus), and in other characteristics of the fission process for which parameter Z^2/A plays a role similar to the one of the usual liquid-drop parameter Z^2/A of compound nuclei.

1 Introduction

Fission cross sections of W (isotope ^{184}W) in the energy region up to the 200 MeV was included in the High Priority Request List [1] due to its importance for development of ADS and nuclear reaction models. Recently, evaluated cross section data libraries have been created at LANL for all stable tungsten isotopes up to 150 MeV [2]. However, there are no evaluated data sets for fission cross sections. The experimental database up to now consisted only of data for ^{nat}W(n,f) cross sections in the energy range 50–200 MeV [3,4] and ^{nat}W(p,f) one at 190 MeV [5].

Our preliminary results on fission cross sections for separated tungsten isotopes have already been published in ref. [6] together with calculation by CEM03.01 generator [7]. In this work the final experimental data are presented. In addition, they are supplemented by our recent results for ^{181}Ta. The results are analyzed in comparison with the (n,f) and (p,f) cross sections data for bismuth and separated isotopes of lead in the 50–200 MeV energy range.

General regularities are discussed in some characteristics of the fission process in the intermediate energy region for which the parameter Z^2/A of the composite system (incident nucleon + target nucleus) plays a role similar to the one of the usual liquid-drop parameter Z^2/A of compound nuclei.

2 Experimental results

The measurements have been carried out at the upgraded neutron beam facility [8] and at the broad proton beam facility [9] of the TSL. Similar to our previous work [10], the same fission chambers based on thin-film breakdown counters (TFBC) were used at both neutron and proton fluxes. Fissile targets were made from separated isotopes of tungsten in the WO_3 chemical form by means of vacuum evaporation onto aluminum backings. The thicknesses of the deposited layers, about 2 mg/cm^2, have been defined by direct weighting and by method of Rutherford backscattering of α-particles [11]. The measurements of relative counting rates of fission events induced by neutrons were carried out for all separated tungsten isotopes simultaneously. Measurements in wide proton beam were carried out simultaneously for two or three target sets only (depending on proton energy) while one of them was used as a relative monitor of the proton flux. The total statistical uncertainties of the relative results depend on the projectile energy and amount to not more than 10% for the neutron measurements. For proton measurements, they vary from 5–10% above 90 MeV to 15–25% below 60 MeV. In the data reduction process, the corrections were introduced, connected with:

- the TFBC detection efficiency, taking into account of properties of fission fragments,
- the shape of the neutron spectrum (for the neutron part of the measurements),
- the background of fission events due to the presence of heavy fissile admixtures in the aluminum backings.

The main aspects of the data processing have been described in details in refs. [3,12]. Absolute (n,f) and (p,f) cross sections for separated isotopes of tungsten (^{182,183,184,186}W) and ^{181}Ta have been obtained by multiplication of the measured cross section ratios to parameterized ^{209}Bi(n,f) [3] and ^{209}Bi(p,f) [10] cross section, respectively. In view of their practical importance, we present also the (n,f) and (p,f) cross section data for ^{nat}W obtained both by direct measurements using the ^{nat}W samples and calculations on a basis of results for separated isotopes taking into account their contributions in the natural element. The results are presented in tables 1

[a] Presenting author, e-mail: smirnov@atom.nw.ru

Table 1. Neutron-induced fission cross sections.

E_n MeV	^{182}W mb	^{183}W mb	^{184}W mb	^{186}W mb	^{nat}W exp. mb	^{nat}W calc. mb
46.6±1.0	≤ 0.003		≤ 0.006	≤ 0.0016	<0.0040	
65.1±1.7	0.035±0.004	0.027±0.003	0.021±0.002	0.009±0.001	0.020±0.010	0.020±0.002
74.1±1.4	0.071±0.009	0.065±0.008	0.039±0.005	0.023±0.007	0.042±0.009	0.046±0.007
94.6±1.2	0.26±0.03	0.19±0.02	0.14±0.02	0.071±0.008	0.14±0.02	0.16±0.02
142.5±3.1	1.0±0.1	0.64±0.09	0.62±0.08	0.33±0.05	0.56±0.08	0.64±0.09
172.4±3.0	1.4±0.2	1.16±0.13	1.0±0.1	0.48±0.06	1.04±0.15	0.96±0.11

Table 2. Proton-induced fission cross sections.

E_p MeV	^{182}W mb	^{183}W mb	^{184}W mb	^{186}W mb	^{181}Ta mb	^{nat}W exp. mb	^{nat}W calc. mb
40.4±0.2	0.0048±0.0007	0.0045±0.0007	0.0041±0.0006	0.0026±0.0004	–	–	0.0039±0.0006
43.5±0.9	0.011±0.002	0.0104±0.0017	0.0087±0.0014	0.0045±0.0008	–	–	0.008±0.001
59.2±1.0	0.09±0.02	0.07±0.01	0.039±0.007	0.024±0.005	–	0.050±0.006	0.054±0.006
64±1.0	–	–	–	–	0.039±0.017	–	–
93.2±1.0	1.24±0.17	0.88±0.12	0.62±0.09	0.34±0.04	0.36±0.07	0.71±0.10	0.74±0.10
130.5±1.0	2.93±0.35	2.2±0.3	1.8±0.2	0.98±0.12	0.94±0.18	1.98±0.23	1.92±0.23
166±1.0	–	–	–	–	1.53±0.23	–	–
169.6±1.0	4.85±0.58	3.9±0.5	3.2±0.4	2.0±0.2	1.91±0.28	3.5±0.4	3.4±0.4

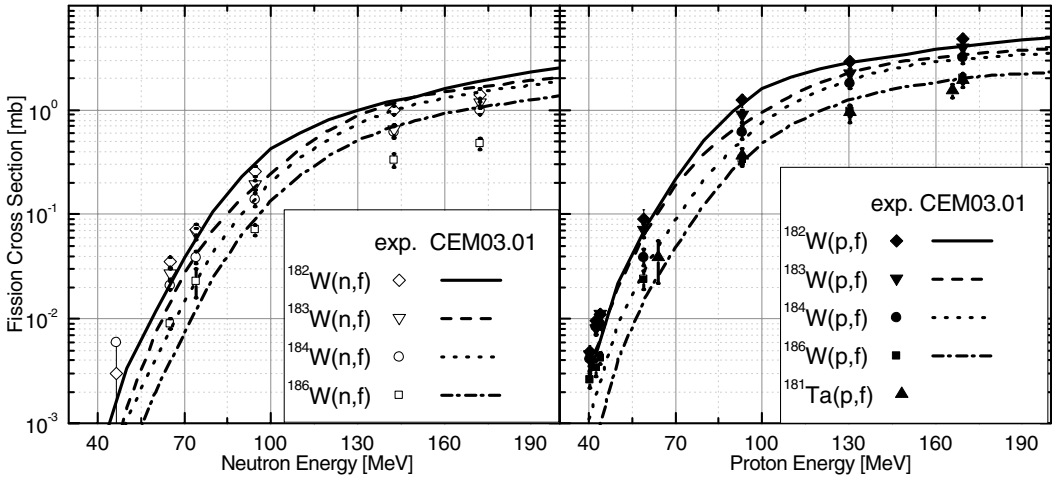

Fig. 1. The (n,f) and (p,f) cross sections of ^{182}W, ^{183}W, ^{184}W, ^{186}W and ^{181}Ta(p,f) versus incident nucleon energy. Symbols are experimental results of the present work, and curves are results of calculations by the CEM03.01 event generator.

and 2 and are shown in figure 1 (only for tungsten isotopes and Ta).

In figure 1 the experimental data are compared with the results of updated calculations for tungsten isotopes by the CEM03.01 event generator [7]. It is seen that the calculations agree satisfactory with the (p,f) data, while problems are seen in description of the (n,f) data. At present this is an open question of CEM03.01 still to be solved.

3 Isotopic dependence of the cross sections

A low contribution of the shell correction (~1 MeV) to the fission barrier (~30 MeV) and a large deformation ($\beta \approx 0.25$) for the tungsten isotopes distinguish them significantly from the lead isotopes studied earlier. The latter are of spherical shape and have the largest microscopic contribution to the barrier of all nuclei (~15 MeV). Thus, the tungsten isotopes can be considered as representatives of the typical liquid-drop fission.

It is seen from the figure 1 that the values of the (n,f) and (p,f) cross sections increase with decrease of the isotope mass number and with the energy of incident particles increase. On the other hand, the cross section ratios for tungsten isotopes to one of them become approximately constant with the incident nucleon energy increase. The values of these ratios were used for estimation of the difference in the fission barriers for neighbouring isotopes: $B_f(A-1) - B_f(A)$. Using the same approach which we applied in ref. [13] for lead isotopes, we have obtained the following values: ≈0.55 MeV for neutrons and ≈0.50 MeV for protons. These differences are close to those obtained for the lead isotopes (0.38 MeV for neutrons

and ≈0.30 MeV for protons) in ref. [13] and seem to be too large for liquid-drop fission. At present it is hard to make a conclusion whether this fact is a result of coarseness of the present suppositions (simplified relation for fission cross section, averaging on wide spectrum of fissioning nuclei) or it has a physical sense. More detailed calculations are necessary.

4 Comparison of the (p,f) and (n,f) cross sections

The dependence of the (p,f)/(n,f) cross section ratio on the parameter Z^2/A of a target nuclei was first studied in ref. [14] for a range of nuclei from Ta to Np. It has been observed that the σ_{pf}/σ_{nf} ratio depends strongly on the incident nucleon energy in the low-energy region (20–70 MeV) and then approaches a plateau slowly. In figure 2, up-to-date results for the incident nucleon energy of about 180 MeV are shown. It is seen that the σ_{pf}/σ_{nf} ratio increases with the Z^2/A parameter decrease. However, it is also seen that the dependency is not monotonous, but it has a "hollow" in transition from the lead isotopes group to the tungsten one. This effect has been predicted earlier in ref. [15] and was ascribed to connection of the fission cross section ratio with a value of the fission barrier. The fission barrier changes weakly for heavy actinide nuclei, increases rapidly in the region of lighter nuclei and reaches a maximum value for ^{208}Pb due to large value of the shell correction to the liquid-drop barrier. Since the shell correction decreases, the barrier reaches a plateau that can lead to slowing down of the σ_{pf}/σ_{nf} rise in the region of tungsten.

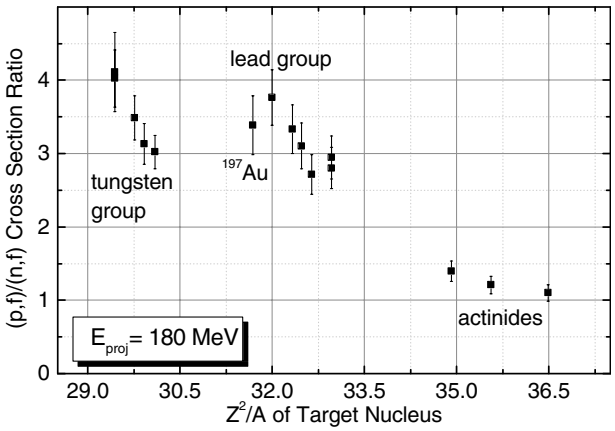

Fig. 2. The (p,f)/(n,f) cross section ratios versus parameter Z^2/A of the target nucleus.

5 Effect of "compound nucleus" in intermediate energy region.

Comparative analysis of data on (p,f) and (n,f) cross sections for ^{205}Tl, $^{204,206-208}$Pb and ^{209}Bi in the energy range up to about 180 MeV [10] and results of the present work has given an additional confirmation of a regularity we recently observed in ref. [16], which can be interpreted as an effect

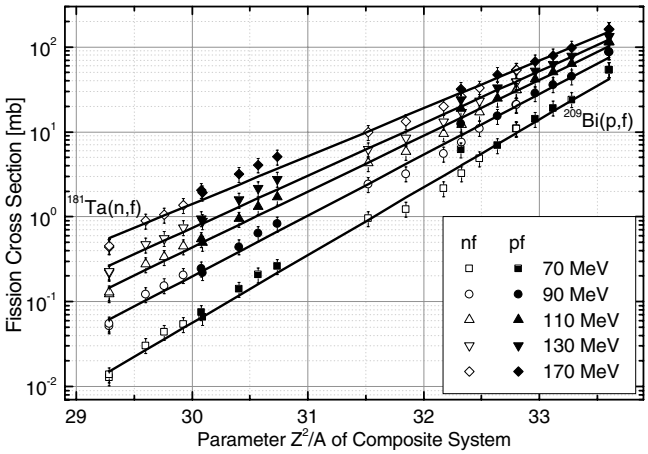

Fig. 3. The (n,f) and (p,f) cross sections versus parameter Z^2/A of the composite system for the different incident nucleon energies.

of "compound nucleus" in intermediate energy region. The regularity is an equality of fission cross sections (within experimental errors, 10–20%) in reactions of nuclei with protons and neutrons, characterizing by composite systems with the same sum charge, Z, and mass, A, at the same energy of incident particles.

In figure 3 the dependences are presented of the (n,f) and (p,f) cross sections for nuclei from ^{181}Ta to ^{209}Bi on the parameter Z^2/A of a composite system. It is seen from figure 3 an exponential character of the dependences – straight lines in semi-logarithmic scale, the slope of which is decreases with the projectile energy increase. Thus the dependency of the fission cross section values in these reactions is traced analogously to the dependence of the fission probability on the parameter $Z^2/A$of the compound nucleus:

$$P_f \sim \exp\{-[B_f(Z^2/A) - B_n]/T\},$$

where B_f and B_n are the fission barrier and neutron binding energy, respectively, and T is the temperature of an excited nucleus. Increase of the temperature, which results from increasing projectile energy, thus leads to a weakening of the dependence of the fission probability on the parameter Z^2/A.

The effect is seen in other earlier observed properties of the fission process induced by intermediate energy nucleons too. In particular, as it was already discussed in section 4, the (p,f) cross sections exceed the (n,f) ones systematically. Fission fragment angular anisotropy in intermediate energy region show a similar behaviour for proton- and neutron-induced fission [17].

Recently, measured fragment mass distributions in the fission of ^{232}Th, ^{238}U, ^{235}U and ^{237}Np, induced by protons with energies of 50 and 96 MeV, have been compared with calculations from the code TALYS [18,19] and experimental data on neutron-induced fission of ^{238}U for the neutron energy range up to 200 MeV [20]. It has been shown that the most striking characteristic of the fragment mass distribution – the ratio of symmetric and asymmetric fission fractions – in the case of neutrons is manifested in the same way as in the case of protons, i.e., at the same particle energy the fraction of symmetric fission drops with increasing number of neutrons

in the composite nucleus, N: from N = 142–143 (for ^{232}Th+p, ^{235}U+p, ^{237}Np+p) to N = 146 (^{238}U+p) and further to N = 147 (^{238}U+n). Such a result was established earlier for protons and neutrons at an energy of about 15 MeV (leading to excitation energies above the barrier, near 14 MeV) [21], when almost each interaction of a proton or neutron with the target leads to a veritable compound nucleus, the decay mode of which does not depend on the way of formation.

The above mentioned experimental manifestations of the effect of "compound nucleus", pointing to a large resemblance of the behaviour of composite systems formed at intermediate energies and real compound nuclei at low energies, can be understood in the framework of the modern model codes. As a result of the first stage of the interaction of intermediate-energy nucleons with a nucleus (i.e., a cascade, followed by pre-equilibrium nucleon emission), a variety of nuclei is created, with different charges, masses and excitation energies, $W(Z_i, A_i, E_i^*)$. These nuclei reach thermal equilibrium, (i.e., compound nucleus formation), and finally undergo fission, thus contributing to the observed characteristics of fission. Calculations for the two reactions ^{208}Pb+p and ^{209}Bi+n performed in frame of the codes TALYS [16] and CEM03.01 [17] show that the average values $\langle Z \rangle$, $\langle A \rangle$, and $\langle E^* \rangle$, versus the incident nucleon energy as well as the shapes of their distributions are very close to each other.

This work was performed in framework of the ISTC project 2213 and partially supported by US DOE.

References

1. A.J. Koning et al., Nucl. Instrum. Meth. Phys. Res. A **414**, 49 (1998).
2. M.B. Chadwick et al., Report LA-UR-98-1825 (1998); Nucl. Sci. Eng. **131**, 293 (1999).
3. A.N. Smirnov et al., Phys. Rev. C **70**, 054603 (2004).
4. A.B. Laptev et al., in *Proc. International Conf. on Nuclear Data for Sci. Technol.*, *Santa Fe, 2004*, AIP Conf. Proc. **769** (2005), p. 865.
5. M.C. Duijvestijn et al., Phys. Rev. C **59**, 776 (1999).
6. A.N. Smirnov et al., LANL Report LA-UR-05-3757 (2005).
7. S.G. Mashnik et al., LANL Report LA-UR-05-7321; E-print: nucl-th/0503061; J. Phys. Conf. Series **41**, 340 (2006).
8. S. Pomp et al., in. *Proc. International Conf. on Nuclear Data for Sci. Technol.*, *Santa Fe, 2004*, AIP Conf. Proc. **769** (2005), p. 780.
9. O. Jonsson et al., *TSL Progress Report 1998–1999*, edited by A. Ingemarsson, Uppsala University (2000), p. 43.
10. V.P. Eismont (Project Manager), *Final Project Technical Report of ISTC 1309–99*, V.G. Khlopin Radium Institute, St.-Petersburg, 2002.
11. S.M. Soloviev, Nucl. Instrum. Meth. Phys. Res. A **397** (1997), p. 159.
12. V.P. Eismont (Project Manager), *Final Project Technical Report of ISTC 2213-03*, V.G. Khlopin Radium Institute, St.-Petersburg, 2006.
13. V.P. Eismont et al., in. *Proc. International Conf. on Nuclear Data for Sci. Technol*., *Santa Fe, 2004*, AIP Conf. Proc. **769** (2005), p. 629.
14. V.P. Eismont et al., in *Proc. 2nd Conf. on ADTT*, *Kalmar, Sweden, June 3-7, 1996*, pp. 592–598.
15. V.P. Eismont et al., J. Nucl. Sci. Technol., Suppl. 2, 238 (2002).
16. A.N. Smirnov et al., in. *Proc. International Conf. on Nuclear Data for Sci. Technol.*, *Santa Fe, 2004*, AIP Conf. Proc. **769** (2005), p. 633.
17. V.P. Eismont et al. (these proceedings).
18. O.I. Batenkov et al., in *Proc. International Conf. on Nuclear Data for Sci. Technol.*, *Santa Fe, 2004*, AIP Conf. Proc. **769** (2005), p. 625.
19. M.C. Duijvestijn et al., Phys. Rev. C **64**, 014607 (2001).
20. C.M. Zoller, Ph.D. thesis, University of Darmstadt, 1995.
21. T. Ohtsuki et al., Phys. Rev. C **44**, 1405 (1991).

International Conference on Nuclear Data for Science and Technology 2007
DOI: 10.1051/ndata:07759

Studies of neutron-induced light-ion production with the MEDLEY facility

U. Tippawan[1,2], S. Pomp[2], P. Andersson[2], G. Ban[5], R. Bevilacqua[2], V. Blideanu[5], J. Blomgren[2], Ph. Eudes[6], Y. Foucher[6], A. Guertin[6], F. Haddad[6], M. Hayashi[2,3], C. Lebrun[5], F.R. Lecolley[5], J.F. Lecolley[5], T. Lefort[5], L. Nilsson[2], N. Marie[5], A. Öhrn[2], M. Österlund[2], A. Prokofiev[4], V. Simutkin[2], I. Slypen[7], P.A. Söderström[2], and Y. Watanabe[3]

[1] Fast Neutron Research Facility, Chiang Mai University, P.O. Box 217, 50200 Chiang Mai, Thailand
[2] Department of Neutron Research, Uppsala University, Box 525, 75120 Uppsala, Sweden
[3] Department of Advanced Energy Engineering Science, Kyushu University, Japan
[4] The Svedberg Laboratory, Uppsala University, Box 533, 75121 Uppsala, Sweden
[5] LPC, ENSICAEN, Université de Caen, CNRS/IN2P3, Caen, France
[6] SUBATECH, Université de Nantes, CNRS/IN2P3, France
[7] Institut de Physique Nucléaire, Université Catholique de Louvain, Louvain-la-Neuve, Belgium

Abstract. The growing interest in applications involving high-energy neutrons (E > 20 MeV) demands high-quality experimental data on neutron-induced reactions. Such data have been measured with the MEDLEY setup at the The Svedberg Laboratory (TSL), Uppsala, Sweden. It has been used to measure differential cross sections for elastic nd scattering and double-differential cross sections for light-ion production (A ≤ 4) with targets ranging from C to U and at incident neutron energies around 96 MeV. We summarize the experimental results obtained so far and compared with theoretical reaction model calculations. A new method for correcting charged-particle spectra for thick target effects has been used for data obtained with the MEDLEY facility. The new quasi-monoenergetic neutron beam facility of TSL offers the possibility to extend these measurements up to neutron energies of 175 MeV. In January 2007, the neutron beam facility at TSL has been equipped with improved shielding and pre-collimator to reduce the background observed with MEDLEY during the first experimental campaigns at 175 MeV to an acceptable level. We present the current status of the MEDLEY facility after the shielding upgrade. We summarize also our ongoing projects including both measurements of light-ion production at 175 MeV from C to U targets and fission studies of U-238 in the energy region of 11 to 175 MeV.

1 Introduction

Over the past years development has been made in a wide variety of different applications involving interactions of fast neutrons (20–200 MeV) with nuclei. Examples are dosimetry at commercial aircraft altitudes and in space [1,2] and radiation treatment of cancer within the field of medicine [3], soft-error effects in computer memory within electronics [4], and energy production and transmutation of nuclear waste [5] within energy applications. For all these applications, an improved understanding of neutron interactions is needed for calculations of neutron transport and radiation effects. It should be emphasized that for these applications, it is beyond reasonable efforts to provide complete data sets. Instead, the nuclear data needed for a better understanding must come to a very large extent from nuclear scattering and reaction model calculations, which all depend heavily on nuclear models, which in turn are benchmarked by experimental nuclear reaction cross section data.

The MEDLEY facility [6], located at the The Svedberg Laboratory (TSL) in Uppsala, Sweden, has over the past years performed measurements of double-differential cross sections for the production of light ions by 96 MeV neutrons [6–9]. Recently, we have started a program on measuring angular distributions of fission fragments [10]. The facility has also proven to be a valuable tool in the search for three-body force effects [11]. All these measurements have been performed at the "old" neutron beam at TSL [12]. At this beam, the neutron fluence above 100 MeV, where the cyclotron has to operate in FM mode, becomes too low to collect good statistics within reasonable time and it was therefore decided to construct a new neutron beamline with shorter distance from the neutron production point to the experimental area, thus delivering higher neutron fluxes. This new beamline is in operation since 2004 [13] and opens up the possibility to extend the experimental program and measure neutron-induced reactions at energies up to 175 MeV.

2 Light-ion production studies with MEDLEY

2.1 Experiments and typical results

During the last few years, we have performed a "complete" set of experiments in order to measure double-differential cross sections of the (n,px), (n,dx), (n,tx), (n,^{3}Hex), and (n,αx) reactions from light to heavy nuclide such as carbon, oxygen, silicon, calcium, iron, silver, holmium, lead and uranium around incident neutron energies of 96 MeV. As an illustration, some results for carbon, oxygen, silicon, iron, lead and uranium are presented in figures 1–3. More details can be found in the refs. [6–9]. Note that carbon data are preliminary and calcium, silver and holmium data are under analysis.

Examples of the double differential (n,px) spectra for carbon, oxygen, silicon, iron, lead and uranium are shown at some angles (20°, 60° and 100°) in figures 1–3. The main difference among the data is found at low energy (below

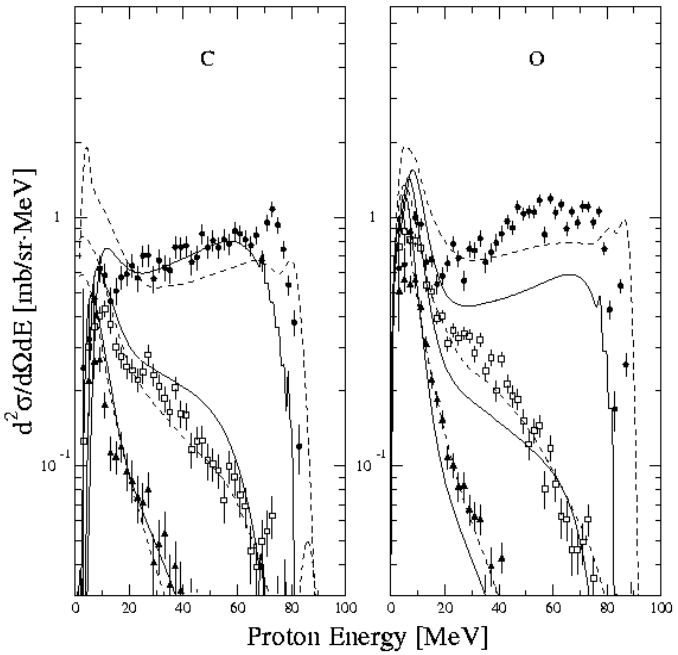

Fig. 1. Experimental double-differential cross sections of the C(n,px) and O(n,px) reactions (left and right, respectively) at 96 MeV at 20°(filled circles), 60° (open squares), and 100° (filled triangles). Solid and dashed curves represent calculations with the TALYS and GNASH codes, respectively.

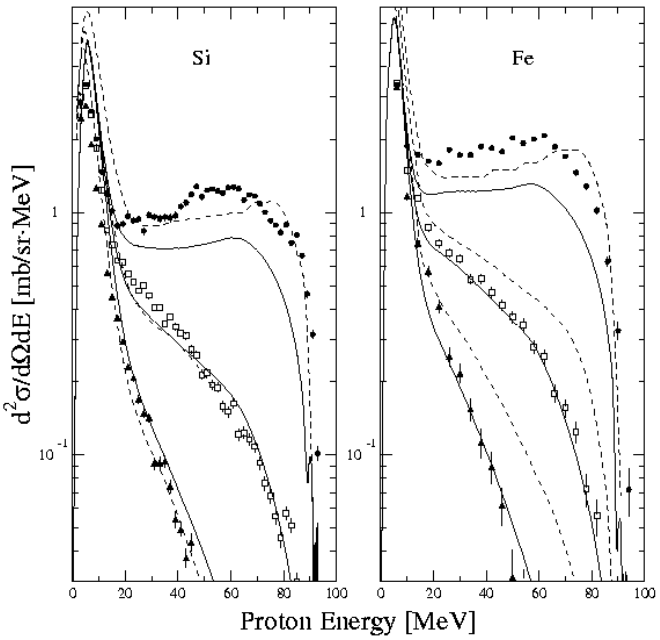

Fig. 2. Same as figure 1, but for Si(n,px) and Fe(n,px).

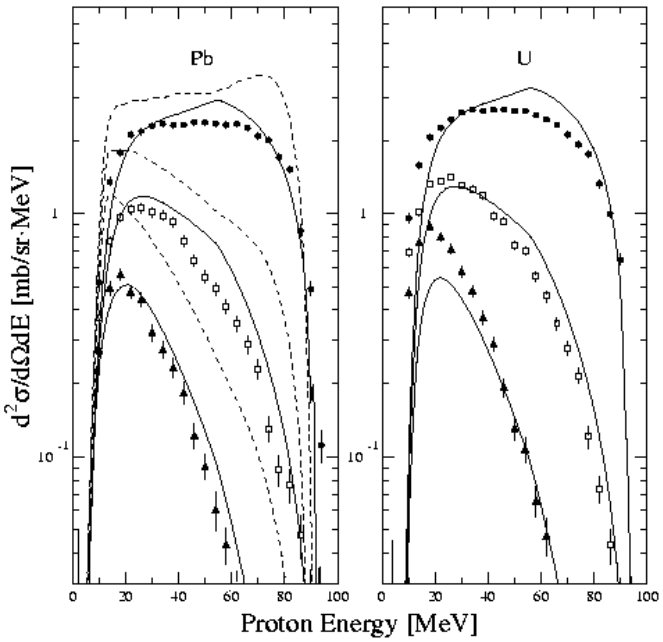

Fig. 3. Same as figure 1, but for Pb(n,px) and U(n,px).

20 MeV) where a compound component is dominant for medium-weight nuclides, i.e., silicon and iron. These low-energy particles are emitted mainly following the evaporation process of excited nuclei; for carbon and oxygen, the process is less prominent because of low level density while for lead and uranium, this emission is strongly inhibited by the Coulomb barrier. The emission of high-energy protons is strongly forward-peaked and hardly visible in the backward hemisphere. It is a sign of the preequilibrium process. The general trend of the preequilibrium emission becomes dominant with increasing mass number.

2.2 Comparison with theoretical predictions

In figures 1–3, the experimental results are presented together with model calculations. The solid lines show calculations with the TALYS code [14] whereas the dashed lines were obtained by the GNASH code [15]. Overall, both predictions give a fair description of the shape of the spectra for all nuclides. At the forward angles (20°), the GNASH predictions give a better description in the mid-energy region for the light to medium-weight nuclide. Note that there is no calculation by GNASH for uranium. The TALYS results account better for the absolute magnitude of the experimental cross sections at large angles for all nuclide while the GNASH calculations overestimate the high-energy parts of the spectra for the medium-weight and heavy nuclides.

For a detailed comparison with theoretical models, angular distributions are needed. In figures 4–5, experimental angular distributions at low, medium, and high proton energies for carbon and oxygen, respectively, are shown together with angular distributions calculated on the basis of the TALYS and GNASH models (see ref. [9] for iron, lead and uranium cases). In general, both models give a good description of the data. In the ref. [8], we have compared the experimental data with a preliminary of TALYS code. They show large discrepancies, especially at low energy regions. Using TALY code, version 0.64, we get a reasonable agreement.

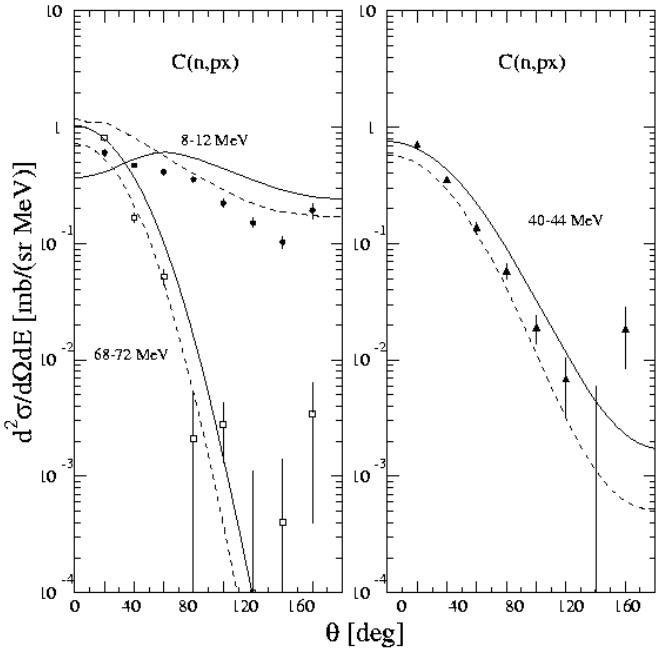

Fig. 4. Angular distributions of C(n,px) cross section at ejectile energies of 8–12 MeV (filled circles), 40–44 (filled triangles), and 68–72 (open squares). Solid and dashed curves represent calculations based on the TALYS and GNASH models, respectively.

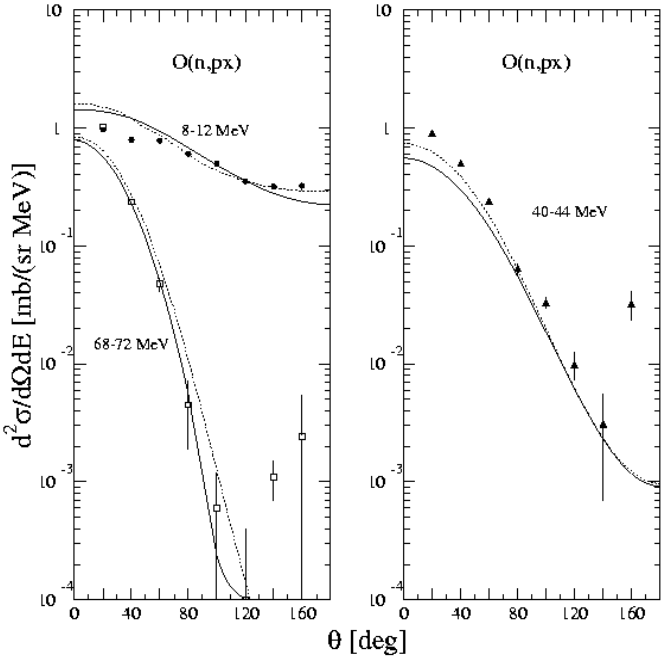

Fig. 5. Same as figure 4, but for O(n,px) cross section.

3 nd elastic scattering

Neutron-deuteron (nd) elastic scattering in the 60–200 MeV range is one of the most promising ways of investigating three-nucleon (3*N*) forces. Recent calculations, (see ref. [11] and reference therein), have indicated that the presence of 3*N* forces should appear as a measurable effect in the angular range of the differential cross section minimum.

The nd elastic scattering differential cross section has been performed at 95 MeV incident neutron energy. Models based on inclusion of 3*N* forces describe nd data in the angular region of the cross-section minimum very well, while models without 3*N* forces cannot account for the data [11] (see fig. 6).

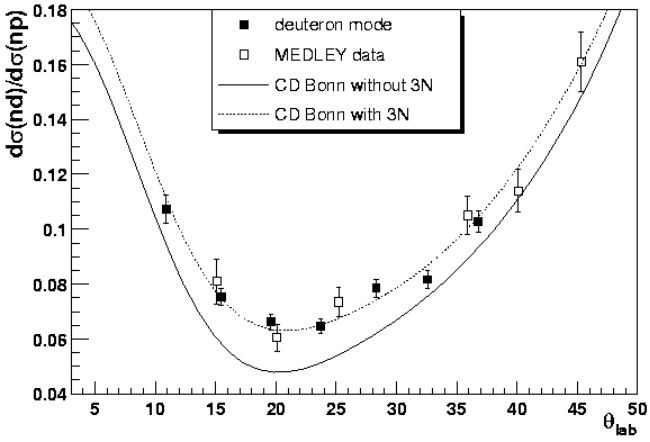

Fig. 6. Ratio of the nd and the np cross sections at 95 MeV as a function of the laboratory angle of the recoiling proton or deuteron [11]. The solid (dotted) line is a cross section calculation, based on the CD-Bonn nucleon-nucleon potential, without (with) three-nucleon effects included.

4 The MEDLEY facility

The charged particles are detected by the MEDLEY setup [6]. It consists of eight three-element telescopes mounted inside a 90 cm diameter evacuated reaction chamber. Each telescope has two fully depleted ΔE silicon surface barrier detectors and one E CsI(Tl) detector. MEDLEY has been equipped with larger CsI detectors to be able to stop protons up to 180 MeV. These new detectors have now been used during several runs and perform according to expectations. The CsI crystals have a total length of 100 mm. The first 70 mm is made cylindrical with a diameter of 50 mm and the remaining 30 mm is tapered to 18 mm diameter to match the size of the readout system. The readout is performed by Hamamatsu S3204-08 photodiodes (PD). The crystals, toghether with the PDs, are mounted inside an aluminum tube and have been manufactured by Saint-Gobain, France. The CsI response function has been tested with 170 MeV proton beam and compared with Monte Carlo simulations, which is decribed elsewhere at this conference [16].

A new method for correcting charged-particle spectra, distorted by energy and particle loss in a thick target [17], has been used for data obtained with the MEDLEY facility [7,8]. It uses an iterative procedure to obtain improved guesses on the inverse response functions for each measured particle energy. The procedure is easy to use, includes a correct treatment of cutoff energies, and has been validated by some test cases.

4.1 Background

During the first runs we have found a rather large background probably due to neutrons from the production target penetrating the concrete shielding. Exchanging the concrete wall to an iron wall has achieved improved background conditions. Available iron blocks from the old CELSIUS ring have actually been used when this reconstruction was undertaken in January 2007. The first data with the new shielding had been taken during February and March 2007. In addition, a pre-collimator, built by holed lead blocks, has been installed temporally inside the clearing magnet. It showed significant improvement of the signal-to-background ratio.

4.2 Data-taking and analysis

As mentioned above, we have collected data on ^{12}C(n,lcp) induced by 175 MeV neutrons early this year. Preliminary double-differential cross sections for carbon are presented in another contribution to this conference by M. Hayashi et al. [16].

5 Outlook

Using the MEDLEY facility at the new Uppsala neutron beam, we plan to measure double-differential cross sections for light-ion production on oxygen, silicon, iron, lead, bismuth and uranium at 175 MeV. Furthermore we will measure the ^{238}U(n,f) cross section, together with angular distributions of the fission fragments, over the energy region of 20 to 175 MeV. The proposed target nuclei are of highest interest within the applications listed above, and, in addition, of key interest for model development.

References

1. D. O'Sullivan, D. Zhou, E. Flood, *Investigation of cosmic rays and their secondaries at aircraft altitudes*, Radiat. Meas. **34**, 277 (2001).
2. T.W. Armstrong, B.L. Colborn, *Predictions of secondary neutrons and their importance to radiation effects inside the international space station*, Radiat Meas. **33**, 229 (2001).
3. D.L. Schwartz, J. Einck, J. Bellon, G.E. Laramore, *Fast Neutron Radiotherapy For Soft Tissue And Cartilaginous Sarcomas At High Risk For Local Recurrence*, Int. J. Radiat. Oncol. Biol. Phys. **50**, 449 (2001).
4. *Single-Event Upsets in Microelectronics, topical issue*, edited by H.H.K. Tang, N. Olsson, Mat. Res. Soc. Bull. 28 (2003).
5. J. Blomgren, *Experimental activities at high energies*, invited lecture at *Workshop on Nuclear Data for Science & Technology: Accelerator Driven Waste Incineration, Trieste, Italy, Sept. 10–21, 2001*.
6. S. Dangtip et al., *A facility for measurements of nuclear cross sections for fast neutron cancer therapy*, Nucl. Instrum. Meth. Phys. Res. A **452**, 484 (2000).
7. U. Tippawan et al., *Light-ion production in the interaction of 96 MeV neutrons with silicon*, Phys. Rev. C **69**, 064609 (2004) and Phys. Rev. C **73**, 039902(E) (2006).
8. U. Tippawan et al., *Light-ion production in the interaction of 96 MeV neutrons with oxygen*, Phys. Rev. C **73**, 034611 (2006).
9. V. Blideanu et al., *Nucleon-induced reactions at intermediate energies: New data at 96 MeV and theoretical status*, Phys. Rev. C **70**, 014607 (2004).
10. A. Prokofiev et al., *A new facility for high-energy neutron-induced fission studies*, *Proceedings of the International Conference on Nuclear Data for Science and Industry*, AIP Conf. Proc. **769** (Melville, New York, 2005), p. 800.
11. P. Mermod et al., *Evidence of three-body force effects in neutron-deuteron scattering at 95 MeV*, Phys. Rev. C **72**, 061002(R) (2005).
12. J. Klug et al., *SCANDAL – a facility for elastic neutron scattering studies in the 50–130 MeV range*, Nucl. Instrum. Meth. Phys. Res. A **489**, 282 (2002).
13. S. Pomp et al., *The new Uppsala neutron beam facility*, *Proceedings of the International Conference on Nuclear Data for Science and Industry*, AIP Conf. Proc. **769** (Melville, New York, 2005), 780.
14. ICRU Report 63, International Commission on Radiation Units and Measurements, Bethesda, MD, March 2000.
15. A.J. Koning, S. Hilaire, M.C. Duijvestijn, *TALYS-0.64 User Manual*, December 5, 2004, NRG Report 21297/04.62741/P FAI/AK/AK.
16. M. Hayashi et al., *Measurement of light-ion production at the new Uppsala neutron beam facility*, in *International Conference on Nuclear data for Science and Technology, 2007*.
17. S. Pomp, U. Tippawan, *An iterative procedure to obtain inverse response functions for thick-target correction of measured charged-particle spectra*, Nucl. Instrum. Meth. Phys. Res. A **572**, 893 (2007).

International Conference on Nuclear Data for Science and Technology 2007
DOI: 10.1051/ndata:07747

Measurement of light-ion production at the new Uppsala neutron beam facility

M. Hayashi[1,a], Y. Watanabe[1], R. Bevilacqua[2], J. Blomgren[2], L. Nilsson[2], A. Öhrn[2], M. Österlund[2], S. Pomp[2], A. Prokofiev[3], V. Simutkin[2], P.A. Söderström[2], and U. Tippawan[4]

[1] Department of Advanced Energy Engineering, Kyushu University, Kasuga, Fukuoka 816-8580, Japan
[2] Department of Neutron Research, Uppsala University, P.O. Box 525, 751 20 Uppsala, Sweden
[3] The Svedberg Laboratory, Uppsala University, P.O. Box 533, 751 21 Uppsala, Sweden
[4] Fast Neutron Research Facility, Chiang Mai University, P.O. Box 217, Chiang Mai 500200, Thailand

Abstract. A collaborative research project has been launched on neutron-induced light-ion production measurements using the new Uppsala neutron beam facility. The available energy range of quasi mono-energetic neutron beams is extended up to 175 MeV. Double-differential cross sections (DDXs) of light-ion production (p, d, t, ^{3}He, and α) are measured using a conventional spectrometer system which consists of eight counter telescopes. Each telescope is composed of two silicon surface barrier detectors as the ΔE detectors and a CsI(Tl) scintillator as the E detector. Response of the scintillators to 160 MeV protons is measured to test the performance. The measured response is reproduced well by a PHITS transport calculation. The DDXs of light-ion production are measured for Ca at 94 MeV and C at 175 MeV at angles between 20° to 160° in steps of 20°. The preliminary experimental (n,xp) data are shown in comparison with a model calculation using the TALYS code and the evaluated cross sections in the JENDL high-energy file.

1 Introduction

Recently, there have been increasing nuclear data needs for neutron-induced light-ion production at intermediate energies, especially 20 to 200 MeV, for a wide variety of applications, such as radiation treatment of cancer therapy, neutron dosimetry at high altitude and space, single event effects in microelectronics, and accelerator-driven transmutation of nuclear waste. To satisfy these needs, a series of experiments have successfully been performed for several targets (C, O, Si, Fe, Pb, and U) at 96 MeV using the quasi mono-energetic neutron facility at the The Svedberg Laboratory (TSL) [1–3]. Similar light-ion production measurements have been carried in the incident energy range below 100 MeV at other facilities as well [4,5]. However, there has been no systematic measurement at energies between 100 and 200 MeV until now.

The Uppsala neutron beam facility has recently been upgraded [6], so that quasi mono-energetic neutron beams are available with higher intensity than the previous one for energies up to 175 MeV. Using the new facility, systematic measurements have been planned of double-differential cross sections (DDXs) for light-ion production induced by 175 MeV neutrons. The MEDLEY spectrometer setup used in the previous experiments at 96 MeV [1,3] is partly modified by installing such a thick CsI scintillator as the E-detector that light ions generated from reactions by 175 MeV neutrons are fully stopped in the scintillator. In the present work, some preliminary measurements are performed as the feasibility demonstration. One of them is to measure the response of CsI scintillators to 160 MeV protons as the performance evaluation test, i.e., estimation of the reaction tail. The DDXs of (n,xp) reactions on Ca at 94 MeV (hereafter, measurement-I) and on C at 175 MeV (measurement-II) are measured using the MEDLEY setup. The experimental DDXs for Ca are compared with a model calculation using the TALYS code [7]. Also, a preliminary result is presented for comparison between the measured C(n,xp) spectrum at 20° and the evaluated cross sections in the JENDL high-energy file [8].

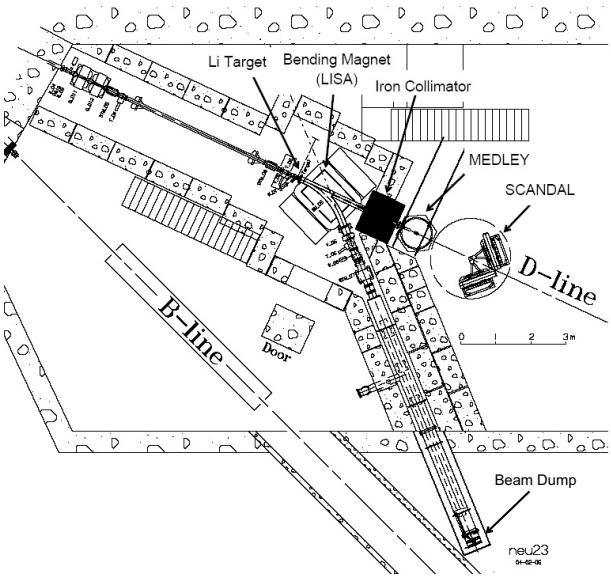

Fig. 1. New neutron beam facility at TSL and experimental setup.

2 Experimental methods

Figure 1 shows the new Uppsala neutron beam facility [6] at the TSL and the experimental setup of MEDLEY experiments [9]. Protons from the cyclotron impinge on an enriched ^{7}Li target, and neutrons are produced by the ^{7}Li(p,n)^{7}Be

[a] Corresponding author, e-mail: teru@aees.kyushu-u.ac.jp

reaction. In measurement-I, the 98.5 MeV protons produces neutrons with a peak energy of 94 MeV using a lithium target 8 mm thick, while the 180 MeV protons produces neutrons with a peak energy of 175 MeV using a 23.5 mm thick target in measurement-II. The neutrons are transported to the MEDLEY chamber passing through a 100-cm long and conical iron collimator whose diameter is 54 mm at the end of collimator. The neutron flux was about 3.1×10^5 n/(cm^{2}s) with a proton beam intensity of 3.4 μA in measurement-I, while it was about 4.3×10^4 n/(cm^2 s) with a proton beam intensity of 0.3 μA in measurement-II. The proton beam passing through the Li target is deflected by a bending magnet into the beam dump and integrated in a Faraday cap in order to monitor the beam current. In addition, a pre-collimator made out of lead blocks was installed temporarily inside the bending magnet to reduce a background component and improve the signal to background ratio. The distance from the Li target to the center of MEDLEY chamber was 3.74 m. The relative neutron beam intensity is monitored by the integrated proton beam current at the beam dump and by both a thin film breakdown counter and an ionization chamber mounted downstream of the MEDLEY setup.

The MEDLEY setup and construction details of each telescope are illustrated in figure 2. MEDLEY consists of eight three-element telescopes mounted inside a vacuum chamber with a diameter of 90 cm. Each telescope consists of two fully depleted silicon surface barrier detectors serving as ΔE detector and a CsI(Tl) scintillator serving as E detector. The thickness of the ΔE detectors is in the range of 50–60 μm for the first one, and 400–500 μm for the second one. The CsI(Tl) scintillators were upgraded from the previous ones [1–3], and have a total length of 100 mm which is enough to stop high-energy protons produced in the 175 MeV measurement. They have a cylindrical shape with 50 mm diameter, where the last 30 mm are tapered to 18 mm diameter to match the size of a Hamamatsu S3204-08 photodiode for the light readout. The signals from each telescope are processed using the same data acquisition system as in the previous 96-MeV measurements [1–3].

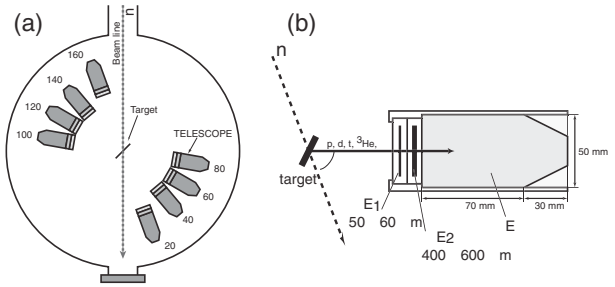

Fig. 2. MEDLEY setup: (a) arrangement of eight telescopes inside the MEDLEY chamber, and (b) construction details of each telescope.

Calcium and carbon targets are placed at the center of the MEDLEY chamber. The carbon target was 22 mm in diameter and 1.0 mm thick, and the calcium target was 29 mm in diameter and 230 μm thick. For absolute cross section normalization, a polyethylene (CH_2) target with 25 mm diameter and 1.0 mm thickness was used. Instrumental backgrounds are also measured by removing the target from the neutron beam.

Since the ^{7}Li(p,n) reaction produces peak neutrons and low-energy tail neutrons, time-of-flight (TOF) measurements are used to reject the tail neutrons. The TOF data are measured as a time difference between master trigger signal and RF timing signal from the cyclotron.

3 Data reduction procedure

The data reduction procedure based on the ΔE-E technique is the same as in the previous 96-MeV measurement and explained in detail in refs. [1,3,16]. Here the procedure for the measurement-II is briefly described.

Energy calibration of all detectors is obtained using the data themselves. Events in the ΔE-E bands are fitted with respect to the energy deposited in the two ΔE silicon detectors, which is determined from the thicknesses and the energy losses calculated with the SRIM code [10]. One example is shown in figure 3(a) for the present 175-MeV measurement.

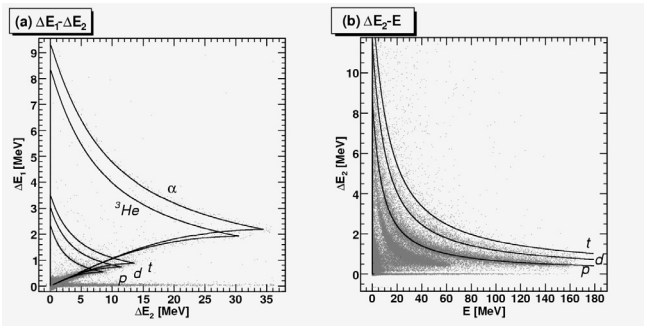

Fig. 3. Calibrated ΔE_1-ΔE_2 plot for telescope 1 at 20 degree in the left panel (a). The solid lines correspond to calculation results of energy-loss values for proton, deuteron, triton, ^{3}He and α particles. Calibrated ΔE_2-E plot for telescope 1 at 20 degree in the right panel (b). The solid line corresponds to calculated energy-loss values for protons.

For the energy calibration of the CsI(Tl) scintillator, the following approximate expression is applied to hydrogen isotopes [9]:

$$E = a + bL + c\,(bL)^2\,, \qquad (1)$$

where L is the light output and a, b, and c are the fitting parameters. The parameter c depends on the kind of charged particles. For the small CsI(Tl) scintillators, the c parameter was found by Tippawan [12] to be 0.0032 for protons. For the new CsI(Tl) scintillators, the derived c parameter was found to be ~0.001 for protons. Figure 3(b) shows a result of the energy calibration for ΔE_2 and E detectors for the 175-MeV measurement.

The measured TOF data are used for selection of light-ion events induced by neutrons in the main peak of the source neutron spectrum.

Some corrections are necessary to obtain final DDX data. Background events measured in target-out runs are subtracted from the target-in runs after normalization to the same neutron

fluence. Corrections due to the finite target thickness are made in the method described in ref. [1]. However, it should be noted that this correction has not yet been applied in the present analysis of the 175-MeV measurement. The finite efficiency of the CsI(Tl) scintillator is corrected using the Monte Carlo simulation method discussed below.

The number of the net counts due to np scattering is obtained using measurements of the (n,p) spectrum at 20° for both the targets, CH_2 and C. The result is shown in figure 4. Finally, the absolute values of the measured cross sections are determined using the reference np cross sections in the same method as in refs. [1,3]. The np scattering cross sections are taken from NN-online [13].

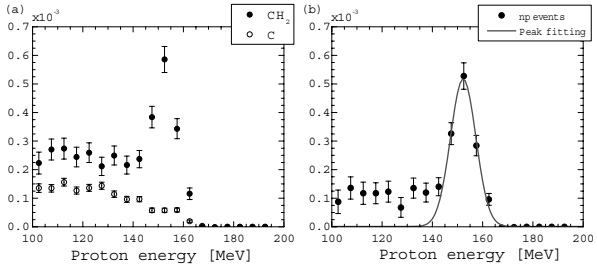

Fig. 4. Measured np scattering peak: (a) the contribution from C in the CH_2 data and (b) the net np peak with a Gaussian fitting.

4 Results and discussion

4.1 Response of CsI(Tl) scintillator to protons

The performance of the newly-installed CsI(Tl) scintillators was investigated using a 160-MeV proton beam with very low intensity, i.e., about 100 protons per second, prior to the 175 MeV neutron measurement. The proton beam was formed by installing a collimator system into the B-line shown in figure 1, which consists of a combination of a tantalum scatterer with a thickness of 4 mm and a graphite collimator with a diameter of 4 mm. The counter telescope depicted in figure 2(b) was placed near the exit of the B-line to measure the response of the Cs(Tl) scintillator to 160-MeV protons.

In figure 5(a), the measured proton spectrum normalized to the observed peak corresponding to 160 MeV is presented together with a Monte Carlo simulation using the PHITS code [14]. Note that the energy resolution of the oberved peak was 1.7 MeV in FWHM, although it is not shown in the figure. Due to nuclear interactions a certain fraction of incident protons does not fully deposit their energies into the CsI(Tl) scintillator. This leads to the so-called reaction tail which is seen in the low-energy region. The PHITS simulation reproduces the measurement well. The fraction of the reaction tail for simulated and experimental data is plotted as a function of proton energy in figure 5(b). The PHITS simulation is in excellent agreement with both the previous work [15] given by the solid line and the present measurement denoted by the full circle with the error. The efficiency of the CsI(Tl) is finally corrected using the PHITS calculation in the data analysis of the C(n,xp) reaction at 175 MeV.

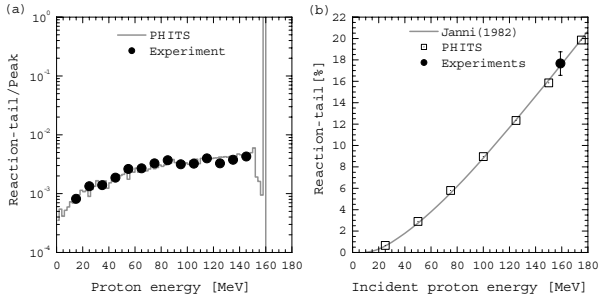

Fig. 5. Measured response of CsI(Tl) scintillator to 160 MeV protons: (a) the ratio of reaction tail to peak with the PHITS calculation, and (b) the fraction of the reaction tail as a function of incident proton energy. The explanation of the symbols and lines is given in the text.

4.2 Ca(n,xp) at 94 MeV

In figure 6, experimental double-differential cross sections of the 94 MeV (n,xp) reaction on Ca are presented for four angles and compared with a model calculation using the TALYS-0.64 code [7]. The detail of the data analysis and the model calculation is reported elsewhere [16]. The TALYS calculation overestimates the low energy region where the evaporation process is dominant, while underestimating the intermediate continuum region at forward angles where the preequilibrium emission is expected to have a large contribution.

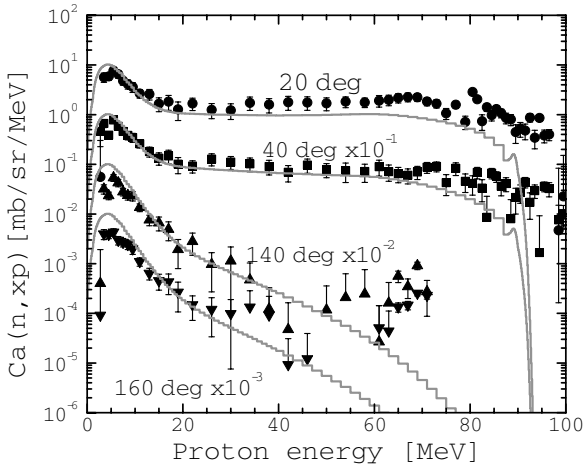

Fig. 6. Comparison of experimental double-differential cross sections for the Ca(n,xp) reaction at 94 MeV (filled symbols with error bar) with the TALYS-0.64 calculation (solid histograms).

4.3 C(n,xp) at 175 MeV

The incident neutron spectrum accepted by the TOF gate was estimated from data analysis of the recoil protons from np scattering in the measurement of the CH_2 target. Figure 7 shows the result together with the source neutron spectrum calculated using an empirical formula [17]. Both the spectra are normalized so that each peak corresponding to 175 MeV is unity. The calculated spectrum is folded using a Gaussian function with the same width as the experimental energy resolution. The measured neutron spectrum is in good agreement

with the calculated one. The hatched region above 95 MeV corresponds to the accepted neutron spectrum in the present measurement.

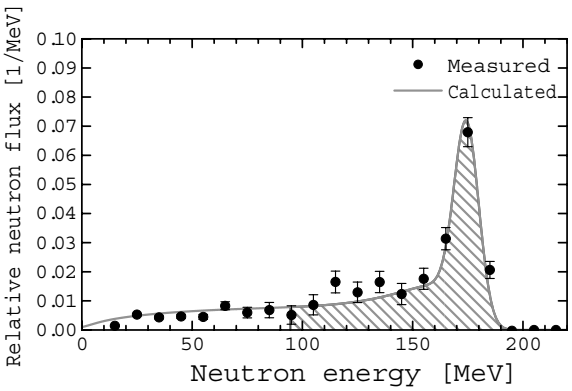

Fig. 7. Comparison between the measured neutron spectrum and calculated one. The hatched region corresponds to the accepted neutron spectrum.

The C(n,xp) spectrum measured at 20° is shown in figure 8. The measured spectrum is compared with a folding spectrum $\sigma^{cal}\left(E_p, \theta_p\right)$ obtained by the following equation:

$$\sigma^{cal}\left(E_p, \theta_p\right) = \int_{95MeV}^{175MeV} \sigma^{eval}\left(E_n, E_p, \theta_p\right) f\left(E_n\right) dE_n, \quad (2)$$

where $f(E_n)$ is the accepted source neutron spectrum shown in figure 7 and the calculated one [17] is used. The JENDL/HE evaluated cross sections [8] are used as $\sigma^{eval}(E_n, E_p, \theta_p)$ in equation (2). As can be seen in figure 8, the calculated (n,xp) spectrum shows good agreement with the measured one in the intermediate proton energy range.

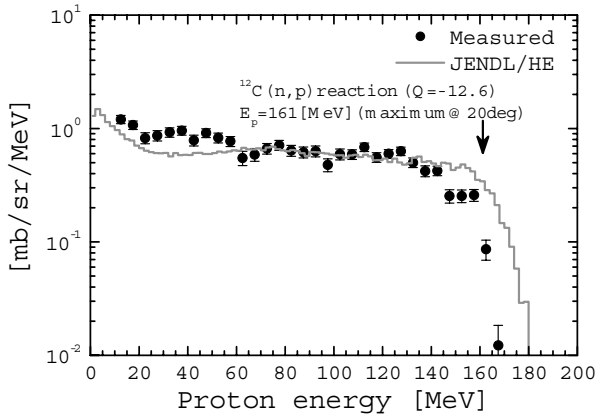

Fig. 8. Comparison of the experimental C(n,xp) spectrum at 20 ° with the folding spectrum calculated from the JENDL/HE evaluated cross sections and the accepcted neutron spectrum.

5 Summary

We have measured the double-differential cross sections of (n,xp) reactions on Ca at 94 MeV and on C at 175 MeV using the new Uppsala neutron beam facility for the first time. The measured Ca data were in reasonable agreement with the TALYS calculation, although the calculation overestimated the evaporation region at all angles and underestimated the preequilibrium region at 20°. Since the background contribution from source neutrons having continuous energies between 95 MeV and 175 MeV could not be subtracted from the measured proton spectra for C, the present measurement was compared with the proton spectrum obtained by folding the JENDL high-energy data and the expected source neutron spectrum. The proton spectrum measured at 20° showed overall good agreement with the JENDL high-energy data. Further analysis including other angles will be required for detailed comparison. In addition, it was confirmed that the measured response of the new CsI(Tl) scintillators to 160 MeV proton was reproduced well by the PHITS transport calculation.

A series of light-ion production measurements is planned for other targets, O, Si, Fe, Pb, and U, at 175 MeV in order to meet nuclear data needs for fast neutron applications.

M.H. is grateful to the Kyushu Industrial Technology Center for the Grants-in-Aid for human resource development.

References

1. U. Tippawan et al., Phys. Rev. C **69**, 064609 (2004).
2. V. Blideanu et al., Phys. Rev. C **70**, 014607 (2004).
3. U. Tippawan et al., Phys. Rev. C **73**, 034611 (2006).
4. Y. Nauchi et al., J. Nucl. Sci. Technol. **36**, 143 (1999).
5. I. Slypen et al., Phys. Rev. C **51**, 1303 (1995).
6. S. Pomp et al., in *Proceedings of the International Conference on Nuclear Data for Science and Technology*, *Santa Fe, USA, Sept. 26–Oct. 1*, edited by R.C. Haight, M.B. Chadwick, T. Kawano, P. Talou (AIP, New York, 2005), p. 780.
7. A.J. Koning, S. Hilaire, M.C. Duijvestijn, *ibid.*, p. 1154.
8. Y. Watanabe et al., *ibid.*, p. 326.
9. S. Dangtip et al., Nucl. Instrum. Meth. A **452**, 484 (2000).
10. J.F. Ziegler et al., *The Stopping and Range of Ion in Solids* (Pergamon Press, New York, 1985).
11. D. Horn et al., Nucl. Instrum. Meth. A **320**, 237 (1992).
12. U. Tippawan, Ph.D. thesis, Graduate School Chiang Mai University, Chiang Mai, May 2004, Thailand.
13. SAID Nucleon Nucleon scattering database. Available from Center for Nuclear Studies, Department of Physics, George Washington University, USA, URL: http://gwdac.phys.gwu.edu.
14. H. Iwase et al., J. Nucl. Sci. Technol. **39**, 1142 (2002).
15. J.F. Janni, At. Data Nucl. Data Tables **27**, 147 (1982).
16. P.A. Söderström, Diploma thesis, Uppsala University Neutron Physics Report, Feb. 2007.
17. A. Prokofiev et al., in *Proceedings of the International Conference on Nuclear Data for Science and Technology*, *Tsukuba, Japan, Oct. 7–12, 2001*, J. Nucl. Sci. Technol., Suppl. 2 (2002), p. 112.

International Conference on Nuclear Data for Science and Technology 2007
DOI: 10.1051/ndata:07562

Comparison of prompt-fission neutron multiplicities and energy spectra for intermediate energy proton-and neutron-induced fission

Oleg Batenkov[1,a], Georgy Boikov[1], Vilen Eismont[1], Mikhail Majorov[1], Sergey Soloviev[1], Jan Blomgren[2], and Walter Loveland[3]

[1] V.G. Khlopin Radium Institute, 2oi Murinskiy Prospect 28, Saint-Petersburg 194021, Russia
[2] Department of Neutron Research, Uppsala University, Box 525, 751 20 Uppsala, Sweden
[3] Oregon State University, USA

Abstract. The number and spectra of neutrons, in particular the number and spectra of prompt neutrons from the fission of actinides, at the intermediate energies represent important physical quantities, which determine the possibility of applying of one or another design of ADS. The multiplicities and energy distributions of prompt neutrons in interactions of ^{232}Th, ^{235,238}U and ^{237}Np with 50 and 96 MeV protons were measured by our group. The data are compared with results of recent measurements of the average multiplicities and spectra of prompt neutrons at the fission of ^{235,238}U induced by neutrons of the same energies. The correlation of the measured characteristics with neutron-proton compositions of composite nuclei is discussed. The similarity of characteristics for fission induced by neutrons and protons is noted.

1 Introduction

The number and spectra of prompt neutrons from the fission of actinides, at intermediate energies, determines the applicability of different variants of ADS designs. At the same time a knowledge of these characteristics is of great importance for theory because it leads to a better understanding of the mechanism of the interaction of fast neutrons with nuclei and properties of the fission of heated nuclei–the dynamics of the sharing of energy brought in into a nucleus by an incident nucleon between the collective and single-particle degrees of freedom, features of the de-excitation of high excited states of fission fragments. But numerous measurements, which have been made, were carried out for a restricted energy range of incident neutrons- i.e., nuclear reactor energies (E < 20 MeV). Only recently, have results of measurements of the average multiplicity of prompt neutrons of the fission of ^{238}U and ^{235}U [1] and spectra of such neutrons for ^{238}U [2] carried out at incident nucleon energies from 0.7 to 200 MeV been published. It is supposed that significant, additional, information on the energy dependence of characteristics of fission may be obtained in more easily performed measurements using proton beams (the intensity of proton beams is higher than the intensity of neutron beams by some orders of magnitude). For intermediate energy protons only data for E < 60 MeV for ^{238}U [3] and E = 155 MeV for ^{238}U [4] exist. Moreover, in the latter work published in 1970 only average multiplicities were measured. The present work is intended to fill the gap using modern experimental techniques, in the range of investigated nuclei and to compare results of measurements with protons and neutrons.

2 Experimental apparatus and techniques

The experimental apparatus and techniques used to make this measurement are very similar to that described previously [5].

[a] Presenting author, e-mail: obatenkov@atom.nw.ru

In this study, beams of 50 and 96 MeV protons from the Gustav Werner synchrocyclotron at the T. Svedberg Laboratory, Uppsala University, Uppsala, Sweden were used to irradiate targets of ^{232}Th, ^{235}U, ^{238}U and ^{237}Np. The actinide targets were mounted in the center of a thin-walled (0.8 mm) stainless steel chamber. (The time structure of the proton beam involves a 3 ns wide bunch with 70 ns between bunches.) The targets were 100–320 μg/cm^2 of ThF_4, UF_4 and NpO_2 evaporated onto a 60 μg/cm^2 Al_2O_3 backing and covered by 20 μg/cm^2 Au. After passing through the scattering chamber, the beam was stopped in a well-shielded Faraday cup ~25 m downstream of the target.

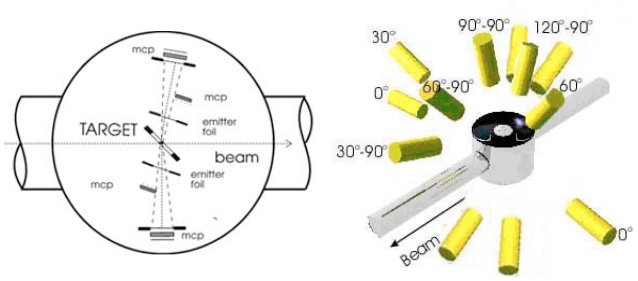

Fig. 1. Experimental arrangement. The location of the neutron detectors are shown in the right panel, and a schematic drawing of the scattering chamber is shown in the left panel.

In figure 1, we show a schematic diagram of the arrangement of the fission detectors inside the chamber and the placement of the twelve stilbene neutron detectors used in this study. The fission detectors consisted of two time-of-flight telescopes mounted at +80° and –90° with respect to the incident proton beam. Start and stop signals for the time-of-flight detectors were obtained from microchannel plate (MCP) detectors. The fission fragments passed through 60 μg/cm^2 Al_2O_3 emitter foils, knocking out a shower of electrons that

are detected in the MCPs. The time resolution of each telescope was ~80 ps with a fragment registration efficiency of 98%. For each fission event, the velocities of both fragments were measured and assuming, the mass number of the fissioning system was (A+1 - $\nu_{prefission}$) where the mass number of the target nucleus is A and $\nu_{prefission}$ is the average number of pre-fission neutrons, the fragment masses were calculated on an event-by-event basis.

The energy of any neutrons associated with each fission event was measured using time-of-flight methods. The stop signal for the neutron time-of-flight was taken to be the fission-fission coincidence with the start signal being from the stilbene neutron detectors. Typical time resolutions of ~1 ns were obtained with neutron flight paths of 46–50 cm. This corresponds to an energy resolution for 2 MeV neutrons of ~9%. Neutrons were separated from γ-rays using pulse shape discrimination. The n/γ separation was > 10^4 for E_n > 0.5 MeV.

The efficiency of the neutron detectors for E_n < 9 MeV was defined as the ratio of the measured neutron spectrum from ^{252}Cf spontaneous fission to the known distribution. Calibration spectra using ^{252}Cf were measured before and after each experiment by placing a small ionization chamber containing ^{252}Cf in the target position. For E_n > 9 MeV, the detector efficiencies were calculated.

Neutron detectors were at angles of 0, 30, 54, 60, and 90° with respect to the direction of motion of the fission fragments. Detectors were also at angles of 30, 36, 50, 60, 90, 120, and 144° with respect to the proton beams. As described earlier, the neutron flight paths were 46–50 cm with detector diameters of 5–7 cm and with detector thicknesses of 2–3 cm. The time-of-flight distribution of background events was obtained for each detector from gating on a subsequent beam burst. The number of fission-neutron events collected for each energy for each target was ~10^6, with typical proton beam currents of 15 nA.

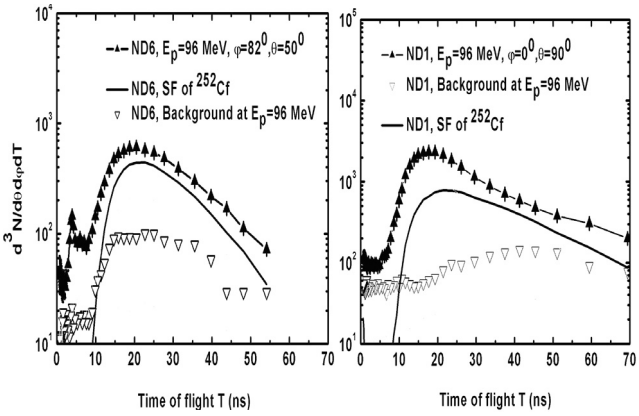

Fig. 2. Representative time-of-flight spectra for the interaction of 96 MeV protons with ^{235}U.

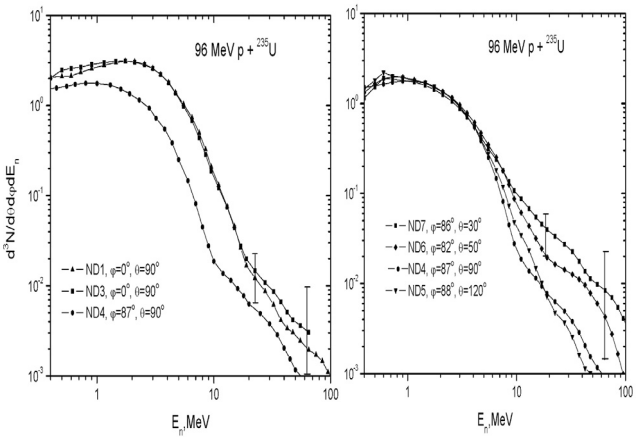

Fig. 3. Representative neutron energy spectra for the interaction of 96 MeV protons with ^{235}U.

3 Data analysis and results

For each beam-target combination, the experimental results of these measurements are a series of neutron time-of-flight spectra, measured at twelve different angles and their associated fission fragment distributions. (The data are collected on an event-by-event basis with each event including time-of-flights of the emitted neutron and the two fission fragments.)

In figure 2, we show some representative neutron time-of-flight spectra for the interaction of 96 MeV protons with ^{235}U along with background spectra and calibration spectra taken with ^{252}Cf. These time-of-flight spectra were converted into neutron energy spectra. In figure 3, we show some representative fission-associated neutron spectra for the reaction of 96 MeV protons with ^{235}U at fission-neutron angles of 0 and 87° (beam-neutron angle of 90°), while in figure 3 we show typical fission-associated neutron spectra at beam-neutron angles of 30, 50, 90, and 120° (at fission-neutron angles ~90°). As expected, the high energy neutrons (E_n > 15 MeV) from direct processes are strongly forwardly peaked with respect to the beam axis. Also the angular distributions of the neutrons with respect to the fragment direction of motion are forward-peaked with the higher energy neutrons being more isotropic.

The number of neutrons emitted per fission, ν, for the 50 MeV proton induced fission of ^{232}Th, ^{235}U, ^{238}U and ^{237}Np is 7.35 ± 0.07, 6.86 ± 0.06, 7.44 ± 0.07, and 7.24 ± 0.06 while the same quantities for the 96 MeV proton induced fission are 9.17 ± 0.10, 8.57 ± 0.08, 9.27 ± 0.08, and 8.58 ± 0.1. The average neutron energy in the laboratory system for the 50 MeV proton induced fission of ^{232}Th, ^{235}U, ^{238}U and ^{237}Np is 2.63 ± 0.02, 2.77 ± 0.02, 2.72 ± 0.02, 2.83 ± 0.02 MeV while the same quantities for the 96 MeV proton induced reaction are 3.09 ± 0.04, 3.09 ± 0.03, 3.12 ± 0.03, and 3.12 ± 0.04 MeV, respectively. The average neutron energies in the laboratory system are largely independent of the target nucleus and increase with the beam energy. (Typical average laboratory neutron energies in the low energy neutron induced fission of these nuclei are about 2.0 MeV.)

In figure 4, we show, for typical projectile energy-target system, the decomposition of the neutron energy spectra into three components: (a) pre-equilibrium neutrons emitted in the initial nucleon-nucleus interaction, consisting of two stages, an intranuclear cascade in which the primary particles are re-scattered several times before absorption or leaving the nucleus and a second "exciton" stage where conventional

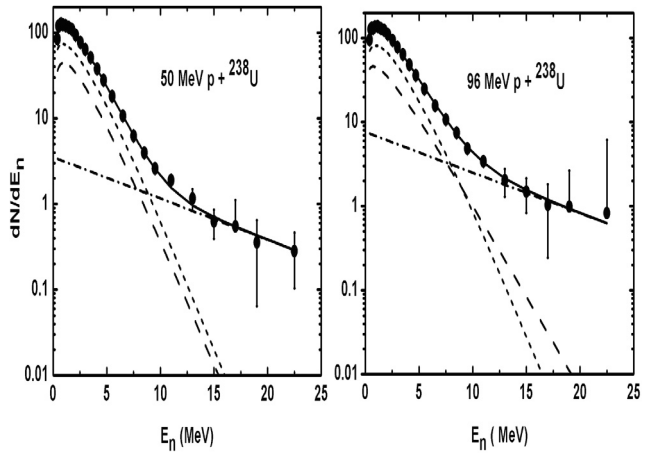

Fig. 4. Decomposition of the neutron energy spectra into their components. Solid lines and symbols indicate the overall spectra, the dot-dashed line the pre-equilbrium component, the short dashed line the post fission component and the long dashed line the equilibrium component.

pre-equilibrium emission takes place (dot-dashed line), (b) equilibrium neutrons emitted by the equilibrated nucleus prior to fission (long dashed line) and (c) post fission neutrons emitted by the fully accelerated fission fragments (short dashed line). As remarked earlier, the so-called scission neutrons and neutron emitted by the accelerating fragments are grouped into the "equilibrium component".

To do this decomposition, one begins by removing the pre-equilibrium component from each angle resolved spectrum. This is done by assuming that all neutrons above 15 MeV are due to pre-equilibrium processes and fitting the energy spectra with an equation of the form

$$dN/dE_n = \nu_{pre-1}\, A\exp[-(E_n - C)/T)$$

where A and C are normalizing constants and T is a slope parameter giving the slope of the pre-equilibrium energy distribution. The slope parameter T was found to be 9 MeV^{-1} for all systems. The values of ν_{pre-1} are tabulated in table 1 along with the average energy (in the rest frame of the emitting system) of each pre-equilibrium neutron. This component does not depend on the nature of the target nucleus and only weakly depends on the beam energy. (The additional energy carried away by these pre-equilibrium neutrons only increases only about 4.5 MeV as the beam energy increases 46 MeV.) While the pre-equilibrium neutrons include the most energetic neutrons, these high energy neutrons are very few in number making their contributions to the energetics relatively small.

Once the pre-equilbrium neutrons have been removed from the spectra, the components due to the equilibrium and post-fission neutrons are resolved. In a first approximation, all neutrons emitted at 0° with respect to the fragment direction of motion are assumed to be due to post fission neutrons while all neutrons emitted at 90° are assumed to be equilibrium neutrons. The energy spectra in the rest frame of the emitting nucleus of these two components are fitted using the equations

$$dN/dE_n = \nu_{post} B\, E_n{}^{b} \exp[-E_n/T_{post}]$$

Table 1. The average energy (in the rest frame of the emitting system) and number of neutrons emitted in pre-equilibrium processes, by the fully accelerated fission fragments and prior to fission.

Target	E_p = 50 MeV		E_p = 96 MeV	
	ν_{pre-1}	$\langle E_n\rangle$ (MeV)	ν_{pre-1}	$\langle E_n\rangle$ (MeV)
^{232}Th	0.5 ± 0.3	8.8 ± 1.0	1.1 ± 0.3	9.1 ± 1.0
^{235}U	0.5 ± 0.3	8.8 ± 1.0	1.1 ± 0.3	9.1 ± 1.0
^{238}U	0.5 ± 0.3	8.8 ± 1.0	1.1 ± 0.3	9.1 ± 1.0
^{237}Np	0.5 ± 0.3	8.8 ± 1.0	1.0 ± 0.3	9.1 ± 1.0
Target	E_p = 50 MeV		E_p = 96 MeV	
^{232}Th	4.4 ± 0.3	1.65 ± 0.03	4.9 ± 0.3	1.76 ± 1.0
^{235}U	4.9 ± 0.3	1.74 ± 0.03	5.0 ± 0.3	1.76 ± 1.0
^{238}U	4.4 ± 0.3	1.65 ± 0.03	5.1 ± 0.3	1.76 ± 1.0
^{237}Np	4.8 ± 0.3	1.76 ± 0.03	4.9 ± 0.3	1.76 ± 1.0
Target	E_p = 50 MeV		E_p = 96 MeV	
	ν_{eq}	$\langle E_n\rangle$ (MeV)	ν_{eq}	$\langle E_n\rangle$ (MeV)
^{232}Th	2.4 ± 0.3	2.30 ± 0.03	3.4 ± 0.3	2.60 ± 1.0
^{235}U	1.5 ± 0.3	2.50 ± 0.03	2.7 ± 0.3	2.70 ± 1.0
^{238}U	2.6 ± 0.3	2.40 ± 0.03	2.9 ± 0.3	2.70 ± 1.0
^{237}Np	1.9 ± 0.3	2.40 ± 0.03	3.0 ± 0.3	2.90 ± 1.0

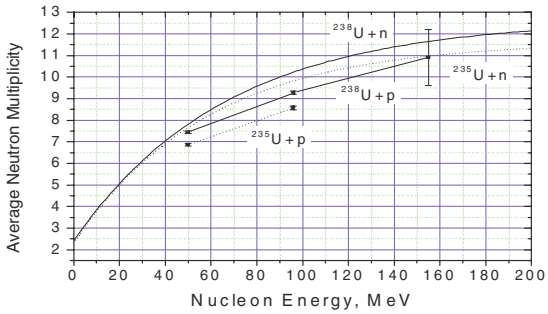

Fig. 5. Prompt fission-neutron average multiplicity for ^{235}U and ^{238}U as a function of incident nucleon energy, the approximating functions – for neutrons (solid line - ^{238}U, dashed line - ^{235}U) [1], points – for protons (solid square connected by a solid line - for ^{238}U including data for E = 155 MeV from [4], solid circles connected by a dashed line – for ^{235}U).

$$dN/dE_n = \nu_{eq} D\, E_n{}^{d} \exp[-E_n/T_{cn}]$$

where the constants B, D, b, d, T_{post} and T_{cn} are determined in the fitting process. Following the determination of these constants, they are used with the above equations to fit, in an iterative manner, the angle-resolved energy spectra to give the values of ν_{post}, the post scission neutron multiplicity per fission event and ν_{eq}, the multiplicity of equilibrium neutrons emitted per fission event. The values of these quantities are tabulated in table 1.

4 Discussion

In figure 5 our data on the average multiplicity of neutrons, $\langle\nu_p\rangle$ produced in the fission of ^{235}U and ^{238}U are compared with fitting functions for these values obtained in [1] (for the same energy region of fission-neutrons).

It is seen that the energy dependence of the average multiplicity for the (p,f) and (n,f) reactions looks similar.

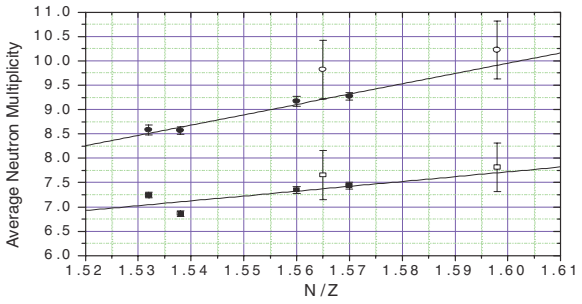

Fig. 6. Prompt fission-neutron average multiplicity for systems ^{237}Np+p, ^{235}U+p, ^{232}Th+p, ^{235}U+n, ^{238}U+p and ^{238}U+n as a function of the ratio of the number of protons to the number neutrons for composite nuclei (systems are listed by way of N/Z). Open symbols are for neutron-induced reactions.

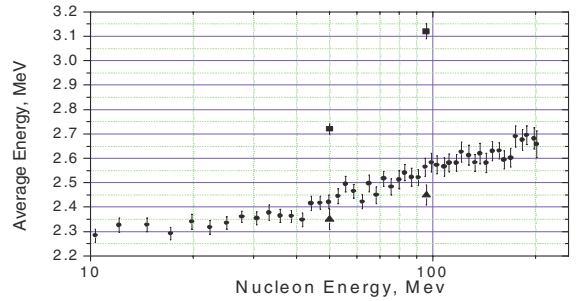

Fig. 7. Prompt fission-neutron average energy for ^{238}U as a function of incident nucleon energy: circles – neutrons [2], squares – for protons for the range of fission neutrons 0.4 to 22.5 MeV, triangles – for protons for the range of fission neutrons 0.65–7.5 MeV.

All points for ^{238}U(p,f) including the point at 155 MeV [4] and for ^{235}U(p,f) lie lower than the corresponding (n,f) reaction points. As in the case of reactions with neutrons [1] $\langle\nu_p\rangle(^{238}U)\rangle\langle\nu_p\rangle(^{235}$U). The comparison of data on ^{235}U and ^{238}U with data on other nuclides demonstrates an increase of $\langle\nu_p\rangle$ with the increase of N/Z (where N and Z numbers of neutrons and protons in composite nuclei). The slope of $\langle\nu_p\rangle$ increases with incident nucleon energy.

This is illustrated in figure 6, which includes both data on protons and on neutrons.

It may be noted that the similarity of energy dependence and the absolute values of $\langle\nu_p\rangle$ also occurs in the comparison of the average energies of prompt neutrons at the neutron and proton induced fission of ^{238}U. This may be seen in figure 7, where together with data from [2], our results on the average energies of spectra of all detected neutrons including cascade neutrons with energies up to 22.5 MeV and spectra "deduced" from the latter, are presented.

The authors of [2] found that at energies higher than 50 MeV the average energy of fission-neutrons in the laboratory frame slightly increases with the energy of incident neutrons due to both the rise of energy in a center-of mass frame (CMF) and the rise of the kinetic energy of fission fragments. We suppose that this may be a result of the rise of the excitation energy of fission fragments that in turn leads to the rise of the temperature of neutron spectra in CMF and to a more early emission of neutrons from fragments – up to the moment of the beginning of acceleration that increases the detected kinetic energy of fission fragments. The effect of emitting neutrons from fission fragments before the stage of being fully accelerated was treated in [7].

5 Conclusion

The similarity of fission properties in (p,f) and (n,f) reactions is considered to be the result of the effect of the "compound nucleus". As calculations made with contemporary codes TALYS [9,10] and CEM03 [11,12] show, this effect is a consequence of the similar characteristics of the intermediate compound nuclei, formed after a intra-nuclear cascade and pre-equilibrium emission. Due to the fact that intensities of protons beams are some orders of magnitude higher than intensities of neutron beams, the possibility of investigating, in detail, the dependence of the characteristics of fission-neutrons on the excitation energy of a nucleus, including determining various differential characteristics, correlations with fission fragments masses and kinetic energies, for a wide circle of actinides becomes more realistic. The investigation of such correlations is necessary for the development of our understanding of such a multi-parameter process as fission to apply the process in nuclear plants using intermediate energy neutrons.

References

1. Th. Ethvignot et al., in *Proc. Int. Conf. on Nuclear Data for Science and Technology*, *Santa Fe, NM, Sept. 26–Oct. 1, 2004,* AIP Conf. Proc. **769** (2005), p. 656.
2. Th. Ethvignot et. al., Phys. Lett. B **575**, 221 (2003).
3. V.A. Rubchenya et al., Nucl. Instrum. Meth. Phys. Res. A **463**, 653 (2001).
4. E. Cheifetz et al., Phys. Rev. C **2**, 256 (1970).
5. O. Batenkov et al., Nucl. Instrum. Meth. Phys. Res. A **394**, 235 (1997).
6. W. Mannhart, IAEA Tecdoc-410, 158 (1986).
7. V.P. Eismont, At. Energy **19**, 133 (1965).
8. A.N. Smirnov et al. (these proceedings).
9. A.J. Koning et al., in *Proc. Int. Conf. on Nuclear Data for Science and Technology*, *Santa Fe, NM*, *Sept. 26–Oct. 1, 2004,* AIP Conf. Proc. **769** (2005), p. 1154.
10. A.N. Smirnov et al., *ibid.*, p. 637.
11. S.G. Mashnik et al., LANL Report LA-UR-05-2686, Los Alamos, 2005; E-prints: nucl-th/0502019; nucl-th/0503061.
12. K.K. Gudima (private communication).

International Conference on Nuclear Data for Science and Technology 2007
DOI: 10.1051/ndata:07703

A neutron beam facility at SPIRAL-2

X. Ledoux[1], M. Aïche[2], G. Ban[3], G. Barreau[2], P. Baumann[4], P. Bem[5], V. Blideanu[6], J. Blomgren[7], S. Czajkowski[2], P. Dessagne[4], E. Dupont[6], D. Doré[6], T. Ethvignot[1], U. Fischer[8], F. Gunsing[6], B. Jacquot[9], B. Jurado[2], M. Kerveno[4], F.R. Lecolley[3], J.L. Lecouey[4], F. Negoita[10], S. Oberstedt[11], M. Petrascu[10], A.J.M. Plompen[11], F. Rejmund[9], D. Ridikas[6], G. Rudolf[4], O. Shcherbakov[12], S.P. Simakov[8], and J. Taïeb[1]

[1] CEA/DIF, DPTA/SPN, BP. 12, 91980 Bruyères-le-Châtel Cedex, France
[2] Centre d'Études Nucléaires de Bordeaux-Gradignan, 33175 Gradignan, France
[3] LPC, ISMRa et Université de Caen, CNRS/IN2P3, France
[4] Institut Pluridisciplinaire Hubert Curien, Strasbourg, France
[5] Nuclear Physics Institute, 25068 Řež, Czech Republic
[6] CEA Saclay, DSM/DAPNIA, 91191 Gif-sur-Yvette, France
[7] Department of Neutron Research, Uppsala University, Uppsala, Sweden
[8] Forschungszentrum Karlsruhe, Institute for Reactor Safety, Karlsruhe, Germany
[9] GANIL, CEA/DSM-CNRS/IN2P3, Caen, France
[10] NIPNE, Bucharest, Romania
[11] European Commission, JRC/IRMM, Geel, Belgium
[12] PNPI, Gatchina, Leningrad district, Russia

Abstract. The future SPIRAL-2 facility is mainly composed of a high-power superconducting driver LINAC, delivering a high-intensity deuteron, proton and heavy ions beams. The first two beams are particularly well suited to the construction of a neutron beam and irradiation facility called Neutrons for Science (NFS). Thick C and Be target-converters with incident deuteron beam will produce an intense white neutron spectrum, while thin ^{7}Li target and incident proton beam allows generating quasi-monoenergetic neutrons. The 1–40 MeV neutron energy range will be covered and characterized by very intense fluxes available. The primary ion beam characteristics (energy, time resolution, intensity, etc.) are adequate to create a neutron time-of-flight facility. Irradiation stations for neutron, proton and deuteron induced reactions could also be built in order to perform cross-sections measurements by activation techniques. In this paper we will discuss the potential of this new installation to investigate numerous topics, both in fundamental and applied physics. In particular, cross section measurements could be performed for different purposes like nuclear data evaluation, fission and fusion technology, Accelerator Driven Systems, nuclear medicine, astrophysics, etc.

Introduction

The future SPIRAL-2 facility, currently under construction at GANIL, Caen (France) will produce radioactive ion beam (RIB) in the mass range from A = 60 to A = 140. These nuclei will be produced by the fission of ^{238}U induced by fast neutrons, which are generated from deuterons interacting with a carbon converter [1]. The high-power superconducting driver LINAG (LINear Accelerator of Ganil) will deliver a high-intensity deuteron as well as proton and heavy ions beams. The delivered beams will also be used for other purposes than RIB production [2]. We can mention the atomic physic facility or the S^3 experiment where high intensity heavy ions beams will be used for super-heavy studies. Finally, LINAG's characteristics are also particularly well suited to the construction of a neutron beam and irradiation facility, called Neutrons for Science (NFS). This facility will be a very powerful tool for physics with neutron beams from fundamental research to applications like the transmutation of nuclear waste, design of future fission and fusion reactors, nuclear medicine or the test and development of new detectors. We will describe in this paper the technical characteristics of the facility and give some examples of the physics case which could be achieved.

1 Description of NFS

1.1 The neutron hall

The NFS project will be composed of two parts: a pulsed neutron beam for in-flight measurements and an irradiation station for activation measurements. The facility will be composed of the primary proton/deuteron beam extension in a dedicated cave with a target converter (neutron production target). Behind the converter a thick concrete wall with a collimated channel defines the neutron beam (see figure 1). The size of the neutron hall downstream of the collimator will be around

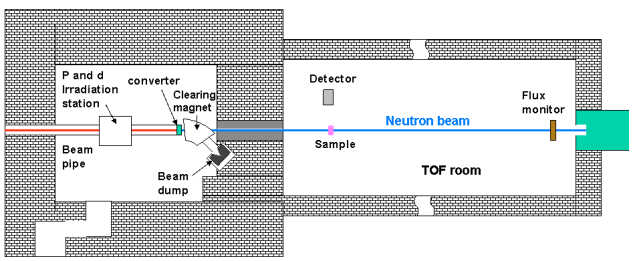

Fig. 1. Schematic view of the NFS facility.

L ~ 25 m × l ~ 8 m. This size would allow using large experimental set-ups and performing measurements at desired distances from 5 up to 30 m. This flexibility is very interesting in terms of flux and energy measurement resolution (see sect. 1.3). The clearing magnet placed between the converter and the collimator allows the deviation of an outgoing beam (in case of thin converter) to the beam dump and clean up of the neutron beam from the secondary charged particles created in the converter.

1.2 Neutron production

The LINAG is designed to accelerate deuterons up to 40 MeV and protons up to 33 MeV. The accelerator frequency is 88 MHz, the burst duration is 200 ps and the nominal intensity is 5 mA. Two types of production reactions are conceivable to produce neutrons.

The first is the deuteron break-up reaction on 1 cm thick converter. A continuous spectrum is generated with an average energy of around 14 MeV at 0 degrees and the impinging deuteron is stopped in the target. We can see on figure 2 that the use of beryllium instead carbon allows to gain a factor of 2 in the neutrons yield. The second production mode is obtained by the ^{7}Li(p,n)^{7}Be reaction on a thin target (~1 mm). Quasi-monoenergetic neutrons are produced at 0 degree with energy $E_n \approx E_p - 2$ MeV (see fig. 3). The energy resolution and the low energy tail depend mainly on the lithium target thickness. A pulsed beam is required to measure the neutron energy in case of continuous spectrum and to separate quasi-mono-energetic neutrons from the low energy tail.

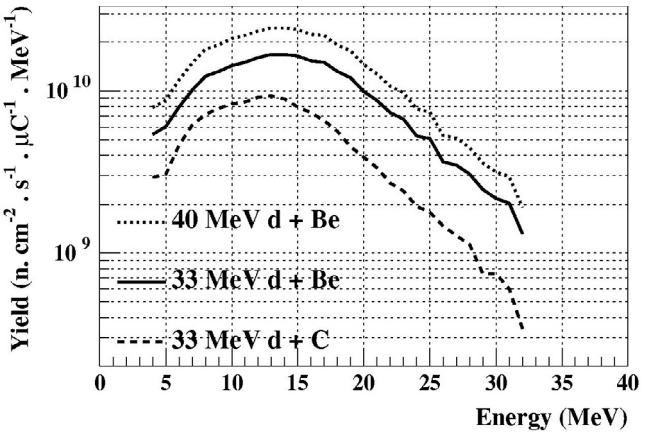

Fig. 2. Neutron spectra produced at 0 degree by deuteron break-up reactions on 1 cm carbon and beryllium converters [4].

1.3 Neutron beam characteristics

Neutron energy resolution and minimum available energy are two very important characteristics of a neutron beam facility. They are directly related to the flight path, the burst duration and the repetition frequency. Due to the beam transport between the LINAG exit and the converter, the initial burst of 200 ps will be somewhat degraded at the converter point. However, a burst duration better than 1 ns should be guaranteed by adding a beam buncher if necessary. Taking into account a 30 m flight path and variable time resolution of different detectors we can calculate the expected resolution on the energy measurement (see eq. 1 and fig. 4).

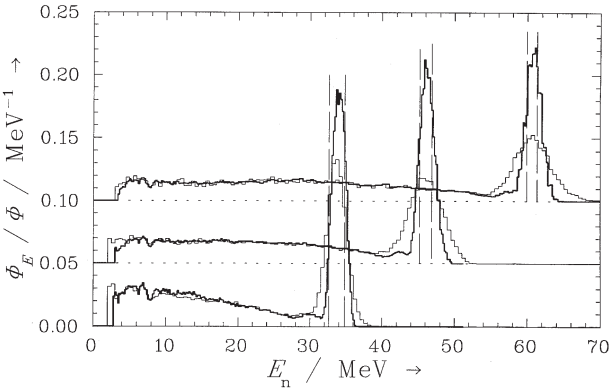

Fig. 3. Neutron spectra produced at 0 degree by ^{7}Li(p,n)^{7}Be reaction at 36, 48 and 63 MeV [5].

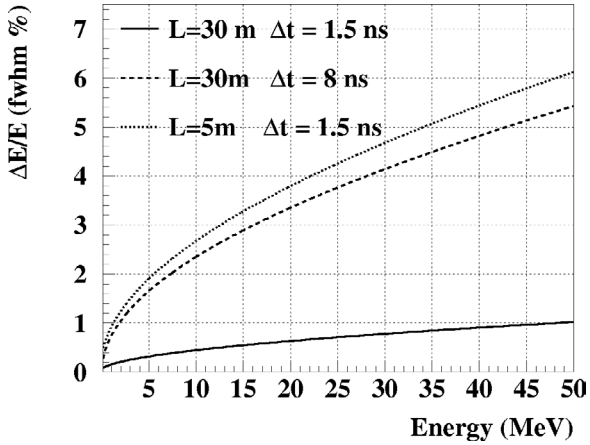

Fig. 4. Energy resolution as a function of the neutron energy.

$$\frac{\Delta E}{E} = \gamma(\gamma+1)\sqrt{\left(\frac{\Delta t}{t}\right)^2 + \left(\frac{\Delta L}{L}\right)^2}. \qquad (1)$$

It can be observed that with fast detectors the energy resolution at 40 MeV is better than 1% and even for slow detectors like HPGe ($\Delta t \approx 8$ ns) the energy resolution remains below than 5%.

The overlap of neutron time-of-flight t from the one of the previous burst with TOF t + T (T is the beam period) limits the available energy range. The period T and the flight path L define the lowest usable energy (threshold energy). For our purpose a unique burst selector is required to divide the initial LINAG frequency (F_0 = 88 MHz) by a factor N. The intensity on the converter is then limited to I = 5 mA/N. The table 1 gives some examples of beam frequency and maximum intensity for several path length and threshold.

By taking into account the neutron yield production, the beam division and the flight path, the neutron flux can be evaluated and compared to other major time-of-flight facilities

Table 1. Time structure parameters and maximum energy for different path lengths and energy threshold.

Path length	E threshold	Frequency	N	Imax
5 m	1 keV	88 kHz	1000	5 μA
5 m	100 keV	875 kHz	100	5 μA
30 m	100 keV	146 kHz	603	8.3 μA
30 m	1 MeV	461 kHz	191	26.2 μA

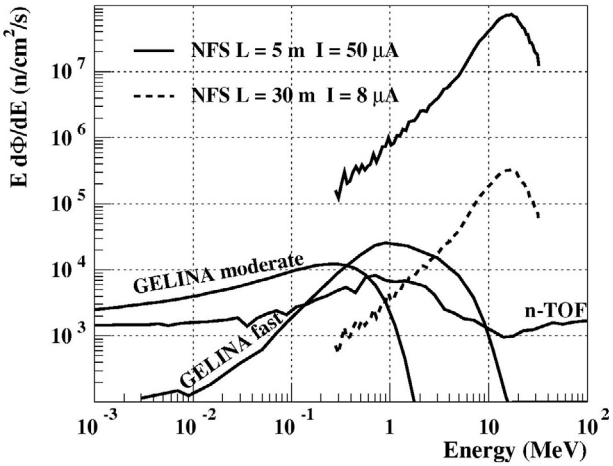

Fig. 5. Neutron flux at NFS for short (5 m) and long (30 m) compared to 2 other n-tof facilities in Europe.

in Europe namely n_TOF at CERN and Gelina at Geel. A flight path between 5 and 30 m is available at NFS allowing high intensity flux (5 m) and high resolution measurement (30 m). We can see on figure 5 that between 1 and 35 MeV NFS is very competitive in terms of average flux in comparison with n_TOF and Gelina. It has to be stressed that it is mainly due to the high repetition rate, the flux by deuteron burst is clearly lower.

Moreover, NFS presents some advantages thanks to the neutron production mechanism itself. In spallation sources, the high energy neutrons (up to hundreds MeV), can present challenges for collimation and background. Secondly the gamma-flash, which is known to be very penalising especially because it induces a dead time, will be probably strongly reduced at NFS. Note that high energy gammas are produced by π^0 decay in spallation sources and by bremsstrahlung process in photoneutron sources based on electron accelerator.

1.4 Irradiation station

A station dedicated to measurements by activation technique for neutron and deuteron induced reactions is also envisaged. The irradiation sample should be placed as close as possible to the converter in order to maximize available neutron/deuteron flux. No time structure is required in this case and the maximum ion beam intensity will be limited to around 50 μA in order to reduce the radioprotection constraints and make the converter design easier. For quasi-mono-energetic neutrons replacing the magnet by a beam stopper made of carbon seems

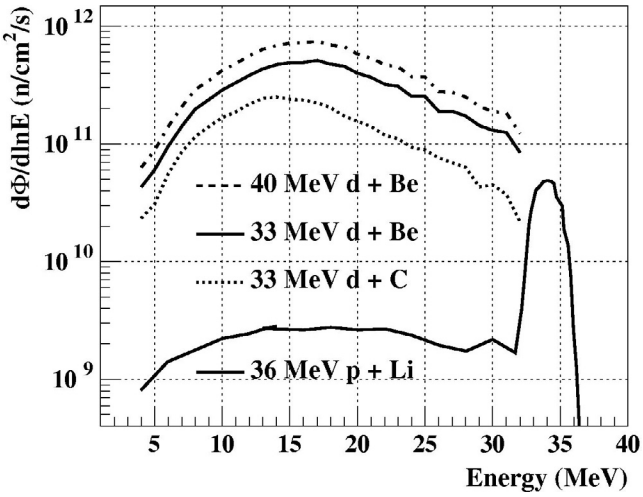

Fig. 6. Available neutron flux for activation experiments.

to be a more adequate solution since in this case the sample could be positioned closer to the Li target. In figure 6 the neutron flux available close to the converter (5 cm) for a beam intensity of 50 μA is presented. Note that even at this reduced intensity the available neutron fluxes are higher than in the existing neutron facilities in Europe, where irradiations by high energy neutrons are performed.

The LINAG offers the possibility of delivering proton and deuteron beams with variable energy up to 33 and 40 MeV respectively. Thus a charged particle irradiation station can be created without major difficulties, although it requires a specific set-up to place and remove the sample, and measure the beam current.

2 Physics case

The NFS facility could be used for cross-section measurements as well as for fundamental research [6,7]. The 1–40 MeV energy range is particularly well suited for studies on the transmutation of nuclear waste in ADS or in the new generation fast reactors.

Required fission cross-sections are often unknown above 14 MeV (or known with big uncertainties). A high neutron flux is absolutely needed because for the actinides of interest being radioactive only small samples can be used. The study of the fission process for fundamental research could also be achieved. Coincidence experiments could be performed, where the fragment mass and charge distribution could be measured. The variable neutron energy allows studying the process at variable excitation energies during the same experiment.

The (n,X) reactions are also of first importance in numerous applications. We saw that measurements using germanium detector are possible with good energy resolution, so (n,n'γ) and (n,xn) can be studied. The impact of such reactions in large systems as nuclear reactors is very important on the energy distribution of the fast neutron spectrum. The NFS energy range allows one to access the opening of new reaction channels like (n,2n), (n,3n), (n,4n)... This is also the region

where the pre-equilibrium process becomes important and measurements are needed to constrain strongly the existing models. The production of charged particles is of primary importance too because it leads to the generation of gases and defaults in the structural materials. If double differential measurements have been performed above 40 MeV, presently no data exist below this energy. It seems that the existing experimental apparatus could be used at NFS.

The fusion technology projects like IFMIF and ITER require activation cross-section measurements in fast neutron, proton and deuteron induced reactions [8,9]. These data are absolutely needed to determine the nuclear safety issues such as gas production, γ-dose rate, heat generation, waste transportation and storage. Such measurements could be achieved by activation techniques in the dedicated irradiation stations.

The neutrons produced in atmosphere by cosmic particles can produce single event upsets (SEUs) in semi-conductor devices on board of aircrafts or satellites. Accurate dosimetric measurements are an important tool for understanding the rate of (SEUs) in semi-conductor devices in neutron environments. The NFS irradiation station would allow performing such measurements in particular with quasi-mono-energetic neutrons.

Conclusions

The NFS characteristics in terms of flux or energy resolution make it a very attractive and powerful tool for neutron physics in the 1–40 MeV range. The high intensity neutron beam will allow performing cross section measurements as well as fundamental physics experiments. This facility is fully complementary to the other existing facilities based on spallation neutron source or electron accelerators. The irradiation facility is particularly well situated for cross-section measurements in neutron, proton or deuteron induced reactions which are needed for the fusion technology. A letter of intent has been presented to the Scientific Advisory Committee of SPIRAL 2 [10] and received encouraging recommendations. The facility could be operational around 2011.

References

1. *Report of the SPIRAL 2 Detail Design Study*, available on http://www;ganil.fr.
2. *The scientific objective of the SPIRAL-2 project*, available on http://www;ganil.fr.
3. D. Ridikas, X. Ledoux et al., *Neutrons for Science (NfS) at SPIRAL-2*, Internal report DAPNIA 05-30, CEA Saclay, France (2005).
4. Meulders et al., Phys. Med. Biol. **20**(2), 235 (1975).
5. Schumacher et al., NIM A **421**, 2843 (1999).
6. *International Workshop on Neutrons for Science (NFS) at SPIRAL-2*, *GANIL, Caen, France, 13–14 December 2004*.
7. A. Plompen, *Nuclear Data Needs for Nuclear Energy (fission) and Possible Contributions of SPIRAL2, 15th Colloque GANIL, Giens, France* (2006).
8. U. Fischer, *Nuclear data needs for fusion technology and possible contribution by SPIRAL2, 15th Colloque GANIL, Giens, France* (2006).
9. P. Bem et al., *Activation cross section benchmarks at NPI cyclotron*, *Workshop on Activation Data – EAF 2007, 02–04 October 2006, Prague, Czech Republic.*
10. *Letters of intents for the SPIRAL 2 facility*, available on http://www;ganil.fr.

Evidence of three-body force effects in neutron-deuteron scattering at 95 MeV

P.Mermod [a], S.Pomp [a,*], J. Blomgren [a], C. Johansson [a], J. Klug [a], L. Nilsson [a,b], N. Olsson [a,c], A. Öhrn [a], M. Österlund [a], U. Tippawan [a,d], O. Jonsson [b], A. Prokofiev [b], P.-U. Renberg [b], B. Bergenwall [e], P. Nadel-Turonski [e,f], Y. Maeda [g], H. Sakai [g], A. Tamii [g],

[a] *Department of Neutron Research, Uppsala University, Box 525, 75120 Uppsala, Sweden*
[b] *The Svedberg Laboratory, Uppsala University, Box 533, 75121 Uppsala, Sweden*
[c] *Swedish Defence Research Agency (FOI), Stockholm, Sweden*
[d] *Fast Neutron Research Facility, Chiang Mai University, Thailand*
[e] *Department of Radiation Sciences, Uppsala University, Sweden*
[f] *George Washington University, Washington, D.C., USA*
[g] *Department of Physics, University of Tokyo, Japan*

Abstract

The neutron-deuteron (*nd*) elastic scattering differential cross section has been measured at 95 MeV incident neutron energy. The neutron-proton (*np*) differential cross section has also been measured for normalization purposes. An inclusion of three-nucleon forces gives a considerable improvement in the theoretical description of the nd data in the angular region of the cross-section minimum. The data cover the full angular distribution by combining neutron detection and deuteron detection, using two different experimental setups, run in several different modes to get the systematical uncertainties under good control. The final data have an unprecedented precision in the region of the cross-section minimum, where three-nucleon forces are expected to be significant. The present data agree well with theoretical descriptions including three-nucleon forces.

Key words: Three-nucleon forces, Neutron-deuteron scattering, Angular distribution
PACS: 21.45.+v, 25.10.+s, 25.40.Dn, 28.20.Cz

* Corresponding author.
Email address: Stephan.Pomp@tsl.uu.se (S.Pomp).

1. Introduction

Nuclear properties and interactions can be understood *ab initio* from the basic knowledge of the nucleon-nucleon (NN) interaction. For this purpose, NN potentials, which are based on meson-exchange theories, have been developed.

In three-nucleon ($3N$) systems, quantitative descriptions can be provided rigorously by using NN potentials in the Faddeev equations [1]. However, theoretical considerations indicate that the description of systems made of more than two nucleons is not complete if three-body forces are not taken into account. As a first experimental evidence, the ^{3}H and ^{3}He binding energies can be reproduced model-independently taking $3N$ forces into account [2], while calculations using only NN interactions underestimate them by typically half an MeV [3]. The ^{4}He binding energy can also be described correctly with combined NN and $3N$ forces [4], indicating that the role of four-nucleon forces is not significant.

Calculations made within the CHPT framework at next-to-next-to-leading order implicitly include $3N$ forces [5,6]. Calculations at the next higher order were made recently [7,8], allowing for instance an excellent description of NN phase shifts.

Besides the ^{3}H and ^{3}He binding energies, a number of observables that may reveal the effects of $3N$ forces have been identified. Significant $3N$-force contributions are expected in the angular distribution of elastic nd scattering [9,10]. Faddeev calculations including a $3N$ potential with parameters adjusted to the triton binding energy predict that $3N$ forces affect substancially the differential cross section in the minimum region of the angular distribution [9]. Around 100 MeV, this effect is of the order of 30%. Several nd scattering experiments [11–15] have been performed. The data show the expected effects of $3N$ forces in the cross-section minimum, while at higher energies, the effects tend to be too large to be accounted for by present theories. This might be due to inadequate modeling of the $2N$ or $3N$ forces in the present calculations rather than the lack of a full relativistic treatment [15].

In the context of our nd scattering experiments, we obtained elastic scattering angular distributions for carbon and oxygen at 95 MeV. Differential cross sections for neutron inelastic scattering on carbon and oxygen to excited states below 12 MeV excitation energy could also be extracted [16]. These data are relevant for medical treatment of tumors with fast neutrons as well as in dosimetry, since the human body contains significant amounts of carbon and oxygen. Recoil nuclei from elastic and inelastic scattering are expected to account for more than 10% of the cell damage, the rest being mainly due to np scattering and neutron-induced emission of light ions [17,18]. The oxygen data may also be relevant for future incineration of nuclear waste in subcritical reactors fed by a proton accelerator, where the nuclear fuel might be in oxide form.

2. Results

By detecting either the scattered neutron or the recoil proton/deuteron, we were able to cover the angular range from 15 to 160 degrees in the c.m. system. By using two different detector setups, MEDLEY [19] and SCANDAL [20] in various configurations, we could keep the systematic uncertainties under control. Additionally, by measuring the np scattering differential cross section and, in the case where scattered neutrons were

detected, also elastic scattering in carbon (i.e., the ^{12}C(n,n) reaction), the systematic error due to uncertainties in the normalization factors was minimized.

The *nd* results at 95 MeV in the minimum region ($80^\circ < \theta_{c.m.} < 160^\circ$) are compared with theoretical predictions based on Faddeev calculations [9] using the AV18 *NN* potential [21] combined with two different $3N$ potentials (Tucson-Melbourne [22] and Urbana IX [23]), as well as predictions from CHPT [5]. It is quantitatively illustrative to compute the reduced χ^2 between our data and the calculations for the *nd* differential cross section in the minimum. When no $3N$ forces are included, the χ^2 is larger than 18. The best description is given by the CD-Bonn potential (version 1996) with the TM99 $3N$ force, with a χ^2 of 2.1. With the AV18 potential, the *nd* differential cross section is slightly better described with the TM99 $3N$ potential ($\chi^2 = 2.3$) than with the Urbana IX potential ($\chi^2 = 3.5$). The CHPT prediction gives a χ^2 of 6.5. Note that the deviations from one may be partly due to the normalization uncertainties in the data [13,16].

Acknowledgements

This work was supported by the Swedish Nuclear Fuel and Waste Management Company, the Swedish Nuclear Power Inspectorate, Ringhals AB, the Swedish Defence Research Agency and the Swedish Research Council.

References

[1] W. Glöckle, H. Witała, D. Hüber, H. Kamada, and J. Golak, Phys. Rep. **274**, 107 (1996).
[2] A. Nogga, A. Kievsky, H. Kamada, W. Glöckle, L.E. Marcucci, S. Rosati, and M. Viviani, Phys. Rev. C **67**, 034004 (2003).
[3] R. Machleidt, F. Sammarruca, and Y. Song, Phys. Rev. C **53**, R1483 (1996).
[4] A. Nogga, H. Kamada, W. Glöckle, and B.R. Barrett, Phys. Rev. C **65**, 054003 (2002).
[5] E. Epelbaum, A. Nogga, W. Glöckle, H. Kamada, Ulf-G. Meissner, and H. Witała, Phys. Rev. C **66**, 064001 (2002).
[6] P.F. Bedaque and U. van Kolck, Annu. Rev. of Nucl. Part. Sci. **52**, 339 (2002).
[7] D.R. Entem and R. Machleidt, Phys. Rev. C **68**, 041001(R) (2003).
[8] E. Epelbaum, W. Glöckle, and Ulf-G. Meissner, Nucl Phys. **A747**, 362 (2005).
[9] H. Witała, W. Glöckle, D. Hüber, J. Golak, and H. Kamada, Phys. Rev. Lett. **81**, 1183 (1998).
[10] S. Nemoto, K. Chmielewski, S. Oryu, and P.U. Sauer, Phys. Rev. C **58**, 2599 (1998).
[11] H. Rühl *et al.*, Nucl. Phys. **A524**, 377 (1991).
[12] P. Mermod *et al.*, Phys. Lett. B **597**, 243 (2004).
[13] P. Mermod *et al.*, Phys. Rev. C **72**, 061002(R) (2005).
[14] J.N. Palmieri, Nucl. Phys. **A188**, 72 (1972).
[15] Y. Maeda *et al.*, Phys. Rev. C **76**, 014004 (2007).
[16] P. Mermod *et al.*, Phys. Rev. C **74**, 054002 (2006).
[17] M.B. Chadwick, P.M. DeLuca Jr., and R.C. Haight, Radiat. Prot. Dosim. **70**, 1 (1997).
[18] J. Blomgren and N. Olsson, Radiat. Prot. Dosim. **103**, 293 (2003).
[19] S. Dangtip *et al.*, Nucl. Instr. Meth. **A 452**, 484 (2000).
[20] J. Klug *et al.*, Nucl. Instr. Meth. **A 489**, 282 (2002).
[21] R.B. Wiringa, V.G.J. Stoks, and R. Schiavilla, Phys. Rev. C **51**, 38 (1995).
[22] J.L. Friar, D. Hüber and U. van Kolck, Phys. Rev. C **59**, 53 (1999); S.A. Coon and H.K. Han, Few-Body Syst. **30**, 131 (2001).
[23] B.S. Pudliner, V.R. Pandharipande, J. Carlson, Steven C. Pieper, and R.B. Wiringa, Phys. Rev. C **56**, 1720 (1997).